

**Dissecting the molecular function of neutral
glycosphingolipids in ovarian cancer
progression**

Inauguraldissertation

zur

Erlangung der Würde eines Doktors der Philosophie
vorgelegt der
Philosophisch-Naturwissenschaftlichen Fakultät der
Universität Basel

von

Md. Shahidul Alam
Aus Chittagong, Bangladesh

Basel, 2017

Genehmigt von der Philosophisch-Naturwissenschaftlichen Fakultät
auf Antrag von:

Prof. Dr. Martin Spiess

Prof. Dr. Viola Heinzelmann-Schwarz

Prof. Dr. Gerhard M. Christofori

Basel, den. 20th June 2017

Prof. Dr. Martin Spiess

Dekan der Philosophisch-
Naturwissenschaftlichen
Fakultät

Table of Contents

1. Summary

2. Introduction

2.1 Ovarian cancer is one of the deadliest malignancies worldwide

2.1.1 Epithelial ovarian cancer is a heterogeneous disease

2.1.2 The uncertain origin of ovarian cancer

2.2 Glycosylation of cellular components in eukaryotes

2.2.1 Aberrant glycosylation in cancer development and progression

2.2.2 Glycosphingolipids in eukaryotic cells

2.2.3 Cellular Function of Glucosylceramide-related GSLs

3. Aim of the thesis

4. Publications

4.1 The glycosphingolipid P₁ is an ovarian cancer-associated carbohydrate antigen involved in migration

4.2 Glucosylceramide synthase inhibitors differentially affect expression of glycosphingolipids

4.3 Naturally occurring anti-glycan antibodies binding to Globo H-expressing cells identify ovarian cancer patients

4.4 Altered (neo-) lacto series glycolipid biosynthesis impairs α 2-6 sialylation on N-glycoproteins in ovarian cancer cells

4.5 Transition of mesenchymal and epithelial cancer cells depends on globosides

5. Further discussion and conclusion

6. References

7. Abbreviations

8. Appendix

8.1 Supplementary information for publication 4.1

8.2 Supplementary information of Publication 4.4

8.3 Supplementary information of Publication 4.5

9. Acknowledgements

10. Curriculum vitae

1. Summary

Glycosphingolipids (GSLs) are essential structural components of each eukaryotic cell and comprise a heterogeneous group of membrane lipids covalently linked to a glycan moiety. GSLs play fundamental role in proliferation, differentiation, adhesion, protein and lipid trafficking, signaling events and binding ligands of bacterial toxin and viruses. Aberrant glycosylation on GSLs has been associated with malignant transformation. The presence of tumor associated GSLs has also been observed in epithelial ovarian cancer, which is the eight most common cause of cancer in the women worldwide bearing the highest mortality rate among all gynecological cancers. Several studies from our group suggest a potential role of GSLs (Gb3 and P₁) in ovarian cancer. Both are the members of neutral GSLs belonging to globo series (Gb3) and (neo-) lacto series (P₁). The α 1-4 galactosyltransferase (*A4GALT*) terminates both Gb3 and P₁ in the GSLs biosynthesis pathway. Gb3 is expressed on different human cell types (erythrocytes, monocytes, granulocytes, fibroblasts, smooth muscle cells of digestive tract and urogenital system, and various cancer cell lines) as well as in cancer tissues (primary lesions of metastatic colon cancer and the colon cancer metastases to liver) while the presence of P₁ is only known to be on erythrocytes. The functional role of these neutral GSLs has not been well understood in general and particular in context of ovarian cancer. To address this question, here we utilized two strategies: 1) enzymatic inhibition of key glycosyltransferase glucosylceramide synthase (GCS) and 2) CRISPR-*Cas9* mediated genome editing to generate homozygous, stable, and heritable knockout cell lines to consequently establish an experimental tool depleted for specific glycans. The effects of inhibition and abolishment of these GSLs on cellular process is investigated with the appropriate assays. Our results displayed that ablation of (neo-) lacto series GSLs by CRISPR-*Cas9* mediated genome editing (*ΔB3GNT5*) leads an unexpected loss of α 2-6 sialylation on *N*-glycoproteins. Profiling of α 2-6 sialyltransferase encoding genes revealed that loss of α 2-6 sialylation is due to the silencing of *ST6GAL1* expression. Another study reported that globoside glycosyltransferases are elevated in epithelial signature and depletion of globosides by CRISPR-*Cas9* mediated *A4GALT* deletion induce epithelial to mesenchymal transition (EMT) and consequently enhance chemo resistances. Cells undergoing EMT lost E-cadherin expression through epigenetic silencing at the promoter of *CDH1* via DNA methylation, however, in *A4GALT*

deleted cells demethylation was only able to rescue E-cadherin expression while wild type *A4GALT* was provided. Our data demonstrated another class of biomolecules vital for epithelial homeostasis to maintaining cell integrity and function. Taken together, our studies demonstrate that GSLs, and in particular globosides, play an important role in the transition of ovarian cancer cells towards epithelial (MET) or mesenchymal (EMT) phenotypes. Thus, these data suggest that particular GSLs are involved in a complex network affecting molecular events such as alteration of α 2,6-sialylation on *N*-glycoproteins and influencing E-cadherin mediated cell-cell adhesion in intermediate EMT ovarian cancer cell lines. In summary this PhD thesis highlights a close relationship between the EMT process and GSLs, which allows a new direction for targeting new therapies.

2. Introduction

2.1 Ovarian cancer is one of the deadliest malignancies worldwide

Ovarian cancer is the seventh most common type of cancer in women with highest mortality rate among all gynecological cancer, representing 4% of all cancer in women [1, 2]. Worldwide 239,000 new cases of ovarian cancer are diagnosed each year, with 152,000 cancer-specific deaths [2-6]. The incidence and survival rates vary by country; 55% of all new cases occurred in countries with high or very high levels of human development, whereas 37% of new cases and 39% of deaths occurred in Europe and North America [2, 7, 8]. Interestingly, the annual incidence rates are declining in certain countries with very high levels of human development, notably in Europe and North America [2]. This might have been influenced by the use of oral contraceptives and changing pattern of hormonal replacement therapy [9, 10]. The high mortality rate has several reasons, which are discussed in more details in the introductory sections below.

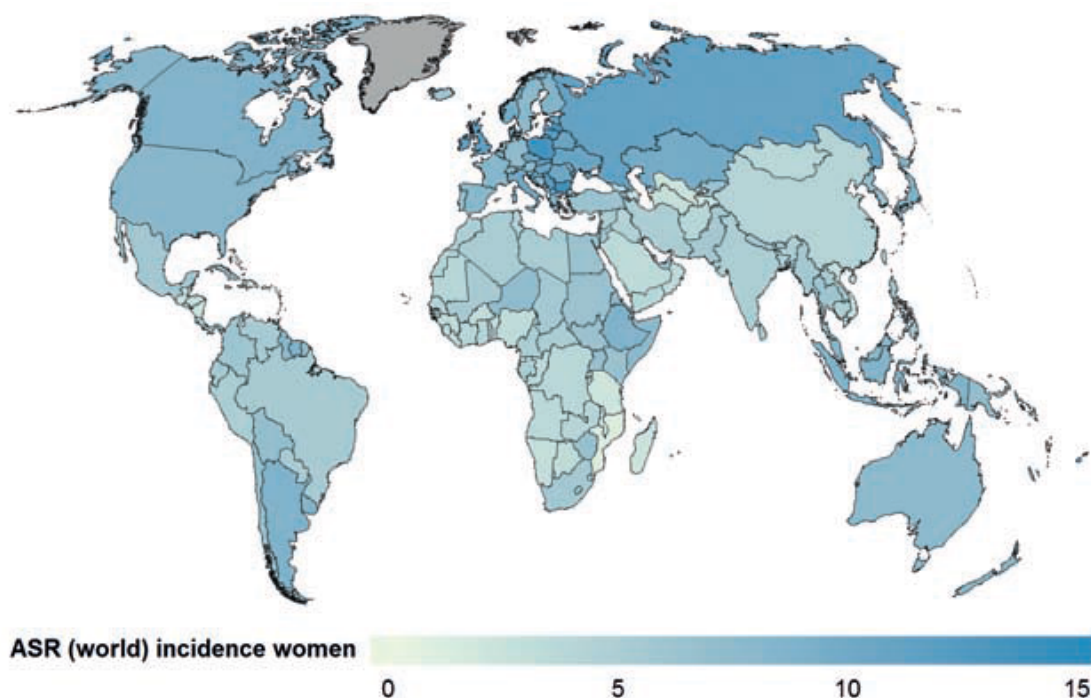


Figure 1: Global distribution of estimated age-standardized (world) incidence rates (ASR) per 100,000 for ovarian cancer, 2012 (adapted from [2]).

2.1.1 Epithelial ovarian cancer is a heterogeneous disease

Epithelial ovarian tumors/carcinomas account for approximately 90% of the all-ovarian tumors and are classified into five major subtypes: high grade serous carcinoma (HGSC), low grade serous carcinoma (LGSC), clear cell carcinoma, endometrioid adenocarcinoma and mucinous adenocarcinoma, that vary in biological behavior, response to treatment and overall prognosis (Table 1) [10, 11]. There is considerable heterogeneity within specific subtypes, particularly most frequent serous cancers [12, 13]. Although international federation of gynecology and obstetrics (FIGO) stage and grade are still used to classify ovarian cancer, two separate and quite distinct groups (Type 1 and Type 2) have been recently re-organized according to their molecular profiles [14, 15]. Type 1 tumors include LGSC, endometrioid, clear cell and mucinous carcinoma, which are characterized by indolent course and early stage detection, when the tumor is microinvasive and confined to the ovary. They commonly have mutations in *KRAS*, *BRAF*, *ARID1A*, *PIK3CA*, and *PTEN* [15]. By contrast, Type 2 tumors include HGSC, malignant mixed mesodermal tumors and undifferentiated carcinomas [14, 15], which are more aggressive and detected in advanced stages (stages III-IV) in more than 75% of cases. A very high frequency of *TP53* mutation (>95%) and *BRCA1/2* alteration (15%) are associated with Type 2 tumors [16].

Table: 1 Types of ovarian cancer by histology, clinical findings and genomic characteristics (adapted from [10])

Histological subtype	Clinical findings	Genetic characteristics
High grade serous carcinoma	Present with peritoneum, ascites and/or pelvic mass. Typically advanced stage	Associated with <i>BRCA</i> (15%) and <i>TP53</i> (>95%) mutations & >50% tumors with HR deficiencies
Low grade serous carcinoma	Presents in young patients (43-55 years). Early or late stages	<i>KRAS</i> (20-40%) and <i>BRAF</i> (5%) mutations. Tumors with genomic instability
Clear-cell carcinoma	Parenchymal metastasis (in the liver and lungs)	<i>ARID1A</i> (46-57%) and <i>PIK3CA</i> (33%) mutations
Endometrioid adenocarcinoma	Potentially associated with endometriosis	<i>PTEN</i> (35-50%), <i>ARID1A</i> (30%) and <i>PIK3CA</i> (30%) mutations. Microsatellite instability (20-40%)
Mucinous adenocarcinoma	Presents in younger patients and typically early stage	<i>KRAS</i> mutations (43-57%)

2.1.2 The uncertain origin of ovarian cancer

Ovarian cancer strikes silently, usually revealing no obvious symptoms until disease advances to a metastatic stage [17]. Approximately 70% of ovarian cancer patients are often diagnosed when disease metastasized to a distant site because of nonexistence screen methods and only 20% of women with such cancers can expect to survive 5 years [18-20]. Therefore a better insight into the biology of the disease is needed in order to detect at an early and potentially curable stage and to develop more targeted and effective treatment strategies. As implicit in the name, ovarian cancer is supposed to be a cancer originating in the ovary [21]. Yet the exact cell of origin has been unclear whether the cancer actually arises from the ovary, especially for HGSC, the most common and deadliest ovarian cancer [22, 23]. HGSC is rarely detected in stage I (<1.5% cases) [24-26], when tumors are confined to ovary, most cases are in advanced FIGO stage with wide spread metastases in the peritoneal cavity [27]. However, mostly non-epithelial tumors – such as granulosa-cell and germ-cell tumors or epithelial ovarian cancers like endometrioid, clear-cell, mucinous, and borderline tumors are limited to ovary without metastasis [28, 29].

Several sites have been proposed to give rise to the cell of origin for EOC, including ovarian surface epithelium (OSE), fallopian tubes and other derivatives of secondary Mullerian system [30-33]. Epithelial ovarian tumors have long been considered to originate from the OSE or the cortical inclusion cysts [34, 35], but a convincing precursor for HGSC has not been identified yet. A recent study has been proposed that the transitional zone (named as hilum) between OSE, mesothelium and tubal epithelium may also be a candidate for the EOC cell of origin because of their plastic and presumably, less differentiated states [36-38]. The study demonstrated that the hilum OSE cells are cycling slowly and display long-term stem cell properties *ex vivo* and *in vivo*, shown by serial sphere formation and long-term lineage tracing assay. The increased transformation potential was also identified after inactivation of *Trp53* and *Rb1*, whose pathways are altered frequently in the most aggressive and common type of human EOC (HGSC) [39].

Another hypothesis is based pathologist observations in the late 1990s and early 2000s where meticulously sections of the fallopian tubes and ovaries from women at high risk of developing ovarian cancer were investigated. Women with high risk to develop ovarian cancer usually display a family history of breast or ovarian cancer

and carry germline mutations in *BRCA1* and *BRCA2* [40]. Surprisingly, they found no ovarian lesions but instead discovered occult noninvasive and invasive carcinomas in the fallopian tubes, typically in the fimbria, named as serous tubal intraepithelial carcinomas (STIC), [41-46]. The STIC lesions carry *TP53* mutation positive cells and show increased proliferative capacity in at least 60% of women with HGSC [47, 48] and similar lesions are not observed in OSE [49]. These early lesions exhibit shortened telomerase, which is a notable hallmark of early molecular carcinogenesis [50, 51]. Subsequently, Piek *et al.* proposed that these occult tubal carcinomas might shed malignant cells to ovary [52]. According to this concept, STIC cells detach from the distal fimbriated end of fallopian tube and implant on the ovarian surface, stimulating primary ovarian cancer [53-55]. Therefore, it has been suggested that additional sites of origin exist and a substantial proportion of cases may arise from precursor lesions located in the fallopian tubal epithelium. The hypothesis is also supported by clinical observations in which STICs can originate from secretory epithelial cells of the fallopian tube and progress to HGSC by rapidly disseminating to involve ovarian and peritoneal surfaces. The shared morphologic and immunophenotypic features of STICs and HGSCs is further supported by this hypothesis. Moreover, injection of transformed primary human fallopian tube secretory epithelial cells (FTSECs) into the peritoneum of nude mice induces tumors that grossly, histologically, immunophenotypically, and genomically resemble human HGSCs [56-58]. In the most recent study, demonstrated that HGSOC can originate in fallopian tube secretory epithelial cells (FTSEC) and also established STIC as a precursor lesion to HGSC and peritoneal carcinoma in mouse model targeting the *Brca*, *Tp53* and *Pten* [59].

2.2 Glycosylation of cellular components in eukaryotes

Glycans are the most abundant biological molecules on our planet and represent one of the four fundamental building blocks (protein, lipid, nucleic acid and glycan) of life [60]. They are assemblies of carbohydrates (oligosaccharides and polysaccharides), which exist in either free form or in covalent complexes with proteins or lipids, named as glycoconjugates [61]. These glycoconjugates are primarily defined according to the nature and their non-glycosyl part, whether glycoproteins or glycolipids [62].

Several main families of glycoconjugates have been identified in the past. Secreted and transmembrane proteins can be modified with oligosaccharides at the amino acid asparagine (Asn) referring to *N*-glycoproteins, at the amino acids serine (Ser)- or threonine (Thr)- forming *O*-glycoproteins. In contrast, intracellular proteins such as glycosylphosphatidylinositol (GPI)-linked proteins bear a glycan chain linked to phosphatidylinositol. Nuclear and cytoplasmic proteins are modified with the monosaccharide as *O*-linked *N*-acetylglucosamine (*O*-GlcNAc) linked to serine, often at sites that are normally phosphorylated [63] (Figure 2). Beside proteins, glycosaminoglycans present as free polysaccharides (such as hyaluronan) or as part of proteoglycans (such as heparan sulphate and chondroitin sulphate). The remaining glycosphingolipids (GSLs) usually linked to ceramides being part of the cell surface membrane [63] (Figure 2).

Most of these glycans exist in the glycocalyx as membrane-bound glycoconjugates or secreted molecules, which can become integral parts of the extra cellular matrix (ECM) [61]. These locations place glycans in a position to mediate cell adhesion and motility, as well as intracellular signaling events [64]. The enzymatic process that produces glycosidic linkages of saccharides to other saccharides, proteins or lipids usually catalyzed through glycosyltransferases is defined as glycosylation [65, 66] and act as a key regulatory mechanism controlling several pathophysiological processes. Glycosylation defects in humans and their links to disease have shown that the mammalian glycome contains a remarkable amount of biological information [67]. It has also been shown that characterizing the biological functions of each glycan [68], as well as glycan-binding proteins and lipids made important contributions to the cancer field [61, 69-71].

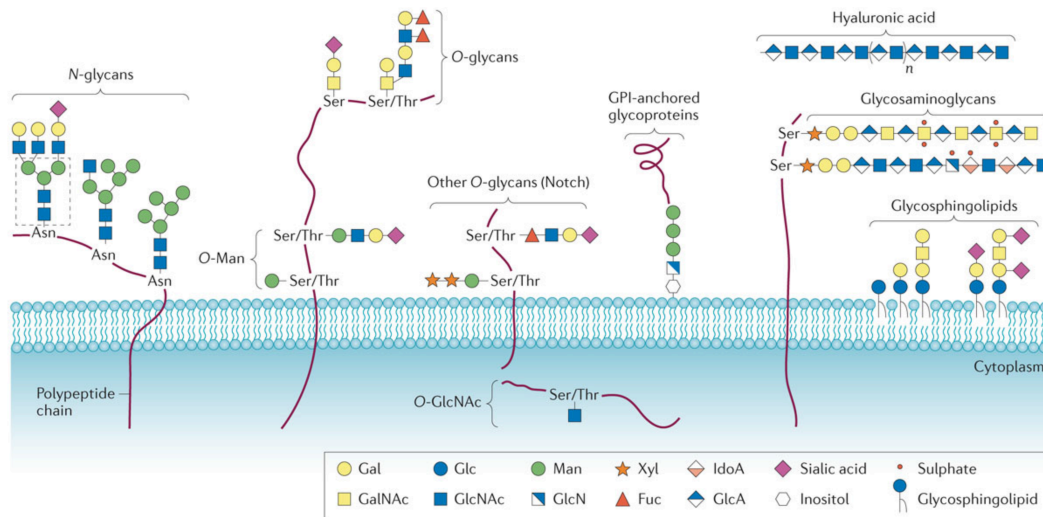


Figure 2: Common classes of glycans in mammalian cells (adapted from [62])

Glycans have been found in various types of macromolecules. Ceramide-linked glycans are composed of a variable series of structures, which can be further modified with terminal sialic acids [64, 72]. Proteins are glycosylated by the covalent attachment of a monosaccharide to a polypeptide backbone, *via* *N*-linkage to Asn or *O*-linkage to Ser/Thr. *O*-glycans can be extended, producing various ‘cores’ and different terminal structures that are usually fucosylated and sialylated [73]. Other types of *O*-glycans include the *O*-mannose (*O*-Man), *O*-fucose (*O*-Fuc), *O*-galactose (*O*-Gal) and nucleocytoplasmic *O*-linked β -*N*-acetylglucosamine (*O*-GlcNAc) [74, 75]. *N*-glycans share a common pentasaccharide core region (highlighted in the figure as a dotted line box) that can be further diversified into oligomannose, hybrid or complex types and further modified by the terminal structures GlcNAc, Gal and sialic acid [64]. Some glycoproteins can also be found in the outer leaflet of the plasma membrane linked to a phosphatidylinositol; known as GPI-anchored proteins [64]. Glycosaminoglycans are linear co-polymers of acidic disaccharide repeating units mostly found attached to the so-called proteoglycans [64]. An exception is hyaluronic acid, which is a glycosaminoglycan found free in the extracellular matrix.

2.2.1 Aberrant glycosylation in cancer development and progression

More than six decades ago, it was first described that changes in glycosylation are associated with oncogenic transformation [76, 77]. Tumor cells display a wide range of aberrant glycosylation, which may affect cell glycoconjugates such as *N*-glycans and *O*-glycans on glycoproteins, glycolipids or glycosaminoglycans compared with their non-transformed counter cells [78, 79]. This might be due to the expression levels of glycosyltransferases, sugar nucleotide donors, as well as disorganization of the Golgi, which may contribute to significant changes between normal and diseased states [79]. Malignant transformation is often accompanied by the expression of oncofetal antigens-epitopes and those observations were further investigated with advent monoclonal antibody technology, which showed that tumor specific antibodies were directed against glycan epitopes [80, 81]. Thus, cancer associated carbohydrates are potential targets for new diagnostic biomarkers or as therapeutic targets. Interestingly, the majority of the cancer-associated biomarkers that are clinically applied nowadays are either glycoproteins or glycolipids (Table 3). This might be because of human serum proteomes, most of which are made up of glycoproteins [82]. Glyconjugates are entering to the circulatory system from tissues or blood cells through active secretion or leakage, including necrotic and apoptotic processes, which displayed great complexity fluctuate in carbohydrate structures and reflecting the physiological and pathological state of the organism. Thus, serum with its ease of accessibility from peripheral blood and reduced risk to the patient due to minimally invasive nature of harvesting is an attractive option from a clinical and diagnostic perspective [83].

Current strategy to detect the ovarian cancer involves ultrasonography and monitoring levels of the serum glycoprotein CA125 also referring to MUC16 [84, 85]. However, CA125 is inadequate as it is non-specific for ovarian cancer and thus unreliable for diagnosing early stage for this disease [86]. For the last two decades, numerous studies (including large clinical trails) have been conducted to develop potential biomarker for ovarian cancer. Several markers are currently being investigated including OVX1, M-CSF, inhibin, kallikreins, TPS, and lysophosphatidic acid [86, 87].

Table 3: List of FDA approved biomarkers (adapted from [64])

Biomarker	Type	Source	Cancer Type	Clinical Use
α -Fetoprotein	Glycoprotein	Serum	Liver	Monitoring
α -Fetoprotein-L3	Glycoprotein	Serum	Liver	Risk
DCP	Protein	Serum	Liver	Risk
Human chorionic gonadotropin-3	Glycoprotein	Serum	Testicular	Staging
CA19-9	Carbohydrate	Serum	Pancreatic	Monitoring
CA125	Glycoprotein	Serum	Ovarian	Monitoring
Pap smear	Cervical smear	Cervix	Cervical	Screening
CEA	Glycoprotein	Serum	Colon	Monitoring
EGF receptor	Glycoprotein	Colon	Colon	Selection of therapy
KIT	Protein (IHC)	GI tumor	GI stromal tumors	Diagnosis & selection of therapy
Thyroglobulin	Glycoprotein	Serum	Thyroid	Monitoring
PSA	Glycoprotein	Serum	Prostate	Monitoring
CA15-3	Glycoprotein	Serum	Breast	Monitoring
CA27-29	Glycoprotein	Serum	Breast	Monitoring
Cytokeratins	Protein (IHC)	Breast tumor	Breast	Prognosis
Estrogen & progesterone receptors	Protein (IHC)	Breast tumor	Breast	Selection of therapy
HER2/NEU	Glycoprotein	Breast tumor	Breast	Prognosis & selection of therapy
HER2/NEU	Glycoprotein	Serum	Breast	Monitoring
HER2/NEU	DNA (FISH)	Breast tumor	Breast	Prognosis & selection of therapy
Chromosome 3,7, 9, and 17	DNA (FISH)	Urine	Bladder	Screening & Monitoring
NMP22	Protein	Urine	Bladder	Screening & Monitoring
Fibrin/FDP	Protein	Urine	Bladder	Monitoring
BTA	protein	Urine	Bladder	Monitoring
CEA and mucin	Glycoprotein	Urine	Bladder	Monitoring

In regards to glycoconjugates as biomarkers, recent work identify glycan-based markers, efforts have been made with array technologies searching for glycan-binding proteins [88-91]. In a recent study we used the first custom made high throughput printed glycan array, consist of a library of over 200 glycans including well-known tumor associated carbohydrate antigens, and identified plasma-derived anti-glycan antibody signatures in blood of ovarian cancer patients compared to healthy controls

[92]. In comparison to the clinically applied tumor markers CA125, anti-glycan antibodies to individual glycan structures on the array showed a comparable sensitivity and specificity in this cohort, which was increased by a combination of up to 6 glycans with a sensitivity (79.2%) and specificity (84.8%). A combination of both, the top candidate P₁ and CA125 only marginally improved the sensitivity (76%) and specificity (73.9%) [92]. The subsequent studies validate the predictive value of printed glycan array using two independent glycan based immunoassay, suspension array and ELISA [93]. Within the top five candidates two of them were glycosphingolipids (Gb3 and P₁). These data demonstrated that specific GSLs might play a role in ovarian cancer patients, however, their cellular function in this context remains to be elucidated.

2.2.2 Glycosphingolipids in eukaryotic cells

Glycosphingolipids (GSLs) were first discovered and named by Ernst Klenk after their isolation from brain tissue in 1942 [94]. GSLs represent the major components of outer leaflet of each eukaryotic cell plasma membrane, which are a heterogeneous class of amphipathic compounds that constituted by complex glycan moieties linked to a ceramide lipophilic backbone by a β -glycosidic bond [95]. GSLs comprising ceramide is synthesized in endoplasmic reticulum (ER) [96, 97] and then transported to Golgi *apparatus* and converted to glucosylceramide (GlcCer) by the activity of glycosyltransferase, then it flips to the Golgi lumen [98, 99]. Glycosyltransferases are enzymes that establish natural glycosidic linkages *via* catalyzing the transfer of saccharide moieties from an activated nucleotide sugar to a nucleophilic glycosyl acceptor target, which can be oxygen-, carbon-, nitrogen-, or sulfur-based. It is estimated that glycosyltransferases in mammals utilize at least nine sugar nucleotide donors: CMP-sialic acid, UDP-glucose, -galactose, -GlcNAc, -GalNAc, -xylose, -glucuronic acid, -mannose, and -fucose. Specific carbohydrates from the appropriate activated sugar nucleotide (e.g. UDP-Galactose, CMP-sialic acids, UDP-Fucose, etc.) are then added to the non-reducing end of the growing carbohydrate chain linked to GlcCer [100]. The GSLs ceramide seems to part of the membrane and sugars are facing the extracellular space of the cells [101].

The structural and functional classifications of GSLs have traditionally been based on their glycan part [64]. The first monosaccharides β 1-1-linked to ceramide in higher

animals are typically galactose or glucose forming galactosylceramide (GalCer) and glucosylceramide (GlcCer), respectively. The latter is further elongated by the addition of β 1-4-linked galactose resulting in lactosylceramide (galactosyl-1,4- β -glucosylceramide). The further extension of the GSL generates a series of neutral “core” structures, which are divided into three major series: ganglio-series (Gal β 1-3GalNAc β 1-4Gal β 1-4Glc β 1-1Cer), (neo-) lacto-series (GlcNAc β 1-3Gal β 1-4Glc β 1-1Cer), and globo-series (Gal α 1-4Gal β 1-4Glc β 1-1Cer) (Figure 3) [64].

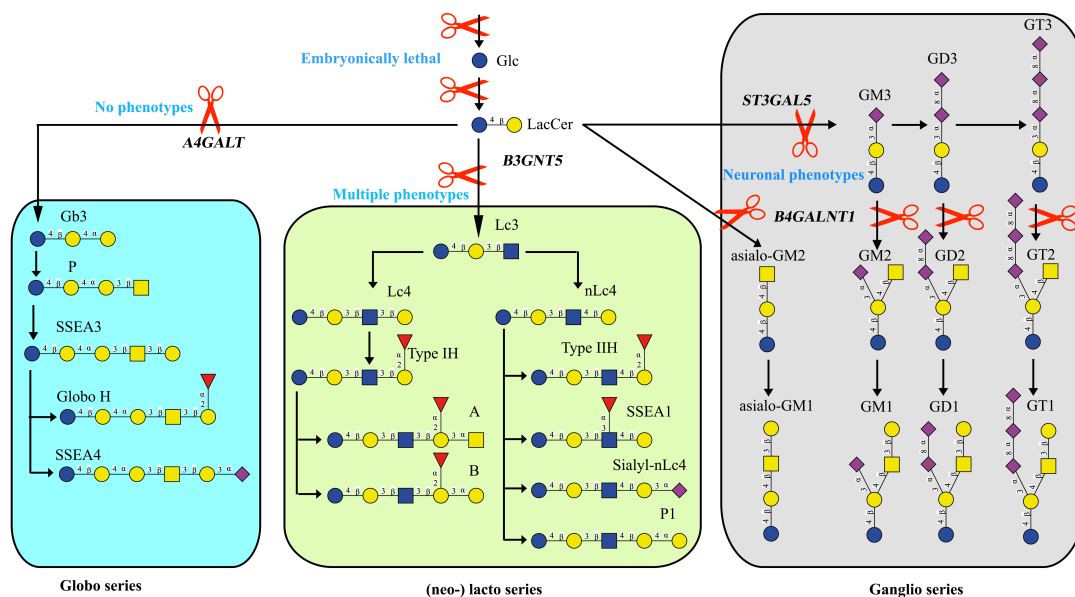


Figure 3: GSLs biosynthesis pathway Depiction of the three major glycosphingolipid series - globo, (neo-) lacto, and ganglio series shown in light blue, green and grey box, respectively. LacCer is the precursor of all three glucosylceramide-related GSL series. Extensions of globo and (neo-) lacto series GSLs are occurred by the action of *A4GALT* and *B3GNT5*, respectively, whereas the ganglio series biosynthesis occurred by *ST3GAL5* & *B4GALNT1*. Glycosidic linkages are displayed next to CFG annotated monosaccharides. The red scissor indicated the deletion of the particular glycosyltransferase. The phenotypic consequences of different genetic manipulations of GSL synthesis pathway in mice are indicated in blue text.

The GSL expression varies among different tissue-specific patterns. For example, in mammals gangliosides are broadly distributed predominately in the brain and the

(neo-) lacto-series GSLs are in secretory organs and certain hematopoietic cells including leukocytes. In contrast, globo-series are the most abundant in erythrocytes [64]. This diversity showed the important differences in GSLs functions [64]. GSLs can also sub-divided as neutral (no charged sugars or ionic groups), sialylated (having one or more sialic acid residues), or sulfated groups [64], where all sialylated GSLs are known as “gangliosides,” regardless of whether they are based on the ganglio-series neutral core structure mentioned above [64].

2.2.3 Cellular Function of Glucosylceramide-related GSLs

2.2.3.1 Physiological role of GSLs in mice

GSLs have been extensively studied using genetic, biochemical, biophysical and cell biology approaches to identify their physiological roles. A general framework for the understanding of functions of GSLs in mammals has been provided by mouse genetics. Studies have shown that ablation of the key glycosyltransferase of glucosylceramide-related GSLs, *Ugcg* leads to embryonic lethality during gastrulation as a result of massive apoptosis in mice [102]. Similarly, depletion of the *B4galt5*, responsible for LacCer synthesis expression [103], gives rise to embryonic lethality by embryonic day 10.5, possibly as a result of growth inhibition [104]. These results suggest that glucosylceramide-related GSLs are cumulatively required for correct embryo development. On the other hand, the GM3 synthase (*St3gal5*) knockout does not impair to any major abnormalities, although this is associated with enhanced insulin sensitivity [105], impaired neuropsychological behaviour [106] and hearing loss [107]. Downstream GA2/GM2/GD2 synthase (*B4galnt1*) [108] ablation leads to male infertility [109], axonal degeneration, myelination defects [110], motor deficit [111] and Parkinsonism [112]. Depletion of *St8sial* (GD3 synthase) promotes thermal hyperalgesia, mechanical allodynia [113] and reduced neuroregeneration [114]. All of these gangliosides strongly involve in neuronal function. Along the same lines, combined deletion of the GM3 and GA2/GM2/GD2 synthases showed severe neurodegeneration [115], whereas, combined ablation of GD3 and GA2/GM2/GD2 synthases induces lethal audiogenic seizures [116] and peripheral nerve degeneration, leading to reduced sensory function and skin lesions as a result of over-scratching [117] in mice. (Neo)-lacto series depletion by *B3gnt5* knockout, which is responsible for Lc3 synthesis, leads to either preimplantation lethality [118] or multiple postnatal

defects, such as: early death, growth inhibition, loss of fur, obesity, reproductive problems and B-cell functional defects [119]. By contrast, *A4galt* knockout mice showed loss of globoside synthesis with no overt phenotypes [120] (Figure 3). Results from all of these studies made GSLs as an important player, which might have an influence with several human diseases including cancer.

2.2.3.2 Glycosphingolipids in cancer

GSLs have been actively modulate various features of the cell, including apoptosis, cell proliferation, endocytosis, intracellular transport, cell migration and senescence, and inflammation [121], which are the crucial aspects related to tumorigenesis and cancer progression, as well as the responses to anti-cancer therapies [122]. In addition, a large number of GSLs have also been identified as tumor-associated carbohydrate antigens [123]. In different cancer cells, it has been shown that alterations of cell surface GSL-expression patterns are associated with tumor-relevant phenotypes [122]. For example, the exogenous addition of gangliosides Gt1b, GD1A, GM3 and GM1 inhibit human neuroblastoma (NBL-W) cell proliferation and epidermal growth factor (EGF) receptor tyrosine phosphorylation [124]. By contrast, the globosides Gb4 and Gb5 strongly enhance colon cancer cell proliferation and motility [125]. The disialyl GSL has been demonstrated to enhance tumor phenotypes [126] such as GD3 for cell growth and invasiveness in malignant melanoma [127-130], by activating Src family kinases [130] and Focal adhesion kinase activation [128], whereas GD2 promotes proliferation in small cell lung cancers [131] and GD3/GD2 enhance malignant properties in osteosarcoma cells [132]. On the same line, in highly metastatic osteosarcoma cells the ganglioside GD1a inhibits cell migration [133] by suppressing matrix metalloproteinase-9 (MMP-9) [134], tumor necrosis factor α [135], nitric oxide synthase 2 [136] and hepatocyte growth factor (HGF) expression [137], thus impacting on HGF induced c-Met phosphorylation [138]. In addition, Gt1b has been shown to inhibit integrin dependent keratinocyte adhesion to fibronectin [139]. In cancer cells, the same effect has been shown for GM3 and GM2, inhibition of integrin-dependent cancer cell motility *via* promoting the formation of a ganglioside/tetraspanine/integrin complex and inactivating Src or Met [140, 141]. Collectively, all these data demonstrated the specific roles in mammalian physiology and pathology to different classes of GSLs, and the molecular mechanisms through which they exert these functions involve interactions of GSLs with proteins and glycans [123].

Over the last three decades, GSLs have been identified to interact with a number of plasma membrane located signaling receptors to modulate their activation [124, 142-159] (Table 2) and the best-characterized example is the interaction between EGF receptor and GM3. The exogenously added GM3 inhibits cell growth [160, 161] through the modulation of EGF receptor phosphorylation, which is dependent on the presence of the Neu5Ac residue in GM3 and of lysine 642 in the EGFR [142]. The GM3 binding to EGFR inhibits homo-dimerization and are not allowing the ligand (EGF) to activate EGFR phosphorylation [142]. A similar interaction was also reported between the insulin receptor and GM3, which again involves a key lysine (IR944) positioned in the proximity of the transmembrane portion of the insulin receptor [157].

Table 2: Known interaction between GSLs and proteins

Protein	GSLs	References
EGFR	GM1, GM3, GD1, GT1, Gb4	[124, 142-147]
FGFR	GM3	[148, 149]
PDGFR	GM1, GM3, GD1, GT1	[150, 151]
NGFR/TrK	GM1	[152, 153]
NgR1	GT1	[154]
VEGFR	GM3	[155]
TGFβ1R	Gb4, GM3	[144, 156]
IR	GM3	[157, 158]
Lyn/Cbp	GD3, GD1	[159]
Tetraspanins	GM3, GM2	[162-164]
CD11b/CD18	LacCer	[165]
α5β1 integrin	GT1	[166]
Caveolin-1	GM3	[166, 167]
PMCA	GM3, GM2, GM1, GD1	[168]
Galectin-1	GM1	[169]
Galectin-3	GM1	[170]

GSLs have also been shown to interact with a number of non-receptor plasma membrane proteins, including tetraspanins, integrins, caveolin-1 [139, 162-168], and galectins [169, 170]. Some of these interactions involve the binding of glycans to

protein modules or specific amino acids [142, 157, 169, 170] known as carbohydrate-protein interactions, whereas a GSLs interacting with glycan moieties on proteins or lipids are termed carbohydrate-carbohydrate interactions [171]. The carbohydrate-carbohydrate interactions can be established both in *cis* (*i.e.* glycans on the cell membrane of one cell) and in *trans* (*i.e.* glycans on the cell membrane of adjacent cells) [171]. The *cis* carbohydrate-carbohydrate interactions include the interactions between GM3 and the terminal GlcNAc moieties of the EGFR and HGF receptor glycans modulating properties of receptor activation [171]. Similarly, GSLs Gt1b/GD3 bind to mannose residues in integrin $\alpha 5$ and modulating integrin $\alpha 5$ - $\beta 1$ function that is cell-ECM (fibronectin) adhesion [139]. The *trans* carbohydrate-carbohydrate interactions were described for the interaction of GM3-Gg3 and GM3-LacCer contributing to the adhesion of tumor cells to endothelial cells [172, 173].

In addition to that GSLs also have the unique feature of forming molecular clusters by acting as both hydrogen bond donors and acceptors [95, 123, 174, 175] and promoting self-aggregation [174], which are defined as lipid rafts, GSL-enriched membranes or glycosynapses [123]. These lipid rafts on the plasma membrane serve for signaling, cargo sorting at the different traffic stations along the secretory and endocytic pathways [174] and adhesion molecules, to regulate their functions (e.g. integrin) [176]. Recent reports also suggest that ceramide heterogeneity impacts the molecular function of GSLs [177, 178]. Taken together, the current literature indicates that GSLs are involved in membrane-organization [123, 179], as well as they can interact with specific proteins and/or lipids [123]. These properties concur with the role that GSLs have in ‘environment sensing’, both in terms of modulation of cell responsiveness to extracellular stimuli and of cell-cell adhesion/recognition. These concepts position GSLs as important modulators of multicellularity, and more generally relate to ‘cell sociology’ [123]. Thus, GSLs have emerged to be key controllers in processes that imply cell differentiation and tissue patterning, whereas their deregulation plays a driving role in diseases such as cancers [180]. It should also be noted that, although these concepts are supported by a number of studies, only a few GSLs have been studied in more detail, thus, leaving the understanding of the specific roles of most GSLs to future research.

3. Aim of the thesis

Previous results by the Heinzemann group have been demonstrated that blood plasma-derived anti-glycan antibodies vary in levels discriminating ovarian cancer patients from healthy controls [181]. Interestingly, most of the glycan structures identified are supposed to be naturally attached to lipids presented on the cell surface membrane, also referring to glycosphingolipids (GSLs). GSLs have been found to participate in numerous biological processes involved in cancer, such as inflammation, immune surveillance, cell–cell adhesion, cell–matrix interaction, inter- and intracellular signaling, and cellular metabolism. Despite these observations, there remains a considerable lack of knowledge about the functional implications of GSLs in relation to ovarian cancer. In order to gain insight into the function of GSLs in ovarian cancer, the overall goal of this project is to understand the role of glucosylceramide-related glycosphingolipids, and in particular the function of globo (Gb3, SSEA3, etc.) and (neo-) lacto series GSLs (nLc4 and P₁).

Specific aims of the project are:

1. To establish a workflow for characterizing cancer samples from patients and cell lines for the GSLs expression using flow cytometry and mass spectrometry.
2. To elucidate whether circulating anti-glycan antibodies from patient samples specifically bind GSLs on ovarian cancer cells.
3. To establish an experimental strategy for studying GSLs by developing an experimental workflow through testing GSLs-synthesizing glycosyltransferase inhibitors and the use of genome editing in ovarian cancer cell lines. The latter comprised the design and establishment of a strategy to site-specifically and heritably knock out specific glycosyltransferase-encoding genes using zinc finger nucleases or the CRISPR-*Cas9* system ('glyco-engineered cell lines') together with re-expression of the enzyme for establishment of a functional rescue system.
4. To study the role of GSLs using fully characterized glyco-engineered ovarian cancer cell lines *in vitro* and *in vivo* in regards to Epithelial-to-Mesenchymal transition, a process in embryonic development and cancer progression, in particularly well reported in ovarian carcinogenesis. Moreover, the impact of glyco-engineering on the entire glycome was also of interest.

4. Publications

4.1 The glycosphingolipid P₁ is an ovarian cancer-associated carbohydrate antigen involved in migration

F. Jacob, M. Anugraham, T. Pochechueva¹, B. W. C. Tse, S. Alam, R. Guertler, N. V. Bovin, A. Fedier, N. F. Hacker, M. E. Huflejt, N. Packer and V. A. Heinzelmann-Schwarz

British Journal of Cancer, 2014

My contributions to this paper:

I contributed to this work by profiling GSLs on different ovarian cancer cell lines using flow cytometry. I have also characterized naturally occurring anti-P1 antibodies present in ovarian cancer ascites capable in binding or cancer cell lines. I was involved in analyzing the data and designing the corresponding figures as well as in writing parts of the manuscript.

Keywords: Gb3 (Pk); Gb4 (P); TACA; CD77; ovarian cancer; anti-glycan antibodies

The glycosphingolipid P₁ is an ovarian cancer-associated carbohydrate antigen involved in migration

F Jacob^{*1,2}, M Anugraham³, T Pochechueva¹, B W C Tse^{2,4}, S Alam¹, R Guertler^{1,2}, N V Bovin⁵, A Fedier¹, N F Hacker⁶, M E Huflejt⁷, N Packer³ and V A Heinzelmann-Schwarz^{1,2,6}

¹Gynecological Research Group, Department of Biomedicine, University Hospital Basel, University of Basel, Hebelstrasse 20, Basel 4031, Switzerland; ²Ovarian Cancer Group, Adult Cancer Program, Lowy Cancer Research Centre, University of New South Wales, Prince of Wales Clinical School, Building C25 Kensington Campus, Sydney, NSW 2052, Australia; ³Department of Chemistry and Biomolecular Sciences, Biomolecular Frontiers Research Centre, Faculty of Science, Macquarie University, Balaclava Road, North Ryde, Sydney, NSW 2109, Australia; ⁴Australian Prostate Cancer Research Centre Queensland, Institute of Health and Biomedical Innovation, Queensland University of Technology, Translational Research Institute, Brisbane, QLD 4102, Australia; ⁵Shemyakin-Ovchinnikov Institute of Bioorganic Chemistry, Russian Academy of Sciences, Ul. Miklukho-Maklaya, 16/10, Moscow 117997, Russian Federation; ⁶Gynaecological Cancer Centre, Royal Hospital for Women, School of Women's and Children's Health, Barker Street, Randwick, NSW 2031, Australia and ⁷Division of Thoracic Surgery and Thoracic Oncology, Department of Cardiothoracic Surgery, New York University School of Medicine, 550 First Avenue, New York, NY 10016, USA

Background: The level of plasma-derived naturally circulating anti-glycan antibodies (AGA) to P₁ trisaccharide has previously been shown to significantly discriminate between ovarian cancer patients and healthy women. Here we aim to identify the Ig class that causes this discrimination, to identify on cancer cells the corresponding P₁ antigen recognised by circulating anti-P₁ antibodies and to shed light into the possible function of this glycosphingolipid.

Methods: An independent Australian cohort was assessed for the presence of anti-P₁ IgG and IgM class antibodies using suspension array. Monoclonal and human derived anti-glycan antibodies were verified using three independent glycan-based immunoassays and flow cytometry-based inhibition assay. The P₁ antigen was detected by LC-MS/MS and flow cytometry. FACS-sorted cell lines were studied on the cellular migration by colorimetric assay and real-time measurement using xCELLigence system.

Results: Here we show in a second independent cohort ($n = 155$) that the discrimination of cancer patients is mediated by the IgM class of anti-P₁ antibodies ($P = 0.0002$). The presence of corresponding antigen P₁ and structurally related epitopes in fresh tissue specimens and cultured cancer cells is demonstrated. We further link the antibody and antigen (P₁) by showing that human naturally circulating and affinity-purified anti-P₁ IgM isolated from patients ascites can bind to naturally expressed P₁ on the cell surface of ovarian cancer cells. Cell-sorted IGROV1 was used to obtain two study subpopulations (P₁-high, 66.1%; and P₁-low, 33.3%) and observed that cells expressing high P₁-levels migrate significantly faster than those with low P₁-levels.

Conclusions: This is the first report showing that P₁ antigen, known to be expressed on erythrocytes only, is also present on ovarian cancer cells. This suggests that P₁ is a novel tumour-associated carbohydrate antigen recognised by the immune system in patients and may have a role in cell migration. The clinical value of our data may be both diagnostic and prognostic; patients with low anti-P₁ IgM antibodies present with a more aggressive phenotype and earlier relapse.

*Correspondence: Dr F Jacob; E-mail: francis.jacob@unibas.ch

Received 19 March 2014; revised 5 June 2014; accepted 21 July 2014; published online 28 August 2014

© 2014 Cancer Research UK. All rights reserved 0007–0920/14



Glycosphingolipids (GSLs) have critical roles in embryonic development, signal transduction, cell signalling, apoptosis, receptor modulation, cell adhesion, growth and cell differentiation and carcinogenesis (Jarvis *et al*, 1996; Hakomori, 1998; Kasahara and Sanai, 1999). The presence of tumour-associated GSLs antigens have been observed in epithelial ovarian cancer (Pochechueva *et al*, 2012), which is the fifth most common cause of death from all cancers in women and the leading cause of death from gynaecological malignancies (Ozols, 2006).

Printed glycan array technology (a glycan-based discovery approach) previously demonstrated that naturally occurring anti-glycan antibodies (AGA) in plasma of ovarian cancer patients exhibited specificities towards synthetic P₁ trisaccharide. In our previous study, we have demonstrated using a printed glycan array that anti-P₁ antibodies can discriminate healthy controls from ovarian cancer patients (Jacob *et al*, 2012). This study (on a Swiss Discovery Cohort) showed that anti-P₁ antibodies of IgM, IgG and IgA together were significantly lower in ovarian cancer patients, thereby discriminating them from healthy controls. The predictive value of the printed glycan array was validated by two independent glycan-based immunoassays, ELISA and suspension array (Pochechueva *et al*, 2011b).

The P^k, P and P₁ carbohydrate antigens, commonly expressed on GSL, are members of the P blood group system that differ in their specificity based on their oligosaccharide sequences. In cancer, the globo (P^k and P) and neolacto (P₁) series are precursor GSL that give rise to well-known tumour-associated carbohydrate antigens, such as Forssman antigen (Hakomori *et al*, 1977; Taniguchi *et al*, 1981) and Globo H (Gilewski *et al*, 2001; Chang *et al*, 2008; Wang *et al*, 2008). High levels of P^k (Gal α 1-4Gal β 1-4Glc β 1-1Ceramide; Gb3, CD77), P (GalNAc β 1-3Gal α 1-4Gal β 1-4Glc β 1-1Ceramide; Gb4) and Globo H were described in the past (Wenk *et al*, 1994).

As shown previously, naturally occurring AGA to P₁ have the potential to be used diagnostically in plasma of ovarian cancer patients. However, it remains unknown whether P₁-bearing GSL are present on ovarian cancer cells and whether naturally occurring anti-P₁ antibodies to chemically synthesised carbohydrates in glycan-based immunoassays bind to these GSL antigens. To our knowledge, no published reports regarding the role of P₁ in malignant transformation, particularly in ovarian cancer, are available, and the molecular mechanisms underlying GSL expression on the cell surface, as well as its function, have yet to be elucidated. Therefore, this study aims (A) to determine the responsible naturally occurring AGA immunoglobulin class discriminating cancer from normal; (B) to determine whether the level of these antibodies are predictive of patient outcome; (C) to investigate whether the related P₁ glycan epitopes are present on cells isolated from ovarian cancer tissues as well as on ovarian cancer cell lines; (D) to compare the AGA profiles in ascites and matched plasma; (E) to compare monoclonal anti-P₁ antibodies produced in humans and affinity purified anti-P₁ antibodies isolated from ascites; and finally (F) to investigate the functional role of the P₁ antigen in ovarian cancer.

MATERIALS AND METHODS

Biospecimens. Two independent patient cohorts from two different continents were used for the experiments: (A) matched plasma and ascites from 11 serous FIGO stage III/IV cancer patients from the previously described Swiss Discovery Cohort (Jacob *et al*, 2012); (B) plasma from 155 Australian samples (Australian Validation Cohort) comprising healthy controls, borderline tumour and ovarian cancer patients. The Australian Validation Cohort was split into: (1) borderline tumours and

adenocarcinomas of the ovary, tube and peritoneum ('tumour group'), and (2) healthy control women ('control group'). Patients were either admitted with an adnexal mass to the Gynaecological Cancer Centre of the Royal Hospital for Women, Randwick, Australia or were seen as outpatients to the Hereditary Cancer Centre of The Prince of Wales Hospital, Randwick, Australia. All patients were prospectively included after giving informed consent in accordance with ethical regulations (Hunter Area Research Ethics 04/04/07/3.04; South Eastern Sydney Illawarra HREC/AURED Ref:08/09/17/3.02). The processing of blood plasma samples was performed constantly on ice within 3 h after collection as previously described (Jacob *et al*, 2011a, 2012). All clinicopathological data (Supplementary Table S1) such as FIGO stage and grade were incorporated in a specifically designed in-house database ('PEROV'), which was developed using Microsoft Access (Microsoft Corporation, Redmond, WA, USA). Diagnosis and histopathological features were independently re-evaluated by a pathologist specialised in gynaecological oncology (JS). Blood samples were stored in aliquots at -80°C .

Glycan-based immunoassays (printed glycan array, suspension array and ELISA). The printed glycan array was performed as previously described (Huflejt *et al*, 2009; Bovin *et al*, 2012; Jacob *et al*, 2012). AGA were detected by ImmunoPure goat anti-human IgA + IgG + IgM conjugated to long chain biotin (1:100, 'Combo', Pierce, Rockford, IL, USA). To detect the immunoglobulin class, developed printed glycan array slides were individually incubated with 1:50-diluted biotin-conjugated goat anti-human IgA, IgG or IgM (ZYMED Laboratories, Invitrogen, Carlsbad, CA, USA). The coupling procedures for end-biotinylated glycopolymers and antibody binding were described before (Pochechueva *et al*, 2011a, b). Experimental protocol was performed as described previously (Pochechueva *et al*, 2011b). Exceptions were made with respect to the use of goat anti-human IgG-R-PE or IgM-R-PE secondary antibodies (Southern Biotech Ass. Inc., Birmingham, AL, USA). ELISA was performed as described previously (Pochechueva *et al*, 2011b).

Extraction and identification of GSLs from cancer tissue samples and IGROV1 cell line. Fresh primary tissue samples (~ 100 mg) from a serous ovarian cancer and an endometrioid peritoneal cancer patient were collected to analyse glycolipids by negative ion electrospray ionisation mass spectrometry (LC-ESI-MS/MS). Detailed analysis of the procedure is described in Supplementary Information.

Affinity purification of anti-P₁ antibodies. Ascites fluid was collected from a late-stage serous ovarian cancer patient during primary surgery. The ascites was processed by centrifugation at 4°C , 3000 g for 15 min. Supernatant was aliquoted and kept frozen at -80°C . Thawed ascites (50 ml) was filtered through a 0.22- μm filter (Millipore, Billerica, MA, USA) and diluted three times in PBS (pH 7.4). Glycan-polyacrylamide-Sepharose stored in 20% (v/v) ethanol was washed with 10 volumes 20% ethanol, 20 volumes milliQ water and equilibrated with 10 volumes of PBS. Preprocessed ascites affinity purified against Gal α 1-4Gal β 1-4GlcNAc β -polyacrylamide-Sepharose (P₁-PAA-Seph; 10 ml). A constant flow rate of 1 ml min^{-1} was controlled by the use of an auxiliary pump (Model EP-1 Econo Pump, Bio-Rad, Hercules, CA, USA). Protein content and buffer composition was recorded by UV at 280 nm and conductivity, respectively (BioLogic DuoFlow Workstation, Bio-Rad). The column was washed with PBS containing 0.05% (v/v) Tween 20, unplugged and stored overnight at 4°C . The next day, the column was inserted back into the chromatography system and washed until no protein was detected anymore. Bound anti-P₁ antibodies were eluted using 0.2 M TrisOH (pH 10.2) and neutralised by 2.0 M Glycine HCl (pH 2.5). Eluted anti-P₁ antibodies were concentrated using the Amicon Ultra-0.5

centrifugal filter (Millipore), and their concentration was determined using spectrophotometrically at 280 nm.

Flow cytometry. GSL expression on the cell surface membranes was analysed by flow cytometry (CyAn ADP Analyzer, Beckman Coulter, Nyon, CH, USA) prior to antibody labelling. Unconjugated antibodies included anti-P₁ human IgM (clone P3NIL100; Immucor Gamma, Rödermark, Germany), anti-P₁ murine monoclonal IgM (clone OSK17; Immucor Gamma) and anti-Gb3 monoclonal IgG2b (CD77, P^k) (clone BGR23; Seikagaku Biobusiness Corporation, Tokyo, Japan). Biotin-conjugated antibodies included anti-human mouse IgM (BD Bioscience, Basel, Switzerland), rat anti-mouse IgM and rat anti-mouse IgG2b (BD Bioscience). Streptavidin conjugated to FITC (BD Bioscience) was used for fluorescence detection. Dead and apoptotic cells were separated from live cells using propidium iodide (BD Bioscience). Matching isotype monoclonal antibodies conjugated to FITC were used as controls (BD Bioscience). All investigated cell lines were gated individually to exclude debris, followed by single cell gating to remove dead cells and doublets. Data acquisition was performed using Summit v4.3 (CyAn ADP Analyzer, Beckman Coulter). Data analysis was performed using FlowJo v9 (Tree Star Inc., Ashland, OR, USA).

FACS sorting. IGROV1 cells were grown to 80% confluence, washed twice in PBS and harvested using non-enzymatic cell dissociation buffer (Sigma Aldrich, Buchs, Switzerland). Cells were then washed in PBS containing 1% FCS and resuspended to 10⁶ cells ml⁻¹. Cell suspension (100 µl) was stained with human anti-P₁ IgM (BD Bioscience) as mentioned above and run on a BD FACS Vantage SE DiVa Cell Sorter (BD Bioscience). IGROV1 cell line was sorted using >90% and <10% fluorescence signal intensity for P₁-positive cells to receive P₁-high and P₁-low fractions, respectively.

Flow cytometry-based inhibition assay. Monoclonal human IgM antibody directed to P₁ (Immucor Gamma, Rödermark) was preincubated either with Sepharose-P₁-PAA or Sepharose-P^k-PAA (Lectinity Holdings, Moscow, Russia) in different amounts ranging from 0.015 µmol to 0.06 µmol for 60 min at RT. The supernatant was further processed as described in the flow cytometry section.

Colorimetric cell migration assay. Sub-confluent tumour cells were 'starved' from serum by incubation in serum-free media for 24 h, before harvesting using a non-enzymatic cell dissociation buffer (Sigma Aldrich, Buchs, Switzerland), washed twice and resuspended in serum-free media containing 5% (w/v) BSA. Tumour cells (7.5 × 10⁵ in 300 µl) were loaded into cell culture inserts containing a polyethylene terephthalate membrane with 8-micron pores (Millipore). The inserts were assembled into 24-well plates with each well containing 700 µl of media with 10% supplemented with fetal calf serum, which was used as chemoattractant. After incubation for 18 h at 37 °C, the media in the interior of the insert was removed, and the entire insert was immersed in 400 µl of 0.2% crystal violet/10% ethanol for 20 min. The insert was washed several times in water, and the non-migrated cells in the interior of the insert were removed using a cotton-tip swab. After air-drying, five random areas of the inserts showing the migrated cells were photographed, and cell counts were performed. Colorimetric cell migration assay was performed three times.

In addition, parental IGROV1 cells were preincubated with 1% (w/v) BSA in PBS, the corresponding isotype control (ChromPure human IgM, Jackson ImmunoResearch Laboratories, Inc., MILAN Analytica AG, Rheinfelden, Switzerland) and human anti-P₁ IgM (clone P3NIL100), both antibodies in a final concentration of 500 µg ml⁻¹. After 1 h incubation, cells were processed according to previously described cell migration protocol.

MTT assay. Cultures were incubated with 500 µg ml⁻¹ (final concentration) MTT dye (Sigma-Aldrich, Buchs, Switzerland) in PBS for 3 h, followed by removal of the medium and dissolution of the violet crystals in 200 µl of DMSO. The optical density (absorbance at 540 nm) was measured with a SynergyH1 Hybrid Reader (Biotek, Luzern, Switzerland). The data are given as absorbance at 540 nm, representing cell viability as a function of araC concentration. Each experiment was performed independently twice from multiple cultures.

Real-time cell migration analysis (xCELLigence). Real-time cell analysis (RTCA; xCELLigence System, Roche Diagnostics GmbH, Mannheim, Germany) was used to investigate cell migration in P₁-low and -high serous ovarian cancer IGROV1 cells in a label-free environment (Solly *et al*, 2004; Ke *et al*, 2011). Migration was examined on 16-transwell plates (Roche Diagnostics GmbH) with microelectrodes attached to the underside bottom of the membrane for impedance-based detection of the migrated cells. Prior to each experiment, cells were deprived of FCS over a period of 24 h. Initially, 160 µl 'chemoattractant' media (RPMI 1640 containing 10% FCS) and 50 µl RPMI 1640 containing 1% FCS was added to the lower and upper chambers, respectively. Sterile PBS was loaded into the evaporation troughs. CIM-16 plates were further prepared according to the manufacture's protocol. Background signals generated by the cell-free media were recorded. Cells were harvested using trypsin, counted and re-suspended in an appropriate volume of RPMI 1640 containing 1% FCS. Cells (100 000 cells per 100 µl medium) were seeded onto the upper chamber of the CIM-16 plate and allowed to settle onto the membrane. Cell-free media was used as negative control. Each experiment was performed two times in duplicates. The programmed signal detection for quantification of the cell index was measured every 15 min over a period of 30 h. In an independent migration assay, 5 µM of 1-beta-D-arabinofuranosylcytosine (araC; Sigma-Aldrich), a DNA polymerase inhibitor, was added to avoid possible effects on migration caused by cell proliferation.

Statistical analysis. Detailed statistical procedure applied is described in Supplementary Information.

RESULTS

IgM antibodies in plasma against P₁ trisaccharide are reduced in patients with tubal, peritoneal and ovarian cancer. In our previous study, the use of three glycan-based immunoassays (printed glycan array, ELISA and suspension array), detecting IgM, IgG and IgA together, revealed significant AGA interactions with the members of the P blood group system (Pochechueva *et al*, 2011a, b; Jacob *et al*, 2012). Overall, less AGA to P₁ trisaccharide (printed glycan array, ELISA and suspension array) and P^k (printed glycan array) were observed in the plasma of the cancer patient group compared with the control group (Pochechueva *et al*, 2011b; Jacob *et al*, 2012).

In this study, we investigated the levels of IgM and IgG AGA in the plasma of an independent Australian Validation Cohort (*n* = 155). The cohort consisted of a 'benign' control group (healthy controls and benign gynaecological conditions; *n* = 81) and a 'tumour' group (ovarian borderline tumours, ovarian, tubal and peritoneal cancers; *n* = 74) (Supplementary Table S1). Based on suspension array data, AGA to the P₁ trisaccharide belonged mainly to the IgM class (median, IQR; 9.948log(MFI), 9.351–10.090log(MFI)) in all the tested samples. Significantly lower IgM anti-P₁ antibody levels were observed in the blood plasma samples of the tumour as compared with the control group (*P* = 0.0002) (Figure 1A). The tumour group revealed 15/74 (20.3%) samples having lower AGA levels compared with the lowest control group sample. Logistic regression did not reveal any relationship between

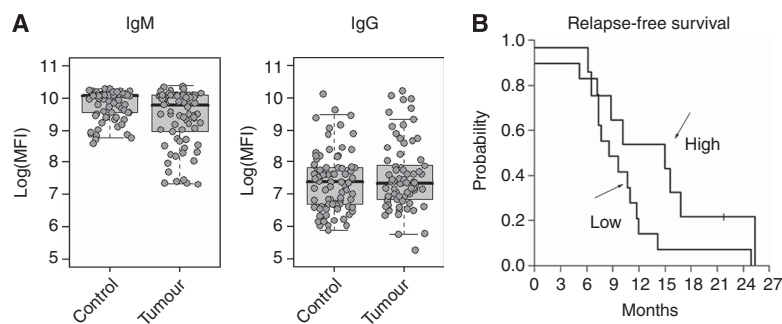


Figure 1. Significantly lower levels of anti-P₁ IgM in cancer patients in the Australian validation cohort ($n = 155$). (A) Box-and-whisker plots showing distribution of AGA levels of IgM and IgG to covalently attached P₁ trisaccharide using suspension array. Decreased AGA levels in cancer patients were observed for IgM. (B) Kaplan–Meier curve on relapse-free survival showing that patients with low antibody levels ($n = 33$; lower than median fluorescence signal) have slightly earlier relapse ($P = 0.055$) than those with high antibody levels ($n = 25$, higher than median fluorescence signal).

clinicopathological parameters and anti-P₁ IgM antibody signatures in the tumour group. In contrast to IgM, generally lower IgG antibody levels (median, IQR; 7.35log(MFI), 6.726–7.858log(MFI)) were observed. Both the control and tumour groups were similar in IgG AGA levels, with no significant difference in between both the groups ($P = 0.7248$, Figure 1A). We have compared various clinical parameters recorded along with collection of plasma samples for each patient. Statistical evaluation revealed a significant discrimination in FIGO stage of the non-mucinous cancer of ovary, tube and peritoneum (FIGO Stage, non-mucinous cancer of the ovary, tube and peritoneum I/II vs III/IV, $P = 0.01773$, t -test). The remaining investigated clinical parameters were not significantly different in their anti-P₁ IgM antibody levels mentioning Grade (G1 vs G2/3, $P = 0.2883$; t -test) or tumour origin (ovary vs tube vs peritoneum, $P = 0.322$; ANOVA). An increasing age has previously been demonstrated to be associated with reduction of AGA in a cohort of 48 control plasma samples using glycopeptide arrays (Oyularan *et al*, 2009). To investigate the influence of age on anti-P₁ antibodies (IgG and IgM), we have applied Pearson's correlation to suspension array data and found a moderate negative correlation ($\rho = -0.33$, $P < 0.01$) in the entire cohort (mean age 56.4 (28–87) years). However, in contrast to the control group that showed a moderate negative correlation ($\rho = -0.37$, $P < 0.01$), there was no correlation between age and anti-P₁ IgM levels in the tumour group ($\rho = -0.18$, $P = 0.123$). This demonstrates that the reduction of anti-P₁ IgM is independent of age in the tumour group and further indicates an association of these lowered IgM levels with the disease. In contrast, we observed no correlation between age and anti-P₁ IgG levels in the control and tumour groups (Supplementary Figure S1). With regards to the risk of cancer recurrence (relapse-free survival), we observed that women with low IgM AGA levels to P₁ (lower than median fluorescence intensity, $n = 33$) were associated with a slightly higher risk ($P = 0.055$) of having an earlier recurrence than patients ($n = 25$) with higher levels of IgM anti-P₁ antibodies (hazard rate ratio 2.328, 95% CI 0.96–5.64) (Figure 1B). The disease-free survival analysis did not reveal any significant effect ($P = 0.605$).

Identification of P blood group-related GSL in cancer tissues.

GSLs were extracted from fresh collected cancer tissues, and the glycans released from the glycolipids in the form of alditols (see 'Materials and methods') were analysed in the negative ion mode using LC-ESI-MS/MS to identify P blood group-related GSLs (Figure 2). The MS² spectra contained adequate information to facilitate the structural assignment of the glycans based on the fragment ions arising from various glycosidic and cross-ring cleavages, which were described previously (Domon and Costello, 1988).

The base peak chromatograms of the glycan alditols released from the GSLs extracted from serous ovarian (Figure 2A (a)) and peritoneal (Figure 2B (a)) cancer tissue showed several components. Globotriaosylceramide (Gb3, P^k) was detected as $[M-H]^{-1-}$ m/z 505.3¹⁻ at low intensities, and the extracted ion chromatogram (EIC) showed it eluting at 15.4 min (Figures 2A b(i) and B b(i)). The MS² spectra of the precursor ion at m/z 505.3¹⁻ (Figure 2C (i)) showed prominent B- and C-type fragment ions (B₁ at m/z 161.1¹⁻, C₁ at m/z 179.2¹⁻ and C₂ at m/z 341.1¹⁻) corresponding to a (Hex)₃ or Gal-Gal-Glc sequence of P_k. Characteristic cross ring fragment ions corresponding to ^{2,4}A₂ at m/z 221.2¹⁻ and ^{0,2}A₂ at m/z 281.0¹⁻ were also present in the spectrum, thereby confirming the presence of the 4-linked terminal Gal to the (Gal-Glc) disaccharide (Karlsson *et al*, 2010). A similar study indicated the absence of ^{0,2}A₂ fragment ion in the MS² spectrum of isoglobotriaosylceramide (Gal α 1-3Gal β 1-4Glc β 1) (Karlsson *et al*, 2010) while previous reports have also noted that this characteristic cross ring cleavage was useful in distinguishing between Type 1 (Gal β 1-3GlcNAc) and Type 2 (Gal β 1-4GlcNAc) chains commonly found in mucins (Chai *et al*, 2001; Robbe *et al*, 2004; Everest-Dass *et al*, 2012).

Globotetraosylceramide (P antigen, Gb4) was detected at $[M-H]^{-1-}$ m/z 708.3¹⁻ and the EIC showed it to elute at 17.0 min (Figures 2A c(ii) and B c(ii)). Despite appearing at low intensities, the MS² spectra of the precursor ion at m/z 708.3¹⁻ (Figure 2C (ii)) was indicated by the B- and C-type fragment ions (B₁ at m/z 202.0¹⁻, B₃ at m/z 526.0¹⁻, C₁ at m/z 220.0¹⁻ and C₂ at m/z 382.1¹⁻), which corresponded to the tetrasaccharide sequence, HexNAc₁Hex₃ or GalNAc-Gal-Gal-Glc of the P antigen. Several Y-ion fragments seen from the reducing-end were also identified at m/z 343.2¹⁻ (Y₂) and m/z 505.2¹⁻ (Y₃) while the diagnostic cross ring cleavages corresponding to ^{2,4}A₃ at m/z 424.1¹⁻ and ^{0,2}A₃-H₂O at m/z 467.1¹⁻ further confirmed the presence of 4-linked Gal to the internal Gal β 1-4Glc β 1 of the Gb4 tetrasaccharide.

The pentasaccharide P₁, HexNAc₁Hex₄ or Gal-Gal-GlcNAc-Gal-Glc, was detected at $[M-H]^{-1-}$ m/z 870.3¹⁻ at 18.0 min in both tissue samples (Figures 2A d(iii) and B d(iii)). The glycosidic fragment ions occurring at m/z 305.1¹⁻ (B₂-H₂O ion) and m/z 341.0¹⁻ (C₂ ion) indicated the presence of the terminal Gal-Gal epitope while the Y-type fragment ions at m/z 546.2¹⁻ (Y₃ ion) and a prominent m/z 708.2¹⁻ (Y₄ ion) corresponded to the loss of the Gal-Gal epitope and terminal Gal, respectively, from the precursor ion, $[M-H]^{-1-}$ m/z 870.3¹⁻ (Figure 2C (iii)). Besides that, the prominent ^{2,4}x₄ fragment ion observed at m/z 648.3¹⁻ in the MS² spectra was also characteristic of the terminal Gal residue linked via a 4-linkage to the Gal-GlcNAc-Gal-Glc tetrasaccharide. The cross ring cleavage at ^{0,2}A₃-H₂O at m/z 425.1¹⁻ and the

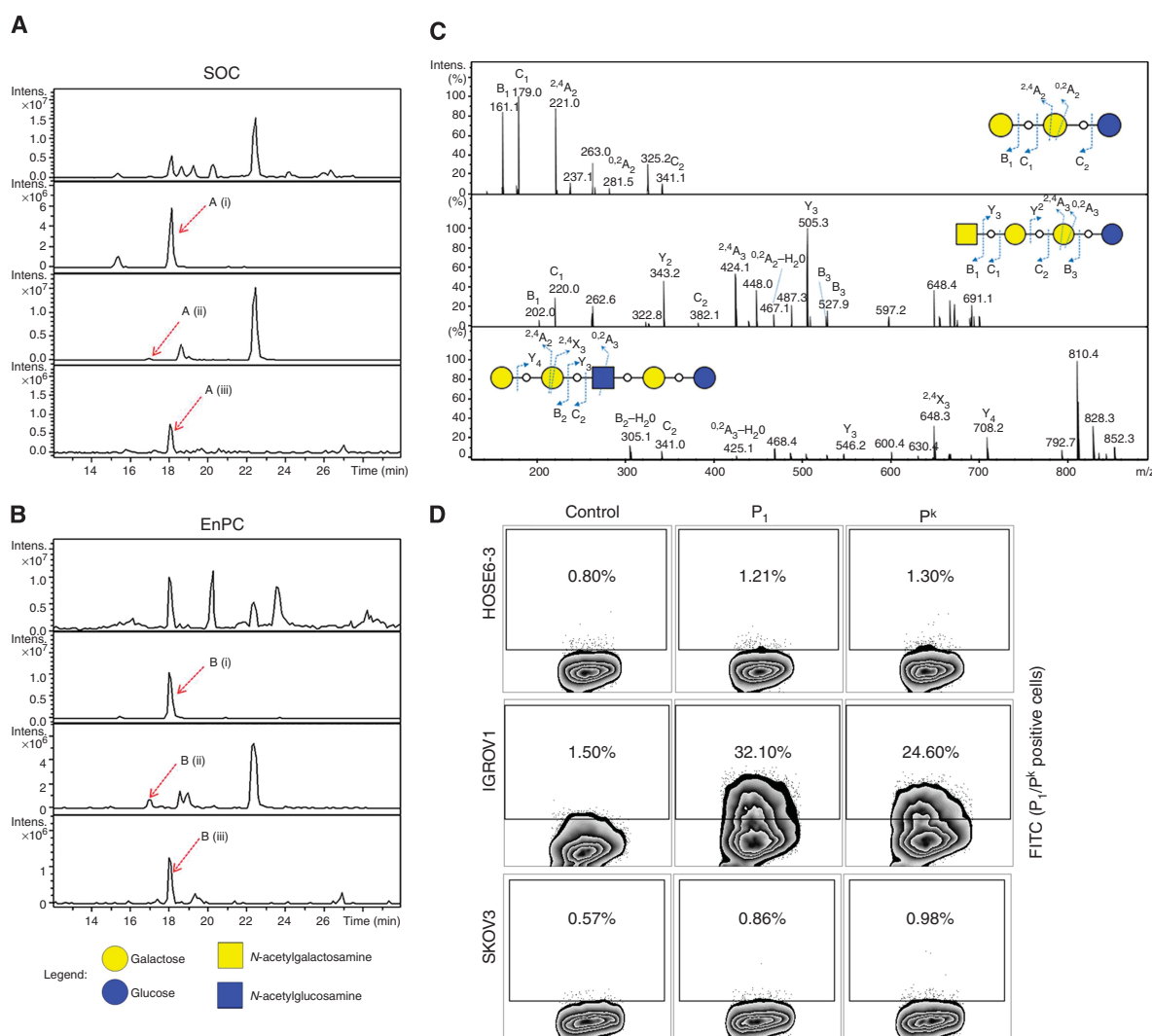


Figure 2. P₁ is expressed on cancer tissue cells. **(A, B)** Base peak chromatograms shown for serous ovarian cancer **(A a)** and endometrioid peritoneal cancer tissue **(B a)**. Selected mass peaks (red arrow) corresponding to the composition of the P^k trisaccharide (Hex₃) **(A and B b(i);** m/z 505.3¹⁻), P tetrasaccharide (Hex₄HexNAc₁) **(A and B c (ii);** m/z 708.3¹⁻), and P₁ pentasaccharide (Hex₄HexNAc₁) **(A and B d(iii);** m/z 870.3¹⁻) are represented as an extracted ion chromatogram (EIC). **(C)** MS² spectrum of P^k trisaccharide (Gal₂-1-4Gal β -1-4Glc β -1) **(i)**, P tetrasaccharide (GalNAc β -1-3Gal α -1-4Gal β -1-4Glc β -1) **(ii)** and P₁ pentasaccharide (Gal α -1-4Gal β -1-4GlcNAc β -1-3Gal β -1-4Glc β -1) **(iii)**. **(D)** Representative flow cytometry results shown as contour plots with outliers demonstrate P₁ and P^k negative cell lines HOSE6-3 and SKOV3. IGROV1 was detected positive with IgMs for both P₁ and P^k. Representative contour plots showing P₁ and P^k expression (FITC; ordinate) and forward scatter (FSC; abscissa). Given percentage corresponds to P₁/P^k-positive cells.

absence of the ^{0,2}A₄ at m/z 646.1¹⁻ further demonstrates the 4-substitution of the GlcNAc residue and the 3-substitution of the internal Gal and thus tentatively identified this compound as Gal α -1-4Gal β -1-4GlcNAc β -1-3Gal β -1-4Glc, the P₁ antigen. The three P blood group antigens were thus shown to be expressed on the GSL of serous ovarian and peritoneal cancer tissues. There was insufficient tubal cancer tissue sample to identify the presence of these antigens.

P₁ is expressed on IGROV1 cell surface. As IgMs were raised against the P₁ antigen in plasma from all types of ovarian cancer patients, and the P₁ (P^k and P) antigens were found to be expressed on the GSL extracted from the cancer tissue of these patients, we established an experimental cell culture model for the investigation into the functional role of P₁. Our panel of immortal cell lines, including human ovarian surface epithelial cells (HOSE6-3 and

HOSE17-1) and various ovarian cancer cell lines ($n=6$), were profiled for P₁ and P^k expression using flow cytometry (Figure 2D). Serous ovarian cancer cell line IGROV1 was heterogenic for P₁ expression (mean 34.1% ranging from 22.8% to 52.8%) based on human anti-P₁ IgM (clone P3NIL100) antibody. The second antibody used in this study, monoclonal murine anti-P₁ IgM (clone OSK17), confirmed P₁ expression on IGROV1 (mean 22.3% ranging from 22.0% to 33.6%). IGROV1 cells were also positive for P^k (mean 33.6% ranging from 12.0% to 54.0%). The normal control cell line HOSE6-3 was negative for both P₁ and P^k as were the remaining ovarian cancer cell lines ($n=5$).

To verify the presence of P₁ on IGROV1 cell line, we isolated GSLs from this cell line and analysed the released glycan alditols using negative ion mode LC-ESI-MS/MS. The P₁ pentasaccharide at m/z 870.3¹⁻ was shown to elute at 20.3 min, and the MS² spectra consisted of B₂ (m/z 323.1¹⁻), Y₃ (m/z 546.3¹⁻) and Y₄

(m/z 708.3¹⁻) fragment ions, which corresponded to the Gal-Gal-GlcNAc-Gal-Glc sequence. The terminal Gal α 1-4Gal linkage was also determined by the cross ring fragment ion at 2⁴x₄ fragment ion observed at m/z 648.3¹⁻ (Supplementary Figure S2).

Monoclonal anti-P₁ IgM bind IGROV1 cells. Both P₁ and P^k share terminal disaccharide structure of composition Gal α 1-4Gal β 1-4Glc(NAc). The monoclonal antibody to P₁ (clone P3NIL100) was used in a flow cytometry-based inhibition assay. Sepharose conjugated PAA-lactose, -N-acetyllactoseamine (LacNAc), -P₁ trisaccharide, -P^k was incubated with the monoclonal antibody to P₁ before immunostaining of IGROV1 cells to observe the degree of inhibition of IgM antibody binding to the expressed P₁ on IGROV1 cell surface. In this experiment, repeated three times, flow cytometry of 52.8% P₁-positive IGROV1 cells revealed complete inhibition of monoclonal anti-P₁ antibody by preincubating with 0.015 μ mol P₁ glycoabsorbents (0.04%). In contrast, less reduction (28.3% by 0.06 μ mol P^k) of bound anti-P₁ antibodies to IGROV1 cells was observed in case of P^k glycoabsorbent (Figure 3). Anti-P₁ antibodies were only slightly inhibited by preincubation with glycoabsorbents Lactose (0.06 μ mol, 46.8%) and LacNAc (0.06 μ mol, 44.8%). This clearly demonstrates that IGROV1 cells express P₁ on their cell surface, and monoclonal antibody to P₁ shows clearly higher affinity to P₁ compared with P^k. It also demonstrates specifically that galactose α 1-4 link is required for antibody binding and that lactose and LacNAc are not primarily epitopes of P₁.

Anti-glycan antibodies levels are similar in ascites and blood plasma. To determine whether anti-tumour antibodies were expressed in ascites as well as plasma of patients, we investigated the presence and distribution of AGA in matched ascites and blood plasma samples ($n=11$ patients) for IgA, IgG and IgM together

and separately using the printed glycan array. This was also done for epitope mapping of ascites-derived human anti-P₁ antibodies.

We detected a broad spectrum of AGA in both plasma and ascites (Figure 4). The fluorescence scan of the binding to the immobilised glycans on the array showed high amplitude of AGA in ascites of IgG, IgM and IgA in both 50 μ M and 10 μ M glycan-printed arrays (Supplementary Figure S3). We observed the highest median relative fluorescence signals in ascites (median, 32.75 $\times 10^4$ RFU) and in plasma (43.33 $\times 10^4$ RFU) for anti-glycan IgM antibodies. Anti-glycan IgG antibodies showed lower interaction with the glycans (ascites (8.11 $\times 10^4$ RFU), plasma (9.80 $\times 10^4$ RFU) as well as anti-glycan IgA (ascites (8.8 $\times 10^4$ RFU), plasma (10.4 $\times 10^4$ RFU)). Different levels of AGA to P₁ trisaccharide were detected in all the tested ascites and plasma samples (Figure 4). Highest binding to P₁ was observed for IgM (ascites (18.1 $\times 10^4$ RFU), plasma (14.3 $\times 10^4$ RFU)) compared with IgG and IgA.

Matched ascites and plasma AGA signals were not dependent on the volume of patient's ascites. Based on raw data sets of 50 μ M printed glycan arrays, strong correlation between matched ascites and blood plasma samples was observed (Figure 4): IgA + IgG + IgM (CCC = 0.889), IgA (CCC = 0.888), IgG (CCC = 0.961), and IgM (CCC = 0.950). Correlations were similar for 10 μ M printed glycans. This demonstrates that detected AGA levels were independent of the volume of ascites.

Naturally occurring anti-P₁ antibodies in ascites bind to cancer cells expressing P₁ on their cell surface. The results achieved from the above experiments demonstrated that (A) anti-P₁ antibodies detected by glycan-based immunoassays are reduced in plasma of cancer patients, (B) P blood group-related glycans are detectable in tissue samples of cancer patients, (C) IGROV1

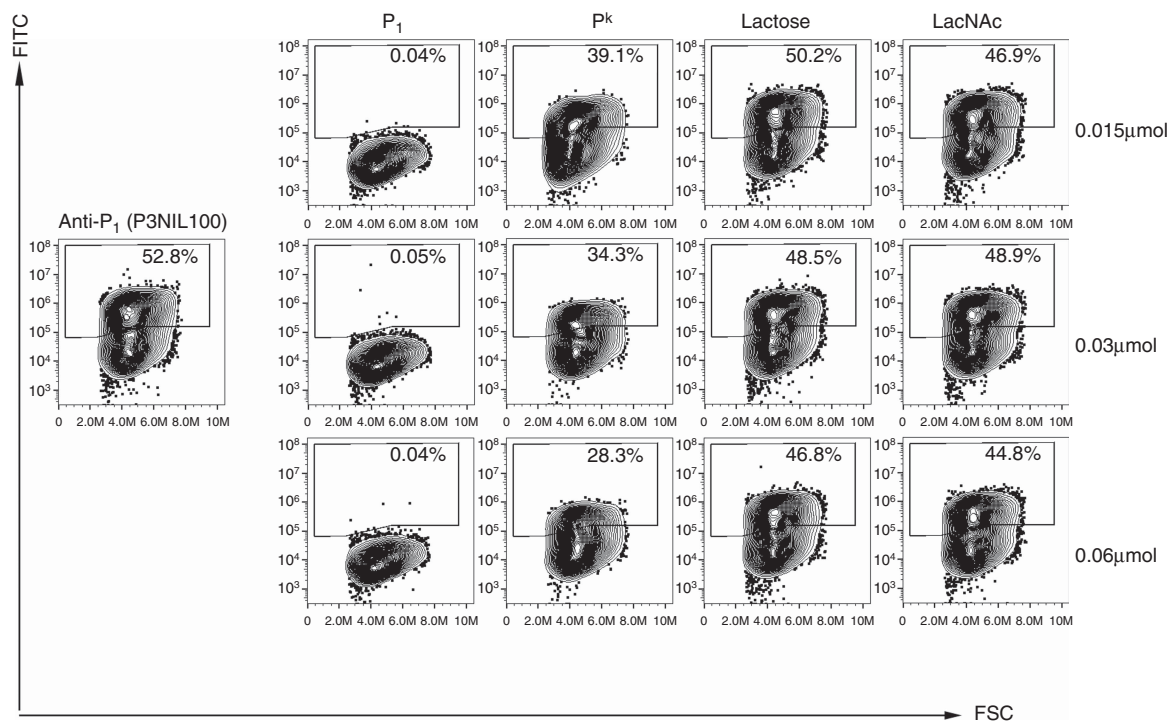


Figure 3. Monoclonal anti-P₁ IgM bind specifically to P₁. Monoclonal anti-P₁ antibody (P3NIL100, positive control) was incubated with different glycan amounts (0.015–0.06 μ mol) prior to flow cytometric measurement of binding to IGROV1 cells. Glycoconjugates Sepharose-PAA (-Lactose, -LacNAc, -P₁, -P^k) were applied to test specificity of antibodies to P₁ by testing the inhibition of binding of the anti-P₁ antibody. Representative contour plots out of three independent experiments showing P₁ expression (FITC; ordinate) and forward scatter (FSC; abscissa). Complete inhibition is shown by increasing Seph-PAA-P₁ amount with only minor inhibition of anti-P₁ antibodies using Seph-PAA-P^k.

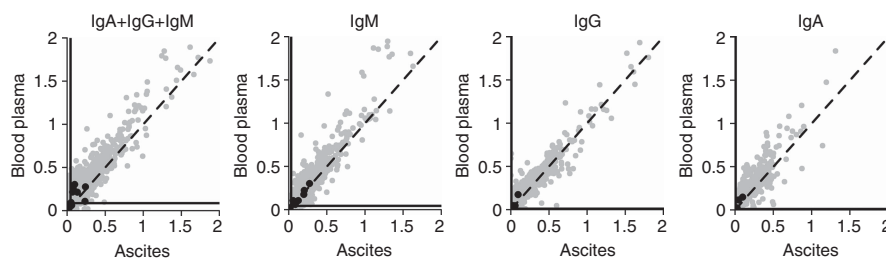


Figure 4. Ascites and blood plasma from cancer patients contain comparable levels of anti-glycan antibodies independent of immunoglobulin class and volume of ascites. Matched ascites and blood plasma samples ($n=11$) were profiled for binding of IgA + IgG + IgM ($n=22$ printed glycan array slides) and independently for IgA ($n=22$), IgG ($n=22$) and IgM ($n=22$) to printed glycan array slides. One scatterplot represents signals for 11 patients each with ascites and blood plasma. AGA to P₁ trisaccharide are highlighted in black. Median signal intensity over all signals calculated for ascites and plasma are shown by horizontal and vertical solid lines, respectively. Antibody signals (RFU $\times 10^6$) are shown on ascites and blood plasma axis. Cutoff (5%) separating background signals from real AGA binding are indicated by a solid line for ascites and plasma in the same scatterplot.

ovarian cancer cell line was found to express P₁ on its cell surface among all the tested cell lines and (D) profiled ascites contained AGA to P₁ trisaccharide. Therefore the following series of experiments were aimed to investigate whether IgM antibodies derived from ascites bind to IGROV1 and in particular to P₁ presented on its cell surface in the same way as the plasma-derived autoantibodies.

We investigated AGA to P₁ trisaccharide from an ascites sample of a late-stage serous ovarian cancer patient. The ascites fluid was first applied to the IGROV1 cell line in a 1:3 dilution, in which 24.3% of cells were stained positive with ascites-derived IgM antibodies (Figure 5A). Based on this result, we proceeded to affinity purify antibodies bound specifically to P₁ trisaccharide conjugated to sepharose beads. Affinity-purified proteins yielded a maximum amount of IgM of 24 μ g after concentration. Detection of purified anti-P₁ antibodies of class IgM revealed binding to P₁-expressing IGROV1 (15.1%) (Figure 5A). In contrast, the ovarian cancer cell line SKOV3, negative for P₁ and P^k expression, had a positive staining of only 0.29% using the purified IgM-P₁ antibodies. This demonstrates for the first time that ascites-derived AGA directed to P₁ trisaccharide also bind to naturally expressed P₁ on cell surface of ovarian cancer cells. In the following ELISA experiment on purified IgM-P₁ antibodies (Figure 5B), higher values for IgM (OD_{450 nm} = mean 3.23 \pm s.d. 0.08) compared with IgG (OD_{450 nm} = 1.08 \pm 0.02) were observed.

Next, we investigated whether purified IgM-P₁ antibodies bind to glycan structures other than P₁ (potential cross-reactivity). ELISA to a limited number of glycoconjugates revealed in the case of IgM specific binding to P₁ trisaccharide, with cross-reactivity to Gal α 1-3GalNAc and Gal α 1-4GlcNAc (Figure 5B). Suspension and printed glycan array were additionally utilised to study the cross-reactivity to broader range of glycan structures, other than P₁. In suspension array, the binding of ascites-derived anti-P₁ antibodies to P₁, P^k, Le^y and α -rhamnose was tested. No preferential binding was observed comparing P₁ and P^k (P₁ 4.11log(MFI); P^k 4.24log(MFI), IgM class). In contrast, Le^y and α -rhamnose coupled beads revealed only minor binding. In the printed glycan array (Figure 5C), we applied a threshold of 5% to the highest median fluorescence signal (19 443 RFU; Gal α 1-4Gal β 1-4Glc-sp3) to eliminate potentially unspecific binding as described previously (Huflejt *et al*, 2009). We identified that affinity-purified IgM-P₁ antibodies bound to P blood group-related structures as the top 10 glycans (Supplementary Table S2). Most of the identified low-affinity binding to glycan structures had substructures of the P₁ antigen such as Gal β 1-4Glc(NAc) with 63.0% and Gal α 1-4Gal β with 22.2% binding reactivity (Supplementary Table S2). This demonstrates that affinity-purified IgM-P₁ antibodies preferentially bound to both P^k and P₁ trisaccharide.

P₁ expression leads to elevated migration rate in ovarian cancer cells. GSLs on the cell surface are described to have several functions in cellular processes, such as pathogen recognition, angiogenesis, cell motility and cell migration (Panjwani *et al*, 1995; Todeschini *et al*, 2008; Hakomori, 2010). Migration is a common feature in cancer cells, and therefore we investigated whether or not the presence of P₁ affects cell migration by using a flow cytometry-based cell sorting of IGROV1 cells to separate P₁-high- from P₁-low-expressing subpopulations. After further sub-cultivation, P₁ expression in P₁-low IGROV1 cells was determined by murine monoclonal anti-P₁ IgM (OSK17; 18%) or human anti-P₁ IgM (P3NIL100; 33.3%). In contrast, P₁-high-expressing IGROV1 cells were 50.0% and 66.1% positive for P₁, respectively, for these antibodies (Figure 6A).

Utilising these P₁-sorted cell lines, we hypothesised that the presence of P₁ affects cell migration. Significantly higher migration was detected in P₁-high-expressing when compared with P₁-low-expressing IGROV1 cells after an 18 h incubation period ($P=0.0006$) (Figure 6B), as shown by colorimetric cell migration assay. In addition to end-point migration assay, real-time and label-free measurement of P₁-sorted IGROV1 cells was performed using the xCELLigence system. A number of 100 000 cells was seeded into each well of the upper chamber, and migration through the microporous membrane were recorded as cell index. IGROV1 cells with higher P₁ were significantly faster after 20 h ($P=0.035$) than low P₁ cells. Longer incubation periods resulted in no difference between both subpopulations (30 h; $P=0.1337$, 40 h; $P=1$; Figure 6C). To avoid the influence of potentially elevated proliferation effects, 5 μ M cytosine arabinoside (araC) was added to the cell culture (Supplementary Figure S4). In concordance with results on the colorimetric cell migration assay and observations on initial xCELLigence experiment, cells with elevated P₁ displayed high basal migratory activity as indicated by the increases in cell index values, reflecting the number of migrating cells. In contrast, P₁-low-expressing cells failed to migrate under experimental conditions. With regard to migratory kinetics, P₁-high-expressing cells migrated rapidly and demonstrated elevated (4.7-fold) cell index of 0.3434 \pm 0.054 (mean \pm s.d.) as compared with P₁-low-expressing cells (0.0726 \pm 0.029; $P=0.004$, CI 0.1–0.45). This difference remained constant throughout the 40 h time course experiment (20 h–3.6-fold ($P<0.001$, CI 0.32–0.66); 30 h–3.6-fold ($P<0.001$, CI 0.40–0.75); 40 h–4.6-fold ($P<0.001$, CI 0.49–0.84); Figure 6C). These findings demonstrate that ovarian cancer cells expressing P₁ on their cell surface migrate faster compared with low-P₁-expressing cells originated from the same parental cell line.

In order to confirm that P₁ is involved in cell migration, we performed the colorimetric cell migration assay with anti-P₁ IgM-pretreated IGROV1 cells. The results (Figure 6D) showed that the

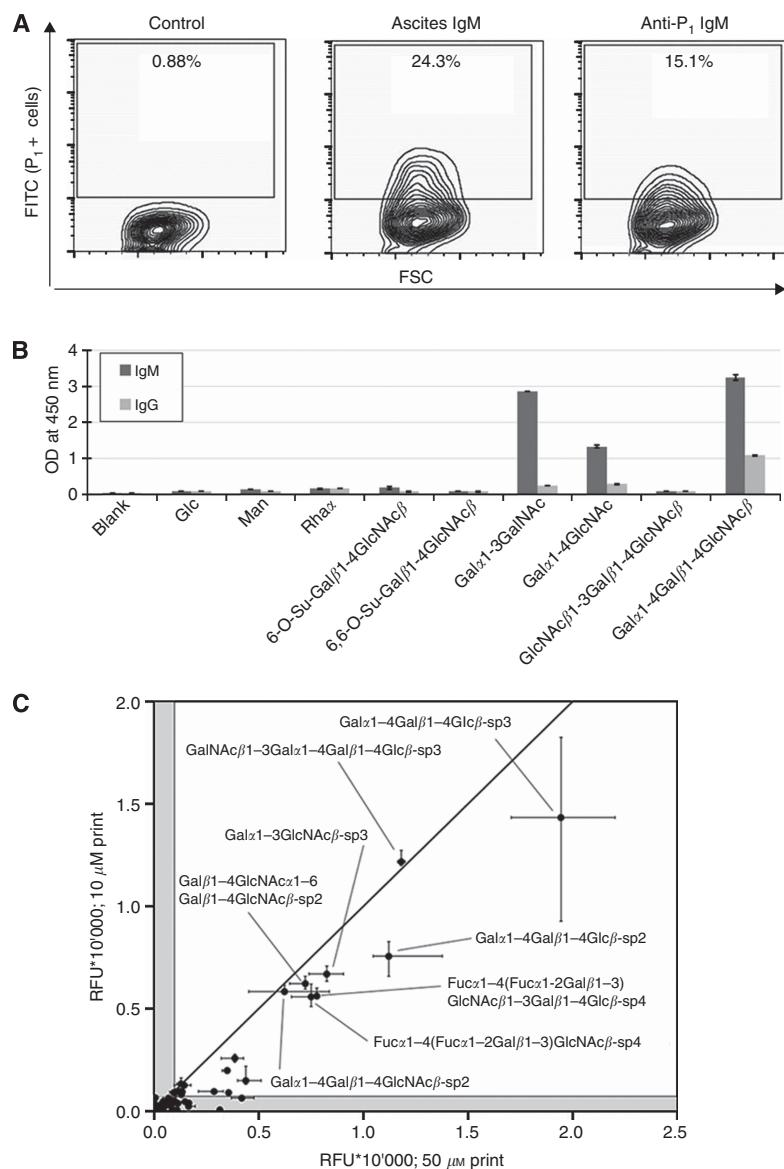


Figure 5. Human ascites-derived affinity-purified anti-P₁ antibodies bind to IGROV1 cells. **(A)** Flow cytometry-based contour plots demonstrate the presence of IgM antibodies in ascites (1 : 3 diluted in PBS) bound to IGROV1 cells (ascites IgM, 24.3%) compared with unstained sample (control). Affinity-purified anti-P₁ IgM (1 : 20) bound to IGROV1 cells (15.1% of P₁-positive cells). **(B)** Representative ELISA demonstrating the cross-reactivity of affinity-purified anti-P₁ antibodies of class IgM (dark grey) and IgG (light grey) to investigated glycans linked to PAA. **(C)** Printed glycan array data (scatterplot for 50 μM vs 10 μM saccharide prints) showing cross-reactivity to glycans sharing related carbohydrate structures. Grey area indicates unspecific binding of AGA as determined by 5% threshold. Inter-quartile range is shown for each glycan horizontally and vertically for 50 μM and 10 μM, respectively.

percentage of migrated cells was significantly lower (reduction by 64%; $P < 0.001$) in cultures preincubated with the anti-P₁ IgM antibody. Pretreatment with the respective IgM isotype control did not affect the migration of IGROV1 cells.

DISCUSSION

Unlike P^k, which has been extensively studied in the areas of verotoxin-mediated cytotoxicity, human immunodeficiency virus infection, immunology and epithelial carcinogenesis, there is, to our knowledge, no published study of P₁ and its potential

presence, immunogenicity and its functional role in oncogenesis. Using glycan-based immunoassays, we have previously demonstrated that naturally occurring AGA significantly distinguishes healthy controls from ovarian cancer patients (Pochechueva *et al*, 2011b; Jacob *et al*, 2012). The present study demonstrates that: (A) an unknown subpopulation of cancer patients show reduced levels of anti-P₁ IgM antibodies in an extended and independent cohort from another continent (Australian Validation Cohort), (B) P^k, P and P₁ carbohydrate antigens are detectable in cancer tissue as well as on the cell surface of cultured ovarian cancer cells, (C) ascites contains similar anti-glycan IgM-P₁ antibody levels compared with blood plasma independent of its volume at the primary diagnosis, (D) naturally occurring AGA of IgM class derived from ascites of a

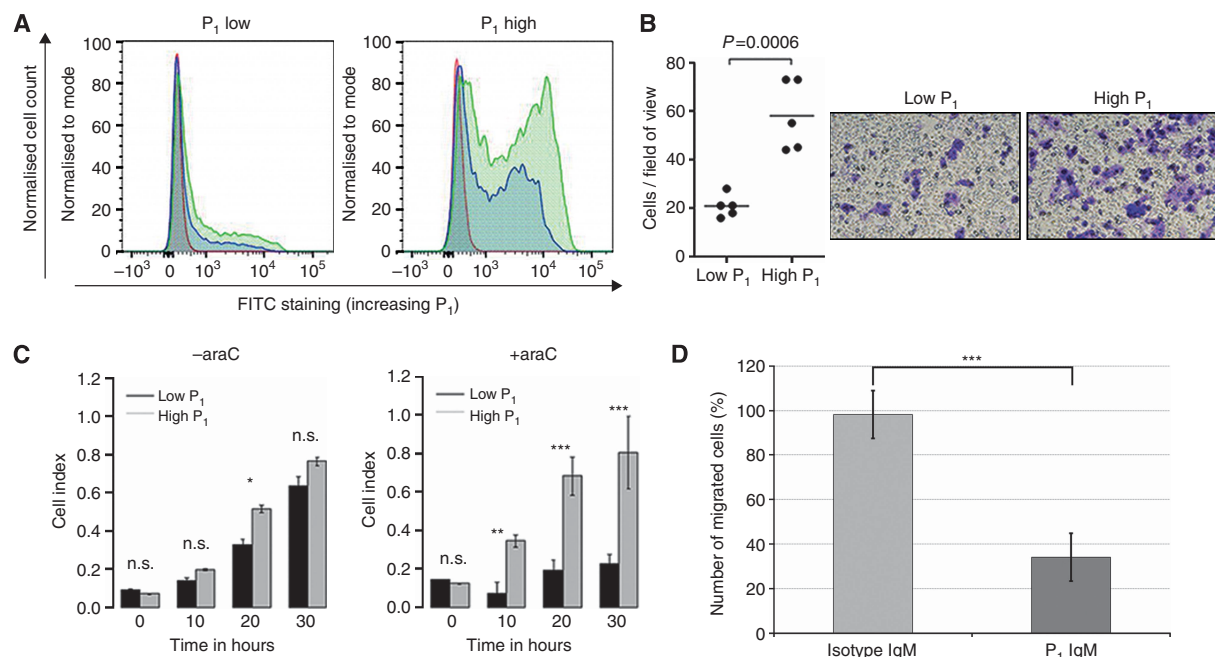


Figure 6. Elevated P₁ expression results in increased migration rate. **(A)** FACS-sorted subpopulations of P₁-low- and -high-expressing IGROV1 cells. Representative histograms showing P₁ expression (abscissa) on cell-sorted IGROV1 cells to normalised cell count (ordinate). P₁ distribution for unstained controls (red), P₁-positivity P3NIL100 antibody (green) and OSK17 antibody (blue). **(B)** Colorimetric cell migration assay showing enhanced migratory ability of IGROV1 cells expressing high compared with low levels of P₁. Stained cells counted in five fields and averaged. Representative image of cell sorted subpopulations of migrated cells (stained violet) after 18 h. **(C)** RTCA assay for P₁-sorted IGROV1 cells showing the migrated cells (cell index) in bar graphs at the time points 0 h, 10 h, 20 h and 30 h. Left bar graph shows RTCA experiment without araC, right bar graph with araC as proliferation inhibitor. Representative figure out of two independent experiments. **(D)** Bar chart showing the inhibition of cell migration of human IGROV1 cells incubated with anti-P₁ IgM compared with corresponding incubation with IgM isotype control. Number of migrated cells was normalised to control. Not significant (NS); *P < 0.05, **P < 0.01, ***P < 0.001.

ovarian cancer patient bind to naturally expressed and chemically synthesised P₁ on glycan arrays, and (E) the presence of P₁ on ovarian cancer cultured IGROV1 cells leads to enhanced migration.

Our results demonstrate that the significantly lower anti-P₁ antibody levels observed in cancer patients were primarily due to the reduction of IgM but not IgG antibodies. This is in full concordance with the literature on the IgM type anti-Thomsen Friedenreich antibodies (Desai *et al*, 1995) and anti-Lewis C antibodies in breast cancer (Bovin, 2013). A very recently published work demonstrated significantly reduced human IgM antibodies to another GSL (*N*-glycolylneuraminy)-lactosylceramide (NeuGcGM3) in non-small cell lung cancer patients (Rodriguez-Zhurbenko *et al*, 2013). Therefore we can assume that IgM class of naturally occurring AGA was able to discriminate between cancer and healthy controls. Natural IgM antibodies belong to the innate immune system and are primarily produced by B1 or CD5+ cells (Boes, 2000; Martin and Kearney, 2001; Viau and Zouali, 2005). As part of the natural immunity, the binding of IgM to conserved carbohydrate structures acts as a first barrier to all invasive particles ('external') and alterations on proteins and lipids within an organism ('internal') (Vollmers and Brandlein, 2007). To date, several human monoclonal antibodies directed to tumour-associated carbohydrate antigens have been isolated. For instance, the monoclonal IgM antibody, SAM-6, specific for cancerous tissue was first derived from a gastric cancer patient (Pohle *et al*, 2004). Later, it was found that the receptor for SAM-6 is a tumour-specific O-linked carbohydrate epitope on GRP78, a central regulator of endoplasmic reticulum in protein folding (Li and Lee, 2006). PAM-1, another monoclonal IgM antibody, binds to a tumour-specific N-linked carbohydrate epitope, a posttranslational modification on cysteine-rich fibroblast growth

factor receptor, CFR-1. This antibody also inhibited tumour growth *in vitro* and in animal model systems by inducing apoptosis (Brandlein *et al*, 2003, 2004a, b). Consistent with the findings of Vollmers and colleagues regarding SAM-6 and PAM-1, our observation based on hierarchical clustering indicates that AGA preferentially bind to substructures of the glycan epitope (Jacob *et al*, 2012). Besides that the decrease of AGA mainly of the IgM class in gynaecological cancer patients (Jacob *et al*, 2012) also points to an involvement of naturally occurring IgM autoantibodies, which recognise GSL structures. We further propose that Gal α 1-4Gal β 1-4Glc(NAc) (present in P, P^K and P₁ antigens) are a result of malignant transformation and could serve as an 'internal' epitope on GSLs that is recognised by naturally circulating anti-glycan IgM antibodies.

The observation of lower levels of anti-P₁ IgM compared with anti-P₁ IgG in cancer patients is very intriguing, and although exploring the underlying mechanisms was beyond the scope of the study, we speculate on a number of possibilities. The elevated presence of corresponding antigens on cancer cells, in our case P₁ GSL, may be bound by circulating anti-P₁ IgM and therefore no longer be freely floating in the plasma and ascites. Another potential mechanism may be tumour-induced immune suppression. It is known that ovarian cancers employ a range of strategies, such as secretion of immunosuppressive cytokines, to facilitate their escape from immune destruction (Lavoue *et al*, 2013). It is possible that this may lead to reduced antibody production against cancer-associated antigens, for example, P₁, conferring a survival advantage to cancer cells. The antibody repertoire in cancer patients would therefore be different. Another possible mechanism is the occupation of anti-P₁ IgMs by cancer cells (including circulating tumour cells) by virtue of their surface expression of

P₁, leading to a reduction in the amount of unbound antibody in plasma and/or ascites. The formation of immune complexes consisting of P₁ antigen shed from cancer cells, and anti-P₁ IgMs, may further contribute to this reduction. A prominent example in the literature for the formation of circulating immune complexes consisting of Lewis x and antibodies has been shown in *Helicobacter pylori*-infected human (Chmiela *et al*, 1998). With regards to no change being observed in the anti-P₁ IgG levels, we expected differences preferentially in the case of IgM rather than of IgG as glycan-based antigens are T-cell-independent antigens and are recognised by the innate immune system.

Our mass spectrometry results demonstrated that these P₁, P^k and P antigens are expressed on ovarian and peritoneal cancer tissues. The functional role of the GSL that carry these structures in carcinogenesis is poorly understood, especially in the case of P₁ and P. It was recently described that a monoclonal anti-P^k antibody (E3E2) inhibited angiogenesis and tumour development (Desselle *et al*, 2012). Enhanced expression of P^k has also been shown to cause doxorubicin resistance in breast cancer cells (Gupta *et al*, 2012). Cisplatin-resistant pleural mesothelioma cells were shown to be sensitised to cisplatin by the addition of sub-toxic concentrations of Verotoxin 1 (Johansson *et al*, 2010). In addition, we also demonstrate that P₁ and P^k antigens are also present on the surface of the IGROV1 serous ovarian cancer cells. IGROV1 is, therefore, to the best of our knowledge, the only immortal cell line from several investigated that expresses P₁. Using monoclonal antibodies against P₁, only minor cross-reactivity to other glycan structures was observed in glycan-based immunoassays (not shown). Furthermore, based on the flow cytometry inhibition assay using IGROV1 cells as an investigative model, the specificity of monoclonal antibodies to P₁ as shown by the full saturation of anti-P₁ antibodies by inhibition with 0.06 μmol glycan on sepharose beads indicates that IGROV1 expresses P₁ on the cell surface.

Serous pelvic masses commonly present with malignant ascites, a plasma-protein-rich intraperitoneal exudate of up to several litres. Several pathophysiological mechanisms are necessary for malignant ascites occur: (a) decreased lymphatic ascites absorption, (b) increased capillary permeability, (c) increased overall capillary membrane-surface area available for filtration, and consequently (d) an increased intraperitoneal oncotic pressure due to intraperitoneal protein concentration (Tamsma *et al*, 2001). Using the printed glycan array, we observed an unexpectedly rich spectrum of AGA with similar amounts in plasma and ascites. These findings suggested that there is an equilibrium between both body fluids. Early lymphatic obstruction is one of the first manifestations of an inflammatory reaction (Feldman, 1975). As IgM has an important role in inflammation with multivalent antigen binding due to its pentameric structure and as the first immunoglobulin class produced in a primary response to an antigen, lymphatic obstruction may result in a rapid increase in IgM secreting plasma cells. Natural circulating AGA have also been described in various inflammatory conditions, including diabetes mellitus type 1 (Gillard *et al*, 1989), chronic inflammatory bowel and Crohn's disease (Malickova *et al*, 2006) and in patients with cancer (Young *et al*, 1979; Springer, 1984; Springer *et al*, 1988; Desai *et al*, 1995).

We also investigated the expression of A4GALT P₁- and P^k-profiled cell lines. As seen in our study, A4GALT is overexpressed in the P₁- and P^k-positive ovarian cancer cell line IGROV1 (Jacob *et al*, 2011b), suggesting that A4GALT is not only involved in P^k but also in P₁ synthesis in ovarian cancer cells. We propose that A4GALT is involved in the progression of various ovarian and peritoneal cancers; however, the molecular link between A4GALT mRNA levels and P₁ expression remains unknown. This is consistent with suspension array results in which no tested clinical parameters were shown to correlate with lower AGA levels to P₁ trisaccharide. A recently identified single nucleotide polymorphism

(CT conversion) encoding an additional exon in the genomic region of A4GALT (Thuresson *et al*, 2011) could probably explain the presence of P₁ in cancer cells. However, it is unclear whether the overexpression of A4GALT is causative for the synthesis of P₁ or P^k in profiled cancer cell lines. The invasive phenotype of colon cells lacking P^k could be induced and inhibited by the transfection of Gb3 synthase (A4GALT) or RNA interference, respectively (Kovbasnjuk *et al*, 2005). Another immunohistochemistry-based study showed that P^k expression was elevated in colorectal cancers and their metastases; however, A4GALT mRNA levels, protein expression or galactosyltransferase activity were not investigated (Falguieres *et al*, 2008). The potential role of A4GALT in cancer initiation or progression needs to be elucidated in future studies with respect to all P blood group-related glycans.

For the first time, we also observed migration rate in P₁-high-expressing cells, and this was even more obvious when araC, a proliferation inhibitor, was added to the cultures (Roy *et al*, 2006). The addition of araC confirmed that the observed difference in migration was indeed due to altered cell migration and not cell proliferation. Our results suggest an involvement of P₁ in cell migration, but the underlying molecular mechanisms are unknown.

Finally, this study provides further evidence that P blood group-related antigens have a role in carcinogenesis and those naturally occurring anti-glycan IgM antibodies against them may have the potential to discriminate ovarian cancer patients from healthy individuals. If these surface antigens prove to be indeed tumour-specific, they may become candidate molecular targets for potential imaging tools for confocal fluorescence endoscopy and positron emission tomography and as tools in targeted immunotherapy (Janssen *et al*, 2006; Viel *et al*, 2008).

ACKNOWLEDGEMENTS

This work was supported by Cancer Institute NSW grant (09/CRF/2-02) to VHS, the William Maxwell Trust, the Mary Elisabeth Courier Scholarship (RANZCOG) to VHS, the Swiss National Foundation grants PBZHP3-133289 (to FJ) and 320030-120543 (to VHS), the OncoSuisse grant (OCS-02115-08-2007) to VHS and the Novartis Foundation (13B093) to FJ. We would like to acknowledge the following people for their various contributions to this publication: Jim Scurry, Andreas Schoetzau, Sheri Nixdorf, Monica Nunez Lopez, Renato Mueller and Daniel Fink.

REFERENCES

- Boes M (2000) Role of natural and immune IgM antibodies in immune responses. *Mol Immunol* **37**(18): 1141–1149.
- Bovin N, Obukhova P, Shilova N, Rapoport E, Popova I, Navakouski M, Unverzagt C, Vuskovic M, Huflejt M (2012) Repertoire of human natural anti-glycan immunoglobulins. Do we have auto-antibodies? *Biochim Biophys Acta* **1820**(9): 1373–1382.
- Bovin NV (2013) Natural antibodies to glycans. *Biochemistry (Moscow)* **78**(7): 786–797.
- Brandlein S, Beyer I, Eck M, Bernhardt W, Hensel F, Muller-Hermelink HK, Vollmers HP (2003) Cysteine-rich fibroblast growth factor receptor 1, a new marker for precancerous epithelial lesions defined by the human monoclonal antibody PAM-1. *Cancer Res* **63**(9): 2052–2061.
- Brandlein S, Eck M, Strobel P, Wozniak E, Muller-Hermelink HK, Hensel F, Vollmers HP (2004a) PAM-1, a natural human IgM antibody as new tool for detection of breast and prostate precursors. *Hum Antibodies* **13**(4): 97–104.
- Brandlein S, Pohle T, Vollmers C, Wozniak E, Ruoff N, Muller-Hermelink HK, Vollmers HP (2004b) CFR-1 receptor as target for tumor-specific apoptosis induced by the natural human monoclonal antibody PAM-1. *Oncol Rep* **11**(4): 777–784.

- Chai W, Piskarev V, Lawson AM (2001) Negative-ion electrospray mass spectrometry of neutral underivatized oligosaccharides. *Anal Chem* **73**(3): 651–657.
- Chang WW, Lee CH, Lee P, Lin J, Hsu CW, Hung JT, Lin JJ, Yu JC, Shao LE, Yu J, Wong CH, Yu AL (2008) Expression of Globo H and SSEA3 in breast cancer stem cells and the involvement of fucosyl transferases 1 and 2 in Globo H synthesis. *Proc Natl Acad Sci USA* **105**(33): 11667–11672.
- Chmiela M, Wadstrom T, Folkesson H, Planeta Malecka I, Czkwianianc E, Rechcinski T, Rudnicka W (1998) Anti-Lewis X antibody and Lewis X-anti-Lewis X immune complexes in *Helicobacter pylori* infection. *Immunol Lett* **61**(2-3): 119–125.
- Desai PR, Ujjainwala LH, Carlstedt SC, Springer GF (1995) Anti-Thomsen-Friedenreich (T) antibody-based ELISA and its application to human breast carcinoma detection. *J Immunol Methods* **188**(2): 175–185.
- Desselle A, Chaumette T, Gaugler MH, Cochonneau D, Fleurence J, Dubois N, Hulín P, Aubry J, Birkle S, Paris F (2012) Anti-gb3 monoclonal antibody inhibits angiogenesis and tumor development. *PLoS One* **7**(11): e45423.
- Domon B, Costello CE (1988) Structure elucidation of glycosphingolipids and gangliosides using high-performance tandem mass spectrometry. *Biochemistry* **27**(5): 1534–1543.
- Everest-Dass AV, Jin D, Thaysen-Andersen M, Nevalainen H, Kolarich D, Packer NH (2012) Comparative structural analysis of the glycosylation of salivary and buccal cell proteins: innate protection against infection by *Candida albicans*. *Glycobiology* **22**(11): 1465–1479.
- Falguieres T, Maak M, von Weyhern C, Sarr M, Sastre X, Poupon MF, Robine S, Johannes L, Janssen KP (2008) Human colorectal tumors and metastases express Gb3 and can be targeted by an intestinal pathogen-based delivery tool. *Mol Cancer Ther* **7**(8): 2498–2508.
- Feldman GB (1975) Lymphatic obstruction in carcinomatous ascites. *Cancer Res* **35**(2): 325–332.
- Gilewski T, Ragupathi G, Bhuta S, Williams LJ, Musselli C, Zhang XF, Bornmann WG, Spassova M, Bencsath KP, Panageas KS, Chin J, Hudis CA, Norton L, Houghton AN, Livingston PO, Danishefsky SJ (2001) Immunization of metastatic breast cancer patients with a fully synthetic globo H conjugate: a phase I trial. *Proc Natl Acad Sci USA* **98**(6): 3270–3275.
- Gillard BK, Thomas JW, Nell LJ, Marcus DM (1989) Antibodies against ganglioside GT3 in the sera of patients with type I diabetes mellitus. *J Immunol* **142**(11): 3826–3832.
- Gupta V, Bhinge KN, Hosain SB, Xiong K, Gu X, Shi R, Ho MY, Khoo KH, Li SC, Li YT, Ambudkar SV, Jazwinski SM, Liu YY (2012) Ceramide glycosylation by glucosylceramide synthase selectively maintains the properties of breast cancer stem cells. *J Biol Chem* **287**(44): 37195–37205.
- Hakomori S (1998) Cancer-associated glycosphingolipid antigens: their structure, organization, and function. *Acta Anat* **161**(1-4): 79–90.
- Hakomori S, Wang SM, Young Jr. WW (1977) Isoantigenic expression of Forssman glycolipid in human gastric and colonic mucosa: its possible identity with "A-like antigen" in human cancer. *Proc Natl Acad Sci USA* **74**(7): 3023–3027.
- Hakomori SI (2010) Glycosynaptic microdomains controlling tumor cell phenotype through alteration of cell growth, adhesion, and motility. *FEBS Lett* **584**(9): 1901–1906.
- Huflejt ME, Vuskovic M, Vasilij D, Xu H, Obukhova P, Shilova N, Tuzikov A, Galanina O, Arun B, Lu K, Bovin N (2009) Anti-carbohydrate antibodies of normal sera: findings, surprises and challenges. *Mol Immunol* **46**(15): 3037–3049.
- Jacob F, Goldstein DR, Bovin NV, Pochechueva T, Spengler M, Caduff R, Fink D, Vuskovic MI, Huflejt ME, Heinzelmänn-Schwarz V (2012) Serum antiglycan antibody detection of nonmucinous ovarian cancers by using a printed glycan array. *Int J Cancer* **130**(1): 138–146.
- Jacob F, Meier M, Caduff R, Goldstein D, Pochechueva T, Hacker N, Fink D, Heinzelmänn-Schwarz V (2011a) No benefit from combining HE4 and CA125 as ovarian tumor markers in a clinical setting. *Gynecol Oncol* **121**(3): 487–491.
- Jacob F, Tse BWC, Guertler R, Nixdorf S, Bovin NV, Hacker N, Heinzelmänn-Schwarz V (2011b) P1 antigen is present on the serous ovarian cancer cell line, IGROV1, correlating with A4GALT overexpression and altered cell behaviour. *Glycobiology* **21**(11): 1454–1531.
- Janssen KP, Vignjevic D, Boisgard R, Falguieres T, Bousquet G, Decaudin D, Dolle F, Louvard D, Tavitian B, Robine S, Johannes L (2006) In vivo tumor targeting using a novel intestinal pathogen-based delivery approach. *Cancer Res* **66**(14): 7230–7236.
- Jarvis WD, Grant S, Kolesnick RN (1996) Ceramide and the induction of apoptosis. *Clin Cancer Res* **2**(1): 1–6.
- Johansson B, Andersson C, Moharer J, Johansson A, Behnam-Motlagh P (2010) Cisplatin-induced expression of Gb3 enables verotoxin-1 treatment of cisplatin resistance in malignant pleural mesothelioma cells. *Br J Cancer* **102**(2): 383–391.
- Karlsson H, Halim A, Teneberg S (2010) Differentiation of glycosphingolipid-derived glycan structural isomers by liquid chromatography/mass spectrometry. *Glycobiology* **20**(9): 1103–1116.
- Kasahara K, Sanai Y (1999) Possible roles of glycosphingolipids in lipid rafts. *Biophys Chem* **82**(2-3): 121–127.
- Ke N, Wang X, Xu X, Abassi YA (2011) The xCELLigence system for real-time and label-free monitoring of cell viability. *Methods Mol Biol* **740**: 33–43.
- Kovbasnjuk O, Mourtazina R, Baibakov B, Wang T, Elowsky C, Choti MA, Kane A, Donowitz M (2005) The glycosphingolipid globotriaosylceramide in the metastatic transformation of colon cancer. *Proc Natl Acad Sci USA* **102**(52): 19087–19092.
- Lavoue V, Thedrez A, Leveque J, Foucher F, Henno S, Jauffret V, Belaud-Rotureau MA, Catros V, Cabillic F (2013) Immunity of human epithelial ovarian carcinoma: the paradigm of immune suppression in cancer. *J Transl Med* **11**: 147.
- Li J, Lee AS (2006) Stress induction of GRP78/BiP and its role in cancer. *Curr Mol Med* **6**(1): 45–54.
- Malickova K, Lukas M, Donoval R, Sandova P, Janatkova I (2006) Novel anti-carbohydrate autoantibodies in patients with inflammatory bowel disease: are they useful for clinical practice? *Clin Lab* **52**(11-12): 631–638.
- Martin F, Kearney JF (2001) B1 cells: similarities and differences with other B cell subsets. *Curr Opin Immunol* **13**(2): 195–201.
- Oyleran O, McShane LM, Dodd L, Gildersleeve JC (2009) Profiling human serum antibodies with a carbohydrate antigen microarray. *J Proteome Res* **8**(9): 4301–4310.
- Ozols RF (2006) Challenges for chemotherapy in ovarian cancer. *Ann Oncol* **17**(Suppl 5): v181–v187.
- Panjwani N, Zhao Z, Ahmad S, Yang Z, Jungalwala F, Baum J (1995) Neolactoglycosphingolipids, potential mediators of corneal epithelial cell migration. *J Biol Chem* **270**(23): 14015–14023.
- Pochechueva T, Chinarev A, Spengler M, Korchagina E, Heinzelmänn-Schwarz V, Bovin N, Rieben R (2011a) Multiplex suspension array for human anti-carbohydrate antibody profiling. *Analyst* **136**(3): 560–569.
- Pochechueva T, Jacob F, Fedier A, Heinzelmänn-Schwarz V (2012) Tumor-associated glycans and their role in gynecological cancers: accelerating translational research by novel-high throughput approaches. *Metabolites* **2**(4): 913–939.
- Pochechueva T, Jacob F, Goldstein DR, Huflejt ME, Chinarev A, Caduff R, Fink D, Hacker N, Bovin NV, Heinzelmänn-Schwarz V (2011b) Comparison of printed glycan array, suspension array and ELISA in the detection of human anti-glycan antibodies. *Glycoconj J* **28**(8-9): 507–517.
- Pohle T, Brandlein S, Ruoff N, Müller-Hermelink HK, Vollmers HP (2004) Lipoptosis: tumor-specific cell death by antibody-induced intracellular lipid accumulation. *Cancer Res* **64**(11): 3900–3906.
- Robbe C, Capon C, Coddeville B, Michalski JC (2004) Diagnostic ions for the rapid analysis by nano-electrospray ionization quadrupole time-of-flight mass spectrometry of O-glycans from human mucins. *Rapid Commun Mass Spectrom* **18**(4): 412–420.
- Rodriguez-Zhurbenko N, Martinez D, Blanco R, Rondon T, Grinan T, Hernandez AM (2013) Human antibodies reactive to NeuGcGM3 ganglioside have cytotoxic antitumor properties. *Eur J Immunol* **43**(3): 826–837.
- Roy AM, Tiwari KN, Parker WB, Secrist 3rd JA, Li R, Qu Z (2006) Antiangiogenic activity of 4'-thio-beta-D-arabinofuranosylcytosine. *Mol Cancer Ther* **5**(9): 2218–2224.
- Solly K, Wang X, Xu X, Strulovici B, Zheng W (2004) Application of real-time cell electronic sensing (RT-CES) technology to cell-based assays. *Assay Drug Dev Technol* **2**(4): 363–372.
- Springer GF (1984) T and Tn, general carcinoma autoantigens. *Science* **224**(4654): 1198–1206.
- Springer GF, Chandrasekaran EV, Desai PR, Tegtmeyer H (1988) Blood group Tn-active macromolecules from human carcinomas and erythrocytes: characterization of and specific reactivity with mono- and poly-clonal

- anti-Tn antibodies induced by various immunogens. *Carbohydr Res* **178**: 271.
- Tamsma JT, Keizer HJ, Meinders AE (2001) Pathogenesis of malignant ascites: Starling's law of capillary hemodynamics revisited. *Ann Oncol* **12**(10): 1353–1357.
- Taniguchi N, Yokosawa N, Narita M, Mitsuyama T, Makita A (1981) Expression of Forssman antigen synthesis and degradation in human lung cancer. *J Natl Cancer Inst* **67**(3): 577–583.
- Thureson B, Westman JS, Olsson ML (2011) Identification of a novel A4GALT exon reveals the genetic basis of the P1/P2 histo-blood groups. *Blood* **117**(2): 678–687.
- Todeschini AR, Dos Santos JN, Handa K, Hakomori SI (2008) Ganglioside GM2/GM3 complex affixed on silica nanospheres strongly inhibits cell motility through CD82/cMet-mediated pathway. *Proc Natl Acad Sci USA* **105**(6): 1925–1930.
- Viau M, Zouali M (2005) B-lymphocytes, innate immunity, and autoimmunity. *Clin Immunol* **114**(1): 17–26.
- Viel T, Dransart E, Nemati F, Henry E, Theze B, Decaudin D, Lewandowski D, Boisgard R, Johannes L, Tavitian B (2008) In vivo tumor targeting by the B-subunit of shiga toxin. *Mol Imaging* **7**(6): 239–247.
- Vollmers HP, Brandlein S (2007) Natural antibodies and cancer. *J Autoimmun* **29**(4): 295–302.
- Wang CC, Huang YL, Ren CT, Lin CW, Hung JT, Yu JC, Yu AL, Wu CY, Wong CH (2008) Glycan microarray of Globo H and related structures for quantitative analysis of breast cancer. *Proc Natl Acad Sci USA* **105**(33): 11661–11666.
- Wenk J, Andrews PW, Casper J, Hata J, Pera MF, von Keitz A, Damjanov I, Fenderson BA (1994) Glycolipids of germ cell tumors: extended globo-series glycolipids are a hallmark of human embryonal carcinoma cells. *Int J Cancer* **58**(1): 108–115.
- Young Jr. WW, Hakomori SI, Levine P (1979) Characterization of anti-Forssman (anti-Fs) antibodies in human sera: their specificity and possible changes in patients with cancer. *J Immunol* **123**(1): 92–96.



This work is licensed under the Creative Commons Attribution-NonCommercial-Share Alike 3.0 Unported License. To view a copy of this license, visit <http://creativecommons.org/licenses/by-nc-sa/3.0/>

Supplementary Information accompanies this paper on British Journal of Cancer website (<http://www.nature.com/bjc>)

4.2 Glucosylceramide synthase inhibitors differentially affect expression of glycosphingolipids

Shahidul Alam, André Fedier, Reto S Kohler, and Francis Jacob

Glycobiology 2015

My contributions to this paper:

For this study, I designed the experimental strategy in supervision by Francis Jacob. I performed literature research and performed all experiments with the help of André Fedier and Reto Kohler. Data were analyzed by myself and prepared for presentation in the manuscript. I have written the manuscript with the help of all co-authors.

Letter to the GlycoForum

Glucosylceramide synthase inhibitors differentially affect expression of glycosphingolipids

Shahidul Alam, André Fedier, Reto S Kohler, and Francis Jacob¹

Gynecological Research Group, Department of Biomedicine, University Hospital Basel, University of Basel, Hebelstrasse 20, Basel 4031, Switzerland

¹To whom correspondence should be addressed: Tel: +41-61-328-6986; Fax: +41-61-265-9399; e-mail: francis.jacob@unibas.ch

Received 2 December 2014; Accepted 17 December 2014

Abstract

Glucosylceramide synthase (GCS) catalyzes the first committed step in the biosynthesis of glucosylceramide (GlcCer)-related glycosphingolipids (GSLs). Although inhibitors of GCS, PPMP and PDMP have been widely used to elucidate their biological function and relevance, our comprehensive literature review revealed that the available data are ambiguous. We therefore investigated whether and to what extent GCS inhibitors affect the expression of lactosylceramide (LacCer), neolacto (nLc4 and P_1), ganglio (GM1 and GD3) and globo (Gb3 and SSEA3) series GSLs in a panel of human cancer cell lines using flow cytometry, a commonly applied method investigating cell-surface GSLs after GCS inhibition. Their cell-surface GSL expression considerably varied among cell lines and more importantly, sublethal concentrations (IC_{10}) of both inhibitors preferentially and significantly reduced the expression of Gb3 in the cancer cell lines IGROV1, BG1, HT29 and T47D, whereas SSEA3 was only reduced in BG1. Unexpectedly, the neolacto and ganglio series was not affected. LacCer, the precursor of all GlcCer-related GSL, was significantly reduced only in BG1 cells treated with PPMP. Future research questions addressing particular GSLs require careful consideration; our results indicate that the extent to which there is a decrease in the expression of one or more particular GSLs is dependent on the cell line under investigation, the type of GCS inhibitor and exposure duration.

Key words: cancer cell lines, flow cytometry, PDMP, PPMP

Introduction

The altered glycan moiety on glycosphingolipids (GSLs) has been connected to malignant transformation (Hakomori 2002). GSLs are made of a hydrophobic ceramide (Cer) lipid tail to which an oligosaccharide head group such as glucose (Glc) or galactose (Gal) is attached to form either glucosylceramide (GlcCer) or GalCer. GSLs are constituents of each eukaryotic cell located at the outer layer of the plasma membrane and play fundamental roles in cell adhesion, cell proliferation and differentiation, protein and lipid trafficking, signaling events, and even function as binding ligands of bacterial toxins and viruses (Hakomori 1992; D'Angelo et al. 2013; Ishibashi et al. 2013; Jennemann and Grone 2013).

GlcCer is the precursor to the synthesis of lactosylceramide (LacCer) that is, in turn, the key precursor for further branching into the neolacto, ganglio and globo series (Figure 1A). The transfer of Glc to Cer is catalyzed by the glucosylceramide synthase [UDP-glucose *N*-asylsphingosine glucosyl transferase (EC 2.4.1.80), GCS] and is the first committed and rate-limiting step in GSL biosynthesis (Kan and Kolesnick 1992). GlcCer and GCS are therefore crucial players in many biological processes and competitive GCS inhibitors have been used to study the biological functions of GSLs in more detail (Park et al. 2012).

We have previously shown that blood plasma-derived anti-glycan antibodies discriminate ovarian cancer patients from healthy controls

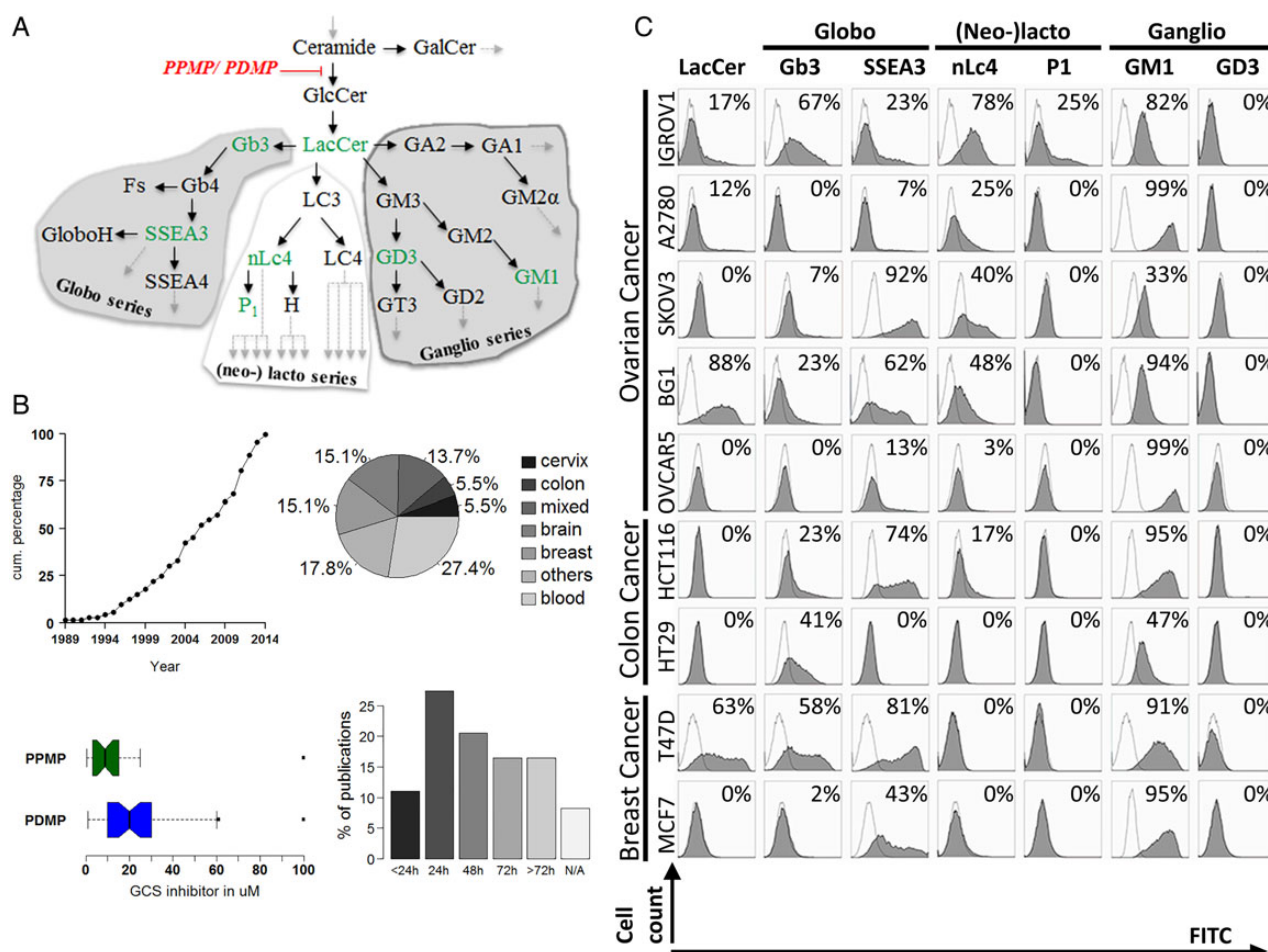


Fig. 1. Glucosylceramide-related biosynthesis, the use of GCS inhibitors in the literature and the differential expression of GlcCer–GSL in a pool of cancer cell lines. **(A)** Depiction of biosynthetic pathway of the globo, neolacto and ganglio series GSLs (respective shaded areas) from GlcCer and LacCer. The key step in this biosynthesis of GlcCer-related GSLs is catalyzed by GCS and is competitively inhibited by PPMP and PDMP (red). GSLs of interest are highlighted in green. Gray arrows indicate further extensions of GSLs. **(B)** Summarized literature showing cumulative increase of publications per year using either both or single inhibitor (top left). Pie chart (top right) presenting the number of studies subdivide according to the origin of the cell lines investigated; >2 organs in one study (mixed) and ≤ 3 publications on one organ investigated summarized by “others”. Box plot (bottom left) showing the median and interquartile range of PPMP (green) and PDMP (blue) concentrations used in the literature. Bar graph depicting the percentage of all studies for categorized time of treatments. **(C)** Flow cytometry data on nine cancer cell lines shown as histogram for negative control (white area under the curve) and GSL-specifically stained sample (dark gray). The value provided in each histogram refers to the percentage of positively stained cells and is a representative of three independent experiments.

using glycan-based immunoassays (Pochechueva et al. 2011; Jacob et al. 2012). More recently, the neolacto series GSL P_1 (Figure 1A) was identified on malignant tissue and cultured cancer cells and therefore may be considered as a cancer-associated carbohydrate (Jacob et al. 2014). To investigate the still poorly understood cellular and molecular functions of neolacto series P_1 and globo series P^k (Gb3), another tumor-associated carbohydrate described in the literature (Kovbasnjuk et al. 2005; Johansson et al. 2009) and encouraged by previous studies showing that GCS inhibitors such as PPMP deplete or reduce the expression of particular GSLs, we evaluated the possibility of depleting cancer cell lines from various cell-surface GSLs using commercially available GCS inhibitors PPMP and PDMP. In order to carefully design our study, we performed a systematic review of the currently available literature in this context and investigated the effect of both inhibitors on representative GSLs of the globo, neolacto and ganglio series in various cell lines.

Results

Literature search

A total of 137 studies have been published since 1989. We identified 73 studies reporting on human cancer cell lines of different tissue that were treated with either with PPMP or PDMP. Since 1989 a continuously growing number of reports have been observed (Figure 1B). In general, both GCS inhibitors were shown to cause cytotoxic, antiproliferative, antiangiogenic and tumor-volume-reducing effects, modulate drug responses in cell lines both cytotoxic (as a drug sensitizer) and -protective (Morjani et al. 2001; Gouaze et al. 2005; Ma et al. 2011; Basu et al. 2012), modulate the level of LacCer and GlcCer and particular reduces the expression of Gb3 in cells (Johansson et al. 2009), modulated the transcription of a set of glycogenes (Ma et al. 2009; Basu et al. 2012), affect protein and lipid trafficking and membrane metabolism (Stefanic et al. 2010) and affect signaling

pathways in cells (Park et al. 2012). Most of the studies investigated cancer cell lines originated from blood (27.5%; Figure 1B). PDMP was generally used in higher concentrations than PPMP (Figure 1B). Information on the mock control [dimethyl sulfoxide (DMSO), isopropanol or water] was provided in only one-fourth (24.7%) of the studies and only 15.0% provided the information (IC_{10-50}) on how the concentration of the inhibitor(s) was determined. The duration of the treatment varied from 30 min up to 168 h (Figure 1B). Particularly interesting to us we found that less than half of the studies (45.2%) addressed the issue of GCS inhibitor-mediated accumulation of Cer or reduction of mainly gangliosides and globosides.

Expression of GSLs in different cancer cell lines

Before addressing the effect of PPMP and PDMP on GSL expression, we measured the GSL content on the cell surface of nine cancer cell lines (Figure 1C). The investigated glycan epitopes include GSLs such as LacCer, globo (Gb3 and SSEA3), neolacto (nLc4 and P_1) and ganglio series (GM1 and GD3) (Figure 1C). We observed a distinct expression of cell-surface GSLs in tested cell lines (Figure 1C). The precursor for all GlcCer-related GSL, LacCer, was highly expressed on BG1 (88%) and T47D (63%), moderately on IGROV1 and A2780 (12 to 30%) and absent on SKOV3, OVCAR5, HCT116, HT29 and MCF7. All cell lines except for HT29 were positive for a globo series GSL, SSEA3. Another member of this series, Gb3, was absent on A2780 and OVCAR5, weakly expressed on SKOV3, HCT116 and MCF7 (2 to 20%) and highly expressed on IGROV1, HT29 and T47D (41 to 67%) (Figure 1C). With regards to neolacto series GSL, more than half of the cell lines were positive for paragloboside (nLc4) except for HT29, T47D, MCF7 and OVCAR5. The second GSL of this series, P_1 , was exclusively present on IGROV1 confirming our previous findings (Jacob et al. 2011, 2014). The ganglio series member GM1 was highly expressed in all cell lines while GD3 was completely absent. In summary, all cancer cell lines expressed at least two GSL on their cell surface but had significant differences in GSL distribution, ranging from 6 positive out of 7 measured GSL (IGROV1) to cancer cells expressing only 2 GSL (OVCAR5 and HT29).

Effect of GCS inhibitors on the survival of cancer cell lines and determination of optimal concentration and incubation period

Based on the flow cytometry data, we selected IGROV1, BG1, HT29 and T47D for further analysis according to the following criteria: (i) at least one cell line from each cancer type, (ii) glycan expression, (iii) moderate or high GSL expression and (iv) whether P_1 and/or Gb3 were expressed in cell lines as these are GSL of our primary interest. HT29 was favored due to its higher expression of Gb3 than HCT116. T47D and MCF7 were negative for the neolacto series but T47D had generally higher expression of GSL compared with MCF7 (Figure 1C).

In order to avoid the effects of PPMP and PDMP on the GSL expression, which are compromised by a reduction in cell survival, we first determined optimal inhibitor concentrations. MTT assay was performed in order to obtain the inhibitory concentrations, i.e. the “sublethal” concentrations for PPMP and PDMP (reduces cell survival by no >10%, i.e. IC_{10}) in combinations with different incubation times (24–72 h). The IC_{10} was chosen since concentrations were previously shown to be sufficient to inhibit the GCS activity leading to accumulation of ceramides in the cells (Baran et al. 2007). We also determined the IC_{50} concentrations in order to

compare the potency of both inhibitors to influence cell viability. PPMP substantially decreased the cell viability (80–90%) and was more cytotoxic in all cell lines than PDMP (50–85%). This observation was independent of the incubation time (Figure 2A). Both inhibitors significantly differed in their molarity based on IC_{10} and IC_{50} among three cell lines. The only exception was T47D, in which case the treatment time over 24 and 72 h did not result in different cell viabilities.

PPMP and PDMP selectively reduce GSLs in a cell line-dependent manner

Both inhibitors were used to treat selected cell lines (IGROV1, BG1, HT29 and T47D) using IC_{10} (Figure 2A) for 48 h following immunostaining and flow cytometry analysis on viable cells. We expected a reduction in all GlcCer-related GSLs on the cell surface. However, our findings clearly demonstrates that Gb3 is the only GSL reduced on the cell surface of almost all investigated cell lines ($n = 4$) and for both inhibitors. The only exception was observed in case of PDMP treatment on T47D (Figure 2B). In contrast, the expression of the other globo series GSL SSEA3 was only affected in BG1.

While PPMP significantly reduced LacCer expression in BG1 cells, PDMP did not affect LacCer expression in all cell lines. Unexpectedly, remaining GSL levels (nLc4, GM1 and P_1) were not changed by either one or both GCS inhibitors.

Discussion

Chemical compounds PDMP and PPMP are structural analogs of ceramide and were designed to inhibit the GCS, the only known glycosyltransferase in the biosynthesis of GlcCer–GSLs. Consequently, an inhibition of this enzyme is expected to result in reduction of GlcCer–GSLs. We have demonstrated that the extent of the inhibitor-induced decrease of GSL expression is different for each cell line. Some GSLs are even not affected. Gb3 seems to be the only GSL which can be generalized, exhibiting in significant reduction in almost all cell lines for both inhibitors (IC_{10}). This is also in concordance with the literature. However, we would expect a similar reduction for SSEA3, a pentasaccharide GSL comprising of Gb3 in its carbohydrate moiety. This was, however, not observed in our experiments, which may be explained by SSEA3 being mentioned to be linked to *N*-glycopeptides (Shevinsky et al. 1982). Another major finding is that we could not observe a marginal extent of reduction within the ganglio (GM1) and the neolacto series (P_1 and nLc4) GSLs. Therefore, our data suggest that both inhibitors are not suitable to reduce GSL of these series in the investigated cell lines.

The unexpected finding on selective reduction of GSLs using GCS inhibitors could possibly be explained by the complex cellular turnover of GSLs. The GSL turnover is dependent on several factors such as metabolic pathways and fluxes, the flow of the endo- and exocytotic routes, the rate of plasma membrane turnover dependent on functional status of a cell, and the occurrence of external stimuli that may influence neosynthesis or degradation. Therefore, the half-life of a certain GSL can vary from only a few hours to several days (Tettamanti 2004). In the case of globosides, Gb3 may have a shorter turnover compared with SSEA3 in our investigated cell lines and is therefore affected by GCS inhibitors. This may also account for neolacto and ganglio series. In addition, the latter may be mostly affected by GCS inhibitors due to the fact that large amounts of gangliosides are expressed in human tumors of the neuroectodermal origin and only minor in normal tissue (Hakomori 1985).

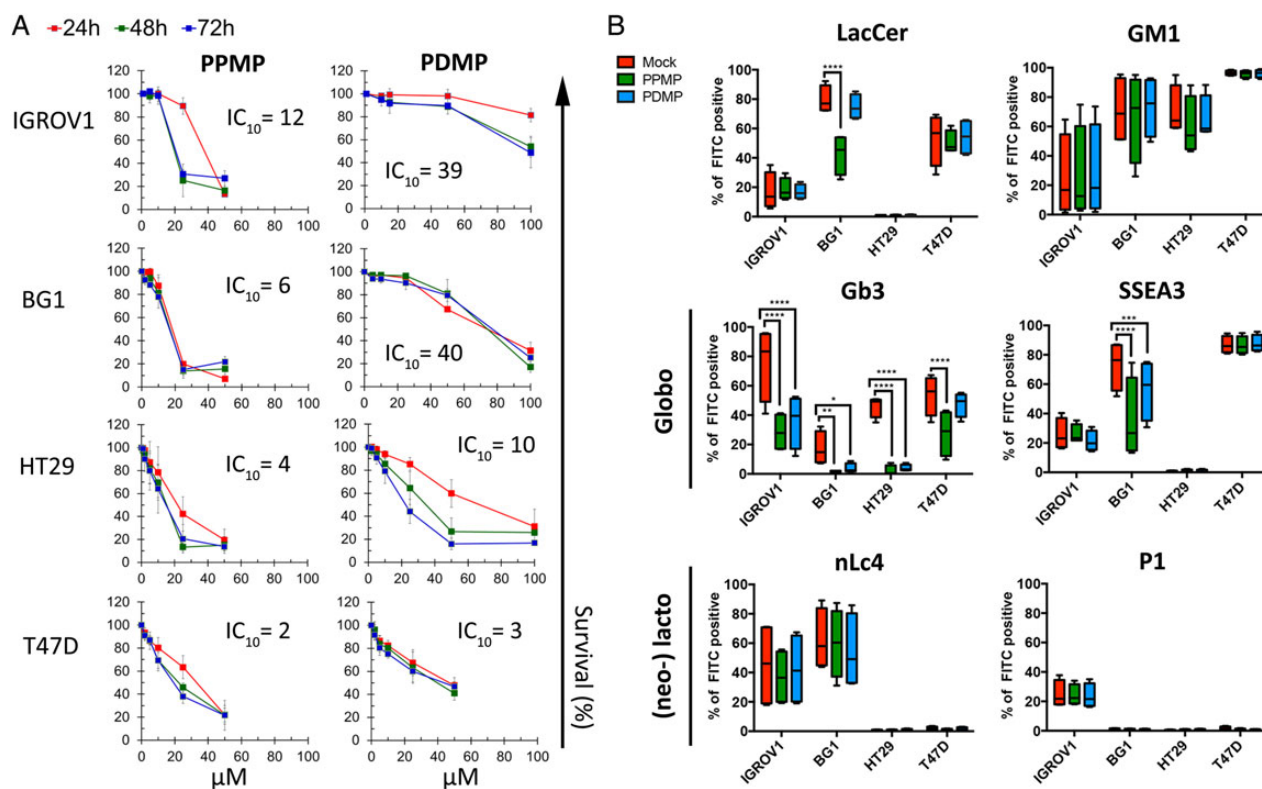


Fig. 2. Effect of PPMP and PDMP on cell survival and on expression of GSLs in IGROV1, BG1, HT29 and T47D cells. **(A)** MTT assay showing cell survival (ordinate) as a function of the indicated concentrations and treatment duration [24 h (red), 48 h (green) and 72 h (blue)] for PPMP (left panel) and PDMP (right panel). Results are presented as percentage of the respective mock-treated control. Mean \pm SD of three independent experiments performed in quadruplet cultures. The IC_{10} used for further flow cytometry experiments is shown for each cell line and inhibitor. **(B)** Box and Whisker plots representing inhibitor-induced (IC_{10}) changes in expression of individual GSLs (percentage of FITC-positive cells, ordinate) for each cell line (abscissa) after a 48 h treatment with DMSO (red), PPMP (green) or PDMP (blue). Data are representative of four independent experiments. * $P < 0.05$, ** $P < 0.01$, *** $P < 0.001$ and **** $P < 0.0001$ were obtained by two-way ANOVA.

Another explanation for our observations may be found in the collected data of our systematic review of the currently available literature for the GCS inhibitor PPMP and PDMP affecting the expression of members of the GlcCer-related GSL in human cancer cells. The literature search revealed that in most cases only one or two cell lines and only a small set of GSL (mostly confined to gangliosides) were investigated within a single study. None of the studies investigated three GSL series in parallel. Moreover, the effect on the expression of GlcCer, the direct product of GCS and LacCer, the branching point for three major GlcCer-related GSL series was only determined in a few cases. In contrast, our experimental setup studied the effect of both inhibitors on a large panel of GSLs representing three GlcCer-GSL series in four cell lines, all measured at the same time. Further discrepancies among studies such as inhibitor concentrations, the treatment duration and the type of the vehicle/mock (if provided) may also cause variable results.

Chemical modifications at various sites of these inhibitors were described in order to enhance their inhibitory effect and to increase the extent of ceramide accumulation or of GlcCer-related GSL reduction. A longer acyl chain in PDMP homologs consisting of various lengths (C6–C18) more efficiently inhibited GlcCer synthesis in MDCK cells. Chemical modifications at the fatty acid chain as well as replacement of the morpholino with a pyrrolidoni ring forming D,L-threo-P4 enhanced the inhibitory activity (Abe et al. 1992). Phenyl group substitutions resulting in the compound EtDO-P4 inhibited GCS at an IC_{50} of 90 nM (Lee et al. 1999) and therefore was more potent compared with respective IC_{50} values in the current literature and to our data.

However, the same inhibitor displayed an IC_{50} at 4 μ M in murine myeloma cells (Manning and Radin 1999). Another important aspect is off-target effects. Enantiomers of GCS inhibitors were shown to raise ceramide levels by inhibition of a pathway forming 1-O-acylceramide that does not involve glucosylceramide synthesis (Shayman et al. 2004). Other GCS inhibitors, Genz-123346 (Silberstein et al. 2011) and EXEL-0346 (Richards et al. 2012), have been recently introduced and may enhance the impact on all GlcCer GSLs.

The initial purpose of our study was to reduce Gb3 and P_1 using PPMP or PDMP in ovarian cancer cell lines. However, a reduction was only seen in case of Gb3 suggesting that both inhibitors can be applied. In case of P_1 , we consider the tested GCS inhibitor strategy not suitable to deplete cells of the neolacto series. We therefore conclude that a careful consideration of the type of the inhibitor, of its appropriate concentration, exposure duration and the type of cell line is recommended for experimental studies in which the depletion of a particular GSL is used to address the research question of interest. This, of course, applies to all inhibitor-based studies.

Material and methods

A systematic literature search was performed for the identification of scientific papers addressing human cell lines in combination with PPMP and PDMP using PubMed (<http://www.ncbi.nlm.nih.gov/pubmed>). The following key words were used: “PPMP” and/or “PDMP”, “PPMP and cancer” or “PDMP and cancer”. The retrieval

was limited from 1989 to August 2014 and included research papers and scientific reports written in English.

Ovarian (IGROV1, A2780, SKOV3, BG1 and OVCAR5), colon (HCT116 and HT29) and breast (T47D and MCF7) cancer cell lines were grown in RPMI-1640 media (Sigma-Aldrich) supplemented with 10% fetal bovine serum (FBS), penicillin (100 U/mL) and streptomycin (100 µg/mL) (Sigma-Aldrich) at 37°C in a 95% humidified atmosphere containing 5% CO₂.

Primary antibodies to detect the cell-surface-associated GSL were applied as follows: mouse IgM anti-LacCer (CD17) conjugated to biotin (Ancell, USA, 1 : 200), rat IgM anti-*P^k* (Gb3) antibody (ABDserotec, Germany, 1 : 200), rat IgM anti-SSEA3 antibody (eBioscience, Austria, 1 : 200), mouse IgM anti-nLc4 (paragloboside) antibody [clone 1B2 kindly provided by Prof. Mandel and Prof. Clausen (Young et al. 1981), 1 : 10], human IgM anti-*P₁* antibody (Millipore, Germany, 1 : 10), mouse IgG anti-GD3 (BD Pharmingen, Switzerland, 1 : 200) and Cholera toxin B subunit (1 mg/mL, Sigma, 1 : 200) to detect GM1. Secondary antibodies (obtained from BD Pharmingen) were used in 1 : 100 dilutions and include: mouse anti-rat IgM antibody conjugated to biotin, rat anti-mouse IgM conjugated to biotin, mouse anti-human IgM conjugated to biotin and anti-mouse IgG/IgM antibody conjugated to fluorescein isothiocyanate. Cell-surface expressed GSL was detected with FITC streptavidin (1 : 200). Non-viable cells were positively stained with 7-amino-actinomycin (BD Pharmingen, 1 : 50). Isotype controls for each primary antibody were used including purified rat IgM (BD Pharmingen), purified mouse IgM and chimpure human IgM (JacksonImmunoResearch, USA).

D,L-Threo-1-Phenyl-2-palmitoylamino-3-morpholino-1-propanol (PPMP; Sigma-Aldrich) and D,L-erythro-1-Phenyl-2-decanoylamino-3-morpholino-1-propanol•HCl (PDMP; Matreya, USA) were aliquoted in DMSO to 20 and 50 mM stocks, respectively, and stored at -20°C.

The MTT assay was performed to define the inhibitor concentration (IC₅₀) and working concentration (IC₁₀) for flow cytometry experiments. Cells seeded in 96-well plates (BD Falcon, Switzerland) were incubated with various concentrations of PPMP, PDMP or respective DMSO concentrations (mock control) for 24, 48 and 72 h. Cell cultures were incubated with MTT-dye (Sigma) at final concentration 500 µg/mL for 3 h. After removal of the supernatant 200 µL DMSO was added to dissolve the crystals. The optical density (OD, absorbance at 540 nm) was measured with a SynergyH1 Hybrid Reader (Biotek, Switzerland). The data (mean ± SD of three independent experiments performed in quadruplets) were presented as the survival (percentage of control) calculated from the OD after subtraction of the contribution of DMSO mock as a function of PPMP and PDMP concentration and incubation time. IC₁₀ and IC₅₀ concentrations of PPMP and PDMP were calculated by linear extrapolation.

To evaluate the distribution of GSL LacCer, Gb3, SSEA3, nLc4, *P₁*, GD3 and GM1, cells grown in T25 cm² flask to 80% confluence were washed with PBS and harvested with 1× Cell Dissociation Solution non-enzymatic (Sigma-Aldrich) at 37°C. Cells were transferred to a 96-well V-bottom micro test plate (10⁵ cells/well), and pelleted at 400 × g for 5 min.

Primary antibodies were added to the cells, resuspended and incubated on ice for 1 h. Cells were then washed twice with FACSWASH (1%, w/v, BSA in PBS) and incubated with the respective secondary antibodies. After additional washing, cells were incubated with streptavidin conjugated to FITC on ice for 30 min. Removal of unbound streptavidin was accomplished by additional washing. Following final washing, cells were re-suspended in 200 µL of FACSWASH and immediately analyzed with the flow cytometer (BD Accuri C6, BD

Pharmingen). Each cell line was gated individually to exclude debris (FSC-A vs. SSC-A) and subjected to single cell gating FSC-A vs. FSC-H. Doublets and non-viable cells were excluded from analysis by gating width vs. 7-AAD. Data acquisition were performed using (BD Accuri C6 software, BD Pharmingen), while data analysis were performed using FlowJo v10.0.4 (Tree Star Inc., Ashland, USA).

All comparisons for the MTT assay were statistically evaluated with two-tailed Student's *t*-test. *P*-values of < 0.05 were considered statistically significant. Flow cytometry data were evaluated with two-way ANOVA comparing mock control with GCS-inhibitor treatments.

Acknowledgements

We are grateful to the Flow Cytometry Facility at the DBM, University Hospital Basel (Emmanuel Traunecker and Toni Krebs) for providing all necessary support.

Conflict of interest statement

None declared.

Funding

This work was supported by Swiss National Foundation (SNF) (grant PBZHP3-133289 and PBZHP3-138752 to F.J.), Novartis Foundation for Biomedical Research (grant 13B093 to F.J.) and the Department of Biomedicine, University Hospital Basel, University of Basel.

Abbreviations

Cer, ceramide; DMSO, dimethyl sulfoxide; FBS, fetal bovine serum; Gal, galactose; Gb3, globotriaosylceramide; Gb4, globotetraose; GCS, glucosylceramide synthase; GD3, *N*-acetylneuraminyl-galactosylglucosylceramide; Glc, glucose; GlcCer, glucosylceramide; GSL, glycosphingolipid(s); IQR, interquartile range; LacCer, lactosylceramide; nLc4, paragloboside; OD, optical density; PDMP, D, L-erythro-1-phenyl-2-decanoylamino-3-morpholino-1-propanol; PPMP, D, L-threo-1-phenyl-2-palmitoylamino-3-morpholino-1-propanol; SSEA3, stage-specific embryonic antigen 3.

References

- Abe A, Inokuchi J, Jimbo M, Shimeno H, Nagamatsu A, Shayman JA, Shukla GS, Radin NS. 1992. Improved inhibitors of glucosylceramide synthase. *J Biochem.* 111:191–196.
- Baran Y, Salas A, Senkal CE, Gunduz U, Bielawski J, Obeid LM, Ogretmen B. 2007. Alterations of ceramide/sphingosine 1-phosphate rheostat involved in the regulation of resistance to imatinib-induced apoptosis in K562 human chronic myeloid leukemia cells. *J Biol Chem.* 282:10922–10934.
- Basu S, Ma R, Moskal JR, Basu M. 2012. Ganglioside biosynthesis in developing brains and apoptotic cancer cells: X. Regulation of glyco-genes involved in GD3 and Sialyl-Lex/a syntheses. *Neurochem Res.* 37:1245–1255.
- D'Angelo G, Capasso S, Sticco L, Russo D. 2013. Glycosphingolipids: synthesis and functions. *FEBS J.* 280:6338–6353.
- Gouaze V, Liu YY, Prickett CS, Yu JY, Giuliano AE, Cabot MC. 2005. Glucosylceramide synthase blockade down-regulates P-glycoprotein and resensitizes multidrug-resistant breast cancer cells to anticancer drugs. *Cancer Res.* 65:3861–3867.
- Hakomori S. 1985. Aberrant glycosylation in cancer cell membranes as focused on glycolipids: overview and perspectives. *Cancer Res.* 45:2405–2414.
- Hakomori S. 1992. Functional role of glycosphingolipids in tumor progression. *Toboku J Exp Med.* 168:211–222.

- Hakomori S. 2002. Glycosylation defining cancer malignancy: New wine in an old bottle. *Proc Natl Acad Sci USA*. 99:10231–10233.
- Ishibashi Y, Kohyama-Koganeya A, Hirabayashi Y. 2013. New insights on glycosylated lipids: Metabolism and functions. *Biochim Biophys Acta*. 1831:1475–1485.
- Jacob F, Anugraham M, Pochechueva T, Tse BW, Alam S, Guertler R, Bovin NV, Fedier A, Hacker NF, Huflejt ME, et al. 2014. The glycosphingolipid P1 is an ovarian cancer-associated carbohydrate antigen involved in migration. *Br J Cancer*. 111:1634–1645.
- Jacob F, Goldstein DR, Bovin NV, Pochechueva T, Spengler M, Caduff R, Fink D, Vuskovic MI, Huflejt ME, Heinzlmann-Schwarz V. 2012. Serum antiglycan antibody detection of nonmucinous ovarian cancers by using a printed glycan array. *Int J Cancer*. 130:138–146.
- Jacob F, Tse BWC, Guertler R, Nixdorf S, Bovin NV, Hacker N, Heinzlmann-Schwarz V. 2011. P1 antigen is present on the serous ovarian cancer cell line, IGROV1, correlating with A4GALT overexpression and altered cell behaviour. *Glycobiology*. 21:1454–1531.
- Jennemann R, Grone HJ. 2013. Cell-specific *in vivo* functions of glycosphingolipids: Lessons from genetic deletions of enzymes involved in glycosphingolipid synthesis. *Prog Lipid Res*. 52:231–248.
- Johansson D, Kosovac E, Moharer J, Ljuslinder I, Brannstrom T, Johansson A, Behnam-Motlagh P. 2009. Expression of verotoxin-1 receptor Gb3 in breast cancer tissue and verotoxin-1 signal transduction to apoptosis. *BMC Cancer*. 9:67.
- Kan CC, Kolesnick RN. 1992. A synthetic ceramide analog, D-threo-1-phenyl-2-decanoylamino-3-morpholino-1-propanol, selectively inhibits adherence during macrophage differentiation of human leukemia cells. *J Biol Chem*. 267:9663–9667.
- Kovbasnjuk O, Mourtzina R, Baibakov B, Wang T, Elowsky C, Choti MA, Kane A, Donowitz M. 2005. The glycosphingolipid globotriaosylceramide in the metastatic transformation of colon cancer. *Proc Natl Acad Sci USA*. 102:19087–19092.
- Lee L, Abe A, Shayman JA. 1999. Improved inhibitors of glucosylceramide synthase. *J Biol Chem*. 274:14662–14669.
- Ma R, Hopp EA, Decker NM, Loucks A, Johnson JR, Moskal J, Basu M, Banerjee S, Basu S. 2011. Regulation of glycosyltransferase genes in apoptotic breast cancer cells induced by L: PPMP and cisplatin. *Adv Exp Med Biol*. 705:621–642.
- Ma R, Matthew Decker N, Anilus V, Moskal JR, Burgdorf J, Johnson JR, Basu M, Banerjee S, Basu S. 2009. Post-translational and transcriptional regulation of glycolipid glycosyltransferase genes in apoptotic breast carcinoma cells: VII. Studied by DNA-microarray after treatment with L-PPMP. *Glycoconj J*. 26:647–661.
- Manning LS, Radin NS. 1999. Effects of the glucolipid synthase inhibitor, P4, on functional and phenotypic parameters of murine myeloma cells. *Br J Cancer*. 81:952–958.
- Morjani H, Aouali N, Belhoussine R, Veldman RJ, Levade T, Manfait M. 2001. Elevation of glucosylceramide in multidrug-resistant cancer cells and accumulation in cytoplasmic droplets. *Int J Cancer*. 94:157–165.
- Park SY, Kwak CY, Shayman JA, Kim JH. 2012. Globoside promotes activation of ERK by interaction with the epidermal growth factor receptor. *Biochim Biophys Acta*. 1820:1141–1148.
- Pochechueva T, Jacob F, Goldstein DR, Huflejt ME, Chinarev A, Caduff R, Fink D, Hacker N, Bovin NV, Heinzlmann-Schwarz V. 2011. Comparison of printed glycan array, suspension array and ELISA in the detection of human anti-glycan antibodies. *Glycoconj J*. 28:507–517.
- Richards S, Larson CJ, Koltun ES, Hanel A, Chan V, Nachtigall J, Harrison A, Aay N, Du H, Arcalas A, et al. 2012. Discovery and characterization of an inhibitor of glucosylceramide synthase. *J Med Chem*. 55:4322–4335.
- Shayman JA, Abe A, Hiraoka M. 2004. A turn in the road: How studies on the pharmacology of glucosylceramide synthase inhibitors led to the identification of a lysosomal phospholipase A2 with ceramide transacylase activity. *Glycoconj J*. 20:25–32.
- Shevinsky LH, Knowles BB, Damjanov I, Solter D. 1982. Monoclonal antibody to murine embryos defines a stage-specific embryonic antigen expressed on mouse embryos and human teratocarcinoma cells. *Cell*. 30:697–705.
- Silberstein C, Lucero MS, Zotta E, Copeland DP, Lingyun L, Repetto HA, Ibarra C. 2011. A glucosylceramide synthase inhibitor protects rats against the cytotoxic effects of shiga toxin 2. *Pediatr Res*. 69:390–394.
- Stefanic S, Spycher C, Morf L, Fabrias G, Casas J, Schraner E, Wild P, Hehl AB, Sonda S. 2010. Glucosylceramide synthesis inhibition affects cell cycle progression, membrane trafficking, and stage differentiation in *Giardia lamblia*. *J Lipid Res*. 51:2527–2545.
- Tettamanti G. 2004. Ganglioside/glycosphingolipid turnover: New concepts. *Glycoconj J*. 20:301–317.
- Young WW Jr, Portoukalian J, Hakomori S. 1981. Two monoclonal anticarbohydrate antibodies directed to glycosphingolipids with a lacto-N-glycosyl type II chain. *J Biol Chem*. 256:10967–10972.

4.3 Naturally occurring anti-glycan antibodies binding to Globo H-expressing cells identify ovarian cancer patients

Tatiana Pochechueva¹†, Shahidul Alam†, Andreas Schötzau, Alexander Chinarev, Nicolai V. Bovin, Neville F. Hacker, Francis Jacob and Viola Heinzelmann-Schwarz

Journal of Ovarian Research 2017

My contributions to this paper:

I contributed to this work by profiling GSLs on different ovarian cancer cell lines using flow cytometry. I have also analyzed the data and designing the corresponding figures as well as in writing parts of the manuscript.

RESEARCH

Open Access



Naturally occurring anti-glycan antibodies binding to Globo H-expressing cells identify ovarian cancer patients

Tatiana Pochechueva^{1†}, Shahidul Alam^{1,2†}, Andreas Schöttau¹, Alexander Chinarev³, Nicolai V. Bovin³, Neville F. Hacker⁴, Francis Jacob^{1,2*} and Viola Heinzlmann-Schwarz^{1,5*}

Abstract

Background: Glycosphingolipids are important compounds of the plasma membrane of mammalian cells and a number of them have been associated with malignant transformation and progression, reinforcing tumour aggressiveness and metastasis. Here we investigated the levels of naturally occurring anti-glycan antibodies to Globo H in blood plasma obtained from high-grade serous ovarian cancer patients (SOC) and women without gynaecological malignancies (control) using suspension glycan array technology employing chemically synthesized glycans as antibody targets.

Results: We found that anti-human Globo H IgG antibodies were able to significantly discriminate SOC from controls ($P < 0.05$). A combination with the clinically used tumour marker CA125 increased the diagnostic performance (AUC 0.8711). We next compared suspension array with standard flow cytometry in plasma samples and found that the level of anti-Globo H antibodies highly correlated ($r = 0.992$). The incubation of plasma-derived anti-glycan antibodies with chemically synthesized (presented on fluorescence microspheres) and native Globo H (expressed on Globo H-positive cell lines) revealed strong reactivity of naturally occurring human anti-Globo H antibodies towards its antigen expressed on ovarian cancer cells.

Conclusions: Our data demonstrate that human plasma-derived antibodies to Globo H as well as the presence of the antigen might be considered as therapeutic option in ovarian cancer.

Keywords: Ovarian cancer, Glycosphingolipids, Suspension array, Glycan

Background

Globo H is a glycosphingolipid of the globo series with a sugar terminus resembling the blood group antigen H determinant. First identified in human teratocarcinoma and breast cancer cells [1, 2], Globo H was found to be overexpressed on the cell surface of several epithelial cancers such as breast, colon, endometrial, gastric, pancreatic, lung, and prostate cancers [3–5]. It is also moderately expressed in normal epithelial tissues (lung, breast, prostate, stomach, pancreas, and ovary), but its distribution is restricted to apical epithelial cells at lumen borders [5]. Functionally, Globo H has been

associated with tumour stem cells [6], to be a potent inducer of angiogenesis [7], and an immunosuppressor through Notch signalling [8]. The high Globo H expression by only cancer and cancer stem cells made it an attractive target for generation of therapeutic cancer vaccines. These vaccines underwent the long history of development and improvement and are currently being tested in clinical trials for treatment [9–11]. Globo H has therefore been considered as one promising tumor-associated glycan biomarker, in particular for breast cancer.

Plasma-derived naturally occurring anti-glycan antibodies (AGA) have been associated to various human diseases including cystic fibrosis [12], Crohn's disease [13], and various malignancies [14–18]. Also healthy humans harbour sets of AGA to blood group-, xeno-

* Correspondence: francis.jacob@unibas.ch; Viola.Heinzlmann@usb.ch

†Equal contributors

¹Ovarian Cancer Research, Department of Biomedicine, University Hospital Basel, University of Basel, Basel, Switzerland

Full list of author information is available at the end of the article



© The Author(s). 2017 **Open Access** This article is distributed under the terms of the Creative Commons Attribution 4.0 International License (<http://creativecommons.org/licenses/by/4.0/>), which permits unrestricted use, distribution, and reproduction in any medium, provided you give appropriate credit to the original author(s) and the source, provide a link to the Creative Commons license, and indicate if changes were made. The Creative Commons Public Domain Dedication waiver (<http://creativecommons.org/publicdomain/zero/1.0/>) applies to the data made available in this article, unless otherwise stated.

(heterophil), and infection-related glycan motifs [19]. Globo H was also shown to be an antigen for naturally occurring plasma-derived AGA in breast and some other epithelial cancers with high specificity [20]. These antibodies were assessed by the glycan microarray technology and their levels were significantly different in serum of breast cancer patients and healthy individuals [21]. Despite these few reports, there is limited knowledge on Globo H antigen expression on cell lines and the presence of naturally circulating AGA in plasma from ovarian cancer patients.

We assessed the levels of anti-Globo H antibodies of IgG and IgM isotypes in healthy and serous ovarian cancer (SOC) patients. We used our “in house” developed suspension glycan array (SGA), a robust tool for AGA profiling [15, 22], to detect anti-Globo H antibodies in human plasma samples for discrimination of ovarian cancer patients and normal controls. We also compared SGA and standard flow cytometry in order to address the following questions; a) whether AGA levels are comparable in both methods, and b) whether those antibodies can recognize native Globo H epitope on the cell surface of cancer cell lines.

Methods

Human subjects

Two groups of female donors were involved in the current study. All patients were over the age of 18 and were prospectively included after giving informed consent in accordance with ethical regulations (Hunter Area Research Ethics 04/04/07/3.04; South Eastern Sydney Illawarra HREC/AURED Ref:08/09/17/3.02). The serous ovarian cancer (SOC) group consisted from patients with serous ovarian cancer with Grade 2 and 3 of all FIGO stages (SOC $n = 19$). The control group ($n = 29$) consisted of women without macroscopically confirmed gynaecological malignancy including comprising of benign donors, patients with benign gynaecological tumours (leiomyoma, cystadenoma, or fibroadenoma) and patients undergoing medical control due to previous family history of breast cancer or bearing known *BRCA* mutations. Women in the control group had no other type of malignancy at the date of collection. Patients were either admitted with an adnexal mass to the Gynaecological Cancer Centre of the Royal Hospital for Women, Randwick, Australia or were seen as outpatients to the Hereditary Cancer Centre of The Prince of Wales Hospital, Randwick, Australia. The processing of blood plasma samples was performed as previously described [15, 23].

Suspension glycan array

Glyco-polymers with end-biotin group- Sialylated and sulfated glycans were chemically synthesised (Lectinity

Holdings, Moscow, Russia). The glycopolymers, Glyc(20)–PAA–biot₁, used for coupling to fluorescent beads were produced in-house as previously described [24]. The glycopolymers are composed of a polyacrylamide carrier (PAA, number of the average polymerisation degree, $n = 220$) provided with end biotin groups and side-pendant Glyc residues, that are statistically distributed along the polymer backbone. The content of monomer units with glycan substitution is 20 mol %. Non-glycosylated monomer units are substituted with an ethanolamine residue for the regular Glyc(20)–PAA–biot₁. GD₃ and GM₂ glycans were purchased from Elicityl (Crolles, France) and then used for synthesis of Glyc(20)–PAA–biot₁, as described above.

Modification of fluorescent microbeads- Biotinylated glycopolymers were coupled to fluorescent Bio-Plex Pro™ Magnetic COOH beads of 6.5 μm diameter with distinct spectral “addresses” (Bio-Rad Laboratories Inc., Cressier, Switzerland). Each bead’s region was embedded with a precise ratio of red and infrared fluorescent dyes allowing its identification using Bio-Plex 200 Suspension Array System (Bio-Rad Laboratories Inc., Hercules, CA, USA). Coupling of biotinylated glycopolymers using biot–PEG₂₃–NH₂ (Hetero-bifunctional PEG, MW = 1300, Iris Biotech GmbH, Marktredwitz, Germany) modification of microbeads was accomplished as described previously [25]. All remaining steps were performed as described previously [25]. Data are presented as median MFI and interquartile range (IQR).

ELISA

CA125 levels in blood samples obtained from patients were measured using the human CA125 ELISA kit (MUC16) SimpleStep (Abcam, LucernaChem AG, Switzerland, #ab195213). ELISA was performed according to manufacturer’s protocol.

Cell culture

Ovarian (IGROV1, A2780, SKOV3, BG1, OVCAR3, OVCAR4, OVCAR5, OVCAR8, OAW42, TYK-nu, KUR-AMUCHI, OVSAHO, CAO3, and TOV21G), and breast (T47D and MCF7) cancer cell lines, ovarian surface epithelial cells (HOSE17.1 and HOSE6.3) and normal mammary epithelial cell line MCF10A were grown in RPMI-1640 media (Sigma-Aldrich, Buchs, Switzerland) supplemented with 10% fetal bovine serum (FBS), penicillin (100U/ml) and streptomycin (100 μg/ml) (obtained from Sigma-Aldrich). Fallopian tube secretory epithelial cells (FT237 and FT240) were grown in DMEM-Ham’s F12 medium without HEPES buffer (Sigma) supplemented with Ultrosor™ (PALL corporation, Life Science, Switzerland), penicillin (100U/ml) and streptomycin (100 μg/ml). Another ovarian cancer cell line, EFO27 were grown in RPMI-1640 media supplemented with 20% FBS, penicillin (100U/ml), streptomycin (100 μg/ml) and 1 mM

sodium pyruvate (purchased from Sigma). The culture condition for all cell lines were 37 °C in a 95% humidified atmosphere containing 5% CO₂.

Flow cytometry

Cells were seeded in T25cm² flask cultivated to 70–80% confluence, washed with PBS, harvested with 1x non-enzymatic cell dissociation solution at 37 °C and counted using trypan blue. Cells were then transferred to 96-well- V-bottom micro test plate (10⁵ cells/well) and pelleted at 400xg for 5 min. Analysis of cell membrane-bound Globo H was performed with two-step staining procedure. Anti-Globo H antibodies (Mbr1_IgM_1:500, diluted in FACSWASH (1% BSA in PBS)) were added to cells, resuspended and incubated on ice for 1 h. After two washes with FACSWASH, cells were incubated with R-PE (1:200) on ice for 30 min. Following two washing steps, cells were incubated with 7-AAD (1:100) on ice for 10 min. After the final wash, cells were resuspended in 200 µl of FACSWASH and analyzed with BD Accuri C6 flow cytometer (BD Pharmingen). Analysis of inhibition experiments using microspheres and human cell lines were analyzed with BD LSR Fortessa. Data analysis was done using FlowJo v10.0.4 (Tree Star Inc., Ashland, USA).

Statistical analysis

The raw data (obtained as MFI) were log-transformed. Statistical analysis was either performed by GraphPad Prism 6 software or the statistical software R version 3.1.3 (www.R-project.org). Penalized logistic regression and receiver operating characteristics (ROC) analysis was performed using the R packages 'glmnet' and 'ROCR' [26], respectively. Comparisons between subgroups were performed using Mann Whitney *U*-test. A *p* value < 0.05 was considered significant.

Results and discussion

Studies in the past suggested that levels of anti-Globo H antibodies are predictive for breast cancer [20, 21]. Recent genomic and transcriptomic analyses by the Cancer Genome Atlas (TCGA) revealed that basal-like breast cancer displays significant molecular similarities to undifferentiated (high-grade) SOC [27, 28]: both diseases share molecular signatures (*e.g.* mutations in *TP53*, *BRCA1/2*, and *RBI*). Thus, we investigated the presence of AGA to Globo H in a cohort of 48 blood plasma samples, consisting of high-grade SOC (*n* = 19) and a control group (*n* = 29) comprising women without or benign disease of the gynaecological tract (*e.g.* leiomyoma, cystadenoma, or fibroadenoma).

The SGA utilized to measure AGA [22, 25] incorporated coupling of microspheres with an internal fluorescence to chemically synthesized glycans (Fig. 1a) *via* a linker (Fig. 1b). Using monoplexed SGA levels of

antibodies to alpha-rhamnose (positive control) and Globo H were generally high for both isotypes in all samples (Fig. 1c-e). In contrast, aminoglucitol (negative control) showed AGA levels below the threshold (Fig. 1c). We observed significantly decreased anti-globo H antibody levels of IgG isotype in SOC patients to the control group (IgG 2642 MFI (338; 6067), *p* = 0.009, Fig. 1d-e), hence clearly discriminating cancer patients from healthy controls. The comparison for the IgM isotype showed a similar trend (1526 (492; 4154), *p* = 0.071, Fig. 1d-e). We next performed ROC analysis including the current clinical ovarian cancer biomarker CA125, which was measured by ELISA during clinical examinations at initial diagnosis. The combination of anti-Globo H IgG and IgM revealed an area under the curve (AUC) of 0.7441. The addition of CA125 in a penalized logistic regression model increased the AUC to 0.8711, which was even higher than CA125 alone (AUC 0.8539). This indicates that anti-globo H antibody levels improve the diagnostic performance of CA125 alone (Fig. 1f).

Despite this intriguing finding it remained to be elucidated whether anti-Globo H antibodies are capable to bind the native Globo H antigen expressed on ovarian cancer cells and whether plasma-derived AGA also recognize other glycan structures (epitopes similar to Globo H). Thus, we profiled a panel of ovarian (*n* = 15) and breast (*n* = 2, used as positive control, [11]) cancer cells (Fig. 2a) using the monoclonal antibody MBr1 (Fig. 2a). After the evaluation of the MBr1 in breast cancer cell lines MCF7 and T47D, the working concentration 2.5 µg/ml MBr1 was selected. We observed Globo H expression in only three ovarian cancer cell lines, OVCAR3, BG1, and IGROV1 (Fig. 2a). The remaining ovarian cancer cell lines never showed any positivity for Globo H. The normal ovarian surface epithelial cell lines (HOSE17-1 and HOSE6-3), fallopian tube secretory epithelial cells (FT237 and FT240), and the mammary epithelial cell line MCF10A were also negative for Globo H (Fig. 2a). In contrast to our findings, the literature reported Globo H expression also in TOV21G ovarian cancer cells [29]. This discrepancy might be explained by the use of different monoclonal antibodies to Globo H (MBr1 and VK9) in these two studies.

In order to study the binding of naturally occurring anti-Globo H antibodies from patient samples to Globo H-positive ovarian cancer cell lines, we compared SGA and standard flow cytometry. A total of fourteen plasma samples reflecting the spectrum of antibody levels were selected and profiled using both methods. The comparison revealed a high correlation (*r* = 0.992, *p* < 0.0001) concluding that flow cytometry is suitable for AGA profiling (Fig. 2b).

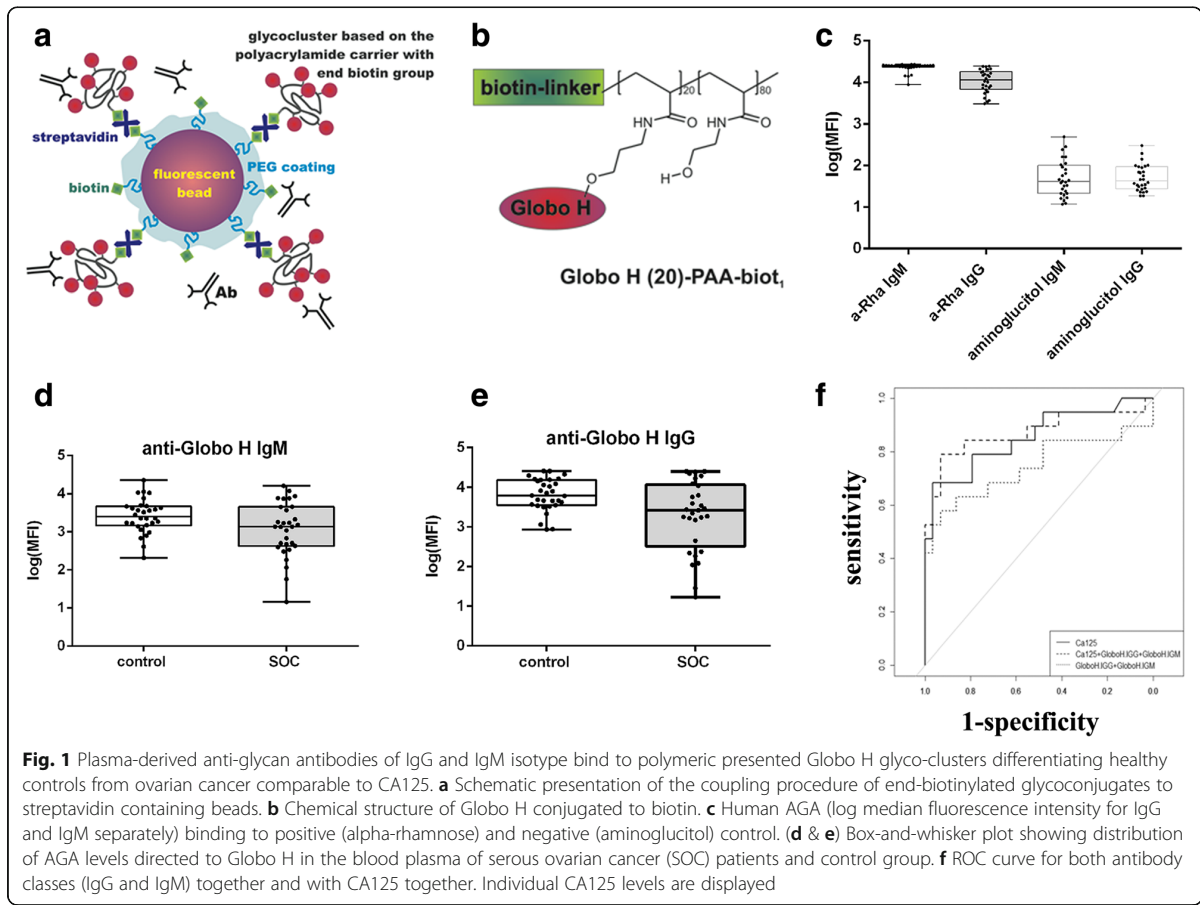


Fig. 1 Plasma-derived anti-glycan antibodies of IgG and IgM isotype bind to polymeric presented Globo H glyco-clusters differentiating healthy controls from ovarian cancer comparable to CA125. **a** Schematic presentation of the coupling procedure of end-biotinylated glycoconjugates to streptavidin containing beads. **b** Chemical structure of Globo H conjugated to biotin. **c** Human AGA (log median fluorescence intensity for IgG and IgM separately) binding to positive (alpha-rhamnose) and negative (aminoglucitol) control. **(d & e)** Box-and-whisker plot showing distribution of AGA levels directed to Globo H in the blood plasma of serous ovarian cancer (SOC) patients and control group. **f** ROC curve for both antibody classes (IgG and IgM) together and with CA125 together. Individual CA125 levels are displayed

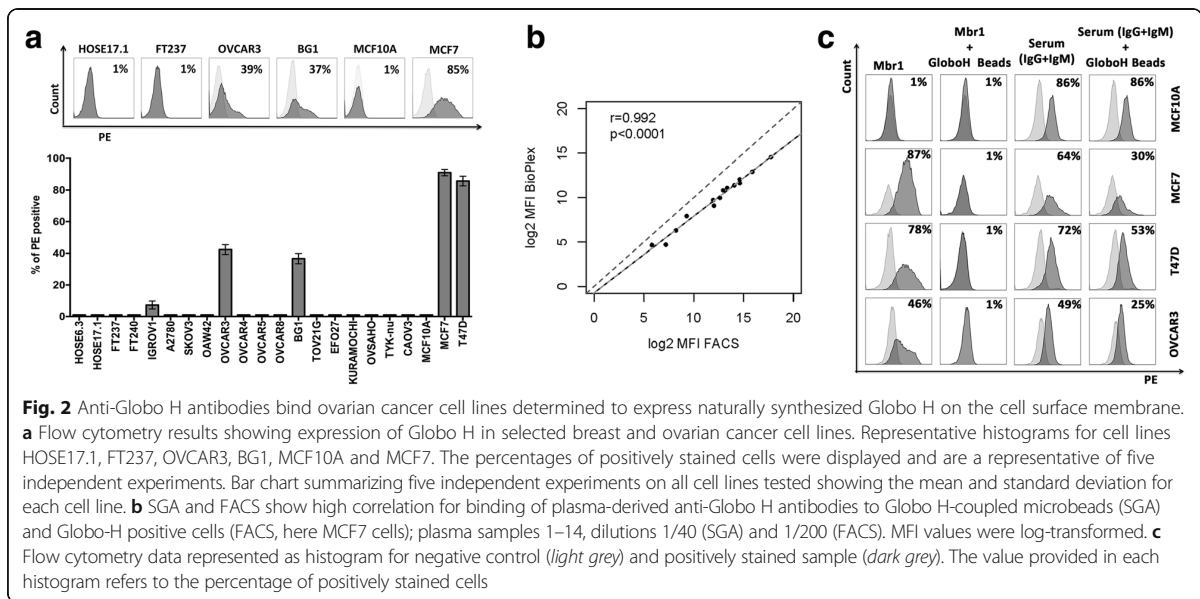


Fig. 2 Anti-Globo H antibodies bind ovarian cancer cell lines determined to express naturally synthesized Globo H on the cell surface membrane. **a** Flow cytometry results showing expression of Globo H in selected breast and ovarian cancer cell lines. Representative histograms for cell lines HOSE17.1, FT237, OVCAR3, BG1, MCF10A and MCF7. The percentages of positively stained cells were displayed and are a representative of five independent experiments. Bar chart summarizing five independent experiments on all cell lines tested showing the mean and standard deviation for each cell line. **b** SGA and FACS show high correlation for binding of plasma-derived anti-Globo H antibodies to Globo H-coupled microbeads (SGA) and Globo-H positive cells (FACS, here MCF7 cells); plasma samples 1–14, dilutions 1/40 (SGA) and 1/200 (FACS). MFI values were log-transformed. **c** Flow cytometry data represented as histogram for negative control (light grey) and positively stained sample (dark grey). The value provided in each histogram refers to the percentage of positively stained cells

To finally prove that plasma antibodies indeed bind to Globo H on the cell surface, we co-incubated anti-Globo H positive plasma (a pool of five individual samples) with Globo H-coupled microbeads (10^5 beads). As a negative control we used MCF10A. We found that plasma antibody binding decreased to different extents among all Globo H positive cancer cell lines (MCF7, T47D, and OVCAR3) tested in flow cytometry (Fig. 2c). We did not achieve pronounced decrease of binding using plasma dilution 1/5–1/100 as well as with combination of less than 0.5×10^5 beads. The plasma binding in case of MCF10A was high (86%) and did not decrease after plasma pre-incubation with Globo H beads (Fig. 2c). These data clearly demonstrate that ovarian cancer cells express Globo H and that the antigen is recognized by naturally occurring anti-Globo H antibodies from human blood plasma.

Taken together, we demonstrate that women with SOC and benign disease display different levels of anti-Globo H antibodies. Moreover, these antibodies are capable to bind Globo H expressing ovarian cancer cell lines.

Conclusions

In this study we report on naturally occurring AGA to a well-known tumour-associated carbohydrate antigen (Globo H) in ovarian cancer. The current study is based on Globo H identified by circulating AGA as well as the monoclonal antibody MBr1. However, future studies have to consider larger cohorts and the measurement of combinations with other representative biomarkers including AGA to evaluate the diagnostic performance of Globo H. Further studies might also incorporate mass spectrometry to confirm the presence of the antigen in ovarian cancer cells. Verification in tissue samples might also support a potential role of Globo H in this malignant disease, e.g. by MALDI imaging mass spectrometry [30]. This knowledge might also contribute to our understanding of the functional role of Globo H as it has been associated with cancer stem (–like) cells previously [31].

Abbreviations

AGA: Anti-glycan antibodies; AUC: Area under the curve; FT: Fallopiian tube; FBS: Fetal bovine serum; HOSE: Human ovarian surface epithelium; MFI: Median fluorescence intensity; ROC: Receiver operating characteristics; SOC: Serous ovarian cancer; SGA: Suspension glycan array; TCGA: The cancer genome atlas

Acknowledgements

We are grateful to the Flow Cytometry Facility at the Department of Biomedicine, University Hospital Basel and University of Basel (Danny Labes and Emmanuel Traunecker) for providing all necessary support.

Funding

Swiss National Foundation (310030_143619 and 32) to V.H.S., Oncosuisse Grant (KFS_3013-08-2012 to V.H.S.), and Krebsliga beider Basel 06-2013/14-2015 to V.H.S and F.J., respectively, and the Department of Biomedicine, University Hospital Basel, University of Basel.

Availability of data and materials

All data generated or analysed during this study are included in this published article.

Authors' contributions

TP, AS, and FJ performed the experiments (suspension array, cell culture, flow cytometry, and competition assay). ASch carried out the statistical analysis. AC and NVB designed, synthesized and provided glycan structures. VHS carried out ethical approval, patient recruitment, and collection of material. NFH participated in cases recruitment of the present study. VHS and FJ designed the study. TP, AS, FJ, and VHS drafted the manuscript. All authors read and approved the final manuscript.

Competing interests

The authors declare that they have no competing interests.

Consent for publication

Not applicable.

Ethics approval and consent to participate

The Hunter Area Research Ethics (04/04/07/3.04) and South Eastern Sydney Illawarra HREC/AURED (08/09/17/3.02) approved this study.

Author details

¹Ovarian Cancer Research, Department of Biomedicine, University Hospital Basel, University of Basel, Basel, Switzerland. ²Glyco-Oncology, Ovarian Cancer Research, Department of Biomedicine, University Hospital Basel, University of Basel, Basel, Switzerland. ³Shemyakin-Ovchinnikov Institute of Bioorganic Chemistry, Russian Academy of Sciences, 117997 Moscow, Russian Federation. ⁴Royal Hospital for Women, Gynecological Cancer Centre, School of Women's and Children's Health, University of New South Wales, Sydney, Australia. ⁵Hospital for Women, Department of Gynecology and Gynaecological Oncology, University Hospital Basel, Basel, Switzerland.

Received: 22 October 2016 Accepted: 4 February 2017

Published online: 10 February 2017

References

- Menard S, Tagliabue E, Canevari S, Fossati G, Colnaghi M. Generation of monoclonal antibodies reacting with normal and cancer cells of human breast. *Cancer Res.* 1983;43(3):1295–300.
- Kannagi R, Levery SB, Ishigami F, Hakomori S, Shevinsky LH, Knowles BB, et al. New globoseries glycosphingolipids in human teratocarcinoma reactive with the monoclonal antibody directed to a developmentally regulated antigen, stage-specific embryonic antigen 3. *J Biol Chem.* 1983;258(14):8934–42.
- Bremer EG, Levery SB, Sonnino S, Ghidoni R, Canevari S, Kannagi R, et al. Characterization of a glycosphingolipid antigen defined by the monoclonal antibody MBr1 expressed in normal and neoplastic epithelial cells of human mammary gland. *J Biol Chem.* 1984;259(23):14773–7.
- Canevari S, Fossati G, Balsari A, Sonnino S, Colnaghi M. Immunochemical analysis of the determinant recognized by a monoclonal antibody (MBr1) which specifically binds to human mammary epithelial cells. *Cancer Res.* 1983;43(3):1301–5.
- Zhang S, Cordon-Cardo C, Zhang HS, Reuter VE, Adluri S, Hamilton WB, et al. Selection of tumor antigens as targets for immune attack using immunohistochemistry: I. Focus on gangliosides. *Int J Cancer.* 1997; 73(1):42–9.
- Chang WW, Lee CH, Lee P, Lin J, Hsu CW, Hung JT, et al. Expression of Globo H and SSEA3 in breast cancer stem cells and the involvement of fucosyl transferases 1 and 2 in Globo H synthesis. *Proc Natl Acad Sci U S A.* 2008;105(33):11667–72. doi:10.1073/pnas.0804979105.
- Cheng JY, Wang SH, Lin J, Tsai YC, Yu J, Wu JC, et al. Globo-H ceramide shed from cancer cells triggers translin-associated factor X-dependent angiogenesis. *Cancer Res.* 2014;74(23):6856–66. doi:10.1158/0008-5472.CAN-14-1651.
- Tsai YCHJ, Cheng JY, Lin JJ, Hung JT, Wu YY, Yen KT, Yu AL. A prevalent cancer associated glycan, Globo H ceramide, induces immunosuppression by reducing Notch 1 signalling. *J Cancer Sci Ther.* 2013;5(7):264–70.
- Slovin SF, Ragupathi G, Fernandez C, Jefferson MP, Diani M, Wilton AS, et al. A bivalent conjugate vaccine in the treatment of biochemically relapsed

- prostate cancer: a study of glycosylated MUC-2-KLH and Globo H-KLH conjugate vaccines given with the new semi-synthetic saponin immunological adjuvant GPI-0100 OR QS-21. *Vaccine*. 2005;23(24):3114–22. doi:10.1016/j.vaccine.2005.01.072.
10. Danishefsky SJ, Shue YK, Chang MN, Wong CH. Development of globo-h cancer vaccine. *Acc Chem Res*. 2015;48(3):643–52. doi:10.1021/ar5004187.
 11. Huang YL, Hung JT, Cheung SK, Lee HY, Chu KC, Li ST, et al. Carbohydrate-based vaccines with a glycolipid adjuvant for breast cancer. *Proc Natl Acad Sci U S A*. 2013;110(7):2517–22. doi:10.1073/pnas.1222649110.
 12. Hirche TO, Stein J, Hirche H, Hausmann J, Wagner TO, Behrens F, et al. Increased levels of anti-glycan antibodies in patients with cystic fibrosis. *Eur J Med Res*. 2011;16(9):385–90.
 13. Rieder F, Lopez R, Franke A, Wolf A, Schleider S, Dirmeier A, et al. Characterization of changes in serum anti-glycan antibodies in Crohn's disease - a longitudinal analysis. *PLoS One*. 2011;6(5):e18172.
 14. Jacob F, Anugraham M, Pochechueva T, Tse BW, Alam S, Guertler R, et al. The glycosphingolipid P(1) is an ovarian cancer-associated carbohydrate antigen involved in migration. *Br J Cancer*. 2014;111(8):1634–45. doi:10.1038/bjc.2014.455.
 15. Jacob F, Goldstein DR, Bovin NV, Pochechueva T, Spengler M, Caduff R, et al. Serum antiglycan antibody detection of nonmucinous ovarian cancers by using a printed glycan array. *Int J Cancer*. 2012;130(1):138–46. doi:10.1002/ijc.26002.
 16. Pochechueva T, Jacob F, Goldstein DR, Huflejt ME, Chinarev A, Caduff R, et al. Comparison of printed glycan array, suspension array and ELISA in the detection of human anti-glycan antibodies. *Glycoconj J*. 2011; 28(8–9):507–17.
 17. Pedersen JW, Blixt O, Bennett EP, Tarp MA, Dar I, Mandel U, et al. Seromic profiling of colorectal cancer patients with novel glycopeptide microarray. *Int J Cancer*. 2011;128(8):1860–71. doi:10.1002/ijc.25778.
 18. Wandall HH, Blixt O, Tarp MA, Pedersen JW, Bennett EP, Mandel U, et al. Cancer biomarkers defined by autoantibody signatures to aberrant O-glycopeptide epitopes. *Cancer Res*. 2010;70(4):1306–13.
 19. Huflejt ME, Vuskovic M, Vasilii D, Xu H, Obukhova P, Shilova N, et al. Anti-carbohydrate antibodies of normal sera: findings, surprises and challenges. *Mol Immunol*. 2009;46(15):3037–49.
 20. Huang CY, Thayer DA, Chang AY, Best MD, Hoffmann J, Head S, et al. Carbohydrate microarray for profiling the antibodies interacting with Globo H tumor antigen. *Proc Natl Acad Sci U S A*. 2006;103(1):15–20. doi:10.1073/pnas.0509693102.
 21. Wang CC, Huang YL, Ren CT, Lin CW, Hung JT, Yu JC, et al. Glycan microarray of Globo H and related structures for quantitative analysis of breast cancer. *Proc Natl Acad Sci U S A*. 2008;105(33):11661–6. doi:10.1073/pnas.0804923105.
 22. Pochechueva T, Chinarev A, Spengler M, Korchagina E, Heinzlmann-Schwarz V, Bovin N, et al. Multiplex suspension array for human anti-carbohydrate antibody profiling. *Analyst*. 2011;136(3):560–9. doi:10.1039/c0an00758g.
 23. Jacob F, Meier M, Caduff R, Goldstein D, Pochechueva T, Hacker N, et al. No benefit from combining HE4 and CA125 as ovarian tumor markers in a clinical setting. *Gynecol Oncol*. 2011;121(3):487–91. doi:10.1016/j.ygyno.2011.02.022.
 24. Chinarev AA, Galanina OE, Bovin NV. Biotinylated multivalent glycoconjugates for surface coating. *Methods Mol Biol*. 2010;600:67–78.
 25. Pochechueva T, Chinarev A, Bovin N, Fedier A, Jacob F, Heinzlmann-Schwarz V. PEGylation of microbead surfaces reduces unspecific antibody binding in glycan-based suspension array. *J Immunol Methods*. 2014;412: 42–52. doi:10.1016/j.jim.2014.06.015.
 26. Sing T, Sander O, Beerenwinkel N, Lengauer T. ROCr: visualizing classifier performance in R. *Bioinformatics*. 2005;21(20):3940–1.
 27. Cancer Genome Atlas N. Comprehensive molecular portraits of human breast tumours. *Nature*. 2012;490(7418):61–70. doi:10.1038/nature11412.
 28. Cancer Genome Atlas Research N. Integrated genomic analyses of ovarian carcinoma. *Nature*. 2011;474(7353):609–15. doi:10.1038/nature10166.
 29. Lou YW, Wang PY, Yeh SC, Chuang PK, Li ST, Wu CY, et al. Stage-specific embryonic antigen-4 as a potential therapeutic target in glioblastoma multiforme and other cancers. *Proc Natl Acad Sci U S A*. 2014;111(7):2482–7. doi:10.1073/pnas.1400283111.
 30. Everest-Dass AV, Briggs MT, Kaur G, Oehler MK, Hoffmann P, Packer NH. N-glycan MALDI Imaging Mass Spectrometry on Formalin-Fixed Paraffin-Embedded Tissue Enables the Delineation of Ovarian Cancer Tissues. *Mol Cell Proteomics*. 2016;15(9):3003–16. doi:10.1074/mcp.M116.059816.
 31. Liang YJ, Kuo HH, Lin CH, Chen YY, Yang BC, Cheng YY, et al. Switching of the core structures of glycosphingolipids from globo- and lacto- to ganglio-series upon human embryonic stem cell differentiation. *Proc Natl Acad Sci U S A*. 2010;107(52):22564–9. doi:10.1073/pnas.1007290108.

Submit your next manuscript to BioMed Central and we will help you at every step:

- We accept pre-submission inquiries
- Our selector tool helps you to find the most relevant journal
- We provide round the clock customer support
- Convenient online submission
- Thorough peer review
- Inclusion in PubMed and all major indexing services
- Maximum visibility for your research

Submit your manuscript at
www.biomedcentral.com/submit



4.4 Altered (neo-) lacto series glycolipid biosynthesis impairs α 2-6 sialylation on N-glycoproteins in ovarian cancer cells

Shahidul Alam* , Merrina Anugraham* , Yen-Lin Huang , Reto S. Kohler, Timm Hettich, Katharina Winkelbach, Yasmin Grether, Mónica Núñez López, Nailia Khasbiullina, Nicolai V. Bovin, Götz Schlotterbeck & Francis Jacob

Scientific Reports 2017

My contributions to this paper:

For this study, I designed the experimental strategy in supervision by Francis Jacob. I performed experiment 1(B) to profile GSLs expression, 2(A, B, C, D, E) to create and validate the knockout cells, 4(E) for SNA staining and 5 (A, B, C, D, F) to generate another knockout cell line and identify the loss of α 2,6 sialylation by *ST6GALI* silencing. Data were analyzed by myself and prepared for presentation in the manuscript. I have written the manuscript with the help of all co-authors.

SCIENTIFIC REPORTS

OPEN

Altered (neo-) lacto series glycolipid biosynthesis impairs α 2-6 sialylation on *N*-glycoproteins in ovarian cancer cells

Received: 24 November 2016

Accepted: 15 February 2017

Published: 30 March 2017

Shahidul Alam^{1,2,*}, Merrina Anugraham^{1,*}, Yen-Lin Huang¹, Reto S. Kohler¹, Timm Hettich³, Katharina Winkelbach¹, Yasmin Grether¹, Mónica Núñez López¹, Nailia Khasbiullina⁴, Nicolai V. Bovin⁴, Götz Schlotterbeck³ & Francis Jacob^{1,2}

The (neo-) lacto series glycosphingolipids (nsGSLs) comprise of glycan epitopes that are present as blood group antigens, act as primary receptors for human pathogens and are also increasingly associated with malignant diseases. Beta-1, 3-*N*-acetyl-glucosaminyl-transferase 5 (B3GNT5) is suggested as the key glycosyltransferase for the biosynthesis of nsGSLs. In this study, we investigated the impact of CRISPR-Cas9-mediated gene disruption of *B3GNT5* ($\Delta B3GNT5$) on the expression of glycosphingolipids and *N*-glycoproteins by utilizing immunostaining and glycomics-based PGC-UHPLC-ESI-QTOF-MS/MS profiling. $\Delta B3GNT5$ cells lost nsGSL expression coinciding with reduction of α 2-6 sialylation on *N*-glycoproteins. In contrast, disruption of *B4GALNT1*, a glycosyltransferase for ganglio series GSLs did not affect α 2-6 sialylation on *N*-glycoproteins. We further profiled all known α 2-6 sialyltransferase-encoding genes and showed that the loss of α 2-6 sialylation is due to silencing of *ST6GAL1* expression in $\Delta B3GNT5$ cells. These results demonstrate that nsGSLs are part of a complex network affecting *N*-glycosylation in ovarian cancer cells.

Glycosphingolipids (GSLs) have been shown to be essential in a wide variety of biological events - such as cell signalling, modification of insulin and EGF-receptor activities, and modulation of Notch ligand activity in *Drosophila*¹. They also interact with well-known proteins such as EGFR², TGF β 1R³, and VEGFR⁴ in various malignancies. GSLs are usually divided into two major families, known as galactosylated or glucosylated ceramides. The latter (glucosylceramide-related glycosphingolipids) is further divided into three major classes based on the action of specific glycosyltransferases: globo- (A4GALT), ganglio- (B4GALNT1 and ST3GAL5), and (neo-) lacto (B3GNT5) -series. Additional elongation of lipid-linked carbohydrate chains is determined by the intracellular localization, which is usually embedded in the endomembrane system and the regulation of specific glycosyltransferases within the GSL-glycan biosynthetic pathway⁵.

The *B3GNT5* gene encodes the glycosyltransferase β -1,3-*N*-acetylglucosaminyl transferase 5, which attaches *N*-acetylglucosamine (GlcNAc) to lactosylceramide (Gal β 1-4Glc β 1-1Ceramide) resulting in the precursor lactotriaosylceramide (Lc3, GlcNAc β 1-3Gal β 1-4Glc β 1-1Ceramide) for synthesis of lacto (Type 1) and neolacto-series (Type 2) GSLs⁶ (Fig. 1A). This enzyme, together with its associated glycosidic product (Lc3), plays a role in human malignant diseases, embryonic development and cell differentiation. Specifically, Lc3 was shown to be elevated on the cell surface of human pro-myelocytic leukemia HL60 cells^{6,7}. Moreover, it has also been suggested as a differentiation-associated GSL in the bone marrow of acute myeloid leukemia patients with corresponding elevated *B3GNT5* expression⁸. In mice experiments, the current data on the potential function of *B3GNT5* seems rather controversial, possibly due to the use of a multicellular organism and different mutation-generating techniques, thereby limiting biological interpretations regarding its role⁹⁻¹¹. Other than

¹Ovarian Cancer Research, Department of Biomedicine, University Hospital Basel, University of Basel, Basel, 4031, Switzerland. ²Glyco-oncology, Ovarian Cancer Research, Department of Biomedicine, University Hospital Basel, University of Basel, Basel, 4031, Switzerland. ³School of Life Sciences, University of Applied Sciences and Arts Northwestern Switzerland, Muttenz, 4132, Switzerland. ⁴Shemyakin-Ovchinnikov Institute of Bioorganic Chemistry, Russian Academy of Sciences, Moscow, 117997, Russian Federation. *These authors contributed equally to this work. Correspondence and requests for materials should be addressed to F.J. (email: francis.jacob@unibas.ch)

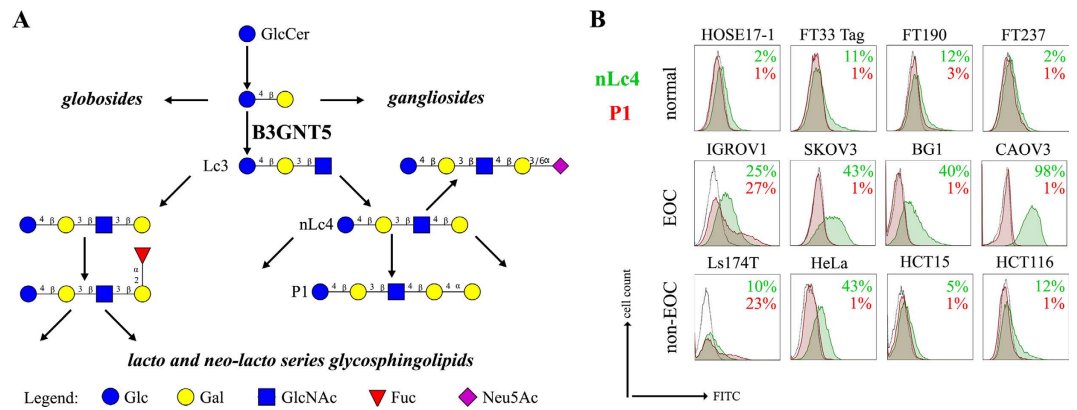


Figure 1. The heterogeneous expression of (neo-) lacto series glycosphingolipids on normal and cancer cell lines. (A) Depiction of the three major glycosphingolipid series - globo, ganglio, and (neo-) lacto series glycosphingolipids. B3GNT5 attaches GlcNAc to the LacCer synthesizing Lc3, the precursor of all nsGSLs. Glycosidic linkages are displayed next to CFG notated monosaccharides. (B) Representative histograms of flow cytometry data on normal and cancer cell lines stained for paragloboside (nLc4, green) and P₁ (red). Grey histogram depicts the negative control. Values within each plot show the mean out of three independent experiments for nLc4 (green) and P₁ (red).

Lc3, it is also known that B3GNT5 is the key enzyme for several GSL structures associated with human diseases such as sialyl-Lewis x¹² and human blood groups ABO and P [based on the Kyoto Encyclopedia of Genes and Genomes (KEGG, <http://www.genome.jp/kegg/>)]. Nevertheless, the biological function of B3GNT5-mediated GSLs is rather limited in the context of cancer and remains to be explained.

In this study, we successfully created a site-specific and heritable *B3GNT5* knockout in human cancer cell lines. By utilizing the CRISPR *Cas9* technology, we established an experimental tool for studying the function of B3GNT5-mediated GSLs, namely the entire (neo-) lacto series (nsGSL). In addition, we also performed a glycomics profiling using mass spectrometry to evaluate the effects of this GSL gene knockout on the entire glycome repertoire of membrane proteins and lipids. The specific glycan alterations described in this study are consistent in two ovarian cancer cell lines and seem to be specific for B3GNT5. It is envisioned that this gene-editing technology will serve as a useful platform to facilitate the downstream investigation of B3GNT5 and its regulation of both GSL and protein glycosylation in cancer development and progression.

Results

(Neo-) lacto- series glycosphingolipids are expressed on cancer cells. As part of our initiative to comprehensively characterize nsGSLs, we have recently reported the presence of paragloboside (nLc4, precursor of P₁) and P₁ pentasaccharide in tumor specimens and immortal ovarian cancer cells using two complementary methods; PGC-LC-ESI-MS/MS and flow cytometry^{13–15}. In this study, we extended the profiling of nsGSLs into three distinct groups; Normal (HOSE17-1, FT33-Tag, FT190 and FT237 which were suggested as a potential origin of epithelial ovarian cancer^{16,17}), Ovarian (IGROV1, SKOV3, BG1, and CAOV3), and Non-ovarian cancer cell lines (Ls174T, HeLa, HCT15, and HCT116). The flow cytometry data revealed a generally lower expression of nsGSLs in normal cells (nLc4 2–12% and P₁ 1–3%), while all four of the ovarian cancer cell lines displayed elevated expression for nLc4 (25–98%). A distinct expression of nLc4 (5–43%) was observed in non-ovarian derived cancer cells (Fig. 1B). P₁ expression was observed only in IGROV1 (27%) and Ls174T (23%) cell lines (Fig. 1B). Based on their nsGSL expression levels, IGROV1 was selected for genome editing to establish a heritable and site-specific *B3GNT5* knockout cell line ($\Delta B3GNT5$), which was then selected to study the influence of nsGSLs on the glycome repertoire.

Genome editing of *B3GNT5* for depletion of nsGSLs and validation using flow cytometry. *B3GNT5* is the key glycosyltransferase involved in synthesis of nsGSLs^{6,18}. We utilized the genome editing technology, CRISPR-*Cas9*, to homozygously delete an 898 bp genomic region, including the translation start site of *B3GNT5* (Fig. 2A). The plasmid pSpCas9(BB)-2A-GFP encoding two specific sgRNA sequences (Supplemental Table S1), was transiently transfected into IGROV1 and tested after 72 h incubation for *Cas9* activity, in which an additional band at 309 bp ($\Delta B3GNT5$) observed below 1208 bp (wildtype *B3GNT5*) indicates an active genome editing. Next, *Cas9*-active cell pools were subjected to single cell sorting (Supplemental Fig. S1) and incubated until further genotyping of single cell clones. The presence of homozygous $\Delta B3GNT5$ was verified by three independent PCRs, which showed the additional band at 309 bp in knockout (PCR₁) and no visible band at 617 bp and 329 bp, respectively for wildtype *B3GNT5* (PCR₂ and PCR₃) (Fig. 2B). We identified two homozygous *B3GNT5*-deleted clones from a total of 320 clones profiled (0.625% efficiency). Despite equal mRNA expression of *B3GNT5* transcripts (*B3GNT5_1*), a truncated transcript length was equally expressed in $\Delta B3GNT5$ cells as compared to wildtype (*B3GNT5_2*, Fig. 2C). The homozygous deletion was confirmed by Sanger DNA sequencing, showing knockout cells with alleles in varying lengths; (*indel*) 898 bp and 899 bp (Fig. 2D). In regards to potential off-target effects, both sgRNAs used for genome-editing did not show off-target effects (Supplemental Fig. S2).

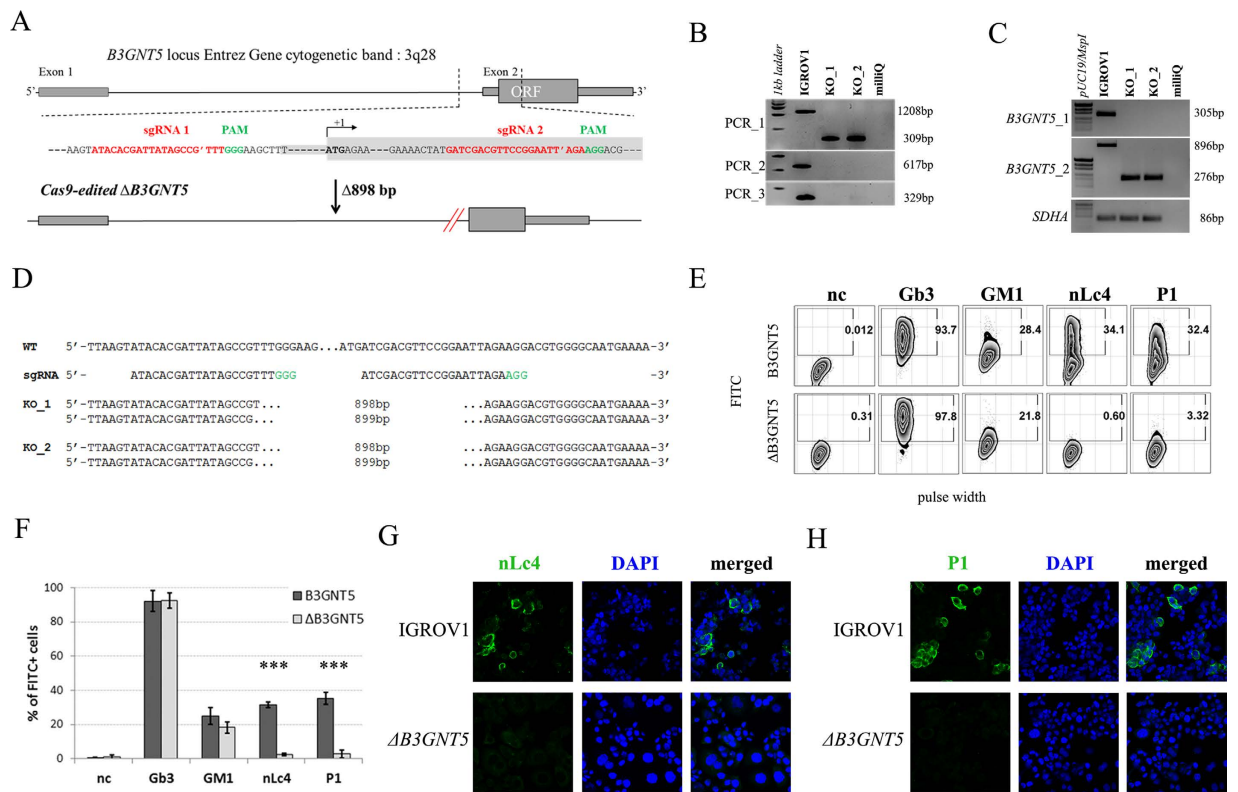


Figure 2. Deletion of *B3GNT5* leads to depletion of nLc4 and P₁. (A) *B3GNT5*-editing strategy using two different sgRNAs (red) contain PAM sequence (green) deleting a genomic region up- and downstream of the transcription start site (+1) including a part of the open reading frame (ORF). *In silico* analysis revealed a deletion of 898 bp. (B) Representative genotyping PCR for characterization of single cell clones. PCR numbers indicate the use of different primer pairs listed in experimental procedures. (C) Semi-quantitative PCR with two different primer pairs (*B3GNT5_1* and *B3GNT5_2*) on wildtype (pIGROV1) and two representative knockout clones. *SDHA* was used as a reference gene. (D) DNA sequencing results for wildtype (WT), and selected biallelically deleted knockout clones (KO_1 and KO_2). (E) Representative counter plots for presence of Gb3, GM1, nLc4 and P₁ before (wildtype *B3GNT5*) and after gene disruption of *B3GNT5* in IGROV1 cells ($\Delta B3GNT5$). Percentage of GSL-positive cells (FITC) is shown in each plot. Negative control (n.c.). (F) Box and Whisker plots representing CRISPR *Cas9*-mediated changes in expression of individual GSLs (percentage of FITC-positive cells, ordinate) for $\Delta B3GNT5$ and parental cells (abscissa). *** $p < 0.001$ was obtained by two-way ANOVA. Data are representative out of four independent experiments. (G,H) Confocal fluorescence images displaying presence and absence of nLc4 (green, G, 40x magnification) and P₁ (green, H) in *B3GNT5* wildtype (*B3GNT5*) and knockout ($\Delta B3GNT5$) cells, respectively. Cells are counterstained with DAPI (blue). Data are represented as mean \pm s.d.

The established $\Delta B3GNT5$ cell line was further investigated for GSL expression using flow cytometry, in which the human anti-P₁ IgM P3NIL100 antibody, previously validated by printed glycan array, was utilized to detect the binding specificities to P₁ epitope on these cells (Supplemental Fig. S3)¹⁴. The GSL pathways affected by the genetic disruption of *B3GNT5* is hypothesized (according to the scheme presented in Fig. 1A) and the binding results were in full concordance with the expression levels for nLc4 and P₁ ($p < 0.001$, Fig. 2E and F). In conclusion, the absence of nLc4 and P₁ epitopes confirmed our hypothesis that the nsGSLs were depleted in these cells, whereas ganglio- and globo- series GSLs were not affected by *B3GNT5*-editing (Fig. 2E and F). In addition, the absence of nLc4 and P₁ in $\Delta B3GNT5$ cells was confirmed by confocal fluorescence microscopy (Fig. 2G and H).

Validation of altered GSL-glycans in $\Delta B3GNT5$ cells by PGC-UHPLC-ESI-QTOF-MS/MS. We also utilized mass spectrometry (MS) to investigate the expression of cell surface glycans, which were subsequently altered due to the genome- editing of *B3GNT5* in IGROV1 cells. This glycomics-based approach was performed to confirm the absence of nsGSLs due to genetic disruption of *B3GNT5*. Glycans were enzymatically released from extracted GSLs of parental and $\Delta B3GNT5$ IGROV1 cells and analyzed using negative mode UHPLC-ESI-QTOF-MS/MS. The assignment of glycan structures was facilitated using diagnostic MS² fragment ions previously described for the analysis of *N*-glycans released from glycoproteins as well as GSL-derived glycans using negative mode LC-ESI-MS/MS^{13,19}.

The MS profiling revealed three neutral GSLs comprising of globo (Gb3)-, paragloboside (nLc4) as well as neolactopentaosylceramide (nLc-penta). All three neutral GSL species differed in chromatographic retention

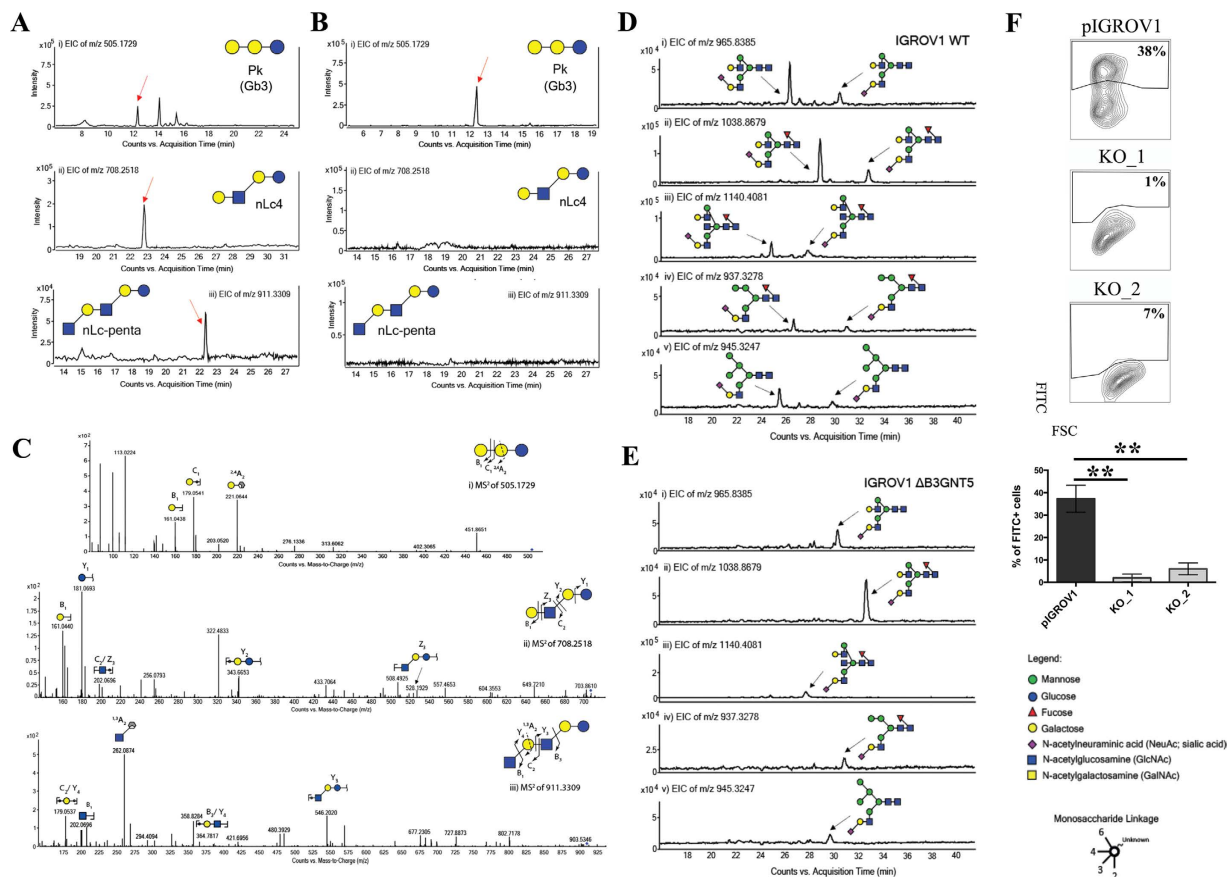


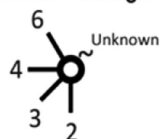
Figure 3. LC-MS profiling of neutral GSLs and monosialylated *N*-glycans extracted from wildtype IGROV1 and genome-edited B3GNT5 cell lines. The extracted ion chromatograms (EIC) obtained from wildtype IGROV1 (A) and genome-edited B3GNT5 (B) cell lines are represented for Gb3 [m/z 505.1729¹⁻-Gal α 1-4Gal β 1-4Glc β 1] (i), nLc4 [m/z 708.2518¹⁻:Gal β 1-4GlcNAc β 1-3Gal β 1-4Glc β 1] (ii) and nLc-pentasaccharide [m/z 911.3309¹⁻:GlcNAc β 1-3-Gal β 1-4GlcNAc β 1-3Gal β 1-4Glc β 1] (iii). (C) MS² spectrum of the precursor ion at m/z 505.1729¹⁻ and m/z 708.2518¹⁻ derived from Gb3 (i), nLc4 (ii) and nLc-penta (iii), respectively. PGC- LC allows for the separation of α 2-6 and α 2-3 sialylated *N*-glycans based on retention time. (D) The EICs obtained from the wildtype IGROV 1 depict three major monosialylated complex *N*-glycans at m/z 965.8385²⁻ [(Neu5Ac)₁(Gal)₂(GlcNAc)₂(Man)₃(GlcNAc)₂] (i), m/z 1038.8679²⁻ [(Neu5Ac)₁(Gal)₂(GlcNAc)₂(Fuc)₁(Man)₃(GlcNAc)₂] (ii) and m/z 1140.4081²⁻ [(Neu5Ac)₁(Gal)₂(GlcNAc)₃(Fuc)₁(Man)₃(GlcNAc)₂] (iii) and two monosialylated hybrid *N*-glycans at m/z 937.3278²⁻ [(Neu5Ac)₁(Gal)₁(GlcNAc)₁(Man)₁(Man)₃(GlcNAc)₂] (iv) and m/z 945.3247²⁻ [(Neu5Ac)₁(Gal)₁(GlcNAc)₁(Man)₂(Man)₃(GlcNAc)₂] (v) which display α 2-3 and α 2-6 sialylated isomers at separate retention times. (E) The EICs of genome-edited B3GNT5 cells depicts the loss of the α 2-6 sialylated isomer for all five of the above mentioned monosialylated complex [m/z 965.8385²⁻ (i), m/z 1038.8679²⁻ (ii), m/z 1140.4081²⁻ (iii)] and hybrid [m/z 937.3278²⁻ (iv), m/z 945.3247²⁻ (v)] *N*-glycans. (F) SNA staining confirmed reduction of α 2-6 sialylation in Δ B3GNT5 cells. Representative counter plot and barograph summarizing three independent experiments on parental IGROV1 cells (pIGROV1) and Δ B3GNT5 cells (KO_1 and KO_2); ** p -value < 0.01. Data are represented as mean \pm s.d.

time, as well as MS² fragmentation patterns facilitating the structural assignment of the GSL-glycans based on the fragment ions arising from various glycosidic and cross-ring cleavages. Table 1 shows the list of GSL-glycans and their relative intensities that were observed in both cell lines. The globo series glycosphingolipid, Gb3, was detected as [M-H]¹⁻ m/z 505.1729¹⁻ in wildtype and Δ B3GNT5 cells and was shown to elute at 12.16 min (Fig. 3A(i) and B(i)). The representative MS² spectra of the precursor ion at m/z 505.1729¹⁻ (Fig. 3C(i)) showed prominent glycosidic-type fragment ions (B₁ at m/z 161.0438¹⁻, C₁ at m/z 179.0541¹⁻) corresponding to the Gal-Gal-Glc trisaccharide sequence. The presence of the 4-linked terminal Gal to the inner (Gal-Glc) disaccharide was further confirmed by the characteristic cross ring fragment ion corresponding to ^{2,4}A₂ at m/z 221.0644¹⁻. The second glycan structure, paragloboside (nLc4), detected as [M-H]¹⁻ m/z 708.2518¹⁻ was found to be present only in the wildtype IGROV1 cell line but not in the Δ B3GNT5 cell line. This glycan was shown to elute at 22.60 mins (Fig. 3A(ii)) and the MS² spectra comprised of a mixture of B and Y ions (B₁ at m/z 161.0440¹⁻, Y₁ at m/z 181.0693¹⁻, Y₂ at m/z 343.6653¹⁻) as well as C and Z ions (Z₃ at m/z 528.1929¹⁻, C₂/Z₃ at m/z 202.0696¹⁻) that corresponded to the tetrasaccharide sequence, Hex-HexNAc-Gal-Glc (Fig. 3C(ii)). The absence of the

Type	No	Glycan Mass [M-H] ⁻	Glycan Structures	PGC-ESI-QTOF-MS/MS		PGC-ESI-IT-MS/MS
				IGROV1	B3GNT5-edited IGROV1	P ₁ -enriched IGROV1 (Anugraham M, et al, 2015)
Neutral GSL	1	505.2 (Pk)		6.34 ± 0.31	4.72 ± 2.38	0.00
	2	546.3		0.00	0.00	0.00
	3a	708.3 (Globo)		0.00	0.00	0.00
	3b	708.3 (Asialo-GM1)		0.00	0.00	0.00
	3c	708.3 (Neo-lacto)		4.52 ± 1.58	0.00	7.64
	4	870.3 (P1)		0.00	0.00	2.43
	5	911.3		1.25 ± 0.48	0.00	Trace
Sialylated GSL	6	634.2 (GM3)		14.18 ± 0.61	23.40 ± 4.32	12.86
	7	837.3 (GM2)		73.71 ± 2.40	71.88 ± 8.13	73.11
	8a	999.3 (GM1)		0.00	0.00	0.68
	8b	999.3 (α2-3 sialyl Paragloboside)		0.00	0.00	2.15
	8c	999.3 (LSTc)		0.00	0.00	1.14

Table 1. Proposed GSL-glycan structures detected on the glycolipid membranes of ovarian cancer cells, IGROV1 (wildtype) and Δ B3GNT5 cells. Structures were assigned based on MS/MS fragmentation (where possible) and known biological GSL synthetic pathway constraints. All structures were depicted according to the CFG (Consortium of Functional Glycomics) notation with linkage placement. Specific linkages corresponding to Gal-GlcNAc (Type 1/Type 2) lactosamine linkages are also indicated (where possible). Values represent mean relative ion intensities ± s.d. of three replicates based on their extracted ion chromatograms (EIC). GSL-glycan structures derived from P₁-enriched IGROV1 cell line previously analyzed with PGC-ESI-IT-MS (20) are also shown for comparative profiling using two different MS platforms. Gb3 (Pk). ● Glucose ● Galactose ■ N-acetylglucosamine (GlcNAc) ■ N-acetylgalactosamine (GalNAc) ◆ N-acetylneruaminic acid (NeuAc)

Monosaccharide Linkage:



cross ring cleavage ions characteristic of 4-linked GalNAc corresponding to ^{0,2}A₃ and ^{2,4}A₃ at *m/z* 484.1672¹⁻ and *m/z* 424.1460¹⁻, respectively, further confirmed the presence of the 3-linked GlcNAc residue to the inner Gal-Glc of the tetrasaccharide. The late elution time observed for this glycan structure has been reported in our previous study demonstrating a similar retention time for nLc4 identified from IGROV1 cell lines using PGC-LC-ESI-IT-MS/MS (20). We also identified a third glycan structure at [M-H]¹⁻ *m/z* 911.3309¹⁻ in wildtype IGROV1 which was shown to elute at 22.10 min (Fig. 3A(iii) and B(iii)). The MS² spectra comprised of mainly B-, C- and Y-type fragment ions (B₁ at *m/z* 202.0696¹⁻, C₂/Y₄ at *m/z* 179.0537¹⁻, B₃/Y₄ at *m/z* 364.7817¹⁻ and Y₃ at *m/z* 546.2020¹⁻) that corresponded to the tentative pentasaccharide sequence, HexNAc-Gal-HexNAc-Gal-Glc corresponding to a poly-LacNAc-type pentaosylceramide (Fig. 3C(iii)). The presence of the ^{1,3}A₂ at *m/z* 262.0874¹⁻ further confirmed the terminal GlcNAc linked to the internal tetrasaccharide. However, this structure was not

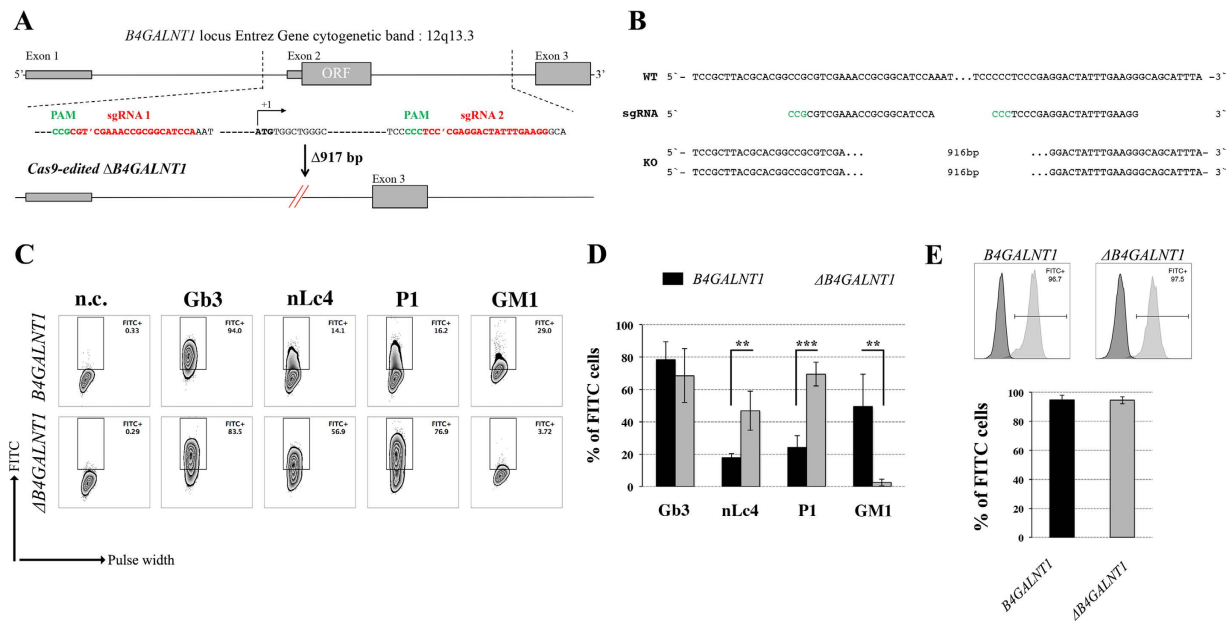


Figure 4. Loss of gangliosides by *B4GALNT1*-editing does not affect $\alpha 2-6$ sialylation in IGROV1 cells. (A) Depiction of CRISPR-Cas9-mediated *B4GALNT1* editing in IGROV1 cells using two different sgRNAs [red; PAM sequence (green)]. *In silico* analysis revealed a deletion of 917 bp including translation start site located at exon 2. (B) Verification of $\Delta B4GALNT1$ cells by DNA sequencing. (C) Representative flow cytometry zebra blot for parental IGROV1 and $\Delta B4GALNT1$ cells. (D) Bar chart summarizing three independent flow cytometry experiments. (E) SNA-staining remains unaffected in $\Delta B4GALNT1$ cells compared to IGROV1 (*B4GALNT1*). Data are represented as mean \pm s.d.

observed in the MS spectra of the $\Delta B3GNT5$ cell line. Whilst we were able to confirm the absence of nLc4 in the $\Delta B3GNT5$ cell line, the presence of the P₁ epitope was not readily detected in both the IGROV1 and $\Delta B3GNT5$ cells analyzed in this study. This could be due to the low expression of the P₁ epitope, coupled with the use of different MS instrumentation in this study (as compared to our previous study using PGC-LC-ESI-IT-MS/MS that was performed on P₁ - enriched cell populations of IGROV1¹³). Moreover, this study used a larger PGC column inner diameter on a conventional LC platform performed which resulted in less sensitivity as opposed to the microflow LC platform performed previously using PGC-ESI-IT-MS/MS. Apart from the neutral GSLs, two gangliosides were also detected in the MS spectra of both the wildtype and $\Delta B3GNT5$ cells. Both GM3 and GM2 were detected as [M-H]¹⁻ *m/z* 634.2142¹⁻ and [M-H]¹⁻ *m/z* 837.2926¹⁻, respectively, while the third ganglioside, GM1, at [M-H]¹⁻ *m/z* 999.3548¹⁻, did not appear to be present in both the cell lines (Table 1). These results indicate that gangliosides remained unaffected by the genome-editing of *B3GNT5*.

Isomeric N-glycan profiling reveals concomitant loss of $\alpha 2-6$ sialylation on membrane proteins in *B3GNT5*-mediated depletion of nsGSL. In addition to the profiling of the GSLs, we also compared the N-glycan profiles of the wildtype and $\Delta B3GNT5$ cell lines to gain an insight into the glycan structural changes, which could potentially be affected as a result of the GSL-related *B3GNT5* genome-editing. We have previously reported an increased relative abundance of $\alpha 2-6$ sialylation as compared to $\alpha 2-3$ sialylation on membrane N-glycans of IGROV1¹⁹. The presence of these isomeric structures in N-glycans can be differentiated based on their retention time on the porous graphitized carbon (PGC)-LC column, whereby glycans bearing the $\alpha 2-6$ sialic acid isomer are less strongly retained on the column and thus elute much earlier as compared to the $\alpha 2-3$ sialylated N-glycans. Likewise, in this study, a similar glycan elution pattern was observed in the wildtype IGROV1 cell lines confirming our previous results (which used another mass spectrometry setup), in which all five N-glycans comprising of the sialylated complex (*m/z* 965.8385²⁻, *m/z* 1038.8679²⁻, *m/z* 1140.4081²⁻) (Fig. 3D(i-iii)) and hybrid (*m/z* 937.3278²⁻ and *m/z* 945.3247²⁻) (Fig. 3D(iv-v)) glycans were found to contain $\alpha 2-6$ and $\alpha 2-3$ isomeric structures which eluted at separate retention times. Surprisingly, we noted that in comparison to the wildtype IGROV1, the genome-edited $\Delta B3GNT5$ cells were shown to display only the $\alpha 2-3$ sialylated glycans but not the $\alpha 2-6$ sialylated N-glycan isomer for all five of the N-glycan masses described above (Fig. 3E(i-v)). We also profiled the membrane protein O-glycans of both cell lines to see if the difference in the sialylation pattern could be attributed to a global glycosylation change across all glycan types. However, we observed no change in the O-glycan sialylation profiles, further demonstrating that the preferential $\alpha 2-6$ sialylation was specific to only the N-glycosylation pathway, as a result of the *B3GNT5* genome-editing. The N- and O-glycans identified in both cell lines and their corresponding relative intensities are shown in Table 2.

In order to confirm the reduction of $\alpha 2-6$ sialylation on membrane glycoproteins, we performed a staining using *Sambucus nigra* agglutinin lectin (SNA), which has been shown to bind preferentially to sialic acid attached to terminal galactose in *via* $\alpha 2-6$ linkage²⁰. The parental IGROV1 revealed positive staining (37% \pm 6% FITC⁺)

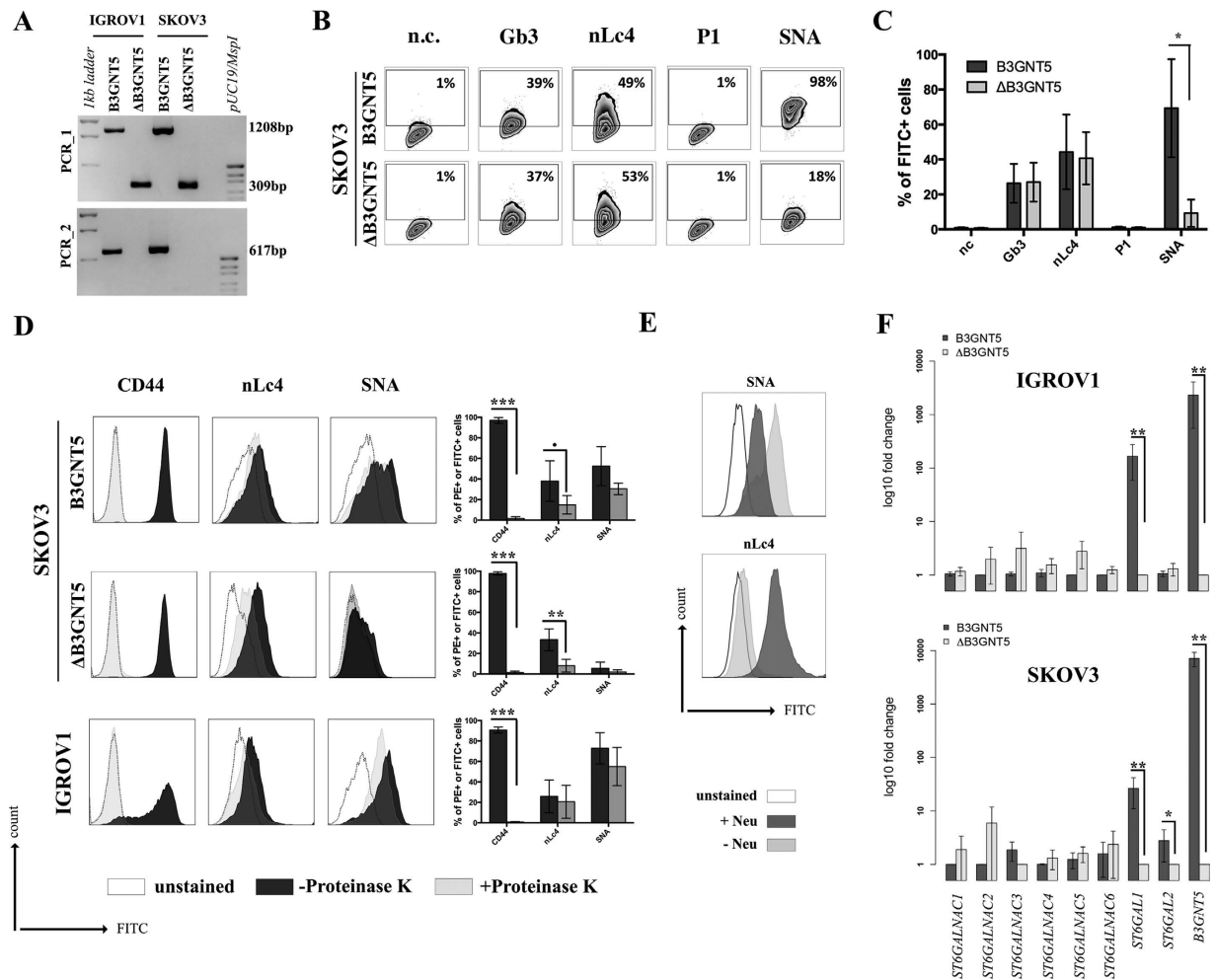


Figure 5. The reduction of α 2-6 sialylation occurs in two $\Delta B3GNT5$ ovarian cancer cell lines. (A) Representative genotyping PCR for $\Delta B3GNT5$ SKOV3 ovarian cancer cells. PCR_1, wildtype-specific PCR; PCR_2, deletion specific PCR. (B) Representative zebra plot for GSL expression in SKOV3 wildtype and $\Delta B3GNT5$ cells. (C) Quantified data from three independent flow cytometry experiments. (D) The epitope for anti-nLc4 antibodies is present on glycoproteins and glycosphingolipids in SKOV3 and IGROV1 cells, respectively. Proteinase K treatment on SKOV3, SKOV3 $\Delta B3GNT5$ and IGROV1 cells following staining for CD44, nLc4 and α 2-6 neuraminic acid (with SNA). Representative histogram for unstained (white), proteinase K untreated (dark gray) and proteinase K treated cells (light gray). Bar chart summarizes three independent experiments. $***p < 0.001$, $**p < 0.01$, $*p$ -value < 0.05 , p -value < 0.1 . (E) Histogram for IGROV1 cells treated with neuraminidase and stained for α 2-6 neuraminic acid (with SNA) and nLc4; unstained (white), neuraminidase treated (dark gray) and untreated cells (light gray). (F) Relative expression of genes encoding glycosyltransferase known to attach α 2-6 neuraminic acid to glycoproteins and glycosphingolipids. Bar chart shows the mean and standard deviation of three independent experiments of target genes (*ST6GALNAC1-6*, *ST6GAL1*, *ST6GAL2*, and *B3GNT5*) in wildtype (IGROV1 and SKOV3) and corresponding $\Delta B3GNT5$ cells. Data are represented as mean \pm s.d.

for α 2-6Neu5Ac whereas for both $\Delta B3GNT5$ cells, the expression of α 2-6 -linked Neu5Ac was significantly reduced (KO_1 = $2\% \pm 1.7\%$ and KO_2 = $6\% \pm 2.6\%$ FITC⁺) ($p < 0.01$; Fig. 3F), thereby confirming the loss of membrane protein α 2-6 sialylation.

α 2-6 sialylation is not affected in *B4GALNT1* ganglioside-depleted IGROV1 cells. Our current data demonstrate that the deletion of *B3GNT5* and consequently, the loss of nsGSLs, have unexpectedly led to the observation that α 2-6 sialylation is reduced on *N*-glycosylated proteins. To investigate whether this effect can be also observed when other GSL series are genome-edited, we utilized the CRISPR-*Cas9* to homozygously delete the *B4GALNT1* gene encoding for the beta-1,4-*N*-acetyl-galactosaminyltransferase-1 glycosyltransferase involved in the synthesis of gangliosides. IGROV1 cells were transfected with two sgRNA *Cas9*-encoding constructs to delete exon 2 of *B4GALNT1*, resulting in a 917 bp deletion (Fig. 4A). Clones identified as homozygously edited *B4GALNT1* knockout cells ($\Delta B4GALNT1$) were confirmed by DNA sequencing based on the deletion of 916 bp (Fig. 4B). Following measurement of GSL expression, as expected, we observed a significant reduction for

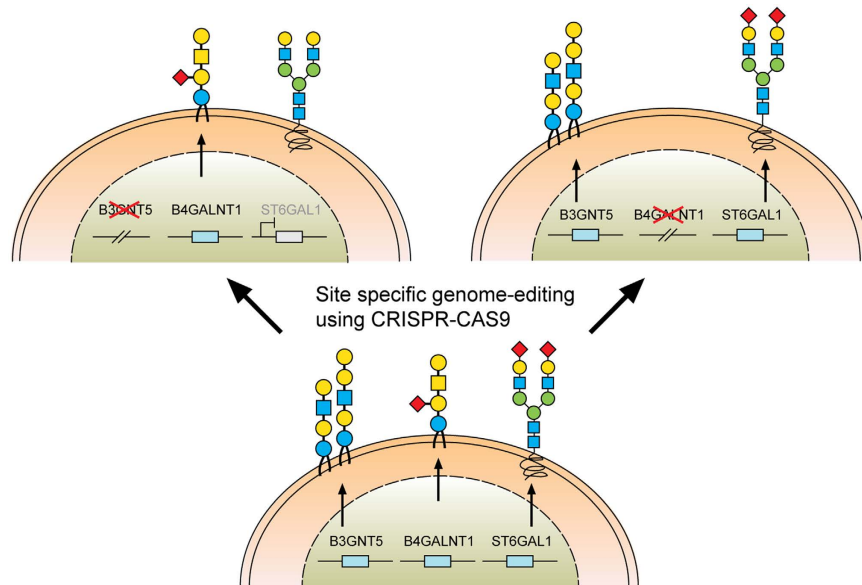


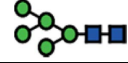
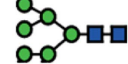
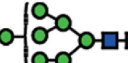
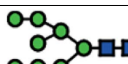
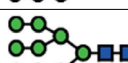
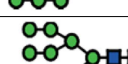
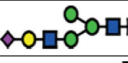

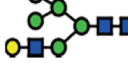


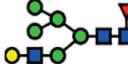
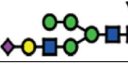
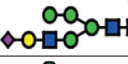
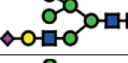

Figure 6. A model summarizing the interaction of specific glycolipid synthases on glycosphingolipids and N-glycosylation of proteins.

GM1 ($p < 0.01$) and no change in the expression of globoside Gb3 (Fig. 4C and D). In line with a previous report showing appearance of nLc4 after sialidase treatment in ganglioside-depleted mice²¹, we found that nLc4 and P₁ are significantly elevated in $\Delta B4GALNT1$ cells ($p < 0.01$, Fig. 4D). In regards to $\alpha 2-6$ sialylation, we did not observe a difference in SNA staining to IGROV1 cells compared to $\Delta B4GALNT1$ cells ($p > 0.05$, Fig. 4E). Taken together, CRISPR-Cas9 mediated disruption of *B4GALNT1* leading to loss of gangliosides did not subsequently alter $\alpha 2-6$ sialylation on glycosylated proteins in contrast to that observed for $\Delta B3GNT5$ cells.






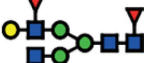
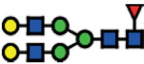
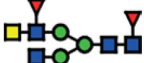



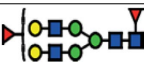
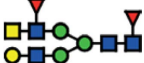

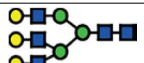



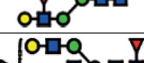




Loss of $\alpha 2-6$ sialylation is a result of silenced *ST6GAL1* expression in $\Delta B3GNT5$ cells. The reduction of $\alpha 2-6$ sialylation in $\Delta B3GNT5$ IGROV1 cells, prompted us to investigate whether this observation is constrained to a specific cell line or reproducible in another ovarian cancer cell line. Thus, we applied the genome-editing strategy as reported for IGROV1 (Figs 2A and 5A) in SKOV3 cells, which were chosen based on their expression of nLc4 and $\alpha 2-6$ sialic acid (Figs 1B and 5B). In contrast, Ls174T being positive for nLc4 and P₁ did not show $\alpha 2-6$ sialylation and was therefore not selected for genome-editing (Supplemental Fig. S4A). Analysis of the GSL expression in parental SKOV3 and corresponding $\Delta B3GNT5$ cells revealed only marginal changes for Gb3 and nLc4, whereas SNA staining was significantly reduced ($p = 0.0232$). This confirms what was previously observed in $\Delta B3GNT5$ IGROV1 cells, and further indicates that the disruption of *B3GNT5* leads to a reduction in $\alpha 2-6$ sialylation and may be a cell line-independent phenomenon (Fig. 5B and C).

It is interesting to note, however, that we did not observe any reduction of nLc4 in SKOV3 $\Delta B3GNT5$ cells (Fig. 5C). Thus, we hypothesized that besides GSLs, the antibody may also recognize the terminal nLc epitope (Gal $\beta 1-4$ GlcNAc) on N- and O-glycoproteins carrying Type II LacNAc (Gal $\beta 1-4$ GlcNAc) terminated antennae and therefore, the binding levels in SKOV3 $\Delta B3GNT5$ cells remained unchanged. To analyze whether the antibody-binding epitope is also carried on cell surface proteins, we treated SKOV3, SKOV3 $\Delta B3GNT5$, and IGROV1 cells with Proteinase K and performed staining for nLc4, SNA, and CD44. The latter was used as a control antigen (sensitive to Proteinase K treatment). As shown in Fig. 5D, cells subjected to Proteinase K treatment showed a complete loss of CD44 epitope, an ubiquitously expressed membrane protein, indicating that proteins on the cell surface are fully digested. In contrast, SKOV3 and SKOV3 $\Delta B3GNT5$ cells showed reduction of nLc4 staining after Proteinase K treatment whereas IGROV1 cells remained positive after nLc4 staining. This suggests that the nLc4 epitope was potentially present on cell surface proteins on SKOV3 as well as Ls174T cells (Supplemental Fig. S4B). In regards to $\alpha 2-6$ sialylation, Proteinase K treated cells showed only marginal reduction in SNA staining (Fig. 5D). Finally, IGROV1 cells (no reduction upon Proteinase K treatment for nLc4) were also treated with a broad-specificity neuraminidase to remove $\alpha 2-6/2-3$ -linked Neu5Ac, resulting in the reduction of SNA staining (Fig. 5E). This observation corroborated with a further increase in nLc4 staining, indicating that nLc4 on GSLs is terminated with Neu5Ac to form sialyl-3 or 6- paralogoside GSLs in IGROV1 cells and is further exposed on the cell surface upon de-sialylation. Taken together, our results provide evidence that apart from nLc4 expression on GSLs, the anti-nLc4 antibody epitope is also preferentially expressed on glycoproteins in SKOV3 cells, as indicated by the sustained presence of nLc4 in SKOV3 $\Delta B3GNT5$ cells and terminal nLc4 in GSLs may further be modified to form sialo-paralogosides, as observed in IGROV1 cells.


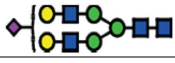
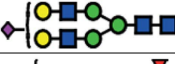







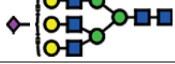






Next, we investigated whether mRNA expression of genes encoding sialyltransferases involved in the synthesis of $\alpha 2-6$ -sialoglycans is altered upon deletion of *B3GNT5*. RT-qPCR was established in concordance with MIQE guidelines²² and glyco-gene expression was normalized to the geometric mean of three independent reference genes (Supplemental Table S2). We profiled *ST6GALNAC1-6* and *ST6GAL1-2* in parental IGROV1 and SKOV3 as

Type	No	Glycan Mass [M-H] ⁻	[M-2H] ²⁻	Glycan Structures	PGC-ESI-QTOF-MS/MS		PGC-ESI-IT-MS/MS
					IGROV1	B3GNT5-edited IGROV1	IGROV1 (Anugraham M, <i>et al</i> , 2014)
N-glycans -High Mannose	1	1235.4	617.2		4.15 ± 0.11	5.54 ± 0.16	0.62 ± 0.06
	2	1397.6	698.3		5.31 ± 0.24	4.88 ± 0.64	7.91 ± 0.15
	3	1559.6	779.3		9.13 ± 0.27	9.48 ± 1.21	13.45 ± 1.35
	4	1721.6	860.3		19.19 ± 1.15	20.85 ± 1.57	16.00 ± 3.73
	5	1883.8	941.4		23.48 ± 2.02	22.29 ± 0.79	24.57 ± 6.02
	6	2045.6	1022.3		1.88 ± 0.21	1.73 ± 0.52	1.43 ± 0.61
N-glycans -Hybrid	7	1567.6	783.3		0.00	0.00	0.19 ± 0.03
	8	1584.6	791.8		0.00	0.00	0.34 ± 0.11
	9	1600.6	799.8		0.63 ± 0.01	0.83 ± 0.12	1.04 ± 0.30
	10	1713.6	856.3		0.00	0.00	1.76 ± 0.21
	11	1729.6	864.3		0.00	0.00	0.68 ± 0.20
	12	1746.6	872.8		0.00	0.00	0.20 ± 0.00
	13a	1875.6	937.3 (α2-6)		0.65 ± 0.03	0.00	0.20 ± 0.25
	13b	1875.6	937.3 (α2-3)		0.42 ± 0.05	0.74 ± 0.07	0.41 ± 0.20
	14a	1891.6	945.3 (α2-6)		1.34 ± 0.09	0.00	0.47 ± 0.22
	14b	1891.6	945.3 (α2-3)		0.67 ± 0.05	1.33 ± 0.17	0.43 ± 0.08

Continued

Type	No	Glycan Mass [M-H] ⁻	[M-2H] ²⁻	Glycan Structures	PGC-ESI-QTOF-MS/MS		PGC-ESI-IT-MS/MS
					IGROV1	B3GNT5-edited IGROV1	IGROV1 (Anugraham M, et al, 2014)
N-glycans -Complex Neutral Hybrid	15	1463.6	731.2		1.25 ± 0.20	1.36 ± 0.35	0.74 ± 0.03
	16	1625.6	812.3		0.00	0.14 ± 0.25	0.64 ± 0.14
	17	1641.6	820.3		0.62 ± 0.01	1.16 ± 0.18	1.59 ± 0.62
	18	1666.4	832.8		0.00	0.00	1.22 ± 0.40
	19	1682.6	840.8		0.00	0.00	0.12 ± 0.05
	20	1771.8	885.4		0.00	0.00	0.00
	21	1787.6	893.3		1.99 ± 0.05	3.48 ± 0.47	3.50 ± 0.22
	22	1812.8	905.9		0.00	0.00	0.24 ± 0.08
	23	1828.8	913.9		0.00	1.30 ± 0.34	0.66 ± 0.12
	24	1844.8	921.9		1.25 ± 0.06	2.01 ± 0.09	1.37 ± 0.19
	25	1869.8	934.4		0.00	0.19 ± 0.33	0.51 ± 0.20
	26	1933.6	966.3		1.23 ± 0.78	1.15 ± 0.13	0.00
	27	1974.8	986.9		0.18 ± 0.31	0.00	0.79 ± 0.28
	28	1990.8	994.9		6.29 ± 1.36	8.23 ± 0.73	2.62 ± 0.60
	29	2006.8	1002.9		1.84 ± 0.39	1.75 ± 0.61	0.31 ± 0.15
	30	2015.8	1007.4		0.00	0.00	0.14 ± 0.06
	31	2079.8	1039.4		0.00	0.00	0.00
	32	2120.8	1059.9		0.00	0.00	0.56 ± 0.19
	33	2136.6	1067.8		2.32 ± 0.27	3.44 ± 0.35	0.31 ± 0.15
	34	2152.8	1075.9		0.77 ± 0.40	1.47 ± 0.95	1.18 ± 0.16
	35	2162	1080.5		1.22 ± 0.22	0.25 ± 0.15	0.39 ± 0.09
	36	2356	1177.5		0.84 ± 0.07	1.13 ± 0.14	0.23 ± 0.02
	37	2518	1258.5		1.88 ± 0.24	1.20 ± 0.22	0.37 ± 0.10

Continued

Type	No	Glycan Mass [M-H] ⁻	[M-2H] ²⁻	Glycan Structures	PGC-ESI-QTOF-MS/MS		PGC-ESI-IT-MS/MS
					IGROV1	B3GNT5-edited IGROV1	IGROV1 (Anugraham M, <i>et al</i> , 2014)
N-glycans -Complex Sialylated Hybrid Complex Sialylated	38	1916.6	957.8		0.00	0.00	0.21 ± 0.06
	39a	1932.8	965.9 (α2-6)		1.41 ± 0.11	0.00	1.38 ± 0.38
	39b	1932.8	965.9 (α2-3)		0.86 ± 0.05	1.28 ± 0.24	1.86 ± 0.49
	40a	2078.8	1038.9 (α2-6)		4.96 ± 0.35	0.00	1.91 ± 0.23
	40b	2078.8	1038.9 (α2-3)		1.68 ± 0.16	3.94 ± 0.27	3.23 ± 0.14
	41	2119.8	1059.4		0.00	0.00	0.36 ± 0.15
	42	2223.8	1111.4		0.00	0.00	0.41 ± 0.07
	43	2265.8	1132.4		0.00	0.00	0.06 ± 0.02
	44a	2282.0	1140.5 (α2-6)		1.35 ± 0.11	0.00	0.35 ± 0.14
	44b	2282.0	1140.5 (α2-3)		1.20 ± 0.34	2.30 ± 0.06	0.30 ± 0.17
	45	2297.8	1148.4		0.00	0.00	0.23 ± 0.02
	46	2370.0	1184.5		0.00	0.00	1.33 ± 0.36
	47	2411.0	1205		0.00	0.00	0.06 ± 0.02
	48	2444.0	1221.5		1.30 ± 0.46	0.00	0.65 ± 0.07
	49	2589.0	1294.0		0.00	0.00	0.03 ± 0.00
	50	2735.0	1367.0		0.00	0.00	0.03 ± 0.00
51	3026.0	1512.5		0.00	0.00	0.19 ± 0.08	

Continued

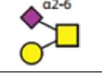

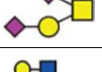
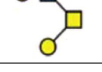
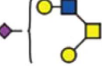
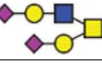






Type	No	Glycan Mass [M-H] ⁻	[M-2H] ²⁻	Glycan Structures	PGC-ESI-QTOF-MS/MS		PGC-ESI-IT-MS/MS
					IGROV1	B3GNT5-edited IGROV1	IGROV1 (Anugraham M, et al, 2014)
O-glycans	1a	675.3	NA		9.10 ± 2.32	13.08 ± 2.43	NA
	1b	675.3	NA		31.55 ± 4.19	27.59 ± 2.21	NA
	2	966.3	NA		52.11 ± 2.60	52.25 ± 0.59	NA
	3	749.3	NA		0.00	0.00	NA
	4	1040.5	NA		7.24 ± 1.26	7.08 ± 0.44	NA
	5	1331.5	NA		0.00	0.00	NA

Table 2. Proposed N- and O-glycan structures detected on the membrane proteins of IGROV1 (wildtype) and Δ B3GNT5 cells. N- and O-glycan structures were separated by PGC-UHPLC-ESI-QTOF and their structures were assigned based on MS/MS fragmentation (where possible), retention time differences and biological pathway constraints. Structures were depicted according to the Consortium of Functional Glycomics (CFG) notation with linkages (α 2, 3 and α 2, 6) indicated for sialic acid (where known). Values represent mean relative ion intensities \pm SD of three replicates based on their extracted ion chromatograms (EIC). N-glycan structures derived from IGROV1 cell line previously analyzed with PGC-ESI-IT-MS^{13,19} are also shown for comparative profiling using two different MS platforms.  Galactose  Mannose  Fucose  N-acetylglucosamine (GlcNAc)  N-acetylgalactosamine (GalNAc)  N-acetylneuraminic acid (NeuAc; sialic acid).

well as their corresponding Δ B3GNT5 cells. Apart from the expected change in *B3GNT5* mRNA levels, *ST6GAL1* expression was found to be significantly decreased in both Δ B3GNT5 cells of up to 166-fold for IGROV1 (Fig. 5F). The expression of the remaining sialyltransferases encoding genes examined was not significantly altered in the wildtype and Δ B3GNT5 cells, except for *ST6GAL2* in SKOV3 cells (Fig. 5F). In addition, *ST6GAL1* expression in parental and IGROV1 Δ B4GALNT1 cells revealed equal gene expression levels (Supplemental Fig. S5), corroborating with no changes observed in SNA staining. In conclusion, these results indicate that the disruption of *B3GNT5* and the corresponding loss of α 2-6 sialylation on N-glycans appear due to the preferential silencing of *ST6GAL1* gene expression in both ovarian cancer cell lines, IGROV1 and SKOV3 (Fig. 6).

Discussion

The advent of novel nuclease-based precision genome-editing techniques is starting to revolutionize the field of glycobiology, enabling stable gene editing and potentially unravelling the roles of glyco-related genes and their corresponding glycosyltransferases in mammalian cell lines. This technology was first demonstrated by Henrik Clausen and his colleagues, through the introduction of the ‘Simple Cell’ strategy, to study the role of truncated O-glycans in malignant diseases^{23,24}, specificity of anti-glycopeptide antibodies²⁵, profile and map the human O-GlcNAc glycoproteome^{26,27}, and produce novel antibodies to defined glycopeptides²⁸. Whilst a majority of this work is based on O-glycans, there is very limited information on the use of genome-editing for glycosphingolipids (GSLs) and in particular, the nsGSLs. Here, we utilized CRISPR-Cas9 nuclease genome-editing to explore the role of *B3GNT5*, the key glycosyltransferase responsible for the synthesis of precursor Lc3 that is extended to form the lacto (Type I) and neo-lacto (Type II) series GSLs⁶. For the first time, using a combination of genomic-level editing and cell surface membrane protein and GSL-glycan profiling, we provide valuable insights into the complex interplay regulating the expression of linkage-specific α 2-6 sialo-N-glycans on proteins as a consequence of GSL disruption. We demonstrate that by mutating *B3GNT5*, the depletion of nsGSLs consequently affects α 2-6 sialylation on N-glycoproteins, not only at the cellular level, but also through the silencing of the corresponding *ST6GAL1* gene.

As evidenced in this study, the genomic deletion of *B3GNT5* resulted in the loss of the (neo-) lacto paragloboside (nLc4, Gal β 1-4GlcNAc β 1-3Gal β 1-4Glc β 1-1Ceramide) as well as P₁ (Gal α 1-4Gal β 1-4GlcNAc β 1-3Gal β 1-4Glc β 1-1Ceramide), a pentasaccharide moiety of which has not been annotated in the KEGG database so far. We recently reported the presence of the P₁ glycan in tissue samples¹⁴ as well as on P₁-enriched IGROV1 ovarian cancer cell lines¹³, serving as a cell-recognition molecule through its binding to naturally occurring anti-glycan antibodies^{14,29}. The presence of nLc4 and P₁ was detected on IGROV1 cells using flow cytometry, in which P₁ was detected using P3NIL100 antibody, a well-validated monoclonal IgM antibody shown to specifically recognize the chemically synthesized P₁ trisaccharide (Gal α 1-4Gal β 1-4GlcNAc β -), as indicated by glycan array profiling performed in this study. Both the flow cytometry and high-resolution ESI-QTOF-MS and MS/MS profiles confirmed that the levels of nLc4 were reduced, while the globo (Gb3) and ganglio (GM3, GM2 and GM1)- series

GSL glycans remained unaffected in $\Delta B3GNT5$ cells. The presence of P_1 , however, was not detected on the parental IGROV1 cells by the mass spectrometry approach applied, possibly due to the low detection levels of P_1 on non- P_1 enriched IGROV1 cells used in this study, as well as the use of a different mass spectrometric platform. Nevertheless, we also observed that apart from IGROV1, the colon cancer cell line, Ls174T, showed detectable levels of P_1 providing further evidence that P_1 is not exclusively present on erythrocytes^{30–32}. The results obtained herein support that the pentasaccharide P_1 is indeed exclusively present as an nsGSL-glycan on membrane glycolipids and not on glycoproteins.

To date, it remains unclear if nLc4- and P_1 - GSL glycans are functionally relevant molecules in diseased states such as cancer and infection or if they are ubiquitously expressed. In regards to pathogenic infections, it has been previously shown that *Helicobacter pylori* induces *B3GNT5* expression and that the ABO(H)/Lewis blood group antigens expressed in *H. pylori*-infected individuals act as receptors for BabA, thereby facilitating colonization of the gastric niche³³. Likewise, the *Shiga* toxin from urinary tract infection-causing enterohemorrhagic *E. coli* was shown to recognize the terminal epitope of P_1 , Gal α 1-4Gal β 1-4 following internalization of the toxin by receptor-mediated endocytosis³⁴. Another study also showed that the *Shiga*-like toxin binds to P_1 trisaccharide on core 2 *O*-glycoproteins in overexpressed CHO cells³⁵. These findings indicate that this toxin may recognize P_1 pentasaccharide. It is evident that the successful *B3GNT5* deletion performed in this study may be further applied to investigate the lectin binding specificities (e.g. *Shiga* toxin) in other human cancer cell lines expressing Gb3, nLc4 and P_1 .

Perhaps, the most intriguing finding from this study is the unexpected loss of α 2-6 sialylation observed using mass spectrometry in $\Delta B3GNT5$ cells which was further substantiated by SNA lectin staining on cultured cells and reduced *ST6GAL1* mRNA expression. We have previously shown in two separate studies, respectively, that ovarian cancer cells, IGROV1 and SKOV3, have higher levels of glycoprotein α 2-6 sialylation as compared to non-cancer ovarian epithelial cells¹⁹ and nLc4 and P_1 are both expressed on IGROV1 and ovarian cancer tissue-derived GSL-glycans¹³. Hence, the reduction of α 2-6 sialylation as a direct consequence of the *B3GNT5* deletion in ovarian cancer cells is indicative of their complex associations within the glycan-processing pathway. A recent publication reported a similar finding in the context of the rare autosomal recessive salt and pepper syndrome³⁶. In this study, a homozygous transition mutation in the gene encoding sialyltransferase *ST3GAL5* (GM3 synthase) was described. More importantly, in addition to the reduced GSL complexity, the comprehensive glycomics analysis performed using mass spectrometry also revealed altered *N*- and *O*-glycans on proteins due to the point mutation in the *ST3GAL5*³⁶. In another study on respiratory chain disorders, the authors observed significant increases of Gb3 and Gb4 and a decrease of LacCer in fibroblasts^{36,37}. Similarly, the appearance of unexpected gangliosides in homozygously deleted *ST3GAL5* murine primary embryonic fibroblast cells was also reported³⁸. Despite the limited number of publications, our current study provides another example on how a loss of a specific glycosyltransferase interferes with glycomic changes, as observed in the reduction of α 2-6 sialylation on *N*-glycoproteins, thereby recognizing the contribution of altered GSL expression in cell development and function. It is not known whether the loss of α 2-6 sialylation is thought to provide a compensation phenotype for the depleted nsGSLs in these cells or enables them to survive despite the glycan changes. It is also unclear as to how the *ST6GAL1* is regulated in the context of their translocation within the Golgi membrane or their accessibility to the membrane proteins. It will be useful to further characterize membrane proteins bearing these sialylated *N*-glycans and observe corresponding changes in the proteome profiles of *B3GNT5*-edited ovarian cancer cells.

Of note, despite similar observations in two independent ovarian cancer cell lines and due to our carefully designed sgRNAs in a way to minimize the probability of off-target activity; we cannot exclude unintended changes in the genome of our genome-edited ovarian cancer cell lines. Here, an unbiased approach would be necessary to exclude mutations anywhere in the genome³⁹. Therefore, the most reliable method would be whole genome sequencing⁴⁰. A direct *in situ* breaks labeling, enrichment on streptavidin, and next-generation sequencing also referring to BLESS⁴¹ as well as linear amplification-mediated high-throughput genome-wide translocation sequencing (HTGTS)⁴² can also be applied as less expensive alternatives to track genomic alterations caused by off target *Cas9*-activity.

In conclusion, the investigation of CRISPR-*Cas9*-mediated deletion of glycosyltransferase in ovarian cancer cells, coupled with the use of MS-based glycomics profiling, serve as a useful model for future studies to elucidate the biological roles of nsGSLs, an important group of GSLs which may be involved in specific cell physiology functions. More importantly, the prominent changes in *N*-glycoprotein sialylation detected in the *B3GNT5* genome-edited cells are reflective of global alterations in one or more regulatory components essential for glycan biosynthesis, thereby warranting further research efforts into the complex and overlapping roles of glycosyltransferases involved in the downstream glycan biosynthesis pathways.

Methods

Cell culture. Cell lines (HOSE17.1, IGROV1, SKOV3, BG1, CAO3, Ls174T, HeLa, HCT15, and HCT116) were grown in RPMI1640 media supplemented with 10% fetal bovine serum (FBS), penicillin (100 U/ml) and streptomycin (100 μ g/ml) (Sigma-Aldrich, Buchs, Switzerland). Fallopian tube cell lines FT33 Tag, FT190, and FT237 (kind gifts by Dr. Drapkin) were cultured in DMEM F12/50 without HEPES supplemented with 2% (v/v) Ultrosor (USG, Pall Corporation, USA) and penicillin/streptomycin. All cell lines were cultured at 37 °C in a 95% humidified atmosphere containing 5% CO₂. Cell lines were short tandem repeat (STR) profiled and routinely tested for mycoplasma infection⁴³.

Antibodies and reagents. Primary antibodies to detect the cell surface-associated GSLs were applied as described previously¹⁵. Briefly, the following primary antibodies were utilized; rat IgM anti- P^k (Gb3) antibody (ABDserotec, Germany); mouse IgM anti-nLc4 (paragloboside) antibody [clone 1B2 kindly provided by Prof.

Mandel and Prof. Clausen, Denmark]⁴⁴; human IgM anti-P₁ antibody (Millipore, Germany), and Cholera toxin B subunit (Sigma-Aldrich, Switzerland) to detect GM1. All secondary antibodies (mouse anti-rat IgM antibody conjugated to biotin, rat anti-mouse IgM conjugated to biotin and mouse anti-human IgM conjugated to biotin) were obtained from BD Pharmingen. Cell surface GSL expression was visualized with FITC conjugated to streptavidin (BD Pharmingen). Non-viable cells were positively stained with 7-amino-actinomycin D (BD Pharmingen). Isotype controls for each primary antibody used included the following: purified rat IgM (BD Pharmingen), purified mouse IgM and chimpure human IgM (Jackson ImmunoResearch, USA). Alpha 2-6 sialylation on the cell surface was investigated using *Sambucus nigra* lectin (SNA) conjugated to biotin (Vector Laboratories, Reactolab, Servion, Switzerland). Lectin staining was visualized with streptavidin conjugated to FITC. Anti human CD44-PE antibody was purchased from Miltenyi Biotec (Bergisch Gladbach, Germany) for use as a positive control in Proteinase K treatment.

CRISPR-Cas9 sgRNA design and construction. The design of sgRNAs was carried out using the online program available from Zhang's laboratory⁴⁵. This program provides additional information about the quality of sgRNA by giving it a score value of up to 100 and additionally, the number and sites of potential off targets. Designed and processed sgRNAs to edit either *B3GNT5* or *B4GALNT1* (Supplemental Table S1) were cloned into pSpCas9(BB)-2A-GFP (addgene PX458) via *BsBI* restriction site using T4 DNA Ligase (Promega, Dübendorf, Switzerland).

IGROV1 and SKOV3 cells were transfected using ViaFect Transfection reagent (Promega, Dübendorf, Switzerland). A total of $4-5 \times 10^5$ cells were seeded into 6-well plates, cultured for 24 h and transfected with 2.5 μ g of pSpCas9(BB)-2A-GFP. Cells were harvested after 72 h and subjected to single cell sorting.

Flow cytometry-based single-cell sorting. IGROV1 transfected with pSpCas9(BB)-2A-GFP targeting either *B3GNT5* or *B4GALNT1* were grown for 72 h, washed twice in PBS and harvested using non-enzymatic cell dissociation buffer (Sigma-Aldrich, Buchs, Switzerland). Cells were then resuspended in RPMI containing 10% FCS before single cell sorting was performed on a BD FACS Vantage SE DiVa Cell Sorter (BD Biosciences). Cells sorted for single DAPI⁻ and GFP⁺ cells were seeded into 96-well flat-bottom plates with pre-warmed RPMI containing 10% FCS. Plates were incubated for 2 to 3 weeks following transfer to 48-well plates, prior to genomic DNA isolation for genotyping PCR to characterize single cell clones.

Genotyping PCR. Selected clones were characterized by three to four PCRs using appropriate primer pairs (Supplemental Table S1). PCR was performed using 1x GoTaq Green Master Mix (Promega, Dübendorf, Switzerland), 200 nM primer (Supplemental Table S1) and 30 ng gDNA and carried out on a Biometra Professional Trio cycler. PCR was performed under the following conditions: initial denaturation at 94 °C for 1 min followed by 33 cycles consisting of denaturation at 94 °C for 15 sec, annealing at 59 °C for 15 sec, and elongation at 72 °C for 15–45 sec depending on the amplicon length. The PCR products were separated on a 1.7% agarose gel.

Sanger DNA Sequencing. PCR products were cloned into pGEM[®]-T Easy Vector System (Promega) according to the manufacturer's protocol. DNA sequencing was performed by Source Bioscience Life Sciences (Berlin, Germany). Samples were shipped at a concentration of 100 ng/ μ l with specific primer (if required) concentration of 3.2 pg/ μ l.

Off target screening. Potential off target sites were amplified (Supplemental Table S1), cloned into pGEM[®]-T Easy Vector System (Promega) and sequenced. A total of three colonies per clone were selected for sequencing.

Reverse transcription semi-quantitative PCR (RT-qPCR) using total RNA. Total RNA was extracted from 80% confluent 6-well plates seeded initially with 1×10^5 cells. Cells were then washed twice with sterile PBS and total RNA was extracted using the ReliaPrep RNA Cell Miniprep System (Promega, Dübendorf, Switzerland). RNA was eluted in 60 μ l RNase free water and RNA concentration was measured using NanoDrop ND-1000 spectrophotometer (Thermo Fisher Scientific, Roskilde, Denmark).

Total RNA (500 ng) was reverse-transcribed using the iScript Reverse Transcription Supermix for RT-qPCR (Bio-Rad Laboratories, Zurich, Switzerland) in a total volume of 10 μ l according to the manufacturer's instructions. RT-qPCR was performed on target and reference genes (*HSPCB*, *SDHA*, and *YWHAZ*) in 10 μ l reactions containing 10 ng cDNA (initial total RNA), 400 nM forward and reverse primer (Supplemental Table S2), nuclease free water and 1x GoTaq[®] qPCR Master Mix with low ROX as the reference dye (Promega, Dübendorf, Switzerland) on a ViiA[™] 7 Real-Time PCR System (Applied Biosystems, Thermo Fisher Scientific, Reinach, Switzerland). Quantitative PCR was performed on three independent experiments, in triplicates, and analyzed as recently described^{19,46}. Each quantitative PCR was further established with a series of six 10-fold dilutions to calculate the efficacy of each reaction and to determine the optimal range of initial mRNA concentration for analysis (Supplemental Table S2).

Flow cytometry. Immuno staining and flow cytometry was performed as previously described^{14,15}. Biotinylated SNA lectin (1:500) containing 10 mM CaCl₂ was applied for detection of α 2-6 neuraminic acid using flow cytometry (BD Accuri[™] C6, BD Bioscience).

Membrane protein extraction and N- and O-glycan release of parental and Δ B3GNT5 IGROV1 cell lines. Membrane protein extraction and glycan release were carried out as previously described¹⁹.

Briefly, approximately 2×10^7 IGROV1 and $\Delta B3GNT5$ IGROV1 cells were washed with PBS and homogenized in lysis buffer (50 mM Tris-HCl, 100 mM NaCl, 1 mM EDTA and protease inhibitor, pH 7.4). Unlysed cells were pelleted through centrifugation and cellular membranes in the supernatant was subjected to ultra-centrifugation at 120,000 g prior to Triton X-114 phase partitioning of membrane proteins. Membrane proteins were acetone-precipitated, solubilized in 8 M urea and spotted onto polyvinylidene difluoride (PVDF) membrane spots placed in a 96-well microtiter plate. Protein spots were treated with PNGase F enzyme and released *N*-glycans were treated with 100 mM ammonium acetate (pH 5.0) and reduced to alditols with 2 M NaBH₄ in 50 mM KOH. For *O*-glycans, the remaining PVDF spots in the 96-well microtiter plate were further subjected to reductive β -elimination by treatment with 0.5 M NaBH₄ in 50 mM KOH to chemically release the *O*-glycans. Both the released *N*- and *O*-glycans were desalted by cation exchange chromatography as previously described and re-suspended in 15 μ l of MilliQ water prior to mass spectrometry analysis.

GSL extraction and enzymatic release of GSL-glycans from cell lines. Lipid extraction and release of GSL-glycans were performed as previously described¹³. Briefly, GSLs were extracted from approximately 2×10^7 parental and $\Delta B3GNT5$ IGROV1 cells using a modified Folch extraction method. Cell pellets were treated with chloroform: methanol (2:1) and subjected to centrifugation. The supernatants were evaporated to dryness and crude GSL fractions were re-dissolved in 50 μ l of chloroform: methanol (2:1). Approximately 10 μ l of GSL standard (neutral glycosphingolipids: LacCer, Gb3 and Gb4) and 50 μ l of extracted GSLs were spotted onto the PVDF membrane and treated with 4 mU (2 μ l) of Endoglycoceramidase II. GSL-glycans released from the immobilized GSL spots were reduced to alditols with 0.5 M NaBH₄ in 50 mM KOH and desalted by cation exchange chromatography as previously described for *N*- and *O*-glycans.

PGC-UHPLC-ESI-QTOF-MS/MS profiling of released GSL- and N- and O-glycan alditols. The separation of glycan alditols was performed using an Agilent UHPLC modular system consisting of a degasser, binary pump, auto-sampler, thermostat and column oven (Agilent Series 1290, Agilent Technologies, Germany). The conventional flow LC system was connected to a mass spectrometer (MS) (Agilent Series 6540 Q-TOF, Agilent Technologies, USA) operating in negative mode and coupled to a jet stream electrospray ion source (ESI) as previously described for *N*- and *O*-linked glycans⁴⁷. Briefly with some slight modifications for GSL-derived glycans, an aliquot of 14 μ l of sample was injected onto the Hypercarb porous graphitized carbon (PGC) analytical column (ID2.1 \times 150 mm column; 3 μ m particle size) (Thermo Fisher Scientific, United Kingdom). The column compartment was maintained at 40 °C. The mobile phase was made up of 10 mM ammonium bicarbonate (A) and 9:1 acetonitrile/water with 10 mM ammonium bicarbonate (B). The chromatographic separation was held with the initial mobile phase composition (1% B; 0–5 mins), followed by a segmented linear gradient to 25% B (5–40 mins), 50% B (40–42 mins) and a fast step at 42.5 mins to 80% B, with a hold for 1.5 mins. The ESI source was operated with the following parameter settings: nebulizer pressure (35 psig), nozzle voltage (0 V), sheath gas flow (11 L/min), sheath gas temperature (375 °C), drying gas flow (8 L/min), drying gas temperature (250 °C), capillary voltage (4000 V) and fragmentor voltage (175 V). High-resolution MS scan (*m/z* 100–1700 at 1.5 Hz) and MS/MS product scan (*m/z* 50–1700 at 3 Hz) were acquired with information-dependent acquisition (IDA) with static exclusion range *m/z* 100–300. An automated mass calibration performed by delivering constantly two reference masses (*m/z* 119.0363 and *m/z* 981.9956) on the end plate of the ESI source to obtain the highest mass accuracy during the measurement. Data analysis was performed with MassHunter B.06.00 (Agilent Technologies, USA). The monosaccharide compositions of monoisotopic masses were determined using GlycoMod tool (<http://web.expasy.org/glycomod/>) with a mass error of ± 0.5 Da. The proposed glycan structures were manually assigned and interpreted based on MS/MS fragmentation patterns of known GSL-derived glycans¹³ and annotated using GlycoWorkBench 2.1 software⁴⁸. In addition, UniCarb KB, a web-based LC-MS/MS database⁴⁹, was also utilized to confirm fragmentation and retention time of sialylated *N*-glycans previously reported to contain sialylated isomers¹⁹. Blank samples, fetuin glycoprotein with isomeric glycan compositions and reference glycolipid standards which served as quality control for sample preparation were randomly measured within each sequence run and checked for background contamination.

Confocal fluorescence microscopy. Cells were grown on polylysine glass slides attached to an 8-well chamber, fixed with 4% para-formaldehyde for 15 min and blocked with 5% (w/v) BSA fraction V (Sigma) dissolved in PBS for 1 h. Cells were then stained with either anti-P₁ IgM¹⁵ (1:5 diluted with incubation buffer (1% BSA in PBS)) or anti-nLc4 (paragloboside) antibody (1:5) for overnight at 4 °C. Following extensive washing corresponding secondary antibodies (Biotin-anti-human IgM (1:100), Biotin-anti-mouse IgM (1:100)) were added to each chamber and incubated for 2 h at 4 °C. Afterwards, cells were washed with PBS and incubated with Streptavidin-FITC (1:200) for 1 h at 4 °C and counterstained with DAPI (Cell Signaling Technology). Fluorescence images were taken with a Zeiss LSM 710 confocal microscope (Zeiss, Feldbach, Switzerland).

Printed Glycan Array. The printed glycan array was performed as previously described with modifications^{29,50,51}. Briefly, glycan arrays were prepared by covalent attachment of amino-spacer synthetic glycans to *N*-hydroxysuccinimide-activated Schott-Nexterion slides. Chemically synthesized carbohydrates with 95–98% purity were used for printing and obtained from Lectinity Holdings (Moscow, Russia) and the Consortium for Functional Glycomics (CFG). The slides were washed for 15 min with 0.1 M PBS (0.01 M Na₂HPO₄, 0.01 M NaH₂PO₄, 0.138 M NaCl, and 0.0027 M KCl, pH 7.4) containing 0.1% Tween-20. Anti-P₁ antibodies were diluted 1:50 in PBS containing 1% BSA. The slides with antibody solution were shaken for 1 h and incubated under relative humidity and temperature of 80% and 37 °C, respectively. The slides were washed with PBS and labeled with secondary antibodies consisting of goat anti-human IgM conjugated with Alexa647 (Invitrogen, USA), which was diluted with PBS (1:250). After incubation, the slides were washed with PBS containing 0.001% Tween 20

and subsequently with bi-distilled water and the fluorescence intensity was measured using a confocal ScanArray Gx scanner (PerkinElmer, USA) with 5 µm resolution. The obtained data were processed using ProScanArray Express 4.0 software.

Proteinase K treatment. Proteinase K treatment was carried out as previously described⁵². Briefly, single-cell suspension of 2×10^6 IGROV1, Ls174T, SKOV3 and B3GNT5 - edited SKOV3 cells were treated with PBS containing 100 µg/mL proteinase K enzyme (Promega) for 1 h at 37 °C with intermittent shaking. At the same cell density the control cells were also resuspended in PBS without proteinase K. The enzymatic reaction was stopped by adding phenyl methyl sulfonyl fluoride (PMSF) at a concentration of 1 mM/mL and incubated on ice for 10 min. Cells were then fixed with 1% PFA on ice for 15 min and washed twice with 5 mL PBS and pelleted at 1200 rpm for 7 min at 4 °C. Finally, fixed cells were stained with SNA, nLc4 or anti-human CD44 antibody for flow cytometric analysis as previously described.

Neuraminidase treatment. To remove the cell surface neuraminic acids, neuraminidase treatment was performed with α 2,3-6, -8,- neuraminidase (New England BioLabs, UK) according to manufacturer's instructions. In brief, IGROV1 cells (1×10^6) were fixed with 4% paraformaldehyde in PBS at room temperature for 15 min, and then washed with PBS twice. Cells were resuspended in 200 µl of glycobuffer (1x) containing 25 Units of the enzyme and incubated at 37 °C for 2 h. Cells were washed with PBS and followed by SNA staining and flow cytometry.

Statistical analysis. Experiments were performed in triplicates and comparisons were statistically evaluated with two-tailed Student's *t*-test. *P* values of <0.05 were considered statistically significant (****p* < 0.001, ***p* < 0.01, **p*-value < 0.05, *p*-value < 0.1.).

References

- Widmer, M. *et al.* Performance of native and recombinant antigens for diagnosis of *Helicobacter pylori* infection. *European journal of clinical microbiology & infectious diseases: official publication of the European Society of Clinical Microbiology* **18**, 823–826 (1999).
- Coskun, U., Grzybek, M., Drechsel, D. & Simons, K. Regulation of human EGF receptor by lipids. *Proceedings of the National Academy of Sciences of the United States of America* **108**, 9044–9048, doi: 10.1073/pnas.1105666108 (2011).
- Kim, S. J. *et al.* Ganglioside GM3 participates in the TGF β 1-induced epithelial-mesenchymal transition of human lens epithelial cells. *The Biochemical journal* **449**, 241–251, doi: 10.1042/BJ20120189 (2013).
- Chung, T. W. *et al.* Ganglioside GM3 inhibits VEGF/VEGFR-2-mediated angiogenesis: direct interaction of GM3 with VEGFR-2. *Glycobiology* **19**, 229–239, doi: 10.1093/glycob/cwn114 (2009).
- D'Angelo, G., Capasso, S., Sticco, L. & Russo, D. Glycosphingolipids: synthesis and functions. *The FEBS journal* **280**, 6338–6353, doi: 10.1111/febs.12559 (2013).
- Togayachi, A. *et al.* Molecular cloning and characterization of UDP-GlcNAc:lactosylceramide beta 1,3-N-acetylglucosaminyltransferase (beta 3Gn-T5), an essential enzyme for the expression of HNK-1 and Lewis X epitopes on glycolipids. *The Journal of biological chemistry* **276**, 22032–22040, doi: 10.1074/jbc.M011369200 (2001).
- Nozaki, H. *et al.* Production and characterization of monoclonal antibodies specific to lactotriaosylceramide. *Glycobiology* **20**, 1631–1642, doi: 10.1093/glycob/cwq117 (2010).
- Wang, Z. *et al.* High expression of lactotriaosylceramide, a differentiation-associated glycosphingolipid, in the bone marrow of acute myeloid leukemia patients. *Glycobiology* **22**, 930–938, doi: 10.1093/glycob/cws061 (2012).
- van Oss, C. J. In *Immunochemistry* (eds van Oss, C. J. & van Regenmortel, M. H. V.) (Marcel Dekker, Inc., 1994).
- Onda, M., Ariga, K. & Kunitake, T. Activity and stability of glucose oxidase in molecular films assembled alternately with polyions. *Journal of bioscience and bioengineering* **87**, 69–75 (1999).
- Brank, A. S., Eritja, R., Garcia, R. G., Marquez, V. E. & Christman, J. K. Inhibition of HhaI DNA (Cytosine-C5) methyltransferase by oligodeoxyribonucleotides containing 5-aza-2'-deoxycytidine: examination of the intertwined roles of co-factor, target, transition state structure and enzyme conformation. *Journal of molecular biology* **323**, 53–67 (2002).
- Holmes, E. H., Ostrander, G. K., Clausen, H. & Graem, N. Oncofetal expression of Lex carbohydrate antigens in human colonic adenocarcinomas. Regulation through type 2 core chain synthesis rather than fucosylation. *The Journal of biological chemistry* **262**, 11331–11338 (1987).
- Anugraham, M., Everest-Dass, A. V., Jacob, F. & Packer, N. H. A platform for the structural characterization of glycans enzymatically released from glycosphingolipids extracted from tissue and cells. *Rapid communications in mass spectrometry: RCM* **29**, 545–561, doi: 10.1002/rcm.7130 (2015).
- Jacob, F. *et al.* The glycosphingolipid P(1) is an ovarian cancer-associated carbohydrate antigen involved in migration. *British journal of cancer* **111**, 1634–1645, doi: 10.1038/bjc.2014.455 (2014).
- Alam, S., Fedier, A., Kohler, R. S. & Jacob, F. Glucosylceramide synthase inhibitors differentially affect expression of glycosphingolipids. *Glycobiology* **25**, 351–356, doi: 10.1093/glycob/cwu187 (2015).
- Flesken-Nikitin, A. *et al.* Ovarian surface epithelium at the junction area contains a cancer-prone stem cell niche. *Nature* **495**, 241–245, doi: 10.1038/nature11979 (2013).
- Perets, R. *et al.* Transformation of the fallopian tube secretory epithelium leads to high-grade serous ovarian cancer in Brca;Tp53;Pten models. *Cancer cell* **24**, 751–765, doi: 10.1016/j.ccr.2013.10.013 (2013).
- Henion, T. R., Zhou, D., Wolfer, D. P., Jungalwala, F. B. & Hennes, T. Cloning of a mouse beta 1,3 N-acetylglucosaminyltransferase GlcNAc(beta 1,3)Gal(beta 1,4)Glc-ceramide synthase gene encoding the key regulator of lacto-series glycolipid biosynthesis. *The Journal of biological chemistry* **276**, 30261–30269, doi: 10.1074/jbc.M102979200 (2001).
- Anugraham, M. *et al.* Specific glycosylation of membrane proteins in epithelial ovarian cancer cell lines: glycan structures reflect gene expression and DNA methylation status. *Molecular & cellular proteomics: MCP* **13**, 2213–2232, doi: 10.1074/mcp.M113.037085 (2014).
- Rogerieux, F. *et al.* Determination of the sialic acid linkage specificity of sialidases using lectins in a solid phase assay. *Analytical biochemistry* **211**, 200–204 (1993).
- Yamashita, T. *et al.* Interruption of ganglioside synthesis produces central nervous system degeneration and altered axon-glia interactions. *Proceedings of the National Academy of Sciences of the United States of America* **102**, 2725–2730, doi: 10.1073/pnas.0407785102 (2005).
- Bustin, S. A. *et al.* The MIQE guidelines: minimum information for publication of quantitative real-time PCR experiments. *Clinical chemistry* **55**, 611–622, doi: 10.1373/clinchem.2008.112797 (2009).
- Radhakrishnan, P. *et al.* Immature truncated O-glycophenotype of cancer directly induces oncogenic features. *Proceedings of the National Academy of Sciences of the United States of America* **111**, E4066–4075, doi: 10.1073/pnas.1406619111 (2014).

24. Ricardo, S. *et al.* Detection of glyco-mucin profiles improves specificity of MUC16 and MUC1 biomarkers in ovarian serous tumours. *Molecular oncology* **9**, 503–512, doi: 10.1016/j.molonc.2014.10.005 (2015).
25. Marcos-Silva, L. *et al.* Characterization of binding epitopes of CA125 monoclonal antibodies. *Journal of proteome research* **13**, 3349–3359, doi: 10.1021/pr500215g (2014).
26. Steentoft, C. *et al.* Precision genome editing: a small revolution for glycobiology. *Glycobiology* **24**, 663–680, doi: 10.1093/glycob/cwu046 (2014).
27. Steentoft, C. *et al.* Precision mapping of the human O-GalNAc glycoproteome through SimpleCell technology. *The EMBO journal* **32**, 1478–1488, doi: 10.1038/emboj.2013.79 (2013).
28. Marcos-Silva, L. *et al.* A novel monoclonal antibody to a defined peptide epitope in MUC16. *Glycobiology* **25**, 1172–1182, doi: 10.1093/glycob/cwv056 (2015).
29. Jacob, F. *et al.* Serum antiglycan antibody detection of nonmucinous ovarian cancers by using a printed glycan array. *International journal of cancer. Journal international du cancer* **130**, 138–146, doi: 10.1002/ijc.26002 (2012).
30. Naiki, M., Fong, J., Ledeen, R. & Marcus, D. M. Structure of the human erythrocyte blood group P1 glycosphingolipid. *Biochemistry* **14**, 4831–4837 (1975).
31. Thuresson, B., Westman, J. S. & Olsson, M. L. Identification of a novel A4GALT exon reveals the genetic basis of the P1/P2 histo-blood groups. *Blood* **117**, 678–687, doi: 10.1182/blood-2010-08-301333 (2011).
32. Dunstan, R. A., Simpson, M. B. & Rosse, W. F. Presence of P blood group antigens on human platelets. *Am J Clin Pathol* **83**, 731–735 (1985).
33. Magalhaes, A. *et al.* Helicobacter pylori chronic infection and mucosal inflammation switches the human gastric glycosylation pathways. *Biochimica et biophysica acta* **1852**, 1928–1939, doi: 10.1016/j.bbdis.2015.07.001 (2015).
34. Ling, H. *et al.* Structure of the shiga-like toxin I B-pentamer complexed with an analogue of its receptor Gb3. *Biochemistry* **37**, 1777–1788, doi: 10.1021/bi971806n (1998).
35. Maria Cherian, R. *et al.* Shiga-like toxin binds with high avidity to multivalent O-linked blood group P1 determinants on mucin-type fusion proteins. *Glycobiology* **24**, 26–38, doi: 10.1093/glycob/cwt086 (2014).
36. Boccutto, L. *et al.* A mutation in a ganglioside biosynthetic enzyme, ST3GAL5, results in salt & pepper syndrome, a neurocutaneous disorder with altered glycolipid and glycoprotein glycosylation. *Human molecular genetics* **23**, 418–433, doi: 10.1093/hmg/ddt434 (2014).
37. Fragaki, K. *et al.* Refractory epilepsy and mitochondrial dysfunction due to GM3 synthase deficiency. *European journal of human genetics: EJHG* **21**, 528–534, doi: 10.1038/ejhg.2012.202 (2013).
38. Shevchuk, N. A. *et al.* Alteration of ganglioside synthesis by GM3 synthase knockout in murine embryonic fibroblasts. *Biochimica et biophysica acta* **1771**, 1226–1234, doi: 10.1016/j.bbali.2007.05.008 (2007).
39. Zischewski, J., Fischer, R. & Bortesi, L. Detection of on-target and off-target mutations generated by CRISPR/Cas9 and other sequence-specific nucleases. *Biotechnol Adv*, doi: 10.1016/j.biotechadv.2016.12.003 (2016).
40. Veres, A. *et al.* Low incidence of off-target mutations in individual CRISPR-Cas9 and TALEN targeted human stem cell clones detected by whole-genome sequencing. *Cell Stem Cell* **15**, 27–30, doi: 10.1016/j.stem.2014.04.020 (2014).
41. Crossetto, N. *et al.* Nucleotide-resolution DNA double-strand break mapping by next-generation sequencing. *Nature methods* **10**, 361–365, doi: 10.1038/nmeth.2408 (2013).
42. Frock, R. L. *et al.* Genome-wide detection of DNA double-stranded breaks induced by engineered nucleases. *Nature biotechnology* **33**, 179–186, doi: 10.1038/nbt.3101 (2015).
43. Uphoff, C. C. & Drexler, H. G. Detection of mycoplasma contaminations. *Methods in molecular biology* **290**, 13–23 (2005).
44. Young, W. W., Jr., Portoukalian, J. & Hakomori, S. Two monoclonal anticarbohydrate antibodies directed to glycosphingolipids with a lacto-N-glycosyl type II chain. *The Journal of biological chemistry* **256**, 10967–10972 (1981).
45. Ran, F. A. *et al.* Genome engineering using the CRISPR-Cas9 system. *Nature protocols* **8**, 2281–2308, doi: 10.1038/nprot.2013.143 (2013).
46. Jacob, F. *et al.* Careful selection of reference genes is required for reliable performance of RT-qPCR in human normal and cancer cell lines. *PLoS one* **8**, e59180, doi: 10.1371/journal.pone.0059180 (2013).
47. Kohler, R. S. *et al.* Epigenetic activation of MGAT3 and corresponding bisecting GlcNAc shortens the survival of cancer patients. *Oncotarget* **7**, 51674–51686, doi: 10.18632/oncotarget.10543 (2016).
48. Damerell, D. *et al.* Annotation of glycomics MS and MS/MS spectra using the GlycoWorkbench software tool. *Methods in molecular biology* **1273**, 3–15, doi: 10.1007/978-1-4939-2343-4_1 (2015).
49. Campbell, M. P. *et al.* UniCarbKB: building a knowledge platform for glycoproteomics. *Nucleic acids research* **42**, D215–221, doi: 10.1093/nar/gkt1128 (2014).
50. Bovin, N. *et al.* Repertoire of human natural anti-glycan immunoglobulins. Do we have auto-antibodies? *Biochimica et biophysica acta* **1820**, 1373–1382 (2012).
51. Huflejt, M. E. *et al.* Anti-carbohydrate antibodies of normal sera: findings, surprises and challenges. *Molecular immunology* **46**, 3037–3049 (2009).
52. Sivasubramanian, K. *et al.* Expression of stage-specific embryonic antigen-4 (SSEA-4) defines spontaneous loss of epithelial phenotype in human solid tumor cells. *Glycobiology* **25**, 902–917, doi: 10.1093/glycob/cwv032 (2015).

Acknowledgements

We are grateful to the Flow Cytometry Facility (Danny Labes and Emmanuel Traunecker) and Microscopy Facility (Michael Abanto and Beat Erne) for providing all necessary support. We would also like to acknowledge the following people for their various contributions to this publication: Viola Heinzlmann-Schwarz, Christian Berchthold, Andreas Schötzau, and Tatiana Pochechueva. We also thank Jolene Molley for final proofreading the manuscript. This work was supported by Novartis Foundation for Biomedical Research (13B093), Krebsliga beider Basel (14-2015), Swiss Cancer League (KLS-3841-02-2016), and FreeNovation 2016 provided by Novartis all to FJ, and the Department of Biomedicine, University Hospital Basel and University of Basel. Work of NVB was supported by the Russian Science Foundation project no. 14-50-00131.

Author Contributions

F.J., S.A., M.A., R.S.K., K.W., and Y.G. designed research; S.A., M.A., Y.L.H., K.W., Y.G., T.H., N.K., and F.J. performed experiments; S.A., M.A., Y.L.H., K.W., Y.G., T.H., N.K. and F.J. analyzed data; N.V.B., G.S., T.H. provided samples, reagents and analytical tools; S.A., M.A., Y.L.H. and F.J. wrote the paper. All authors reviewed and approved the manuscript.

Additional Information

Supplementary information accompanies this paper at <http://www.nature.com/srep>

Competing Interests: The authors declare no competing financial interests.

How to cite this article: Alam, S. *et al.* Altered (neo-) lacto series glycolipid biosynthesis impairs a2-6 sialylation on N-glycoproteins in ovarian cancer cells. *Sci. Rep.* **7**, 45367; doi: 10.1038/srep45367 (2017).

Publisher's note: Springer Nature remains neutral with regard to jurisdictional claims in published maps and institutional affiliations.



This work is licensed under a Creative Commons Attribution 4.0 International License. The images or other third party material in this article are included in the article's Creative Commons license, unless indicated otherwise in the credit line; if the material is not included under the Creative Commons license, users will need to obtain permission from the license holder to reproduce the material. To view a copy of this license, visit <http://creativecommons.org/licenses/by/4.0/>

© The Author(s) 2017

4.5 Transition of mesenchymal and epithelial cancer cells depends on globosides

Francis Jacob*, Shahidul Alam*, Ching-Yeu Liang, Reto S. Kohler, Martina Konantz, Arun V. Everest-Dass, Yen-Lin Huang, Andre Fedier, Andreas Schötzau, Monica Nunez Lopez, Nicolle H. Packer, Claudia Lengerke, Viola Heinzelmann-Schwarz

Manuscript ready to submit

My contributions to this paper:

For this study, I designed the experimental strategy in supervision by Francis Jacob. I performed experiments 1(A, F) to profile GSLs expression, 2(A, B, C, D, E) to generate and validate the heritable and stable knockout cells, 3(A, B, C, D, E, F, G, H) to identify the phenotypic changes, 4(A, B, C) to rescue *A4GALT* and globosides, 5(A, B, C, D, E, G, H, I) to identify EMT status. Data were analyzed by myself and prepared for presentation in the manuscript. I have written the manuscript with the help of all co-authors.

Transition of mesenchymal and epithelial cancer cells depends on globosides

Francis Jacob^{1*}, Shahidul Alam^{1,2*}, Ching-Yeu Liang¹, Reto S. Kohler², Martina Konantz³,
Arun V. Everest-Dass⁴, Yen-Lin Huang², Andre Fedier², Andreas Schötzau², Monica Nunez
Lopez², Nicolle H. Packer^{4,5}, Claudia Lengerke^{3,6}, Viola Heinzelmann-Schwarz^{2,7}

*Shared authorship

¹ Glyco-Oncology, Department of Biomedicine, University Hospital Basel, University of
Basel, 4031, Basel, Switzerland

² Ovarian Cancer Research, Department of Biomedicine, University Hospital Basel,
University of Basel, 4031, Basel, Switzerland

³ Stem Cells and Hematopoiesis, Department of Biomedicine, University Hospital Basel,
University of Basel, 4031, Basel, Switzerland

⁴ Institute for Glycomics, Griffith University, Gold Coast, Queensland, Australia

⁵ Department of Chemistry & Biomolecular Sciences, Biomolecular Discovery & Design
Research Centre, Faculty of Science and Engineering, Macquarie University, North Ryde,
NSW, Australia

⁶ Division of Hematology, University Hospital Basel, University of Basel, 4031, Basel,
Switzerland

⁷ Hospital for Women, Department of Gynecology and Gynecological Oncology, University
Hospital Basel, University of Basel, Basel, Switzerland

Corresponding author(s):

Francis Jacob francis.jacob@unibas.ch

Viola Heinzelmann-Schwarz viola.heinzelmann@usb.ch

Running title: Globosides are vital for mesenchymal-to-epithelial transition

Highlight

- EMT coincides with loss of globoside glycosphingolipids
- Homophilic E-cadherin cell-cell adhesion depends on globosides
- Loss of globosides results in epigenetic silencing of *CDH1*

In brief

Jacob *et al.* demonstrated that globoside glycosphingolipids are elevated in cancer cells with epithelial features and are pre-requisite for E-cadherin-mediated cell-cell adhesion. CRISPR-*Cas9*-mediated depletion of globosides induces reversible epithelial-to-mesenchymal transition (EMT) coinciding with loss of E-cadherin expression due to DNA hypermethylation at the promoter region of *CDH1*.

Summary

The transitions of cancer cells between epithelial and mesenchymal states (EMT and respectively MET) comprise cellular and molecular processes essential for local tumor growth and respective dissemination. The transmembrane glycoprotein E-cadherin is known to induce cell-cell adhesion in epithelial cells and thus to pivotally regulate this process; however, the initiating events remain to be elucidated. Here, we report that globoside glycosphingolipid (GSL) glycosyltransferase-encoding genes are elevated in epithelial cells and correlate with characteristic EMT signatures predicting disease outcome. Importantly, depletion of globosides through deletion of the key enzyme *A4GALT* by CRISPR-*Cas9* induces EMT and consequently enhances chemo-resistance. In regards to cancer stem cells, increase of CD24^{low}/CD44^{high} cells was only observed in wildtype *A4GALT* expressing cancer cells upon cholera toxin treatment inducing MET. Molecularly, cells undergoing EMT lost E-cadherin expression through epigenetic silencing at the promoter region of *CDH1* (*via* DNA methylation), however, in Δ *A4GALT* cells de-methylation was only able to rescue E-cadherin

expression if wildtype A4GALT was provided. Our data suggest GSLs as another class of biomolecule vital for epithelial homeostasis and to maintaining cell integrity and function.

3-7 key words: Glycosphingolipids, Epithelial Ovarian Cancer, CRISPR-*Cas9*, Zebrafish, E-cadherin, Epigenetics, Glycosyltransferases

INTRODUCTION

The requirement for epithelial- to- mesenchymal transition (EMT) is particularly well reported in ovarian carcinogenesis (Tan et al., 2014). Here, metastasis is established by the EMT driven delamination of tumor cells from the *in situ* tumor, followed by their penetration into the surrounding peritoneal cavity (Huang et al., 2013). The adaptation of spreading ovarian cancer cells requires EMT for dissemination while its reversed process, the mesenchymal-to-epithelial transition (MET), then fosters local tumor growth at the metastatic site. Thus, EMT and MET frequently alternate and are actively involved in different phases of tumor progression (Ahmed et al., 2010).

Although the transition of cancer cells between epithelial and mesenchymal states is a central mechanism of tumorigenesis, its molecular regulation is not fully understood (Nieto et al., 2016). Migrating cells are exposed to a different microenvironment, which might conversely again induce morphologic and molecular changes, *in vitro* as well as *in vivo*. During EMT, epithelial cells lose their cell – cell junctions and apical - basal cell polarity and undergo morphological changes to convert into a state of low proliferation, resistance to anoikis, and increased migration and invasion (Diepenbruck and Christofori, 2016). The presence of a specific surface architecture of glycosphingolipids (GSL) in epithelial *versus* mesenchymal cellular states suggests that these surface structures might be important players mediating changes in cell behavior, however, the precise functional role of glycosphingolipids (GSLs) in this context is poorly understood.

Multiple oncogenic events and signaling pathways, especially mediated by the transforming growth factor beta (TGF β), have been implicated in the induction of EMT (Massague, 2008; Teicher, 2001). Beside TGF β , the glucosylceramide synthase inhibitor EtDO-P4 was also capable of inducing partial EMT accompanied with decreased E-cadherin and increased Vimentin expression (Guan et al., 2009). Later, Guan *et al.* pointed out that the GSL repertoire alters during treatment with EtDO-P4 and TGF β in NMuMG, HCV29, and MCF7 cell lines (Guan et al., 2010). An association of the mesenchymal transcription factor Zeb1

with elevated *St3Gal5* and gangliosides was furthermore reported in epithelial NMuMG cells (Mathow et al., 2015). Consistently, we have previously shown that individual glycans, usually linked to lipids, are prognostic markers in ovarian carcinoma (Jacob et al., 2012; Jacob et al., 2011; Pochechueva et al., 2011) and demonstrated that specific GSLs (Figure 1A) of the (neo-) lacto and globo series are heterogeneously expressed in cancer cells derived from cell lines as well as primary patient samples (Alam et al., 2015; Anugraham et al., 2015). However, the functional role of GSLs in EMT/ MET processes, and in particular, the role of globo, (neo-) lacto, and ganglio series GSLs, all determined by specific key glycosyltransferases (Figure 1A), are yet unexplored. Here, we address this question and dissect the role of globosides during EMT exemplified in ovarian carcinoma. We show that globosides are required for E-cadherin mediated cell-cell adhesion, and that loss of globosides triggers EMT through a mechanism involving DNA methylation at the *CDH1* promoter. Our results illustrate a paradigm in which globoside depletion is required to revolve EMT.

RESULTS

Globoside-encoding genes are associated with EMT/MET

In order to gain insight into the involvement of GSL glycosyltransferase-encoding genes (glyco-genes) in reversible transition of cancer cells between epithelial and mesenchymal phenotypes, we investigated the Tothill (Tothill et al., 2008), Bonome (Bonome et al., 2005), and TCGA (Cancer Genome Atlas Research, 2011) transcriptome data sets representing epithelial (E), intermediate epithelial (IE), intermediate mesenchymal (IM), and mesenchymal (M) states. We applied an EMT score, which was previously developed on transcriptomic data to universally predict EMT states across various cancer types (Tan et al., 2014).

First, we tested whether the expression of glycosidase- and glycosyltransferase-encoding genes discriminates epithelial from mesenchymal cancer cells in those transcriptomic data sets. We selected all available Kyoto Encyclopedia of Genes and Genomes (KEGG) annotated glyco-genes involved in synthesis of globo-, neo-lacto, and ganglio-series GSLs and demonstrated that glyco-genes significantly discriminate E from M (Figure 1B). These results suggest that glyco-genes are coordinately altered during transition of cancer cells. EMT was previously shown to predict disease outcome in ovarian cancer (Blechschmidt et al., 2008; Davidson et al., 2000; Hosono et al., 2007), thus, we further tested the EMT score in regards to disease-specific and progression-free survival. Patients with mesenchymal features (IM and M) experienced a shorter overall survival (likelihood ratio test = 14.4, $p = 0.00239$) and earlier disease recurrence (likelihood ratio test = 13.1, $p = 0.00446$) compared to IE and E subtype (Figure 1C). In regards to GSL-encoding genes, the Cox-proportional hazard model revealed *A4GALT* as predictor for longer overall survival and disease recurrence with a hazard ratio (HR) of 0.119. In contrast, the glyco-gene associated with ganglioside *ST8SIAI* predicted disease recurrence with an HR 2.715 ($p = 0.006$) (Figure 1D). Next, we investigated the individual glyco-gene expression and found that all three data sets displayed a classical EMT marker spectrum including *CDHI* and *VIM* revealing a decrease or increase of gene expression among the four different EMT states (E, IE, IM, and M),

respectively (Figure 1E). We observed significantly decreased *A4GALT* expression to particularly associate with a mesenchymal signature (Figure 1A and 1E). The *A4GALT* gene encodes the α 1-4 galactosyltransferase, a key enzyme responsible for synthesis of globoside GSLs. In contrast, IM and M showed elevated expression of *ST3GAL5* encoding α 2-3 sialyltransferase 5 (involved in ganglioside GSL synthesis (Figure 1E)). A more detailed analysis of the Tothill data set in regards to all KEGG annotated glycosyltransferases involved in GSL synthesis revealed generally decreased globoside- and elevated ganglioside-gene expression profiles among the four EMT states (Supplementary Figure S1).

These data demonstrate that globo series related genes, and in particular *A4GALT* are elevated in epithelial cancer cells and associated with improved patient's outcome. In order to set up an experimental model for studies on the relevance of *A4GALT* and globosides during EMT/MET, we next profiled six GSLs (lactosylceramide- LacCer; Gb3, SSEA3, paragloboside-nLc4, P₁, and GM1, Figure 1A and 1F) in 34 cell lines. In general, all healthy and cancer cell lines displayed a heterogeneous expression of GSLs, with a peak of GM1 (82.0 \pm 26.7 % FITC⁺, Figure 1F). In contrast, P₁ displayed the lowest expression among all cell lines (4.6 \pm 15.9 % FITC⁺). The remaining tested GSLs, including globosides Gb3 and SSEA3, displayed a more heterogeneous expression ranging from 0 % to 97.7 % FITC⁺. Interestingly, the ovarian cancer cell line IGROV1 was positive for all GSLs. Moreover, IGROV1 displayed intermediated expression of epithelial and mesenchymal markers in the Cell Line Encyclopedia (Barretina et al., 2012) and has previously been considered as IE ((Huang et al., 2013) and Supplementary Figure S2). We therefore selected IGROV1 as a model to study globoside depletion by genome- editing and the subsequent effects on EMT/ MET.

Establishment of a globoside-depleted ovarian cancer cells using CRISPR-Cas9

As IGROV1 cells express a comprehensive GSL repertoire including globo, (neo-) lacto, and ganglio series, we genome-edited *A4GALT* in this cell line to deplete the glycosidic products of this glycosyltransferase. Our paired-sgRNA-based strategy targets the entire open reading

frame (ORF) of *A4GALT*, a 1'335bp genomic region at chromosome 22q13 (Figure 2A). Transient transfection of PX458 containing two specific sgRNAs following GFP-based clonal selection revealed various genotypes (Supplementary Figure S3 and Figure 2B). We identified three homozygous knockout ($\Delta A4GALT$) clones out of eighty-six clones profiled (3.5% efficiency). Insertions and deletions at the *Cas9*-active sites (indels) were detected by DNA sequencing. However, due to the use of paired sgRNAs targeting the entire ORF, the presence of indels did not influence the knockout of *A4GALT* (Figure 2C). The off-target analysis revealed no sequence variation (insertion/deletion) at predicted off-target sites (Figure 2D). We examined the expression of GSLs in wildtype (*A4GALT*) and $\Delta A4GALT$ cells by flow cytometry. All three $\Delta A4GALT$ cell clones were depleted for the expression of globosides (Gb3 1%, SSEA3 1%) and P₁ (1%), while LacCer (3-20%), nLc4 (50-85%), and GM1 (70-100%) remained largely unchanged (Figure 2E).

According to the transcriptomic data, the gene expression of specific ganglioside synthesizing glycosyltransferases (*e.g.* *ST8SIA1*) increases among the EMT spectrum. Thus, we performed quantitative analysis of the glycosylation of the GSLs expressed by these cells by enzymatically releasing the glycans from the isolated GSLs for analysis using LC-ESI-MS/MS, in order to study the structure of the glycan component of the GSL product after deletion of *A4GALT*. In line with our flow cytometry data, the glycan mass of m/z 505.3¹⁻ corresponding to the monosaccharide composition of globoside Gb3 [(Hex)₃], which is the direct product of *A4GALT*, was not detectable in $\Delta A4GALT$ cells (Supplementary Table S1). Interestingly, the ganglioside GM1 (glycan mass m/z 999.5 ((Hex)₃(HexNAc)₁(NeuAc)₁), Supplementary Figure S4) was increased significantly in $\Delta A4GALT$ cells (29.4%) compared to wildtype (13.4%) indicating that certain gangliosides increased as a consequence of globoside depletion.

Globoside-depleted cells acquire mesenchymal properties *in vitro* and *in vivo*

We next sought to ascertain the phenotypic changes of cells disrupted for *A4GALT*. When compared to wildtype cells, $\Delta A4GALT$ IGROV1 cells (IE) displayed a mesenchymal

morphology (Figure 3A). We also observed a loss of cell-clumps in cell cultures upon disruption of *A4GALT* with $\Delta A4GALT$ cells growing in monolayer instead of on top of each other (Figure 3A). With regards to cell proliferation, we observed no significant differences ($p = 0.05$ at 120 h) (Figure 3B). Next, we examined the influence of *A4GALT* on anchorage-dependent (Figure 3C) and -independent growth in standard tissue culture plates and soft-agar, respectively. Both assays revealed significantly reduced numbers of colonies in $\Delta A4GALT$ cells as compared to parental wild type (anchorage-dependent $p = 0.0001$ and -independent $p = 0.0002$) (Figure 3D).

The striking difference in anchorage-independent growth was further investigated in regards to cell-detachment-induced apoptosis (anoikis), which is a crucial step for tumor cells undergoing malignant transformation or adapting to a new microenvironment. Resistance to anoikis is typical for ovarian cancer cells that can survive in ascites fluids before forming metastatic foci at distant sites (He et al., 2013). We observed prolonged cell viability in $\Delta A4GALT$ cells after 7 and 10 days of cultivation (Figure 3E). This was in line with strongly increased percentage of dead (propidium iodide- positive stained) cells in wildtype compared to $\Delta A4GALT$ IGROV1 cells (Figure 3E). The significant decrease of apoptotic $\Delta A4GALT$ cells coincides with reduced cleaved PARP, another marker of cellular apoptosis (Figure 3F). We next examined the migratory and invasive phenotype of $\Delta A4GALT$ cells using *in vitro* directed cell motility assays (FCS as chemo-attractant). Cells harboring $\Delta A4GALT$ indeed displayed enhanced cell migration (Figure 3G, $p = 0.0015$) and invasion (Figure 3H, $p = 0.024$). Intrigued by this result, we injected both cell types into zebrafish embryo to study cell motility and proliferation *in vivo*. Zebrafish embryos were examined after 3 days post injection (dpi) and in line with our above mentioned *in vitro* data, enhanced *in vivo* dissemination was observed between $\Delta A4GALT$ versus *A4GALT* cells (Figure 3I), while also in this *in vivo* model cell growth was altered, as revealed by flow cytometry quantification of CM-DiL positive cells in corresponding transplanted fish embryos (Figure 3I).

E-cadherin-mediated cell-cell adhesion requires A4GALT-dependent GSLs

Because the gene disruption of *A4GALT* revealed well described phenotypic changes associated with EMT, both *in vitro* and *in vivo*, we characterized cells depleted for globosides in more detail. Specifically, we investigated the major player in EMT- E-cadherin, which has a pivotal role in cell-cell adhesion.

To rule out whether the *A4GALT* deletion mediates its effect as functionally linked to E-cadherin, we restored *A4GALT* levels in $\Delta A4GALT$ cells by ectopically expressing the ORF of *A4GALT* (Rescue DXD) in a doxycycline-inducible manner. The aspartate-any residue-aspartate (DXD) motif, which is present in A4GALT, is important for enzymatic activity of several glycosyltransferases (Ihara et al., 2002; Li et al., 2001; Persson et al., 2007). Thus, a mutant (D194A) of A4GALT was generated as being enzymatically inactive (Rescue DXA) and tested for expression of various GSLs. The Rescue DXD revealed similar expression for LacCer, Gb3, nLc4, P₁, and GM1. However, SSEA3 was not re-expressed in Rescue DXD cells. We also demonstrate for the first time that the DXD-motif in A4GALT is required for enzymatic activity, as none of the A4GALT-mediated GSLs were rescued in DXA cells (Figure 4A and 4B).

Next, we determined the expression of E-cadherin in all four-cell lines- wild type, $\Delta A4GALT$, rescue DXD, and DXA. In addition, we transduced $\Delta A4GALT$ cells with human full-length E-cadherin as well as the cytoplasmic chimera IL2R/ E-cadherin (not capable of engaging hemophilic adhesive activity), and both ORFs generated previously (Gottardi et al., 2001) were cloned into pCW57.1. The wildtype and $\Delta A4GALT$ cells re-expressing E-cadherin and IL2R/E-cadherin revealed high expression of E-cadherin with an expected shift towards lower molecular weight for IL2R/E-cadherin (Figure 4C). We also observed a faint band for E-cadherin in the rescue DXD cells, $\Delta A4GALT$ cells re-expressing A4GALT and globosides. In contrast, both, $\Delta A4GALT$ and rescue DXA cells were not capable expressing E-cadherin (Figure 4C).

Intact cell-cell adhesion *via* E-cadherin usually appears as membranous staining in epithelial cells and becomes intermittent and jagged during EMT, indicating a breakdown of cell-cell junctions (Maeda et al., 2005). This dispersed membrane-associated E-cadherin staining was reported in various epithelial cells undergoing EMT (Bassaganas et al., 2014; Busche et al., 2010; Hoot et al., 2008). To determine whether A4GALT-mediated GSLs affect cell-cell junctions, we analyzed genetically engineered cells for the distribution of E-cadherin, the integral component of the adherens junctions. Despite the low E-cadherin expression in the rescue DXD (Figure 4C), only these cells revealed areas of typical membranous E-cadherin staining as observed in IGROV1 by confocal fluorescence microscopy (Figure 4D). Neither full length nor IL2R fused E-cadherin transduced $\Delta A4GALT$ cells displayed membranous staining as observed in IGROV1. Taken together, these results indicate that A4GALT-mediated GSLs are required for E-cadherin mediated cell-cell adhesion and are important for MET.

The presence of globosides is vital in intermediate EMT cells

CDHI and *A4GALT* expression are positively correlated in epithelial ovarian cancer tissue samples (Tohill, Pearson's correlation 0.26, $p = 6.25e-06$). A4GALT and its enzymatic products seem to be preferentially expressed in cells with epithelial characteristics and are required for cell-cell adhesion *via* E-cadherin. To better understand the connection between A4GALT and E-cadherin in epithelial cells, we asked whether deletion of *A4GALT* affects globosides and function of E-cadherin in ovarian cancer cells representing the full spectrum of EMT. Thus, we tested the transition properties of ovarian cancer cells that have undergone genetic disruption of *A4GALT* in a broader panel of cell lines. A total of 10 ovarian cancer cell lines were selected showing broad variation of *CDHI* and *VIM* expression. *A4GALT* expression coincides with *CDHI* expression in those cell lines (Figure 5A). Next, we tested for expression of E-cadherin and Vimentin together with globosides in matching cell lines. Gb3 and SSEA3 was generally elevated in cell lines being primarily positive for E-cadherin

and almost negative for Vimentin indicating that globosides are preferentially expressed on epithelial cancer cells while losing expression during EMT (Figure 5B).

In addition to IGROV1, cells representing an IE state, we selected BG1, SKOV3 and A2780 cell lines displaying the remaining three different EMT states (E, IM, and M, respectively) and used them for depletion (*via* CRISPR-*Cas9* mediated *A4GALT* editing; BG1, SKOV3,) and respectively over-expression of globosides *via* lentiviral transduction with pUltraA4GALT; A2780). As expected, genomic deletion (Supplementary Figure S5A and S5B) or overexpression of *A4GALT* resulted in the absence or presence of Gb3 and SSEA3, respectively (Figure 5B and Supplementary Figure S5C, S5F). However, E-cadherin expression levels were only reduced in SKOV3 $\Delta A4GALT$ cells whereas BG1 (E) and A2780 (M) did not alter in E-cadherin expression (Figure 5C). Interestingly, BG1 $\Delta A4GALT$ cells showed partly intermittent and jagged staining at the cell-cell borders and significantly reduced colony formation (Supplementary Figure S5D and S5E) supporting previous findings in IGROV1.

To further demonstrate the involvement of globosides in transition of cancer cells, we investigated SKOV3 in more detail, which usually exhibits an IM phenotype (Huang et al., 2013). Studies on SKOV3ip, a derivative of SKOV3 obtained after passaging in mice, showed significantly increased growth rate, enhanced colony formation in soft agar and tumor formation *in vivo* compared with parental SKOV3 (Yu et al., 1993). Here, we observed elevated E-cadherin expression coinciding with increased globosides in SKOV3ip compared to SKOV3 cells (Figure 5C and 5D). There are characteristics of MET shifting parental IM SKOV3 into IE SKOV3ip cells, further supporting our data. Significantly increased anchorage-dependent growth and elevated cell membranous staining correlated with increased E-cadherin expression in SKOV3ip cells (Figure 5D and 5E). These results indicate that especially for IE/IM cancer cells, globosides are essential for epithelial properties involved in E-cadherin expression and cell-cell adhesion.

Cancer cells transitioning towards a mesenchymal state are associated with elevated resistance to a variety of conventional chemotherapeutics (Mani et al., 2008). Here, we tested how loss of *A4GALT* affects resistance to doxorubicin in ovarian cancer cells (Figure 5F). First, we observed increased resistance to doxorubicin in cancer cells reflecting the various EMT states represented by BG1 (E), IGROV1 (IE), and SKOV3 (IM). In contrast to BG1, IGROV1, and SKOV3 displayed 4.25- and 1.80-fold higher resistance to doxorubicin for $\Delta A4GALT$ cells, respectively. The SKOV3ip cell line was 2.12-fold more sensitive to doxorubicin compared to parental SKOV3 (Figure 5F), thus, confirming that intermediate EMT cell lines acquire doxorubicin resistance correlating with expression of globosides.

Next, we studied the impact of *A4GALT* loss on the cancer stem cell (CSC) markers CD24 and CD44 because EMT is usually accompanied by the lack of E-cadherin that enables cancer cells to acquire stem-like properties and enter into a more mesenchymal state (Kalluri and Weinberg, 2009). Thus, we examined whether $\Delta A4GALT$ cell populations undergoing EMT displayed an increase in the proportion of cells carrying the CD24^{low}/CD44^{high} marker profile associated with CSCs. We observed that the percentage of CD24^{low}/CD44^{high} cells was significantly higher in $\Delta A4GALT$ cells (Figure 5G). To prove that globosides are required for MET, we treated $\Delta A4GALT$ cells with cholera toxin (CTx), a MET inducing agent (Pattabiraman et al., 2016), and observed as expected no significant difference in CD24^{low}/CD44^{high} markers, while A2780 (M) and SKOV3 (IM) switched from CD24^{low}/CD44^{high} to CD24^{high}/CD44^{low} phenotypes after CTx treatment (Figure 5G). CSC marker alterations in SKOV3 were accompanied by an increase of the globoside Gb3 (4 to 19% FITC⁺) and enhanced E-cadherin expression (Figure 5H and 5I). Neither globoside nor E-cadherin expression was observed in A2780 and $\Delta A4GALT$ cells (IGROV1, BG1 & SKOV3) treated with CTx (Figure 5G-I). Taken together, these data highlight not only the importance of globosides in MET but also their potential impact on the expression of CD24 and CD44, thus further indicating that GSLs are directly involved in transition of cancer cells from an epithelial to a mesenchymal phenotype.

EMT upon *A4GALT* deletion is accompanied by DNA hypermethylation at the promoter region of *CDH1*

Epigenetic programs, including DNA methylation and chromatin modifications play a key role in EMT (Nieto et al., 2016). Recent work by Pattabiraman *et al.* 2016 suggests that the protein kinase A pathway triggers epigenetic reprogramming by the histone demethylase PHF2. However, in our case CTx treatment only marginally affected expression of E-cadherin, CD24 and CD44 markers, especially in $\Delta A4GALT$ cells (IGROV1, BG1 & SKOV3). Thus, we tested the impact of DNA methylation at the promoter region of *CDH1*. Independent of the program applied, the analysis of the promoter region of *CDH1* predicted a CpG island surrounding the transcription start site (TSS) of *CDH1* (Figure 6A). Since most changes in DNA methylation occur in a region of $-250/+250$ bp relative to the TSS (Kelly et al., 2012), we analyzed the DNA methylation status within the genomic region $-116/+124$ of the TSS *CDH1* comprising 18 CpGs (Figure 6A). Cell lines in the E state (OVCAR3 and BG1) revealed DNA hypomethylation at the investigated locus in contrast to A2780, which showed $84 \pm 2.65\%$ DNA methylation (Figure 6B). Interestingly, we observed increased DNA methylation at the promoter region of *CDH1* in both $\Delta A4GALT$ cell lines compared to parental IGROV1 and SKOV3 (Figure 6B). Next, we hypothesized that E-cadherin expression in $\Delta A4GALT$ cells can be re-expressed by the hypomethylating agent, 5-aza-2'-deoxycytidine (5-Aza), treatment. Parental IGROV1, $\Delta A4GALT$, and rescue DXD cells showed E-cadherin expression after 96 h of treatment with 5-Aza (Figure 6C). Finally, we investigated membranous staining of all three-cell lines and observed increased membranous staining in 5-Aza treated IGROV1 and rescue DXD cells whereas $\Delta A4GALT$ cells did not reveal such a pattern (Figure 6D). Here, we show that we substantially rescued E-cadherin-mediated cell-cell adhesion only in cells with a functional $\alpha 1-4$ galactosyltransferase and its direct glycolipid products (globosides) indicating that DNA methylation coincides with the expression of E-cadherin upon loss of globosides.

DISCUSSION

Glycosphingolipids (GSLs) have been studied for six decades and linked to embryonic development and cell differentiation in normal and diseased cells. They are components of the cell surface membrane acting as mediators for cell adhesion and signal transduction. However, we have identified novel roles for GSLs as mediators of cell-cell adhesion and EMT induction in ovarian cancer. We show that cancer cells undergoing EMT upon depletion of globoside GSLs through genomic deletion of the key glycosyltransferase *A4GALT* display silencing of E-cadherin expression resulting in loss of cell-cell adhesion properties. Remarkably, re-expression of globosides by *A4GALT* rescue partially restored homophilic cell-cell adhesion whereas ectopic E-cadherin was not able to. The pivotal role of globosides in this context was further demonstrated by global de-methylation on genomic DNA with co-expression of *A4GALT* resulting in membranous E-cadherin staining.

Epithelial and intermediate EMT cells were shown to generally express higher levels of globo and neolacto series GSLs. Beside cancer cells undergoing EMT upon *A4GALT* deletion, we also observed elevated levels of Gb3 and E-cadherin expression in SKOV3ip indicating that SKOV3ip cells underwent MET in mice. This is in line with work by Hakomori and colleagues describing a ganglioside enrichment and globoside (*e.g.* SSEA3) reduction in a hydroxytamoxifen inducible TWIST-EMT model system of human mammary epithelial cells (HMLE-TWIST-ER) that correlated with silencing of *CDH1* expression (Liang et al., 2013; Liang et al., 2010). The authors performed knockdown of *ST8SIA1* and *B4GALNT1* (both enzymes involved in ganglioside synthesis) in MCF-7 cells indicating that specific gangliosides might be involved in mammosphere formation with alterations in random cell motility, however without showing E-cadherin expression upon the glyco-gene knockdown. Our transcriptomic data analyses support these findings since all significantly differentially expressed genes encoding for glycosyltransferases involved in the ganglio series GSL synthesis appear upregulated in mesenchymal phenotypes of these tissue samples. Moreover,

our quantitative analysis of glycans released from the expressed GSLs in the tissues demonstrated that gangliosides are increased upon depletion of globosides.

Interestingly, 60.5% of ovarian cancer cell lines can be categorized into IE and IM states (Huang et al., 2013), which was also similarly reflected in ovarian cancer tissue samples and in the cell line encyclopaedia (Tan et al., 2014). Epithelial ovarian cancer seems to be therefore an optimal model for studying EMT/MET. During EMT, cells undergo a series of sequential events to disintegrate cell – cell contacts and the regulatory machinery that controls cell polarity (Nieto et al., 2016). Epithelial cells become progressively separated from mesenchymal-like cells by gradually loosening cell-cell contacts to transit from polarized epithelium to post EMT-mesenchymal state (Huang et al., 2012b). More recent studies point out that a greater flexibility exists in the EMT process, and cells are no longer thought to oscillate between the full epithelial and full mesenchymal state, but rather move through a spectrum of intermediate phases (Nieto et al., 2016). In this state of EMT, cells harbor the greatest plasticity because they are able to either reverse to an epithelial state or progress towards a mesenchymal phenotype (Huang et al., 2012a). Our observations upon GSL depletion support these hypotheses and further point out the importance of GSLs in this context, as here demonstrated in IGROV1 and SKOV3 (both intermediate EMT and E-cadherin⁺/ Vimentin⁺) cell lines. In contrast, epithelial (BG1, E-cadherin⁺/ Vimentin⁻) and stable mesenchymal (A2780, E-cadherin⁻/ Vimentin⁺) cells did not fully undergo transition upon deletion or ectopic expression of A4GALT, respectively. However, we observed changes in cell morphology, E-cadherin cell-cell adhesion and differential expression of CD24 and CD44, all of which are well described to occur in various solid tumors distinguishing CSCs from bulk-tumor populations (Clevers, 2011) and have been related to GSLs (Liang et al., 2013; Pattabiraman et al., 2016).

Interestingly $\Delta A4GALT$ IGROV1 cells also exhibited anoikis resistance as well as higher migratory and invasive phenotypes compared with wildtype, which are the typical characteristics of an EMT transition. In addition, after executing the EMT program,

$\Delta A4GALT$ cells acquired traits associated with metastatic characteristics, which leads to dissemination *in vivo* (Figure 3 and (Tam and Weinberg, 2013)). In light of our results, it becomes more evident that ovarian cancer cells in intermediate EMT/ MET states are characterized by a specific GSL composition which might functionally act upstream of E-cadherin for affecting homophilic cell-cell adhesion.

E-cadherin-mediated cell-cell adhesion usually provides a spatial cue for cells to distinguish an unbounded (apical) from a bounded (basolateral) cell surface and to accumulate acting membrane proteins on the correct surface (Wang et al., 1990), but the mechanisms linking E-cadherin to protein sorting and redistribution to different plasma membrane domains are unknown. Although re-expression of A4GALT resulted only in partial rescue of E-cadherin and cell-cell adhesion, interestingly, no membranous staining was observed in either full-length E-cadherin or IL2R/E-cadherin cytotail expression in $\Delta A4GALT$ IGROV1 cells. Treatment of cells with an agent inducing global DNA de-methylation (5-Aza) increased E-cadherin expression in $\Delta A4GALT$ IGROV1 cells; however, only co-expression of A4GALT in these cells re-stored the wildtype E-cadherin-mediated cell-cell adhesion, indicating that globosides are vital for cancer cells with epithelial features. Thus, we propose that the composition of globosides, herein referred to as a ‘lipid glyco-fingerprint’, intrinsically defines cell-cell adhesion between cells. It remains to be elucidated how the recognition between two cells, before forming adhesion *via* E-cadherin, occurs, either by carbohydrate-carbohydrate (Bucior et al., 2004; Hakomori, 2004) or carbohydrate-protein recognition. Interestingly, examples in the literature show differentially expressed glyco-genes involved in glycosylation of ceramides during EMT/ MET. One study on HMLE-TWIST-ER cell system found 44 genes involved in mesenchymal (CD24^{low} and CD44^{high}) metabolic pathways including genes encoding for enzymes involved in GSL synthesis *UGCG* and *ST6GAL1* (Shaul et al., 2014). Our hypothesis is supported by recent work demonstrating that the CTx induces MET in several cell lines *via* the PKA pathway inducing epigenetic changes that can modulate MET together with loss of mesenchymal characteristics (Pattabiraman et al., 2016).

The cholera toxin is known to bind the ganglioside GM1 (Gal β 1-3GalNac β 1-4(Neu5Ac(α 2-3)Gal β 1-4Glc-ceramide) and associated structures (Merritt et al., 1994). Considering the fact that gangliosides seem to be preferentially expressed in mesenchymal cells, CTx might indeed induce MET by selectively binding to ganglioside-expressing cancer cells with mesenchymal features. Reduced expression of gangliosides on epithelial cells might therefore be an explanation of non-inducible MET in epithelial-like cells. In sum, our current findings identify globoside GSLs as a new major player triggering the transition of ovarian carcinoma cells between epithelial and mesenchymal states.

MATERIAL AND METHODS

Cell culture

A total number of thirty-four different cell lines were acquired *via* different sources and maintained in house in appropriate growth media (Supplementary table S2). All cell lines were cultured at 37°C in a 95 % humidified atmosphere containing 5 % CO₂. All cell lines were authenticated using short tandem repeat (STR) profiling and regularly tested for the absence of mycoplasma (Uphoff and Drexler, 2005).

Reagents, antibodies and enzymes

Antibodies for detection of cell surface-associated GSLs were applied as described previously (Alam et al., 2015). Additional antibodies were applied; primary antibodies E-Cadherin (#3195) and Tubulin (#2148), secondary antibodies HRP-anti-rabbit IgG (#7074) and HRP-anti-mouse IgG (#7076) all obtained from Cell Signaling Technology (BioConcept Ltd, Allschwil, Switzerland). Vimentin (#MS-129-P1) antibody was purchased from Thermo Fisher Scientific (Life technologies, Reinach, Switzerland). Anti-human CD44-PE (#130-098-108) and CD24-PE-Cy7 (#561646) antibodies were obtained from MACS Miltenyi Biotec (Bergisch Gladbach, Germany) and BD Pharmingen (Allschwil, Switzerland), respectively.

Endoglycoceramidase II (EGCase II, recombinant clone derived from *Rhodococcus* sp and expressed in *Escherichia coli*) was purchased from Sigma-Aldrich (MO, USA). Glycosphingolipid standards from Matreya LLC (Neutral Glycosphingolipid Qualmix 1505, globotriosylceramide (CTH), Monosialoganglioside Mixture 1508, Gangliotetraosylceramide 1064) were obtained from Adela Scientific (SA, Australia). Immobilon-P Polyvinylidene Difluoride (PVDF, 0.2 µm) was obtained from Millipore (MA, USA). Microtiter plates (Corning 96-well clear flat bottom, COR3364) were purchased from Invitro (Vic, Australia). Cation exchange resin beads (AG50W-X8) was obtained from BioRad (Hercules, CA, USA) and PerfectPure C18 Zip Tips were obtained from Eppendorf (Hamburg, Germany). Potassium hydroxide and sodium borohydride were obtained from Sigma-Aldrich (MO,

USA). Other reagents and solvents such as methanol, ethanol, chloroform and acetonitrile were of HPLC or LC/MS grade.

Single-guided RNA design and vector construction

Single guided RNAs (sgRNA) targeting exon 3 of *A4GALT* were designed using the web tool of the Zhang laboratory (<http://crispr.mit.edu>) (Ran et al., 2013). sgRNA1 and sgRNA2 (Supplementary table S3, Figure 2) with scores of 91 and 85, respectively, were selected for gene editing of the entire open reading frame (ORF) of *A4GALT*. Intended oligo pairs encoding 20nt targeted sequences (Supplementary table S3) with overhangs (both 5' and 3') from *BsbI* restriction site were ordered, annealed and finally cloned into either pSpCas9(BB)-2A-GFP (addgene, #PX458) or pSpCas9(BB)-2A-puro (addgene, #PX459) via *BsbI* restriction site using T4-DNA ligase (Promega, Dübendorf, Switzerland). Constructs were transformed into DH5alpha *E. coli* strains and sequenced for confirmation of the sgRNA inserted into PX458 by Sanger DNA sequencing using Primer human U6.

Transfection and single cell sorting

IGROV1, BG1 and SKOV3 cell lines were grown in 6-well plate (3×10^5 - 5×10^5 cells/well) for 24 h and transiently transfected using Viafect[®] transfection reagent (Promega) with 2.5 μ g of sgRNA containing either PX458 (Addgene # 48138) or PX459 (Addgene # 62988) donor plasmid to generate homozygous $\Delta A4GALT$. Cells were washed with PBS, harvested using cell dissociation buffer (non-enzymatic, Sigma-Aldrich, Buchs, Switzerland) and finally re-suspended in RPMI containing 10% FCS 72 h after transfection. Following single cell sorting was performed on a BD FACS Aria Cell Sorter (BD Bioscience) sorting for single DAPI⁻ and GFP⁺ cells into 96-well flat-bottom plates with pre-warmed RPMI containing 10% FCS. Plates were incubated for up to 3 weeks following transfer to 48-well plates and genomic DNA isolated for genotyping PCR to characterize single cell clones.

Genotyping PCR

Selected clones were characterized to identify homozygous knockout by using three independent PCR primer pairs (Supplementary table S3). PCR was performed using 2.5x GoTaq Green Master Mix (Promega), 300nM primer, 30ng genomic DNA (gDNA). PCR conditions were 95°C for 2 min, then 32 cycles of 94°C for 15 sec, 58.9°C for 15 sec, 72°C for 30-45 sec (depending on the amplicon length), finished with 1 cycle at 72°C for 5 min. Amplicons were visualized on a 1.5 % agarose gel.

DNA sequencing

PCR products corresponding to genomic modifications were purified and cloned into the pGEM[®]-T Easy Vector System (Promega) according to the manufacturer's protocol and sequenced using T7-F (Supplementary table S3) primer by Sanger DNA sequencing service from Source Bioscience Life Sciences (Berlin, Germany). Samples were shipped at a concentration of 100 ng/μl with specific primer (if required) of 3.2 pg/μl.

Flow cytometry

Immunostaining and flow cytometry was performed as previously described (Alam et al., 2015; Jacob et al., 2014).

Analysis of glycans released from GSLs using PGC LC-ESI-MS/MS

The extraction of GSLs from cell lines was carried out with some modifications based on our previously described method (Anugraham et al., 2015). Briefly, cells (1×10^7) were harvested, washed thrice in 10 ml of phosphate buffered saline and pelleted through centrifugation at 1800 g for 20 min. A total of 5 ml of chloroform: methanol (2:1) was added to the cell pellet and incubated overnight in a 4⁰C incubator shaker. The supernatant was collected after centrifugation at 1800xg for 20 min and the pellet was re-extracted again as described above. The combined supernatants were evaporated to dryness under vacuum and the dried glycosphingolipid mixture was re-dissolved in 50 μl of chloroform: methanol (2:1). Subsequently, GSLs were spotted onto a polyvinylidene difluoride (PVDF) membrane to immobilize the GSLs. PVDF spots were cut and placed in a chloroform-compatible 96-well microplate, to which 50 μl of re-dissolved glycosphingolipid mixtures from cell line samples

were spotted. 10 μl of neutral and acidic glycosphingolipid standards were also on individual PVDF spots and the 96-well microplate was air-dried at room temperature to ensure proper binding of the GSLs. To release the glycans from membrane-bound glycosphingolipids, 2 μl (4mU) of Endoglycoceramidase II in 50 μl of 0.05 M sodium acetate buffer, pH 5.0 was added to each sample well and incubated for 16 h at 37°C. Approximately 50 μl of released glycans was recovered from the individual sample wells and transferred to Eppendorf tubes containing 1ml of chloroform: methanol: water (8:4:3). The sample well was then washed with 50 μl of water and residual glycans were added to the Eppendorf tube. The upper methanol: water layer containing the released oligosaccharides (~400 μl) was dried and kept for subsequent analysis.

The released glycans were reduced to alditols with 20 μl of 200 mM sodium borohydride in 50 mM potassium hydroxide at 50°C for 2 h. The reaction mixture was quenched using 2 μl of 100% glacial acetic acid. The glycan alditols (~20 μl) were applied to individually prepared cation exchange columns which consist of 45 μl of cation exchange resin beads (AG50W-X8) deposited onto reversed phase $\mu\text{C}18$ ZipTips (Perfect Pure, Millipore) and placed in microfuge tubes. The columns were conditioned by a series of pre-washing steps with a) 50 μl of 1 M HCl, b) 50 μl of methanol and c) 50 μl of water as previously described (Jensen et al., 2012). Glycan alditols were eluted with Milli Q water (50 μl , twice) and dried. Subsequent drying steps with methanol (100 μl , thrice) were performed to remove residual borate. Purified glycan alditols were re-suspended in 15 μl of water prior to MS analysis.

The reduced GSL glycans were analyzed by a capillary LC (Dionex) connected to a linear ion-trap mass spectrometer (LTQ Velos Pro, Thermo Scientific). 3 μl of the sample was injected onto a Hypercarb porous graphitized carbon (PGC) capillary column (5 μm Hypercarb KAPPA, 180 μm x 100 mm, Thermo Hypersil, Runcorn, UK). The separation of glycans was carried out over a linear HPLC gradient of 0-70 % (v/v) acetonitrile /10 mM ammonium bicarbonate for 45 mins followed by a 10 min wash-step using 90 % (v/v) acetonitrile /10 mM ammonium bicarbonate at a flow rate of 4 $\mu\text{l}/\text{min}$. The MS spectra were

obtained within the mass range of m/z 400 - m/z 1500. The temperature of the transfer capillary was maintained at 325 °C and the capillary voltage was set at 3.2 kV. Neutral and acidic glycans were detected in the negative ion mode as $[M-H]^{-1}$ and $[M-2H]^{-2}$ ions and their signal intensities and fragmentation were analyzed using the Thermo Xcalibur Qualitative Analysis (Versions 2.2) software.

MTT assay

To identify the proliferation rate cells were seeded at a density of 20'000 cells/ well in 96-well plates and incubated for 24 h to 120 h. At each time point MTT dye (Sigma-Aldrich) was added at a final concentration of 500 $\mu\text{g/mL}$ and incubated for 3 h. After removal of supernatant 200 μl of DMSO was added to dissolve the crystals. The optical density (OD, absorbance at 540 nm) was measured with a Synergy H1 Hybrid Reader (Biotek, Basel, Switzerland). The measurement was performed in quadruplets and experiments were repeated thrice.

Colony formation assay

Cells were harvested and adjusted in cell number for seeding of 500 cells per well of a 12-well plate. The standard culture medium was replaced every 3 days. On the 10th day after seeding, colonies were counted only if they contained more than 50 cells. Finally, the cells were stained using crystal violet and images were taken.

Soft agar assay

Cells were grown in medium containing 1 % base agar and 0.3 % top agar. Additional culture media were overlaid every 3-4 days. After 10-14 days of culture, colonies were enumerated and pictures were taken. The experiments were independently repeated at least three times.

Aggregation or anoikis assay

To evaluate anchorage-independent growth, cells were grown in ultra-low attachment T25cm² flasks. Cells were then harvested at day 4, 7 and 10, washed with PBS and stained with propidium iodide (PI) following the manufactures instructions. The percentage of PI positive cells was analyzed by flow cytometry using BD AccuriTM C6.

Cell motility (migration and invasion)

Directed cell motility assay was performed as described previously (Jacob et al., 2014). In brief, sub-confluent cells were grown in serum-free media for 24 h and 7.5×10^5 cells were seeded into the upper chamber of each insert following incubation at 37°C for 18 h allowing cells to migrate to the chemo-attractant (medium containing 10 % FBS). After incubation, media in the interior part of the insert was removed and the insert was immersed in 0.2% crystal violet/ 10% ethanol for 20 min. The insert was intensively washed and non-migrated cell in the interior of the insert were removed using a cotton-tip swab. Five random areas of the inserts were photographed for migrated cells, and cell counts were performed.

In regards to invasion assay, trans-well inserts were covered with a final volume of 100 μ l Matrigel (diluted with media, 1:80) for 1 h at room temperature to settle down and polymerized. The plate was then placed in the incubator at 37°C for overnight. Cells were then processed according to the previously described cell migration protocol mentioned above and after incubation at 37°C for 24 h, media was removed and the insert was immersed in crystal violet for 20 min and followed the same protocol as described before.

***A4GALT* rescue, mutagenesis and cloning of E-cadherin constructs**

To rescue the *A4GALT* in $\Delta A4GALT$ cells, we utilized IGROV1 genomic DNA as template and designed primer to amplify the *A4GALT* open reading frame. The PCR was performed using 2 U *Pfu* DNA polymerase (Promega), 1 x *Pfu* DNA polymerase buffer, 300nM forward and reverse primer, 30 ng genomic DNA (gDNA), 200 μ M dNTPs and nuclease free water under following conditions: 95°C for 2 min followed by 32 cycles of 94°C for 15 sec, 58°C for 15 sec, 72°C for 3min, and finished with 1 cycle at 72°C for 5 min. Amplicons were visualized on 1 % agarose gel and purified by Wizard SV gel and PCR Clean-Up System (Promega) and finally cloned into plasmid pcDNA3.1 (Addgene #V790-20) which was used as mutagenesis template. After DNA Sanger sequencing the mutagenesis PCR was performed as previously described (Zheng et al., 2004). The PCR amplifications were carried out with Expand[™] High Fidelity PCR system (Roche, Switzerland) in a 50 μ l reaction volume, which

was carried out with 100 ng pcDNA3.1A4GALT open reading frame as template, 1 μ M primer pair, 200 μ M dNTPs and 2 U of DNA polymerase. The PCR was performed under following conditions: 94°C for 5 min; 16 cycles of 94°C for 1 min, 52°C for 1 min and 72°C for 16 min; followed by 72°C for 1 h. The Amplicons were then evaluated by agarose gel electrophoresis and purified by Wizard SV gel and PCR Clean-Up System (Promega) and further treated with restriction enzyme *DpnI* (NEB). An aliquot of 1 μ l PCR product was transformed into DH5 α and plated on LB plate containing 100 μ g/ml ampicillin. Positive mutants were selected by *BsmI* restriction digestion. The desired A4GALT open reading frame was then introduced into pUltra (Addgene #24129, (Lou et al., 2012)) and pCW57.1 (Addgene #41393) via *NheI* and *XhoI/Sall* cloning procedure for further lentiviral transduction. In parallel, full length E-cadherin (addgene #45769) and IL2R/E-cadherin cytotail (addgene #45773) were amplified via Quick Fusion Cloning Kit (bimake.com, Munich, Germany) for cloning into desired lentiviral vector. All primers are listed in supplementary table S3.

Lentivirus production and transduction

HEK293T cells were cultured as described above. One day prior to transfection, cells were seeded at ~40% confluence in a T75cm² flask. Cells were transfected when they reached 70–80% confluence. For each flask, 4 μ g of plasmid pUltra (Addgene #24129, (Lou et al., 2012)) and pCW57.1 (Addgene #41393) encoding the genes of interest (A4GALT (DXD), A4GALT (DXA)), full length E-cadherin, or IL2/E-cadherin cytotail) and 2 μ g of pMD2.G (Addgene #12259) and 2 μ g of pCMVR8.74 (Addgene #22036) were transfected using 24 μ l of jetPEI reagent and 1 ml of 150 mM NaCl solution (Polyplus-transfection, Chemie Brunschwig AG, Basel, Switzerland). Media was changed 24 h after transfection. Virus supernatant was collected 48 h later and filtered with a 0.45 μ m polyvinylidene fluoride filter (Millipore), and stored at -80°C. IGROV1 Δ A4GALT cells were transduced with pUltra and pCW57.1 lentiviral supernatant in 4 ml of media supplemented with 8 μ g/ml polybrene (Sigma) in T25cm² flask and selected after 3 passages by GFP enrichment and 5 μ g/ml puromycin treatment.

Reverse-transcription quantitative polymerase chain reaction (RT-qPCR)

In order to extract RNA, 10^5 cells were seeded in 6-well plates, grown them to 70-80% confluence, then washed twice with sterile PBS prior to total RNA extraction using the ReliaPrep[®] RNA Cell Miniprep System (Promega). RNA was eluted in 60 μ l RNase- free water and RNA concentration measured using a NanoDrop ND-1000 spectrophotometer (Thermo Fisher Scientific, Roskilde, Denmark). An amount of 1 μ g of RNA in a total volume of 20 μ l was reverse transcribed using the iScript[®] Reverse Transcription Supermix for RT-qPCR (Bio-Rad Laboratories, Zurich, Switzerland) according to the manufacturer's instructions. RT-qPCR was performed on *CDH1*, *VIM*, *A4GALT* and reference genes *HSPCB*, *SDHA*, and *YWHAZ* in 10 μ l reactions containing 10 ng cDNA (initial total RNA), 400nM forward and reverse primer (Supplementary table S3), nuclease free water and 1 \times GoTaq[®] qPCR Master mix with low ROX as reference dye (Promega) on a ViiA[™] 7 Real-Time PCR System (Applied Biosystems, Thermo Fisher Scientific, Reinach, Switzerland). Quantitative PCR was performed in triplicates and analyzed as recently described (Kohler et al., 2016).

Western blot

Whole cell lysates were obtained from sub-confluent cultures. Cells were lysed for Western blot analysis according to standard laboratory protocols. The protein concentration of cell lysates was determined by BCA Protein Assay Kit (Pierce, Perbio Science, Lausanne, Switzerland). Equal amounts of protein (20 μ g) were loaded and separated using SDS-PAGE, followed by blotting onto a polyvinylidene difluoride membrane (Amersham Biosciences, Otelfingen, Switzerland). Later, the membrane was blocked with 5 % (w/v) BSA (Sigma) in TBST and incubated with primary monoclonal antibodies E-cadherin (1:1000), Vimentin (1:1000) and tubulin (1:1000) diluted in 5 % (w/v) BSA in TBST at 4°C overnight. Afterwards, membranes were washed in TBST and incubated with corresponding HRP-conjugated secondary antibodies (anti-rabbit and -mouse) in 3 % BSA in TBST for 3 h at room temperature. Finally after washing in TBST, detection was carried out with the Super Signal West Dura Extended Duration Substrate (Life technologies).

Confocal fluorescence microscopy

Cells were grown on polylysine glass slides attached to a 8-well chamber, fixed with 4 % para-formaldehyde (Polysciences, Hirschberg an der Bergstraße, Germany) for 15 min, permeabilized with 0.3 % Triton X-100 (Sigma) and incubated with blocking buffer (5 % (w/v) BSA fraction V (Sigma) in PBS) for 1 h. Cells were then stained with E-cadherin antibody and mounted in ProLong[®] Gold Antifade Reagent with DAPI (Cell Signaling Technology #8961). Fluorescence images were taken on a LSM 780 confocal microscope (Zeiss, Feldbach, Switzerland).

Zebrafish xenograft model

The 'Kantonales Veterinaeramt Basel- Stadt' approved animal experiments and zebrafish husbandry. *A4GALT* and corresponding control cells were labeled with the fluorescent CellTracker CM-DiI (Life Technologies) as previously described (Konantz et al., 2012; Schaefer et al., 2015). In brief, nacre/transparent zebrafish were maintained, collected, grown and staged in E3 medium at 28.5°C according to standard protocols (Krauss et al., 2013). For xenotransplantation experiments, zebrafish embryos were anesthetized in 0.4% tricaine (Sigma-Aldrich) at 48 h post fertilization and 75-100 control or knockdown cells were microinjected into the vessel free area of the yolk. Embryos were incubated for 1 h at 28.5–29 °C for recovery and then screened for the presence of fluorescent human cancer cells in the yolk. Fish harboring red cells were incubated at 35°C as described before (Haldi et al., 2006). Five days after transplantation, embryos were screened microscopically for tumor formation using a Zeiss LSM 710 confocal microscope. Fish were furthermore dissociated into single cells as described (Svoboda et al., 2016) and cells analyzed on a BD Accuri[™] C6 for CM-DiI-positive cells. For each experiment 75–100 cells per fish were transplanted and at least 5 fish for each condition were analyzed.

Bisulfite-sequencing

Four different web-based bioinformatic engines were applied as recently described (Kohler et al., 2016) to predict the genomic location of the CpG island in the *CDHI* gene (UCSC

Genome Browser, CpGPLOT, Methprimer and CpG island searcher). For analysis of the methylation status genomic DNA was isolated from exponentially growing cells as described previously (Kohler et al., 2016). An amount of 1 µg DNA was bisulfite converted using the EZ Methylation-Gold Kit (Zymo Research Inc., Lucerna-Chem AG, Luzern, Switzerland) and was further subjected to PCR reaction using MyTaq™ HS DNA polymerase (Bioline, abc biopply, Solothurn, Switzerland). PCR reactions contained: 1× MyTaq reaction buffer, MyTaq HS polymerase, 300 nM CDH1_Bis_1F and CDH1_Bis_1R (DNA sequence is listed in Supplementary table S2) and nuclease free water to a final volume of 10 µl performed under following conditions; 95°C for 10 min, 35 cycles of 95°C for 15 sec, 50°C for 15 sec, and 72°C for 20 sec, and finished by elongation at 72°C for 3 min. PCR products were subjected to a second PCR using CDH1_Bis_2F and CDH1_Bis_2R following same conditions as described before (Supplementary table S2). The PCR product were visualized on a 2% agarose gel and purified from the gel using the Wizard SV Gel and PCR clean up system (Promega) and cloned into pGEM®-T Easy (Promega). Plasmid minipreps (PureYield™ Plasmid MiniPrep System, Promega) from individually grown colonies were sequenced using SP6 primer. Bisulfite sequencing data were analyzed and visualized using the Quantification tool for methylation analysis (QUMA) web-based application (<http://quma.cdb.riken.jp/top/index.html>).

Cholera toxin and 5-Aza treatments

Cells were treated with 100 ng/ml of CTx (Sigma), which was replenished every 3-4 days over a period of 14 to 16 days. Cells were split to a ratio of 1:6 every 3-4 days during the treatments. In regards to global DNA de-methylation, cells were treated with 2.5 µM 5-aza-2'-deoxycytidine (5-Aza) for up to 96 h with replenishing media every 24 h.

Data acquisition and statistical analysis

Publicly available transcriptomic data sets (GSE26712, GSE68661, and GSE9899) were downloaded from Gene Expression Omnibus (<http://www.ncbi.nlm.nih.gov/geo/>). Statistical analysis and figures were obtained through the use of the software R version 3.1.3 (www.R-project.org/).

project.org). Gene expression data for the “Cancer Cell Line Encyclopedia were accessed through the cbiportal using R (www.cbiportal.org, (Gao et al., 2013)) using cgdsr, a R-based application programming interface (API) that provides a basic set of R functions for querying the Cancer Genomics Data Server (CDGS) hosted by the Memorial-Sloan-Kettering Cancer Center (MSKCC).

Overall survival and relapse-free survival was investigated using Kaplan-Meier curves. Gene expression was dichotomized using tree based model partitioning (“ctree” in R package “party”). Computations of the predicted survivor curves were used for Cox proportional hazards regression model (R package “survival”). Results were presented as hazard ratios (HR) with 95% confidence interval (CI) and corresponding *p*-values.

All experiments were performed in triplicates and statistical evaluation was done using unpaired Student’s *t*-tests. *P* values of < 0.05 were considered statistically significant (*** *p* < 0.001, ** *p* < 0.01, * *p*-value < 0.05, *p*-value < 0.1.)

Acknowledgments

We are grateful to the Flow Cytometry Facility (Danny Labes, Emmanuel Traunecker and Lorenzo Raeli) and Microscopy Facility (Michael Abanto and Beat Erne) for providing all necessary support. We would also like to acknowledge the following people for their various contributions to this publication: Tatiana Pochechueva and Yasmin Grether. Finally, we would like to thank Gerhard Christofori for carefully reading our manuscript and his support on this project.

Financial support

This work was supported by Swiss National Foundation (310030-156982, 310030_143619, -32, and Sinergia 171037) to V.H.S., Oncosuisse Grant (KFS_3013-08-2012 (V.H.S.) and KFS-3841-02-2016 (F.J.), Krebsliga beider Basel (06-2013) to F.J., Novartis Foundation for Biomedical Research (13B093) to F.J, FreeNovation 2016 provided by Novartis to F.J., the Department of Biomedicine, University Hospital Basel and University of Basel. We also acknowledge funding from the Macquarie University Postgraduate Research Scholarship (A.E-D) and Australian Research Council Centre of Excellence in Nanoscale Biophotonics CE140100003 (N.H.P and A. E-D).

Figure legends:

Figure 1

Expression of globoside-encoding genes is elevated in epithelial cancer cells.

A) Glycosphingolipid biosynthesis pathway- glucose is attached to ceramides and further elongated into three major series with the precursor lactosylceramide (LacCer). GSL-series are boxed in colors. Carbohydrate structures provided along with the name were investigated in this study. **B)** Linear discriminant analysis in three transcriptomic ovarian cancer data sets separating epithelial (E, dark green) from mesenchymal (M, red) tissue samples. Wilks lambda and corresponding p-value is provided along with each dot plot. **C)** Kaplan-Meier curves for overall survival and relapse-free survival in four EMT states (E, IE, IM, and M) in the Tothill data set. **D)** Table summarizing globo and ganglio-series synthesizing glycosyltransferase-encoding genes predicting overall and relapse-free survival determined for by Cox proportional hazard model. **E)** Boxplots showing gene expression of *CDHI*, *A4GALT*, *VIM*, and *ST3GAL5* among four different EMT states in three independent ovarian cancer data sets (Tothill, Bonome, and TCGA). Color indicates typical expression of genes up in epithelial (green) or mesenchymal (red), Epithelial (E), intermediate epithelial (IE), intermediate mesenchymal (IM), and mesenchymal (M). **F)** Heatmap of GSL marker expression across normal and cancer cell lines. The heatmap illustrates the unclustered distribution of cell lines from the mean GSL expression out of three independent experiments. GSLs markers arranged by average linkage clustering. Cell line origin is provided along with the heatmap.

Figure 2

Generation of a heritable and site-specific *A4GALT* mutant ovarian cancer cell line using CRISPR-Cas9 technology: **A)** Strategy to delete the *A4GALT* gene ($\Delta A4GALT$) - two different sgRNAs targeting the entire ORF (light blue). *Cas9* active sites are shown in yellow color. $\Delta A4GALT$ cells were identified using three different primers (CRISPR_F, CRISPR_R and ORF_R; blue) resulting 1335bp deletion. **B)** Identification of homozygous $\Delta A4GALT$ cells: Single cell clones were assayed by three genotyping PCRs (1:Deletion PCR; 1863bp and 500bp, 2:wild type specific PCR; 1378bp and 3:inversion PCR; 937bp) showing various genotypes (wild type-wt, deletion-del, inversion-inv; wt/del, inv/del, inv/inv and del/del). **C)** DNA sequence variation (indels) at the CRISPR-Cas9 active sites: homozygous $\Delta A4GALT$ (1335bp) was detected in $\Delta A4GALT$ _1 and $\Delta A4GALT$ _2 while $\Delta A4GALT$ _3 was heterozygously deleted (1335bp and 1208bp). Protospacer adjacent motif (PAM) (red), red arrows indicate predicted deletion sites. **D)** Off target data displayed no sequence variation compare to wild type. Predicted *Cas9*-active off target sites are displayed in red arrows shown in a representative $\Delta A4GALT$ clone. **E)** Depletion of globosides and P₁ in $\Delta A4GALT$ clones: Counter plot represents the data for wild type and $\Delta A4GALT$ showing negative control (unstained cells, red) and GSL positive cells (green). The value provided in each counterplot refers to the percentage of GSL positive cells. Corresponding barchart displays the mean \pm standard deviation (S.D.) of three independent experiments for wildtype (light grey) and three $\Delta A4GALT$ clones (dark grey), student *t*-test, ***p*-value < 0.01, ****p*-value < 0.001.

Figure 3

Appearance of mesenchymal features upon deletion of globosides **A)** Cell morphology of *A4GALT* and $\Delta A4GALT$ (40x magnification): the arrows indicate (a) goblet like epithelial structure (b) formation of clamp and (c) cell protrusions. **B)** Cell growth curve for 120h. The value provided in each time point refers to the number of cells counted every 24h. **C)** MTT cell viability and proliferation assay for wild type (*A4GALT*, grey line) and $\Delta A4GALT$ (black line) cells. **D)** Representative wells with cell colonies and bar chart for quantification of anchorage-dependent growth **E)** Anchorage-independent growth in show reduced colonies in $\Delta A4GALT$ cells compared with wild type cells. **F)** Representative histograms for cell-detachment-induced apoptosis (anoikis) in wildtype and $\Delta A4GALT$ cells showing unstained or negative control (green) and percentage of propidium iodide (PI, stained for dead cells)-stained cells (red). The percentage in each histogram refers to the PI-positively stained cells. Corresponding line chart showing viable cells (y-axis) measured by MTT absorbance ratio (normalized to 100% at day 0) between day 0 and day 10 in both wildtype (*A4GALT*) and $\Delta A4GALT$ cells. **G)** Western-blot data represents more cleaved PARP during day 7 and day 10 in wild type cells compare with $\Delta A4GALT$ cells. **H)** Cell migration assay, **I)** Cell invasion (Matrigel) assay, **J)** Wound healing assay, **K)** phagokinetic track motility. Representative images are shown along with data quantification. A number of 10 images were analyzed for each experiment. Data are presented as bar charts showing mean \pm standard deviation (S.D.) of three independent experiments, student *t*-test, **p*-value < 0.05, ***p*-value < 0.01. Loss of *A4GALT* results in enhanced cancer cell dissemination in tumor xenograft model. **L)** Confocal imaging (z-stack images at 40x magnification) shows that metastatic $\Delta A4GALT$ IGROV1 cells are dispersing throughout the fish body (arrows) whereas non-invasive wild type IGROV1 cells remain in the yolk sac. Corresponding counterplot and bar chart to the right displayed the percentage of CM-Dil positive cancer cells.

Figure 4

E-cadherin mediated cell-cell adhesion depends on the upstream glycosphingolipids A)

Bar chart represents the GSLs expression of different IGROV1 (*A4GALT*, $\Delta A4GALT$, Rescue (DXD) and Rescue mutant (DXD)) cell lines. **B)** Western blot data display the loss of E-cadherin in $\Delta A4GALT$ cells and re-expression of E-cadherin (full length and cytosolic). Second Western blot shows partial rescue of E-cadherin expression in $\Delta A4GALT$ re-expressing *A4GALT* (DXD) in contrast to mutant *A4GALT* (DXA). **C)** Confocal fluorescence images (40x magnification) show loss of membranous E-cadherin staining in $\Delta A4GALT$ compare with wild type *A4GALT* and in DXD rescued cells displaying partial membranous E-cadherin staining, whereas overexpression of E-cadherin (full length and cytosolic) in $\Delta A4GALT$ cells were diminished E-cadherin membranous staining.

Figure 5

The presence of globosides is vital in intermediate EMT cells **A)** *CDH1*, *VIM* and *A4GALT* expression among ovarian cancer cell lines representing the full EMT spectrum. **B)** Corresponding Western blot showing expression of E-cadherin, Vimentin and tubulin. Matching heatmap shows the means of Gb3 and SSEA3 expression of three independent flow cytometry experiments for each cell line. **C)** Deletion or overexpression of *A4GALT* leads to absence or presence of globosides, respectively. Wildtype and $\Delta A4GALT$ cells are shown BG1 and SKOV3. Overexpression of *A4GALT* (OE *A4GALT*) is shown next to parental A2780. E-cadherin expression is lost in SKOV3 $\Delta A4GALT$ cells. SKOV3ip cells show elevated E-cadherin expression. **D)** Representative immunofluorescence images for E-cadherin (green) and DAPI (blue) in SKOV3, SKOV3 $\Delta A4GALT$, and SKOV3ip cells. **E)** Corresponding anchorage-dependent growth (colony formation assay) and Barchart summarizing three independent experiments. **F)** Increasing resistance to doxorubicin in intermediate EMT cells deleted for *A4GALT*. Line charts showing three independent MTT assays. IC_{50} 's for parental (wildtype, black), $\Delta A4GALT$ (red), and SKOV3ip (green) are provided below each line chart. **G)** Representative dot plot for un- and CTx-treated cancer cell lines unstained (red) and double-stained for CD24 and CD44 (light blue). **H)** Alteration of GSLs (LacCer, Gb3, and SSEA3) upon CTx treatment in corresponding cancer cell lines. **I)** Expression of E-cadherin, Vimentin, and tubulin in parental and genetically modified (*A4GALT*) cell lines treated with CTx.

Figure 6

Degree of DNA methylation at the promoter region of *CDH1* correlates with presence of A4GALT and its glycosidic products.

A) CpG island analysis predicts a CpG island at the transcription start site of human *CDH1*. Exon 1 and 2 are shown in black and predicted (depending on the algorithm used) CpG islands are shown as green vertical bars. Genomic region analyzed by bisulfite sequencing in more detail (red bar) and further magnified for CpGs analyzed throughout this study. **B)** Lollipop plots showing degree of DNA methylation at the promoter region of *CDH1* for representing the EMT spectrum based on E-cadherin expression. Total of methylated CpGs are provided along with the standard error between sequences (n=6). **C)** Western blot showing re-expression of E-cadherin in mock (DMSO) and 5-Aza-treated cancer cells IGROV1, IGROV1 Δ A4GALT, and IGROV1 Δ A4GALT Rescue DXD cells. **D)** Membranous staining of E-cadherin is only present in cells being positive for A4GALT and globosides. 5-Aza treatment in IGROV1 Δ A4GALT Rescue DXD cells reveals cell-cell adhesion *via* E-cadherin whereas IGROV1 Δ A4GALT remain negative for membranous E-cadherin staining.

Figures:

Figure 1

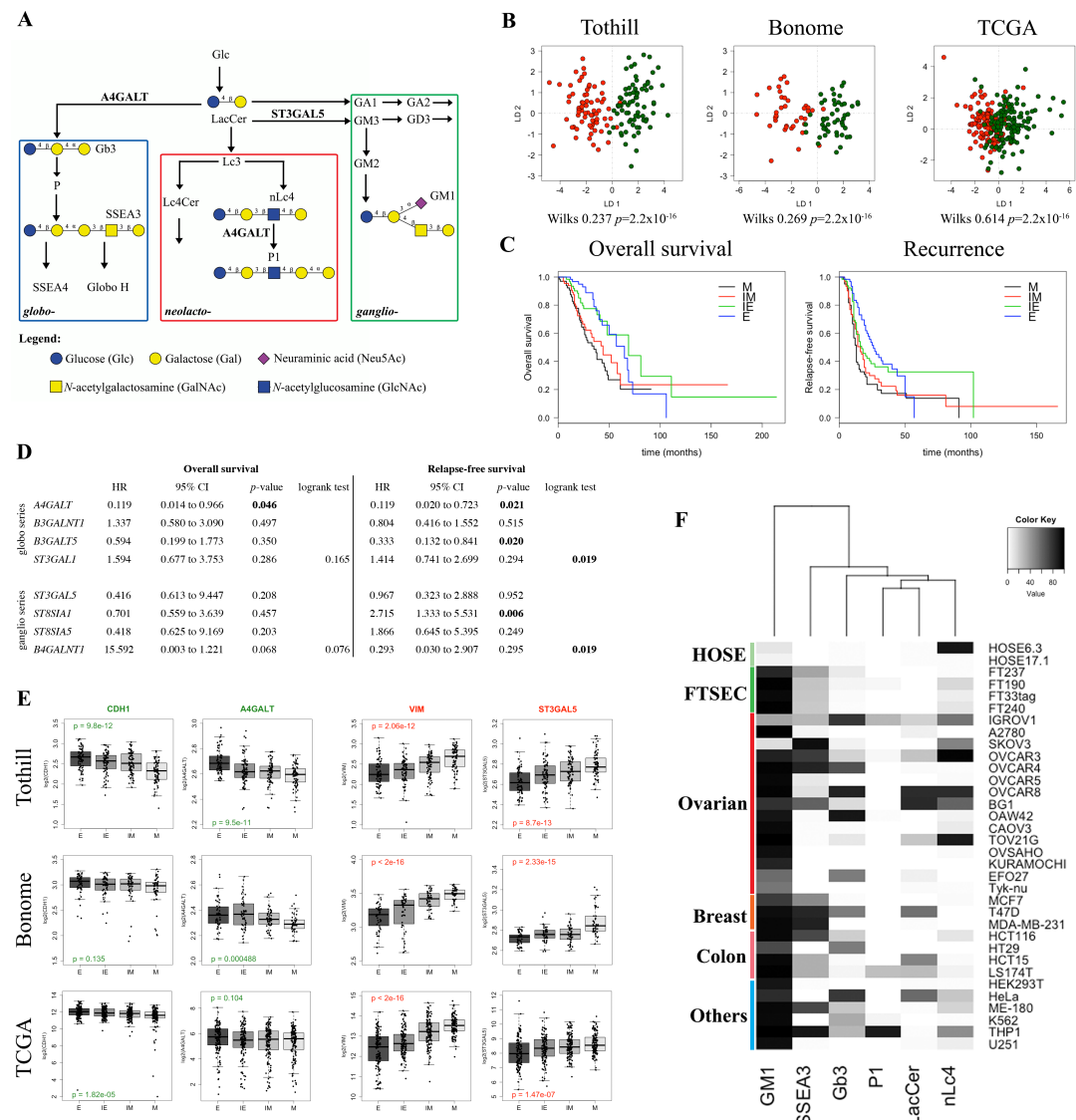


Figure 2

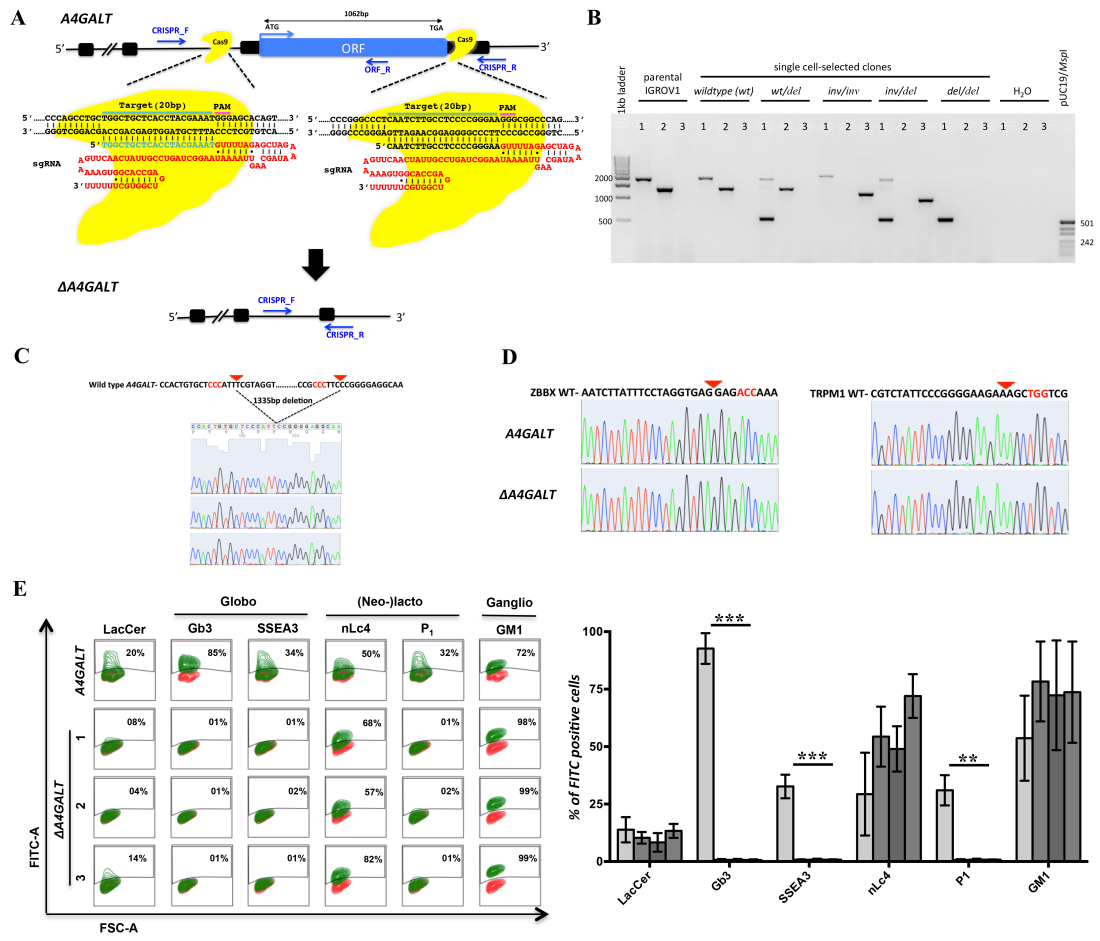


Figure 3

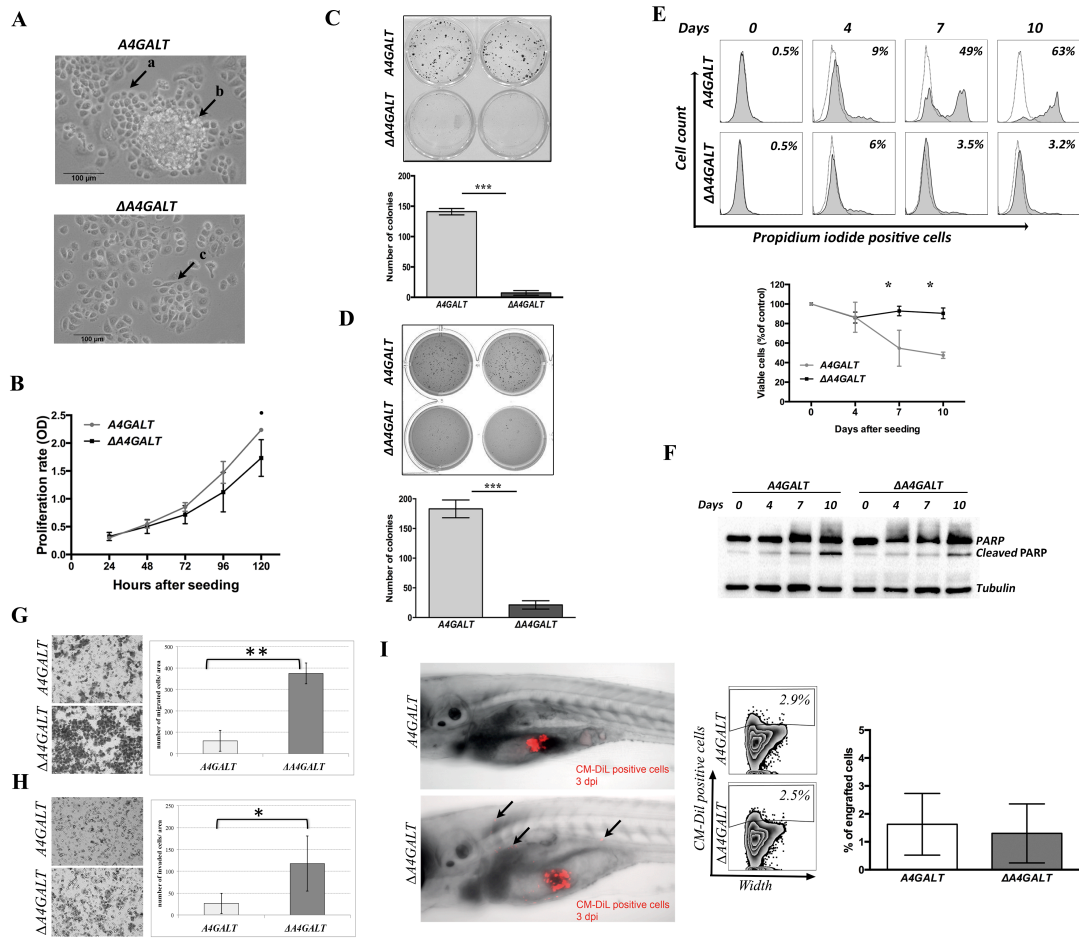


Figure 4

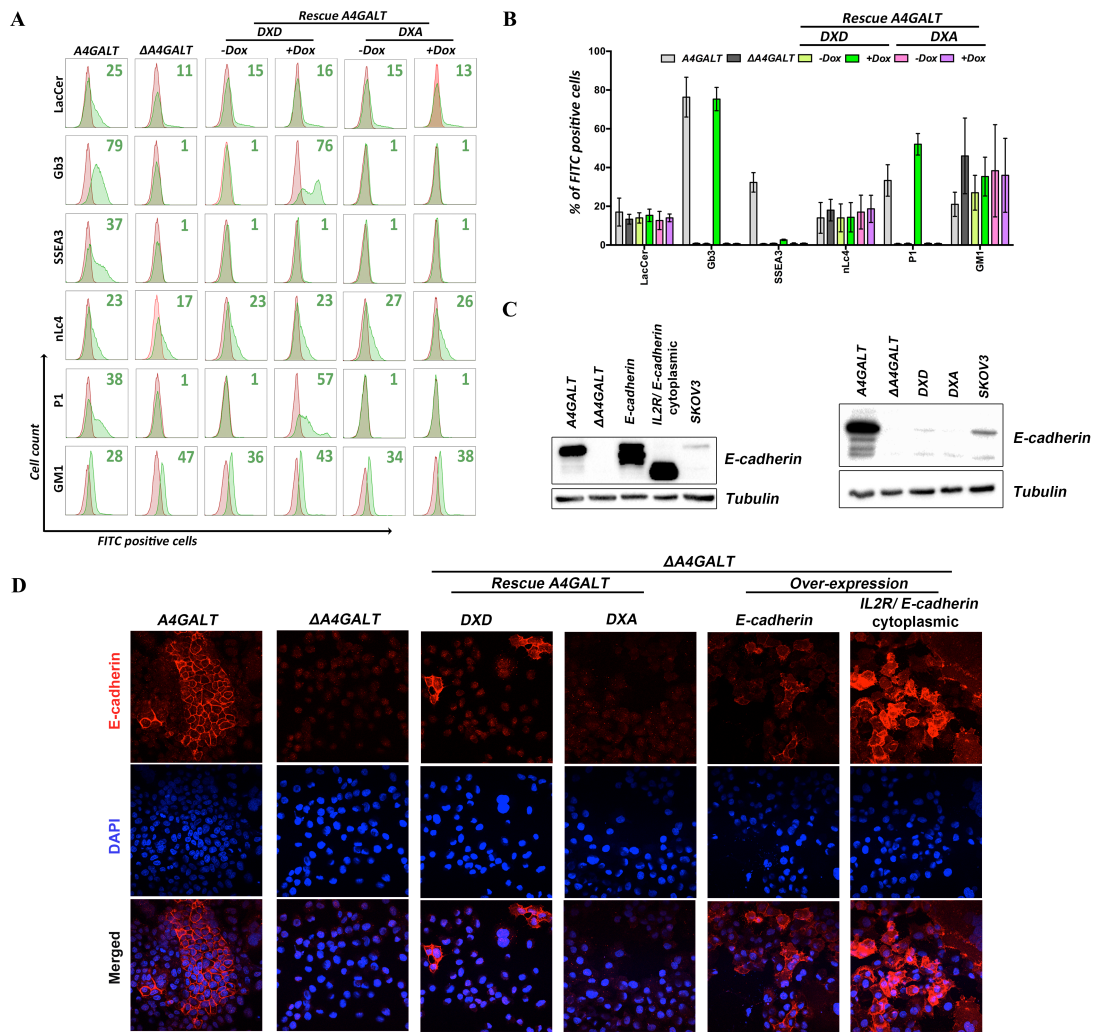


Figure 5

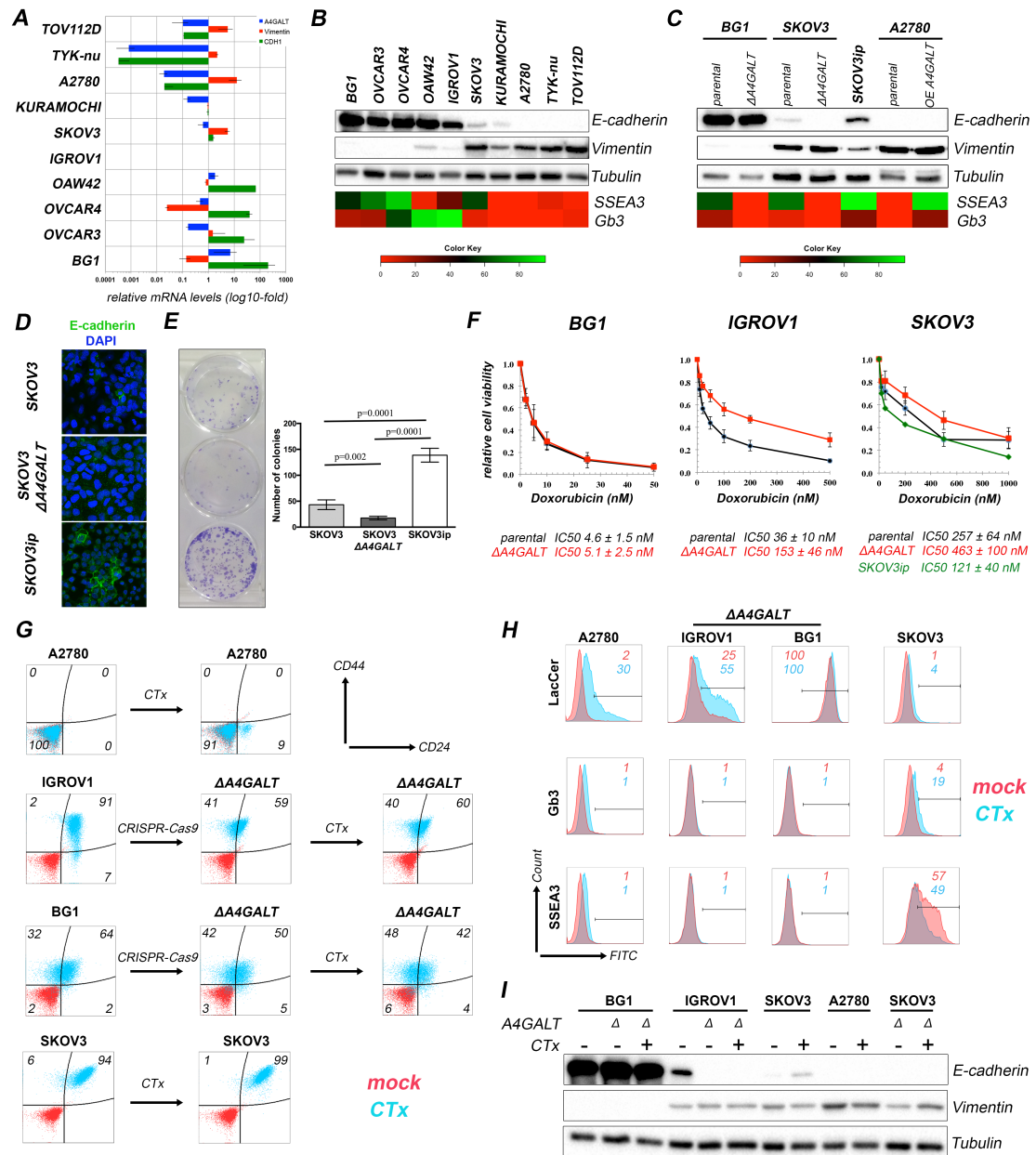
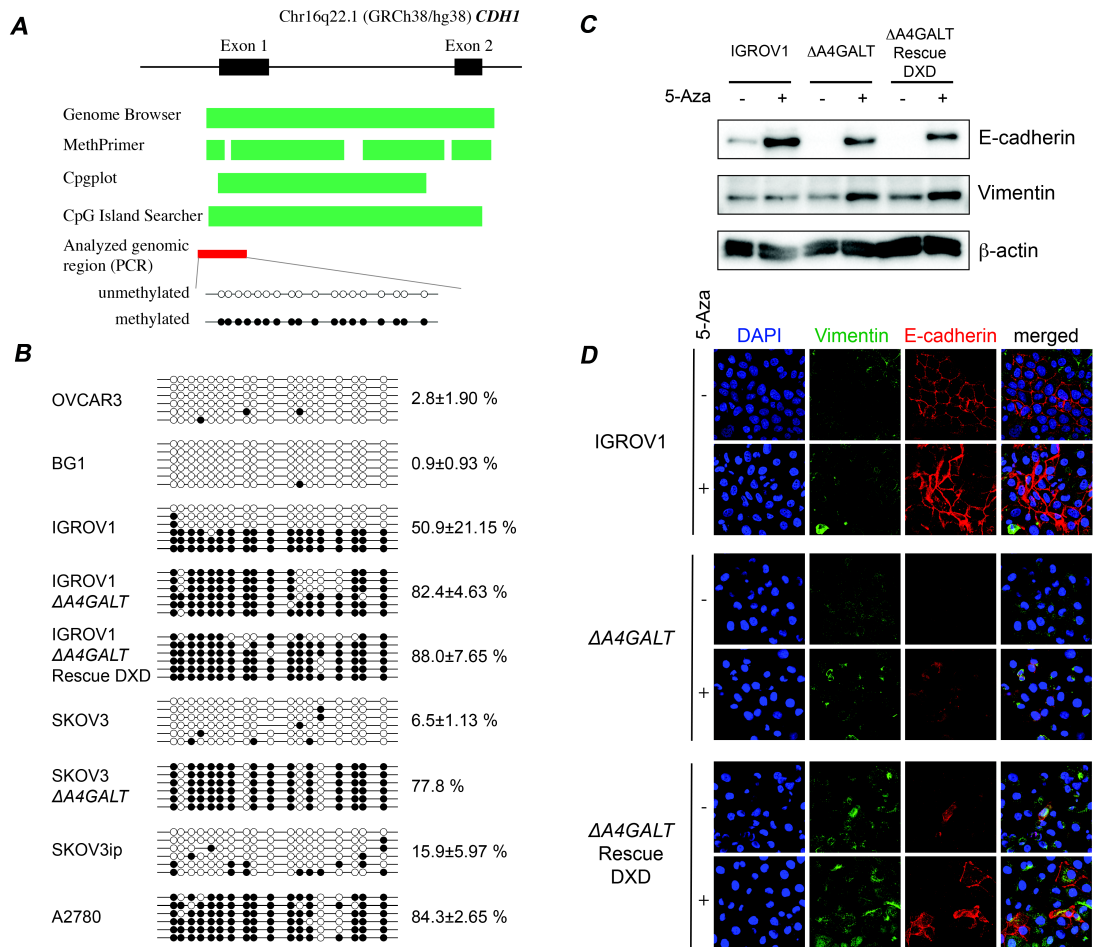


Figure 6



References:

Ahmed, N., Abubaker, K., Findlay, J., and Quinn, M. (2010). Epithelial mesenchymal transition and cancer stem cell-like phenotypes facilitate chemoresistance in recurrent ovarian cancer. *Curr Cancer Drug Targets* 10, 268-278.

Alam, S., Fedier, A., Kohler, R.S., and Jacob, F. (2015). Glucosylceramide synthase inhibitors differentially affect expression of glycosphingolipids. *Glycobiology* 25, 351-356.

Anugraham, M., Everest-Dass, A.V., Jacob, F., and Packer, N.H. (2015). A platform for the structural characterization of glycans enzymatically released from glycosphingolipids extracted from tissue and cells. *Rapid communications in mass spectrometry : RCM* 29, 545-561.

Barretina, J., Caponigro, G., Stransky, N., Venkatesan, K., Margolin, A.A., Kim, S., Wilson, C.J., Lehar, J., Kryukov, G.V., Sonkin, D., *et al.* (2012). The Cancer Cell Line Encyclopedia enables predictive modelling of anticancer drug sensitivity. *Nature* 483, 603-607.

Bassaganas, S., Carvalho, S., Dias, A.M., Perez-Garay, M., Ortiz, M.R., Figueras, J., Reis, C.A., Pinho, S.S., and Peracaula, R. (2014). Pancreatic cancer cell glycosylation regulates cell adhesion and invasion through the modulation of alpha2beta1 integrin and E-cadherin function. *PloS one* 9, e98595.

Blehschmidt, K., Sassen, S., Schmalfeldt, B., Schuster, T., Hofler, H., and Becker, K.F. (2008). The E-cadherin repressor Snail is associated with lower overall survival of ovarian cancer patients. *British journal of cancer* 98, 489-495.

Bonome, T., Lee, J.Y., Park, D.C., Radonovich, M., Pise-Masison, C., Brady, J., Gardner, G.J., Hao, K., Wong, W.H., Barrett, J.C., *et al.* (2005). Expression profiling of serous low malignant potential, low-grade, and high-grade tumors of the ovary. *Cancer research* 65, 10602-10612.

Bucior, I., Scheuring, S., Engel, A., and Burger, M.M. (2004). Carbohydrate-carbohydrate interaction provides adhesion force and specificity for cellular recognition. *The Journal of cell biology* *165*, 529-537.

Busche, S., Kremmer, E., and Posern, G. (2010). E-cadherin regulates MAL-SRF-mediated transcription in epithelial cells. *Journal of cell science* *123*, 2803-2809.

Cancer Genome Atlas Research, N. (2011). Integrated genomic analyses of ovarian carcinoma. *Nature* *474*, 609-615.

Clevers, H. (2011). The cancer stem cell: premises, promises and challenges. *Nature medicine* *17*, 313-319.

Davidson, B., Berner, A., Nesland, J.M., Risberg, B., Berner, H.S., Trope, C.G., Kristensen, G.B., Bryne, M., and Ann Florenes, V. (2000). E-cadherin and alpha-, beta-, and gamma-catenin protein expression is up-regulated in ovarian carcinoma cells in serous effusions. *The Journal of pathology* *192*, 460-469.

Diepenbruck, M., and Christofori, G. (2016). Epithelial-mesenchymal transition (EMT) and metastasis: yes, no, maybe? *Curr Opin Cell Biol* *43*, 7-13.

Gao, J., Aksoy, B.A., Dogrusoz, U., Dresdner, G., Gross, B., Sumer, S.O., Sun, Y., Jacobsen, A., Sinha, R., Larsson, E., *et al.* (2013). Integrative analysis of complex cancer genomics and clinical profiles using the cBioPortal. *Sci Signal* *6*, p11.

Gottardi, C.J., Wong, E., and Gumbiner, B.M. (2001). E-cadherin suppresses cellular transformation by inhibiting beta-catenin signaling in an adhesion-independent manner. *The Journal of cell biology* *153*, 1049-1060.

Guan, F., Handa, K., and Hakomori, S.I. (2009). Specific glycosphingolipids mediate epithelial-to-mesenchymal transition of human and mouse epithelial cell lines. *Proceedings of the National Academy of Sciences of the United States of America* *106*, 7461-7466.

Guan, F., Schaffer, L., Handa, K., and Hakomori, S.I. (2010). Functional role of gangliotetraosylceramide in epithelial-to-mesenchymal transition process induced by hypoxia

and by TGF- β . *FASEB journal* : official publication of the Federation of American Societies for Experimental Biology *24*, 4889-4903.

Hakomori, S. (2004). Carbohydrate-to-carbohydrate interaction in basic cell biology: a brief overview. *Archives of biochemistry and biophysics* *426*, 173-181.

Haldi, M., Ton, C., Seng, W.L., and McGrath, P. (2006). Human melanoma cells transplanted into zebrafish proliferate, migrate, produce melanin, form masses and stimulate angiogenesis in zebrafish. *Angiogenesis* *9*, 139-151.

He, X., Chien, J., and Shridhar, V. (2013). Assessment of resistance to anoikis in ovarian cancer. *Methods in molecular biology* *1049*, 347-354.

Hoot, K.E., Lighthall, J., Han, G., Lu, S.L., Li, A., Ju, W., Kulesz-Martin, M., Bottinger, E., and Wang, X.J. (2008). Keratinocyte-specific Smad2 ablation results in increased epithelial-mesenchymal transition during skin cancer formation and progression. *The Journal of clinical investigation* *118*, 2722-2732.

Hosono, S., Kajiyama, H., Terauchi, M., Shibata, K., Ino, K., Nawa, A., and Kikkawa, F. (2007). Expression of Twist increases the risk for recurrence and for poor survival in epithelial ovarian carcinoma patients. *British journal of cancer* *96*, 314-320.

Huang, R.Y., Chung, V.Y., and Thiery, J.P. (2012a). Targeting pathways contributing to epithelial-mesenchymal transition (EMT) in epithelial ovarian cancer. *Curr Drug Targets* *13*, 1649-1653.

Huang, R.Y., Guilford, P., and Thiery, J.P. (2012b). Early events in cell adhesion and polarity during epithelial-mesenchymal transition. *Journal of cell science* *125*, 4417-4422.

Huang, R.Y., Wong, M.K., Tan, T.Z., Kuay, K.T., Ng, A.H., Chung, V.Y., Chu, Y.S., Matsumura, N., Lai, H.C., Lee, Y.F., *et al.* (2013). An EMT spectrum defines an anoikis-resistant and spheroidogenic intermediate mesenchymal state that is sensitive to e-cadherin restoration by a src-kinase inhibitor, saracatinib (AZD0530). *Cell death & disease* *4*, e915.

Ihara, H., Ikeda, Y., Koyota, S., Endo, T., Honke, K., and Taniguchi, N. (2002). A catalytically inactive beta 1,4-N-acetylglucosaminyltransferase III (GnT-III) behaves as a dominant negative GnT-III inhibitor. *European journal of biochemistry / FEBS* 269, 193-201.

Jacob, F., Anugraham, M., Pochechueva, T., Tse, B.W., Alam, S., Guertler, R., Bovin, N.V., Fedier, A., Hacker, N.F., Huflejt, M.E., *et al.* (2014). The glycosphingolipid P(1) is an ovarian cancer-associated carbohydrate antigen involved in migration. *British journal of cancer* 111, 1634-1645.

Jacob, F., Goldstein, D.R., Bovin, N.V., Pochechueva, T., Spengler, M., Caduff, R., Fink, D., Vuskovic, M.I., Huflejt, M.E., and Heinzelmann-Schwarz, V. (2012). Serum antiglycan antibody detection of nonmucinous ovarian cancers by using a printed glycan array. *International journal of cancer Journal international du cancer* 130, 138-146.

Jacob, F., Tse, B.W.C., Guertler, R., Nixdorf, S., Bovin, N.V., Hacker, N., and Heinzelmann-Schwarz, V. (2011). P1 antigen is present on the serous ovarian cancer cell line, IGROV1, correlating with A4GALT overexpression and altered cell behaviour. *Glycobiology* 21, 1454-1531.

Jensen, P.H., Karlsson, N.G., Kolarich, D., and Packer, N.H. (2012). Structural analysis of N- and O-glycans released from glycoproteins. *Nature protocols* 7, 1299-1310.

Kalluri, R., and Weinberg, R.A. (2009). The basics of epithelial-mesenchymal transition. *The Journal of clinical investigation* 119, 1420-1428.

Kelly, T.K., Liu, Y., Lay, F.D., Liang, G., Berman, B.P., and Jones, P.A. (2012). Genome-wide mapping of nucleosome positioning and DNA methylation within individual DNA molecules. *Genome research* 22, 2497-2506.

Kohler, R.S., Anugraham, M., Lopez, M.N., Xiao, C., Schoetzau, A., Hettich, T., Schlotterbeck, G., Fedier, A., Jacob, F., and Heinzelmann-Schwarz, V. (2016). Epigenetic activation of MGAT3 and corresponding bisecting GlcNAc shortens the survival of cancer patients. *Oncotarget* 7, 51674-51686.

Konantz, M., Balci, T.B., Hartwig, U.F., Dellaire, G., Andre, M.C., Berman, J.N., and Lengerke, C. (2012). Zebrafish xenografts as a tool for in vivo studies on human cancer. *Annals of the New York Academy of Sciences* 1266, 124-137.

Krauss, J., Astrinidis, P., Frohnhof, H.G., Walderich, B., and Nusslein-Volhard, C. (2013). transparent, a gene affecting stripe formation in Zebrafish, encodes the mitochondrial protein Mpv17 that is required for iridophore survival. *Biol Open* 2, 703-710.

Li, J., Rancour, D.M., Allende, M.L., Worth, C.A., Darling, D.S., Gilbert, J.B., Menon, A.K., and Young, W.W., Jr. (2001). The DXD motif is required for GM2 synthase activity but is not critical for nucleotide binding. *Glycobiology* 11, 217-229.

Liang, Y.J., Ding, Y., Levery, S.B., Lobaton, M., Handa, K., and Hakomori, S.I. (2013). Differential expression profiles of glycosphingolipids in human breast cancer stem cells vs. cancer non-stem cells. *Proceedings of the National Academy of Sciences of the United States of America*.

Liang, Y.J., Kuo, H.H., Lin, C.H., Chen, Y.Y., Yang, B.C., Cheng, Y.Y., Yu, A.L., Khoo, K.H., and Yu, J. (2010). Switching of the core structures of glycosphingolipids from globo- and lacto- to ganglio-series upon human embryonic stem cell differentiation. *Proceedings of the National Academy of Sciences of the United States of America* 107, 22564-22569.

Lou, E., Fujisawa, S., Morozov, A., Barlas, A., Romin, Y., Dogan, Y., Gholami, S., Moreira, A.L., Manova-Todorova, K., and Moore, M.A. (2012). Tunneling nanotubes provide a unique conduit for intercellular transfer of cellular contents in human malignant pleural mesothelioma. *PloS one* 7, e33093.

Maeda, M., Johnson, K.R., and Wheelock, M.J. (2005). Cadherin switching: essential for behavioral but not morphological changes during an epithelium-to-mesenchyme transition. *Journal of cell science* 118, 873-887.

Mani, S.A., Guo, W., Liao, M.J., Eaton, E.N., Ayyanan, A., Zhou, A.Y., Brooks, M., Reinhard, F., Zhang, C.C., Shipitsin, M., *et al.* (2008). The epithelial-mesenchymal transition generates cells with properties of stem cells. *Cell* 133, 704-715.

Massague, J. (2008). TGFbeta in Cancer. *Cell* 134, 215-230.

Mathow, D., Chessa, F., Rabionet, M., Kaden, S., Jennemann, R., Sandhoff, R., Grone, H.J., and Feuerborn, A. (2015). Zeb1 affects epithelial cell adhesion by diverting glycosphingolipid metabolism. *EMBO Rep* 16, 321-331.

Merritt, E.A., Sarfaty, S., van den Akker, F., L'Hoir, C., Martial, J.A., and Hol, W.G. (1994). Crystal structure of cholera toxin B-pentamer bound to receptor GM1 pentasaccharide. *Protein science : a publication of the Protein Society* 3, 166-175.

Nieto, M.A., Huang, R.Y., Jackson, R.A., and Thiery, J.P. (2016). Emt: 2016. *Cell* 166, 21-45.

Pattabiraman, D.R., Bierie, B., Kober, K.I., Thiru, P., Krall, J.A., Zill, C., Reinhardt, F., Tam, W.L., and Weinberg, R.A. (2016). Activation of PKA leads to mesenchymal-to-epithelial transition and loss of tumor-initiating ability. *Science* 351, aad3680.

Persson, M., Letts, J.A., Hosseini-Maaf, B., Borisova, S.N., Palcic, M.M., Evans, S.V., and Olsson, M.L. (2007). Structural effects of naturally occurring human blood group B galactosyltransferase mutations adjacent to the DXD motif. *The Journal of biological chemistry* 282, 9564-9570.

Pochechueva, T., Jacob, F., Goldstein, D.R., Huflejt, M.E., Chinarev, A., Caduff, R., Fink, D., Hacker, N., Bovin, N.V., and Heinzelmann-Schwarz, V. (2011). Comparison of printed glycan array, suspension array and ELISA in the detection of human anti-glycan antibodies. *Glycoconjugate journal* 28, 507-517.

Ran, F.A., Hsu, P.D., Wright, J., Agarwala, V., Scott, D.A., and Zhang, F. (2013). Genome engineering using the CRISPR-Cas9 system. *Nat Protoc* 8, 2281-2308.

Schaefer, T., Wang, H., Mir, P., Konantz, M., Pereboom, T.C., Paczulla, A.M., Merz, B., Fehm, T., Perner, S., Rothfuss, O.C., *et al.* (2015). Molecular and functional interactions between AKT and SOX2 in breast carcinoma. *Oncotarget* 6, 43540-43556.

Shaul, Y.D., Freinkman, E., Comb, W.C., Cantor, J.R., Tam, W.L., Thiru, P., Kim, D., Kanarek, N., Pacold, M.E., Chen, W.W., *et al.* (2014). Dihydropyrimidine accumulation is required for the epithelial-mesenchymal transition. *Cell* *158*, 1094-1109.

Svoboda, O., Stachura, D.L., Machonova, O., Zon, L.I., Traver, D., and Bartunek, P. (2016). Ex vivo tools for the clonal analysis of zebrafish hematopoiesis. *Nature protocols* *11*, 1007-1020.

Tam, W.L., and Weinberg, R.A. (2013). The epigenetics of epithelial-mesenchymal plasticity in cancer. *Nature medicine* *19*, 1438-1449.

Tan, T.Z., Miow, Q.H., Miki, Y., Noda, T., Mori, S., Huang, R.Y., and Thiery, J.P. (2014). Epithelial-mesenchymal transition spectrum quantification and its efficacy in deciphering survival and drug responses of cancer patients. *EMBO Mol Med* *6*, 1279-1293.

Teicher, B.A. (2001). Malignant cells, directors of the malignant process: role of transforming growth factor-beta. *Cancer metastasis reviews* *20*, 133-143.

Tothill, R.W., Tinker, A.V., George, J., Brown, R., Fox, S.B., Lade, S., Johnson, D.S., Trivett, M.K., Etemadmoghadam, D., Locandro, B., *et al.* (2008). Novel molecular subtypes of serous and endometrioid ovarian cancer linked to clinical outcome. *Clinical cancer research : an official journal of the American Association for Cancer Research* *14*, 5198-5208.

Uphoff, C.C., and Drexler, H.G. (2005). Detection of mycoplasma contaminations. *Methods in molecular biology* *290*, 13-23.

Wang, A.Z., Ojakian, G.K., and Nelson, W.J. (1990). Steps in the morphogenesis of a polarized epithelium. I. Uncoupling the roles of cell-cell and cell-substratum contact in establishing plasma membrane polarity in multicellular epithelial (MDCK) cysts. *Journal of cell science* *95 (Pt 1)*, 137-151.

Yu, D., Wolf, J.K., Scanlon, M., Price, J.E., and Hung, M.C. (1993). Enhanced c-erbB-2/neu expression in human ovarian cancer cells correlates with more severe malignancy that can be suppressed by E1A. *Cancer research* *53*, 891-898.

Zheng, L., Baumann, U., and Reymond, J.L. (2004). An efficient one-step site-directed and site-saturation mutagenesis protocol. *Nucleic acids research* 32, e115.

5. Further discussion and conclusion

Results obtained throughout this PhD thesis are discussed in greater detail in chapter 4. Here, I will include a general conclusion and discuss how achieved publications are related to each other.

In the present study (Publication I), we demonstrated for the first time that GSLs are expressed in ovarian cancer, in particular, Gb3, P and P₁ are found to be present in patient-derived ovarian cancer tissues as well as in immortal ovarian cancer cell lines [182]. We further show that ascites derived from late-stage ovarian cancer patients contain detectable levels of circulating anti-glycan antibodies compared with matched blood plasma independent of the volume of ascites accumulated [182]. Moreover, affinity purified anti-P₁ antibodies isolated from patient's ascites recognize P₁ expressing ovarian cancer cells [182]. We further demonstrated that fluorescence-activated cell sorted (FACS) IGROV1 cells expressing different levels of P₁ show different capability of *in vitro* directed cell motility [182]. Based on these findings together with previous work published by the Ovarian Cancer Research group, parts of the current PhD thesis aimed to establish an experimental model to elucidate the biological role of certain GSLs in the context of ovarian cancer.

As an initial approach (Publication II) we utilized two widely used glucosylceramide synthase (GCS) inhibitors, PPMP and PDMP, aiming to inhibit the expression of all glucosylceramide-related GSLs. However, our results clearly demonstrated that both, PPMP and PDMP inhibit the GSL synthesis selectively and in a cell line-dependent manner. In contrast to Gb3 which revealed reduced expression on the cell surface of four different cancer cell lines upon GCS inhibitor treatment, the downstream glycosidic product of Gb3 and SSEA3 was only reduced in one out of four cell lines. Moreover, no change was observed for GM1, nLc4, and P₁ indicating that GCS inhibitors selectively inhibit GSL synthesis. Thus, we concluded that our initial strategy was not sufficient for future applications to elucidate the function of GSLs. A plausible approach might apply genome editing (e.g. by utilizing CRISPR-*Cas9*) to generate a GCS synthase deletion ($\Delta UGCG$), which will be an effective method to identify the specific function of glucosylceramide-related related GSLs. However, considering that individual GSLs or series of GSLs have various functions described in the literature, a deletion of the GCS synthase might not be the optimal experimental model to study individual GSLs. We therefore decided to deplete the different GSL

series by knocking out the gene encoding for the key glycosyltransferase (annotated in the KEGG database) (Figure 3). Initially, we tested the use of zinc finger nucleases in combination with single-strand oligonucleotides [183] but found out that CRISPR-*Cas9* system was more efficient and straightforward in our hands.

5.1 Altered α 2-6 sialylation in ovarian cancer cells upon depletion of GSL series

Our previous studies demonstrated using printed glycan array that anti-glycan antibodies can discriminate healthy controls from ovarian cancer patients [181]. The glycan structure with the most significant discriminatory was P₁, which has been shown to present in tissue samples [182] as well as on ovarian cancer cell lines [184]. P₁ glycan structure belongs to (neo)-lacto series GSLs and the biological function of this series GSLs is rather limited in context of cancer and remains to be elucidated. In this study, we utilized the CRISPR-*Cas9* system to deplete (neo-) lacto series GSLs by knocking out the open reading frame encoding for the key glycosyltransferase *B3GNT5* (publication III) and revealed an unexpected loss of α 2-6 sialylation on *N*-glycoproteins due to the silencing of *ST6GALI* expression. The exact mechanism by which the reduction of α 2-6 sialylation on *N*-glycoproteins is still unclear. One of the possibilities might be a direct consequence of the *B3GNT5* deletion, which regulates complex associations within the glycan-processing pathway. A recent study reported similar finding in the context of salt and pepper syndrome [185], in which a homozygous transition mutation in *ST3GAL5* (GM3 synthase) was described. More importantly, in addition to the reduced GSL complexity, altered *N*- and *O*-glycans on proteins was observed due to the point mutation in the *ST3GAL5* [185]. It is still unclear whether the loss of α 2-6 sialylation on *N*-glycoproteins is thought to provide a compensation phenotype for the depletion of (neo-) lacto series GSLs. Another possibility is epigenetic regulation of *ST6GALI*, which might include histone modification, remodeling of microRNA (miR), and DNA methylation (hyper). Histone modifications, such as methylation and acetylation, can either repress or activate gene transcription through alterations in the chromatin structure. For example, expression of gangliosides synthesis enzymes GalNAc transferase and Sialyl transferase II are regulated by histone acetylation during brain development [186]. miRs control the production of the gene product through binding to the mRNA

3' UTR regions, thereby inhibiting protein translation or enhancing mRNA degradation. In metastatic melanoma cells, specific microRNAs (miR-30b and miR-30d) were highly expressed, which has been shown to suppress GALNT7 expression [187]. DNA methylation primarily occurs on CpG rich regions (CpG islands), where a methyl group is covalently attached to a cytosine with the aid of DNA methyltransferases (DNMTs). In cancer cells, some glycosyltransferase genes (*EXT1*, *B4GALNT2*, *ST3GAL6*, *MGAT3*, *MGAT4A*) are suppressed by hypermethylation of gene promoters [188-190]. The use of DNA methylation or histone deacetylation inhibitors and development of the chromatin immunoprecipitation (ChIP) technique with antibodies for these modifications allow analysis of the *ST6GAL1* regulatory mechanisms that link to the deletion of *B3GNT5*.

It has been demonstrated that cell surface sialylated glycans are upregulated in cancer and contribute to increased aggressiveness, metastasis and invasion of a tumor by increasing cancer cell motility, extravasation from the circulation into tissues and resistance to cell death [191-195]. Moreover, hypersialylation of cancer cells enhances the resistance to chemotherapy. Particularly, *ST6GAL1* has been shown to be upregulated in various cancers as a consequence of oncogenic Ras activation [196-198]. For example, the metastatic growth of colon cancer is accompanied by a significant increase of α 2-6 sialylation synthesized by *ST6GAL1* [199] and siRNA knockdown of *ST6GAL1* significantly inhibited cell invasion in various carcinoma cell lines [200-202]. On the other hand, forced expression of *ST6GAL1* in breast (MDA-MB-435) and ovarian (OV4) cancer cells leads to reduced cell-cell adhesion and enhanced capacity for invasion [201, 203]. In addition, the expression of stem cell markers has been also correlated with *ST6GAL1* expression in colon, pancreatic and ovarian cancers, which has been directly shown to promote cell motility and survival/resistance to drug treatment [204-206]. Enzymatic removal of neuraminic acid through neuraminidase treatment of metastatic murine cell lines dramatically decreases the amount of liver metastasis after splenic injection [207]. Recent data suggest that *ST6GAL1* promotes activation of PI3K/Akt signaling pathway [208, 209] for cell migration [208, 209]. However, *in vitro* studies show that the migratory responses are mediated at least in part, by the α 2, 6 sialylation on the glycoprotein β 1 integrin [210]. Cells that do not express integrin β 1, do not exhibit differential invasion upon forced expression of *ST6Gal I* [203, 210, 211].

This is in full concordance with our most recent observations (unpublished data). We found that the loss of α 2-6 sialylation was mostly on the proteins integrin β 1, α 2, α 3, and α 5. Integrins are heterodimeric transmembrane receptors capable of bidirectional signaling (“outside-in signaling” and “inside-out signaling”) [212]. Hypersialylation of β 1-integrin has been shown to impact on cell adhesion (cell to extracellular matrix (ECM)) and cell motility as well as resistance to cell death [213]. The oncogenic Ras expression promotes the upregulation of *ST6GALI* and as a result the hypersialylation of the *N*-glycans on β 1-integrin, which is part of the integrin receptor for collagen (α 1 β 1 and α 2 β 1), fibronectin (α 5 β 1) and laminin (α 3 β 1) [210, 214-217]. It has been demonstrated that hypersialylation of β 1-integrins in ovarian adenocarcinoma cells results in increased cell motility by enhancing collagen binding and migration toward collagen [203, 218]. In addition to that, cell surface α 2-6 sialylation has the ability to block apoptosis and anoikis (cell death related to detachment from other cells or the ECM) [219-223]. For example, the sialylation of α 5 β 1 fibronectin receptor blocks galectin-1 binding and the induction of anoikis [220, 222]. Along with these studies, *ST6GALI* overexpression displayed resistance to chemotherapy agents such as cisplatin, irinotecan and gemcitabine [204-206]. Taken together, all of these studies demonstrated that sialylation plays essential roles in mediating cell-ECM adhesion and migration. Hyper sialylation on integrin has been reported to increase the mobility of cancer cells, thus contributing to tumor progression. Our study displayed depletion of *B3GNT5* leads loss of α 2-6 sialylation on integrin, which plays important role in migration and adhesion. Thus depletion of *B3GNT5* might reduce the metastatic growth of ovarian cancer. The investigation of CRISPR-*Cas9* mediated *B3GNT5* deleted IGROV1 and SKOV3 cells can also be used as a model to role out the possibility of integrin subunits (β 1, α 2, α 3 and α 5) in context of ovarian cancer in a greater detail.

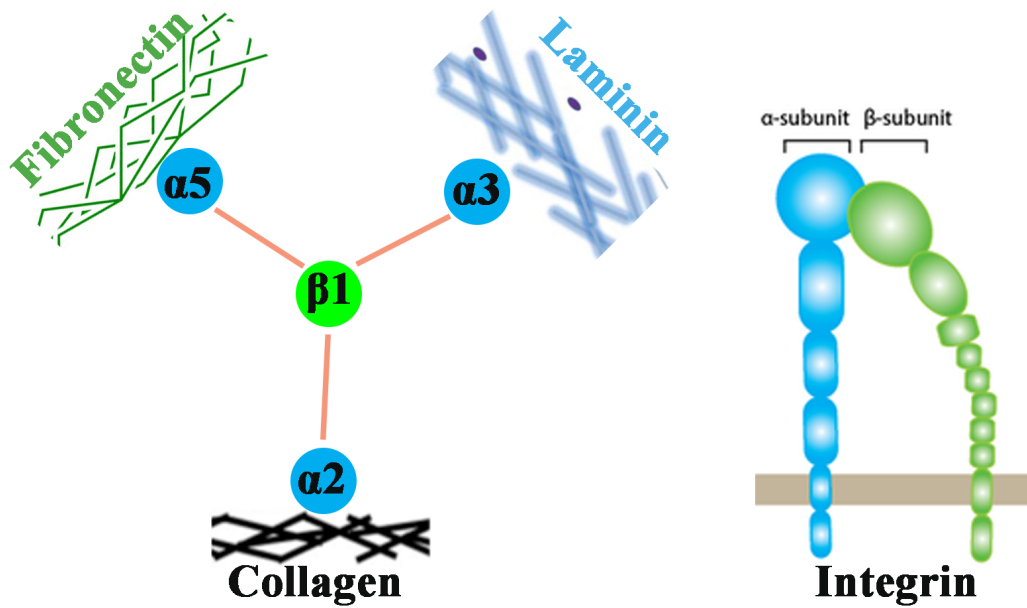


Figure 4: Integrin-ECM interaction. Integrins are heterodimeric cell-surface receptors for ECM proteins and composed of an α and a β subunit. A simplified version of the α - β -subunit pairing displayed the major extracellular ligands for each heterodimer is represented. The same integrin receptor can bind to several different ECM ligands. Intriguingly, engagement of different integrins by the same matrix molecule can elicit very different cellular responses.

5.2 Involvement of GSLs in epithelial to mesenchymal transition (EMT)

Epithelial cells are capable of changing their phenotypes including morphology, growth behaviors, adhesion characteristics and motility, while they encounter a different microenvironment or external stimuli and the well studied process is known as EMT (epithelial mesenchymal transition) [224-227]. Hay and colleagues first observed this phenotype, which was identified as an essential cellular mechanism at several specific stages in ontogenetic development [228-234]. In addition to cell morphology, adhesion and motility, the EMT process has been characterized by a decrease in epithelial markers (E-cadherin, desmoplakin and cytokeratins) while an increase in mesenchymal cell markers (N-cadherin, vimentin, fibronectin) [234, 235]. GSLs have been shown to play an important role in embryogenesis [236], tumorigenesis and cancer progression [237]. Specific types of glycosyl residues are involved in specific signaling pathways and regulate cell phenotypes. For example, GM3 inhibits epithelial growth factor receptor (EGFR) activation [238, 239], GM2 associated with tetraspanin CD82 inhibits the activation of hepatocyte growth factor receptor cMet [240], and O-fucose glycans modulate Notch signaling, which control the fate of many cell types [241, 242]. Because changes in cell adhesion, motility, and growth are an essential phenotypic change in EMT, we considered the possible involvement of GSLs in control of EMT. Our recent study revealed that CRISPR-*Cas9* mediated deletion of *A4GALT* leads to loss of globoside GSLs as well as depletion of E-cadherin (an epithelial molecule) expression in intermediate EMT ovarian cancer cell lines (Manuscript V). Therefore the results displayed a possible correlation of GSLs with EMT process, and in particular, that specific series of GSLs might contribute more to EMT than others.

Several studies have indicated that transcription factors (SNAI1 [243], SNAI2 [244], ZEB1 [245], ZEB2 [246], TCF3 [247], TWIST1 [248], *etc.*), signal transducers (RBFOX2 [249], CK1 [250], MDM2 [251], *etc.*), and microRNAs (miR-200 family [252], miR-205 [253], miR-34 [254], miR-9 [255], miR-101 [256]) are involved as inducers or regulators of the EMT process. The interesting possibility is that GSLs may affect the EMT regulatory networks to initiate the expression of mesenchymal molecules or inhibit the expression of epithelial molecules. The ability of GSLs to interact with various signal transducers, as well as with receptors for growth factors or

integrin's seems to be established. For example, i) ganglioside (GM3) was shown previously to interact with tetraspanin CD9 and integrin $\alpha 3$ to inhibit cell motility and growth [257-259], and ii) GM2-CD82 complex inhibits cMet and its crosstalk with integrin $\alpha 3\beta 1$ provide a basis to control cell motility [240].

Recent reports also demonstrated that the GSL expression dynamically alters during EMT progression [227, 260-262]. For example, i) treatment with TGF β (an EMT inducer) caused Gg4, GM2 reduction in normal murine mammary gland cells (NMuMG) and GM2 depletion in human normal bladder cells (HCV29) [227]. ii) When seeded at low density, MDCK cells undergo progressive epithelialization, which reveal a shift from sphingomyelin expression towards GSLs (GM3, galactosylceramide-sulfate (Sulf), and the globoside derivative Forssman (For)) and the reverse pattern during EMT progression by TGF β treatment [263]. All of these studies mostly focused on the ganglio series GSLs, while the expression of neutral GSLs were not considered. Our studies demonstrated for the first time loss of neutral GSLs (globosides) induced mesenchymal phenotypes in intermediate EMT cells and no significant difference was observed in Gg4 and GM2 expression, while there was two fold increased in GM1 expression pattern. This might be compensation phenotype to survive due to the loss of globosides. In another study on cancer stem cells, the author observed significant increase of ganglio series GSLs (GM2, GD2, GD3, and GD1a) while there was a reduction of globo series GSLs (Gb3) [264]. In line with this study our results displayed that not only increase of ganglio series GSLs but also the reduction of globosides depletion are required for the EMT process.

The EMT markers examined in our study were E-cadherin and Vimentin based on the transcriptomic data and defining the intermediate EMT ovarian cells. However, there are several other epithelial (cytokeratin, desmoplakin, MUC1) and mesenchymal markers (fibronectin, N-cadherin, Snail, Slug, Zeb, TWIST, etc.), which may also be applicable for the future studies. It should be noted that most of the EMT markers follow the classical EMT expression spectrum among our ovarian cancer cell lines tested (n=10) and the gene expression data from the cell line encyclopedia (unpublished data and Manuscript V). The variation of EMT marker expression pattern has been reported previously, and appears to depend on type, origin, and history of the cell lines [230, 232, 233, 265] indicating that the principal EMT markers (E-cadherin, Vimentin, etc.) are necessary to define the intermediate EMT cells. Results of our study clearly indicated that the EMT process is closely correlated

with the expression of neutral GSLs particularly globosides. Based on these results, we hypothesized that a high level of globosides are required for the maintenance of E-cadherin mediated cell-cell adhesion, possibly at junction points. Studies on organizational assembly of globosides with epithelial and mesenchymal molecules and the basis of genetic and epigenetic regulation of specific GSLs involved in EMT or MET process are expected to clarify the detail mechanism. To address this issue, we could introduce (knock-in) a controllable endogenous epithelial molecule (E-cadherin) and look for the possible interaction with globosides.

5.3 GSLs in cancer stem cells and its association to EMT

A specific glycosyl epitope (*e.g.* stem cell markers SSEA3 and SSEA4) in tumor cells whose expression is affected during the EMT process may be associated with the capability of inducing cancer stem cells (CSC) in breast cancer, which is known to provide self-renewing, invasive property of tumor cells [266-268]. Here, we demonstrated that the most commonly applied CSC marker CD24 and CD44 alter upon *A4GALT* deletion in IGROV1 and SKOV3 cell lines. In addition, Pattabiraman *et al.* induced MET (mesenchymal to epithelial transition) by treatment of cells with cholera toxin and forskolin. Interestingly, cholera toxin binds gangliosides, which are supposed to be elevated in cancer cells with mesenchymal characteristics. The study revealed that these agents elevated intracellular cAMP and subsequently activates PKA (protein kinase A). The PKA-C subunit then enters into the nucleus, which in turn regulates PHF2, a histone H3 with acetylated lysine 9 (H3K9) demethylase to induce MET [269]. In order to gain an insight into the function of GSLs in this context, defined number of cells ($\Delta A4GALT$) might be injected into nude mice studying the tumor initiating capability. More importantly, other classical CSC markers should also be considered here. Another possibility to study the tumorigenic ability, cells might be stained with SSEA3, SSEA4, CD24 and CD44 antibodies for the sorting and isolated populations (SSEA3⁺CD44⁺CD24⁻, SSEA4⁺CD44⁺CD24⁻, SSEA3⁻CD44⁺CD24⁻, SSEA4⁻CD44⁺CD24⁻, and CD44⁺CD24⁻) will then injected into the nude mice. It showed also noted whether they are forming local tumors (remaining epithelial state) or metastatic growth (displaying mesenchymal phenotypes). Moreover, mesenchymal breast cancer cells became epithelial upon cholera toxin or forskolin treatment shown by increased E-cadherin expression together with an increase of CD24 and decrease of CD44. However, not all cancer

cell lines investigated in this study were inducible by neither cholera toxin nor forskolin. This is because those cell lines displayed DNA promoter hypermethylation for several key epithelial genomic loci [269]. Another possibility might be due to the different stages of EMT/MET, as intermediated EMT cell lines seem to respond to various inducing agents (manuscript V). In line, CTx-induced MET was only observed in intermediate mesenchymal cells among all ovarian cancer cell lines (characterized by the expression of E-cadherin and Vimentin) tested in Jacob *et al.* (Manuscript V). Of note, we also demonstrated that inducible MET depends on the expression of globosides in ovarian cancer cells. To further investigate the role of globosides in cholera toxin inducible MET system, ectopic expression of mutant PKA (a constitutive expression of PKA) might be the next step to study whether the PKA pathway alters the presence of *A4GALT* and downstream globosides in intermediate EMT ovarian cancer cells.

6. References

1. Ferlay, J., et al., *Cancer incidence and mortality worldwide: sources, methods and major patterns in GLOBOCAN 2012*. Int J Cancer, 2015. **136**(5): p. E359-86.
2. WorldCancerReport, <World Cancer Report.pdf>. World Health Organization, 2014.
3. Siegel, R.L., K.D. Miller, and A. Jemal, *Cancer Statistics, 2016*. Ca-a Cancer Journal for Clinicians, 2016. **66**(1): p. 7-30.
4. Jemal, A., et al., *Global Cancer Statistics*. Ca-a Cancer Journal for Clinicians, 2011. **61**(2): p. 69-90.
5. Sant, M., et al., *Survival of women with cancers of breast and genital organs in Europe 1999-2007: Results of the EURO CARE-5 study*. European Journal of Cancer, 2015. **51**(15): p. 2191-2205.
6. Sant, M., et al., *Survival of women with cancers of breast and genital organs in Europe 1999-2007: results of the EURO CARE-5 study*. Eur J Cancer, 2015.
7. Lowe, K.A., et al., *An international assessment of ovarian cancer incidence and mortality*. Gynecologic Oncology, 2013. **130**(1): p. 107-114.
8. Sung, P.L., et al., *Global distribution pattern of histological subtypes of epithelial ovarian cancer: A database analysis and systematic review*. Gynecologic Oncology, 2014. **133**(2): p. 147-154.
9. Yang, H.P., et al., *Ovarian Cancer Incidence Trends in Relation to Changing Patterns of Menopausal Hormone Therapy Use in the United States*. Journal of Clinical Oncology, 2013. **31**(17): p. 2146-U135.
10. Matulonis, U.A., et al., *Ovarian cancer*. Nature Reviews Disease Primers, 2016. **2**.
11. Gilks, C.B., *Subclassification of ovarian surface epithelial tumors based on correlation of histologic and molecular pathologic data*. Int J Gynecol Pathol, 2004. **23**(3): p. 200-5.
12. Hess, V., et al., *Mucinous epithelial ovarian cancer: a separate entity requiring specific treatment*. J Clin Oncol, 2004. **22**(6): p. 1040-4.
13. Heinzlmann-Schwarz, V.A., et al., *A distinct molecular profile associated with mucinous epithelial ovarian cancer*. Br J Cancer, 2006. **94**(6): p. 904-13.
14. Dehari, R., et al., *The development of high-grade serous carcinoma from atypical proliferative (borderline) serous tumors and low-grade micropapillary serous carcinoma: a morphologic and molecular genetic analysis*. Am J Surg Pathol, 2007. **31**(7): p. 1007-12.
15. Kurman, R.J. and I.M. Shih, *Pathogenesis of ovarian cancer: Lessons from morphology and molecular biology and their clinical implications*. International Journal of Gynecological Pathology, 2008. **27**(2): p. 151-160.
16. Ahmed, A.A., et al., *Driver mutations in TP53 are ubiquitous in high grade serous carcinoma of the ovary*. Journal of Pathology, 2010. **221**(1): p. 49-56.
17. Berry, N.B. and S.A. Bapat, *Ovarian cancer plasticity and epigenomics in the acquisition of a stem-like phenotype*. J Ovarian Res, 2008. **1**: p. 8.
18. Vathipadietal, V., et al., *Identification of a potential ovarian cancer stem cell gene expression profile from advanced stage papillary serous ovarian cancer*. PLoS One, 2012. **7**(1): p. e29079.

19. Berkenblit, A. and S.A. Cannistra, *Advances in the management of epithelial ovarian cancer*. J Reprod Med, 2005. **50**(6): p. 426-38.
20. Fishman, D.A. and K. Bozorgi, *The scientific basis of early detection of epithelial ovarian cancer: the National Ovarian Cancer Early Detection Program (NOCEDP)*. Cancer Treat Res, 2002. **107**: p. 3-28.
21. Kim, J., et al., *The ovary is an alternative site of origin for high-grade serous ovarian cancer in mice*. Clinical Cancer Research, 2015. **21**.
22. Cho, K.R. and M. Shih Ie, *Ovarian cancer*. Annu Rev Pathol, 2009. **4**: p. 287-313.
23. Bast, R.C., Jr., B. Hennessey, and G.B. Mills, *The biology of ovarian cancer: new opportunities for translation*. Nat Rev Cancer, 2009. **9**(6): p. 415-28.
24. Seidman, J.D., et al., *The histologic type and stage distribution of ovarian carcinomas of surface epithelial origin*. International Journal of Gynecological Pathology, 2004. **23**(1): p. 41-44.
25. Seidman, J.D., P. Zhao, and A. Yemelyanova, *"Primary peritoneal" high-grade serous carcinoma is very likely metastatic from serous tubal intraepithelial carcinoma: Assessing the new paradigm of ovarian and pelvic serous carcinogenesis and its implications for screening for ovarian cancer*. Gynecologic Oncology, 2011. **120**(3): p. 470-473.
26. Bell, D., et al., *Integrated genomic analyses of ovarian carcinoma*. Nature, 2011. **474**(7353): p. 609-615.
27. Langyel, E., *Ovarian Cancer Development and Metastasis*. American Journal of Pathology, 2010. **177**(3): p. 1053-1064.
28. Yemelyanova, A.V., et al., *Pathology of stage I versus stage III ovarian carcinoma with implications for pathogenesis and screening*. International Journal of Gynecological Cancer, 2008. **18**(3): p. 465-469.
29. Hogg, R. and M. Friedlander, *Biology of epithelial ovarian cancer: Implications for screening women at high genetic risk*. Journal of Clinical Oncology, 2004. **22**(7): p. 1315-1327.
30. Lengyel, E., *Ovarian cancer development and metastasis*. Am J Pathol, 2010. **177**(3): p. 1053-64.
31. Bowtell, D.D., *The genesis and evolution of high-grade serous ovarian cancer*. Nat Rev Cancer, 2010. **10**(11): p. 803-8.
32. Kurman, R.J. and M. Shih Ie, *The origin and pathogenesis of epithelial ovarian cancer: a proposed unifying theory*. Am J Surg Pathol, 2010. **34**(3): p. 433-43.
33. Dubeau, L., *The cell of origin of ovarian epithelial tumours*. Lancet Oncol, 2008. **9**(12): p. 1191-7.
34. Feeley, K.M. and M. Wells, *Precursor lesions of ovarian epithelial malignancy*. Histopathology, 2001. **38**(2): p. 87-95.
35. Bell, D.A., *Origins and molecular pathology of ovarian cancer*. Modern Pathology, 2005. **18**: p. S19-S32.
36. Auersperg, N., *The origin of ovarian carcinomas: a unifying hypothesis*. Int J Gynecol Pathol, 2011. **30**(1): p. 12-21.
37. Auersperg, N., M.M. Woo, and C.B. Gilks, *The origin of ovarian carcinomas: a developmental view*. Gynecol Oncol, 2008. **110**(3): p. 452-4.
38. Seidman, J.D., et al., *The fallopian tube-peritoneal junction: a potential site of carcinogenesis*. Int J Gynecol Pathol, 2011. **30**(1): p. 4-11.

39. Flesken-Nikitin, A., et al., *Ovarian surface epithelium at the junction area contains a cancer-prone stem cell niche*. Nature, 2013. **495**(7440): p. 241-5.
40. Kurman, R.J., *Origin and molecular pathogenesis of ovarian high-grade serous carcinoma*. Annals of Oncology, 2013. **24**: p. 16-21.
41. Piek, J.M.J., et al., *Dysplastic changes in prophylactically removed Fallopian tubes of women predisposed to developing ovarian cancer*. Journal of Pathology, 2001. **195**(4): p. 451-456.
42. Gross, A.L., et al., *Precursor lesions of high-grade serous ovarian carcinoma: morphological and molecular characteristics*. J Oncol, 2010. **2010**: p. 126295.
43. Saleemuddin, A., et al., *Risk factors for a serous cancer precursor ("p53 signature") in women with inherited BRCA mutations*. Gynecol Oncol, 2008. **111**(2): p. 226-32.
44. Callahan, M.J., et al., *Primary Fallopian tube malignancies in BRCA-positive women undergoing surgery for ovarian cancer risk reduction*. Journal of Clinical Oncology, 2007. **25**(25): p. 3985-3990.
45. Carcangiu, M.L., et al., *Atypical epithelial proliferation in fallopian tubes in prophylactic salpingo-oophorectomy specimens from BRCA1 and BRCA2 germline mutation carriers*. International Journal of Gynecological Pathology, 2004. **23**(1): p. 35-40.
46. Medeiros, F., et al., *The tubal fimbria is a preferred site for early adenocarcinoma in women with familial ovarian cancer syndrome*. American Journal of Surgical Pathology, 2006. **30**(2): p. 230-236.
47. Przybycin, C.G., et al., *Are All Pelvic (Nonuterine) Serous Carcinomas of Tubal Origin?* American Journal of Surgical Pathology, 2010. **34**(10): p. 1407-1416.
48. Kindelberger, D.W., et al., *Intraepithelial carcinoma of the fimbria and pelvic serous carcinoma: Evidence for a causal relationship*. American Journal of Surgical Pathology, 2007. **31**(2): p. 161-169.
49. Folkins, A.K., et al., *A candidate precursor to pelvic serous cancer (p53 signature) and its prevalence in ovaries and fallopian tubes from women with BRCA mutations*. Gynecologic Oncology, 2008. **109**(2): p. 168-173.
50. Kuhn, E., et al., *Telomere length in different histologic types of ovarian carcinoma with emphasis on clear cell carcinoma*. Modern Pathology, 2011. **24**(8): p. 1139-1145.
51. Chene, G., et al., *Early Telomere Shortening and Genomic Instability in Tubo-Ovarian Preneoplastic Lesions*. Clinical Cancer Research, 2013. **19**(11): p. 2873-2882.
52. Piek, J.M.J., et al., *BRCA1/2-related ovarian cancers are of tubal origin: a hypothesis*. Gynecologic Oncology, 2003. **90**(2): p. 491-491.
53. Kurman, R.J. and I.M. Shih, *The Origin and Pathogenesis of Epithelial Ovarian Cancer: A Proposed Unifying Theory*. American Journal of Surgical Pathology, 2010. **34**(3): p. 433-443.
54. Kim, J., et al., *High-grade serous ovarian cancer arises from fallopian tube in a mouse model*. Proceedings of the National Academy of Sciences of the United States of America, 2012. **109**(10): p. 3921-3926.
55. Kurman, R.J., *Origin and molecular pathogenesis of ovarian high-grade serous carcinoma*. Ann Oncol, 2013. **24 Suppl 10**: p. x16-21.

56. Perets, R., et al., *Transformation of the Fallopian Tube Secretory Epithelium Leads to High-Grade Serous Ovarian Cancer in Brca;Tp53;Pten Models*. *Cancer Cell*, 2013. **24**(6): p. 751-765.
57. Karst, A.M., K. Levanon, and R. Drapkin, *Modeling high-grade serous ovarian carcinogenesis from the fallopian tube*. *Proceedings of the National Academy of Sciences of the United States of America*, 2011. **108**(18): p. 7547-7552.
58. Jazaeri, A.A., et al., *Molecular Requirements for Transformation of Fallopian Tube Epithelial Cells into Serous Carcinoma*. *Neoplasia*, 2011. **13**(10): p. 899-U44.
59. Perets, R., et al., *Transformation of the fallopian tube secretory epithelium leads to high-grade serous ovarian cancer in Brca;Tp53;Pten models*. *Cancer Cell*, 2013. **24**(6): p. 751-65.
60. Hart, G.W., *Thematic Minireview Series on Glycobiology and Extracellular Matrices: Glycan Functions Pervade Biology at All Levels*. *Journal of Biological Chemistry*, 2013. **288**(10): p. 6903-6903.
61. Fuster, M.M. and J.D. Esko, *The sweet and sour of cancer: Glycans as novel therapeutic targets*. *Nature Reviews Cancer*, 2005. **5**(7): p. 526-542.
62. Pinho, S.S. and C.A. Reis, *Glycosylation in cancer: mechanisms and clinical implications*. *Nature Reviews Cancer*, 2015. **15**(9): p. 540-555.
63. Wells, L., K. Vosseller, and G.W. Hart, *Glycosylation of nucleocytoplasmic proteins: Signal transduction and O-GlcNAc*. *Science*, 2001. **291**(5512): p. 2376-2378.
64. Varki, A., Cummings, R.D., Esko, J. D., Freeze, H.H., Stanley, P., Bertozzi, C.R., Hart, G.W., and Etzler, M. E., *Essentials of Glycobiology*, 2nd edition, 2009.
65. Fuster, M.M. and J.D. Esko, *The sweet and sour of cancer: glycans as novel therapeutic targets*. *Nat Rev Cancer*, 2005. **5**(7): p. 526-42.
66. Moremen, K.W., M. Tiemeyer, and A.V. Nairn, *Vertebrate protein glycosylation: diversity, synthesis and function*. *Nat Rev Mol Cell Biol*, 2012. **13**(7): p. 448-62.
67. Ohtsubo, K. and J.D. Marth, *Glycosylation in cellular mechanisms of health and disease*. *Cell*, 2006. **126**(5): p. 855-867.
68. Gabius, H.J., et al., *From lectin structure to functional glycomics: principles of the sugar code*. *Trends in Biochemical Sciences*, 2011. **36**(6): p. 298-313.
69. Hakomori, S., *Glycosylation defining cancer malignancy: New wine in an old bottle*. *Proceedings of the National Academy of Sciences of the United States of America*, 2002. **99**(16): p. 10231-10233.
70. Reis, C.A., et al., *Alterations in glycosylation as biomarkers for cancer detection*. *Journal of Clinical Pathology*, 2010. **63**(4): p. 322-329.
71. Pinho, S.S., et al., *Gastric cancer: adding glycosylation to the equation*. *Trends in Molecular Medicine*, 2013. **19**(11): p. 664-676.
72. Julien, S., et al., *How Do Gangliosides Regulate RTKs Signaling?* *Cells*, 2013. **2**(4): p. 751-67.
73. Brockhausen, I., et al., *Pathways of mucin O-glycosylation in normal and malignant rat colonic epithelial cells reveal a mechanism for cancer-associated sialyl-Tn antigen expression*. *Biological Chemistry*, 2001. **382**(2): p. 219-232.

74. Moremen, K.W., M. Tiemeyer, and A.V. Nairn, *Vertebrate protein glycosylation: diversity, synthesis and function*. Nature Reviews Molecular Cell Biology, 2012. **13**(7): p. 448-462.
75. Ma, J.F. and G.W. Hart, *O-GlcNAc profiling: from proteins to proteomes*. Clinical Proteomics, 2014. **11**.
76. Ladenson, R.P., S.O. Schwartz, and A.C. Ivy, *Incidence of the Blood Groups and the Secretor Factor in Patients with Pernicious Anemia and Stomach Carcinoma*. American Journal of the Medical Sciences, 1949. **217**(2): p. 194-197.
77. Hakomori, S. and W.T. Murakami, *Glycolipids of Hamster Fibroblasts and Derived Malignant-Transformed Cell Lines*. Proceedings of the National Academy of Sciences of the United States of America, 1968. **59**(1): p. 254-&.
78. Varki, A., *Biological Roles of Oligosaccharides - All of the Theories Are Correct*. Glycobiology, 1993. **3**(2): p. 97-130.
79. Adamczyk, B., T. Tharmalingam, and P.M. Rudd, *Glycans as cancer biomarkers*. Biochimica Et Biophysica Acta-General Subjects, 2012. **1820**(9): p. 1347-1353.
80. Feizi, T., *Carbohydrate antigens in human cancer*. Cancer Surv, 1985. **4**(1): p. 245-69.
81. Holmes, E.H., et al., *Oncofetal Expression of Lex Carbohydrate Antigens in Human Colonic Adenocarcinomas - Regulation through Type-2 Core Chain Synthesis Rather Than Fucosylation*. Journal of Biological Chemistry, 1987. **262**(23): p. 11331-11338.
82. Anderson, N.L. and N.G. Anderson, *The human plasma proteome - History, character, and diagnostic prospects*. Molecular & Cellular Proteomics, 2002. **1**(11): p. 845-867.
83. Kirwan, A., et al., *Glycosylation-Based Serum Biomarkers for Cancer Diagnostics and Prognostics*. Biomed Res Int, 2015. **2015**: p. 490531.
84. Sasaroli, D., G. Coukos, and N. Scholler, *Beyond CA125: the coming of age of ovarian cancer biomarkers. Are we there yet?* Biomark Med, 2009. **3**(3): p. 275-288.
85. Jacob, F., et al., *Proteogenomic studies in epithelial ovarian cancer: established knowledge and future needs*. Biomark Med, 2009. **3**(6): p. 743-56.
86. Duffy, M.J., et al., *CA125 in ovarian cancer: European Group on Tumor Markers guidelines for clinical use*. Int J Gynecol Cancer, 2005. **15**(5): p. 679-91.
87. Bast, R.C., Jr., et al., *New tumor markers: CA125 and beyond*. Int J Gynecol Cancer, 2005. **15 Suppl 3**: p. 274-81.
88. Pochechueva, T., et al., *Comparison of printed glycan array, suspension array and ELISA in the detection of human anti-glycan antibodies*. Glycoconj J, 2011. **28**(8-9): p. 507-17.
89. Culf, A.S., M. Cuperlovic-Culf, and R.J. Ouellette, *Carbohydrate microarrays: survey of fabrication techniques*. OMICS, 2006. **10**(3): p. 289-310.
90. Shin, I., S. Park, and M.R. Lee, *Carbohydrate microarrays: an advanced technology for functional studies of glycans*. Chemistry, 2005. **11**(10): p. 2894-901.

91. Zhao, J., et al., *Protein biomarkers in cancer: natural glycoprotein microarray approaches*. *Curr Opin Mol Ther*, 2008. **10**(6): p. 602-10.
92. Jacob, F., et al., *Serum antiglycan antibody detection of nonmucinous ovarian cancers by using a printed glycan array*. *International Journal of Cancer*, 2012. **130**(1): p. 138-146.
93. Pochechueva, T., et al., *Comparison of printed glycan array, suspension array and ELISA in the detection of human anti-glycan antibodies*. *Glycoconjugate Journal*, 2011. **28**(8-9): p. 507-517.
94. Zhang, X.B. and F.L. Kiechle, *Review: Glycosphingolipids in health and disease*. *Annals of Clinical and Laboratory Science*, 2004. **34**(1): p. 3-13.
95. Merrill, A.H., *Sphingolipid and Glycosphingolipid Metabolic Pathways in the Era of Sphingolipidomics*. *Chemical Reviews*, 2011. **111**(10): p. 6387-6422.
96. Linn, S.C., et al., *Regulation of de novo sphingolipid biosynthesis and the toxic consequences of its disruption*. *Biochemical Society Transactions*, 2001. **29**: p. 831-835.
97. Mullen, T.D., Y.A. Hannun, and L.M. Obeid, *Ceramide synthases at the centre of sphingolipid metabolism and biology*. *Biochemical Journal*, 2012. **441**: p. 789-802.
98. Lannert, H., et al., *Functional organization of the Golgi apparatus in glycosphingolipid biosynthesis. Lactosylceramide and subsequent glycosphingolipids are formed in the lumen of the late Golgi*. *J Biol Chem*, 1998. **273**(5): p. 2939-46.
99. Sonnino, S., et al., *Fine tuning of cell functions through remodeling of glycosphingolipids by plasma membrane-associated glycohydrolases*. *Febs Letters*, 2010. **584**(9): p. 1914-1922.
100. Maccioni, H.J.F., R. Quiroga, and M.L. Ferrari, *Cellular and molecular biology of glycosphingolipid glycosylation*. *Journal of Neurochemistry*, 2011. **117**(4): p. 589-602.
101. Russo, D., S. Parashuraman, and G. D'Angelo, *Glycosphingolipid-Protein Interaction in Signal Transduction*. *International Journal of Molecular Sciences*, 2016. **17**(10).
102. Yamashita, T., et al., *A vital role for glycosphingolipid synthesis during development and differentiation*. *Proceedings of the National Academy of Sciences of the United States of America*, 1999. **96**(16): p. 9142-9147.
103. Kumagai, T., et al., *Involvement of murine beta-1,4-galactosyltransferase V in lactosylceramide biosynthesis*. *Glycoconjugate Journal*, 2010. **27**(7-9): p. 685-695.
104. Kumagai, T., et al., *Early lethality of beta-1,4-galactosyltransferase V-mutant mice by growth retardation*. *Biochemical and Biophysical Research Communications*, 2009. **379**(2): p. 456-459.
105. Yamashita, T., et al., *Enhanced insulin sensitivity in mice lacking ganglioside GM3*. *Diabetes*, 2003. **52**: p. A315-A315.
106. Niimi, K., et al., *Impairment of neuropsychological behaviors in ganglioside GM3-knockout mice*. *Biochemical and Biophysical Research Communications*, 2011. **406**(4): p. 524-528.
107. Yoshikawa, M., et al., *Mice lacking ganglioside GM3 synthase exhibit complete hearing loss due to selective degeneration of the organ of Corti*.

- Proceedings of the National Academy of Sciences of the United States of America, 2009. **106**(23): p. 9483-9488.
108. Takamiya, K., et al., *Mice with disrupted GM2/GD2 synthase gene lack complex gangliosides but exhibit only subtle defects in their nervous system.* Proceedings of the National Academy of Sciences of the United States of America, 1996. **93**(20): p. 10662-10667.
 109. Takamiya, K., et al., *Complex gangliosides are essential in spermatogenesis of mice: Possible roles in the transport of testosterone.* Proceedings of the National Academy of Sciences of the United States of America, 1998. **95**(21): p. 12147-12152.
 110. Sheikh, K.A., et al., *Mice lacking complex gangliosides develop Wallerian degeneration and myelination defects.* Proceedings of the National Academy of Sciences of the United States of America, 1999. **96**(13): p. 7532-7537.
 111. Chiavegatto, S., et al., *A functional role for complex gangliosides: Motor deficits in GM2/GD2 synthase knockout mice.* Experimental Neurology, 2000. **166**(2): p. 227-234.
 112. Wu, G.S., et al., *Mice Lacking Major Brain Gangliosides Develop Parkinsonism.* Neurochemical Research, 2011. **36**(9): p. 1706-1714.
 113. Handa, Y., et al., *GD3 synthase gene knockout mice exhibit thermal hyperalgesia and mechanical allodynia but decreased response to formalin-induced prolonged noxious stimulation.* Pain, 2005. **117**(3): p. 271-279.
 114. Okada, M., et al., *b-series ganglioside deficiency exhibits no definite changes in the neurogenesis and the sensitivity to Fas-mediated apoptosis but impairs regeneration of the lesioned hypoglossal nerve.* Journal of Biological Chemistry, 2002. **277**(3): p. 1633-1636.
 115. Yamashita, T., et al., *Interruption of ganglioside synthesis produces central nervous system degeneration and altered axon-glia interactions.* Proceedings of the National Academy of Sciences of the United States of America, 2005. **102**(8): p. 2725-2730.
 116. Kawai, H., et al., *Mice expressing only monosialoganglioside GM3 exhibit lethal audiogenic seizures.* Journal of Biological Chemistry, 2001. **276**(10): p. 6885-6888.
 117. Inoue, M., et al., *Refractory skin injury in complex knock-out mice expressing only the GM3 ganglioside.* Journal of Biological Chemistry, 2002. **277**(33): p. 29881-29888.
 118. Biellmann, F., et al., *The Lc3-synthase gene B3gnt5 is essential to pre-implantation development of the murine embryo.* BMC Developmental Biology, 2008. **8**.
 119. Kuan, C.T., et al., *Multiple phenotypic changes in mice after knockout of the B3gnt5 gene, encoding Lc3 synthase-a key enzyme in lacto-neolacto ganglioside synthesis.* BMC Developmental Biology, 2010. **10**.
 120. Okuda, T., et al., *Targeted disruption of Gb3/CD77 synthase gene resulted in the complete deletion of globo-series glycosphingolipids and loss of sensitivity to vVerotoxins.* Journal of Biological Chemistry, 2006. **281**(15): p. 10230-10235.
 121. D'Angelo, G., et al., *Glycosphingolipids: synthesis and functions.* FEBS J, 2013. **280**(24): p. 6338-53.

122. Patwardhan, G.A. and Y.Y. Liu, *Sphingolipids and expression regulation of genes in cancer*. Progress in Lipid Research, 2011. **50**(1): p. 104-114.
123. Hakomori, S.I., *Structure and function of glycosphingolipids and sphingolipids: Recollections and future trends*. Biochimica Et Biophysica Acta-General Subjects, 2008. **1780**(3): p. 325-346.
124. Mirkin, B.L., S.H. Clark, and C. Zhang, *Inhibition of human neuroblastoma cell proliferation and EGF receptor phosphorylation by gangliosides GM(1), GM(3) GD(1A) and GT(1B)*. Cell Proliferation, 2002. **35**(2): p. 105-115.
125. Kovbasnjuk, O., et al., *The glycosphingolipid globotriaosylceramide in the metastatic transformation of colon cancer*. Proceedings of the National Academy of Sciences of the United States of America, 2005. **102**(52): p. 19087-19092.
126. Furukawa, K., et al., *Disialyl gangliosides enhance tumor phenotypes with differential modalities*. Glycoconjugate Journal, 2012. **29**(8-9): p. 579-584.
127. Hamamura, K., et al., *Ganglioside GD3 promotes cell growth and invasion through p130Cas and paxillin in malignant melanoma cells*. Proceedings of the National Academy of Sciences of the United States of America, 2005. **102**(31): p. 11041-11046.
128. Hamamura, K., et al., *Focal adhesion kinase as well as p130Cas and paxillin is crucially involved in the enhanced malignant properties under expression of ganglioside GD3 in melanoma cells*. Biochimica Et Biophysica Acta-General Subjects, 2008. **1780**(3): p. 513-519.
129. Ohkawa, Y., et al., *Essential roles of integrin-mediated signaling for the enhancement of malignant properties of melanomas based on the expression of GD3*. Biochemical and Biophysical Research Communications, 2008. **373**(1): p. 14-19.
130. Hamamura, K., et al., *Functional Activation of Src Family Kinase Yes Protein Is Essential for the Enhanced Malignant Properties of Human Melanoma Cells Expressing Ganglioside GD3*. Journal of Biological Chemistry, 2011. **286**(21): p. 18526-18537.
131. Yoshida, S., et al., *Ganglioside G(D2) in small cell lung cancer cell lines: Enhancement of cell proliferation and mediation of apoptosis*. Cancer Research, 2001. **61**(10): p. 4244-4252.
132. Shibuya, H., et al., *Enhancement of malignant properties of human osteosarcoma cells with disialyl gangliosides GD2/GD3*. Cancer Science, 2012. **103**(9): p. 1656-1664.
133. Hyuga, S., et al., *Inhibition of highly metastatic FBJ-LL cell migration by ganglioside GD1a highly expressed in poorly metastatic FBJ-S1 cells*. Biochemical and Biophysical Research Communications, 1997. **231**(2): p. 340-343.
134. Hu, D., et al., *Ganglioside GD1a negatively regulates matrix metalloproteinase-9 expression in mouse FBJ cell lines at the transcriptional level*. Connective Tissue Research, 2007. **48**(4): p. 198-205.
135. Wang, L., et al., *Ganglioside GD1a suppresses TNF alpha expression via Pkn1 at the transcriptional level in mouse osteosarcoma-derived FBJ cells*. Biochemical and Biophysical Research Communications, 2008. **371**(2): p. 230-235.

136. Cao, T., et al., *Ganglioside GD1a Suppression of NOS2 Expression Via ERK1 Pathway in Mouse Osteosarcoma FBJ Cells*. Journal of Cellular Biochemistry, 2010. **110**(5): p. 1165-1174.
137. Zhang, L., et al., *Ganglioside GD1a negatively regulates hepatocyte growth factor expression through caveolin-1 at the transcriptional level in murine osteosarcoma cells*. Biochimica Et Biophysica Acta-General Subjects, 2011. **1810**(8): p. 759-768.
138. Hyuga, S., et al., *Ganglioside GD1a inhibits HGF-induced motility and scattering of cancer cells through suppression of tyrosine phosphorylation of c-Met*. International Journal of Cancer, 2001. **94**(3): p. 328-334.
139. Wang, X.Q., et al., *Carbohydrate-carbohydrate binding of ganglioside to integrin alpha(5) modulates alpha(5)beta(1) function*. Journal of Biological Chemistry, 2001. **276**(11): p. 8436-8444.
140. Mitsuzuka, K., et al., *A specific microdomain ("glycosynapse 3") controls phenotypic conversion and reversion of bladder cancer cells through GM3-mediated interaction of alpha 3 beta 1 integrin with CD9*. Journal of Biological Chemistry, 2005. **280**(42): p. 35545-35553.
141. Todeschini, A.R., et al., *Ganglioside GM2-tetraspanin CD82 complex inhibits met and its cross-talk with integrins, providing a basis for control of cell motility through glycosynapse*. Journal of Biological Chemistry, 2007. **282**(11): p. 8123-8133.
142. Coskun, U., et al., *Regulation of human EGF receptor by lipids*. Proceedings of the National Academy of Sciences of the United States of America, 2011. **108**(22): p. 9044-9048.
143. Liu, Y.H., et al., *Ganglioside depletion and EGF responses of human GM3 synthase-deficient fibroblasts*. Glycobiology, 2008. **18**(8): p. 593-601.
144. Park, S.Y., et al., *Globoside promotes activation of ERK by interaction with the epidermal growth factor receptor*. Biochimica Et Biophysica Acta-General Subjects, 2012. **1820**(7): p. 1141-1148.
145. Guan, F., K. Handa, and S.I. Hakomori, *Regulation of Epidermal Growth Factor Receptor Through Interaction of Ganglioside GM3 with GlcNAc of N-Linked Glycan of the Receptor: Demonstration in Id1D Cells*. Neurochemical Research, 2011. **36**(9): p. 1645-1653.
146. Huang, X., et al., *Ganglioside GM3 inhibits hepatoma cell motility via down-regulating activity of EGFR and PI3K/AKT signaling pathway*. Journal of Cellular Biochemistry, 2013. **114**(7): p. 1616-1624.
147. Milani, S., et al., *Gangliosides influence EGFR/ErbB2 heterodimer stability but they do not modify EGF-dependent ErbB2 phosphorylation*. Biochimica Et Biophysica Acta-Molecular and Cell Biology of Lipids, 2010. **1801**(6): p. 617-624.
148. Bremer, E.G. and S. Hakomori, *Gm3 Ganglioside Induces Hamster Fibroblast Growth-Inhibition in Chemically-Defined Medium - Ganglioside May Regulate Growth-Factor Receptor Function*. Biochemical and Biophysical Research Communications, 1982. **106**(3): p. 711-718.
149. Toledo, M.S., et al., *Cell growth regulation through GM3-enriched microdomain (glycosynapse) in human lung embryonal fibroblast WI38 and its oncogenic transformant VA13*. Journal of Biological Chemistry, 2004. **279**(33): p. 34655-34664.

150. Bremer, E.G., et al., *Ganglioside-Mediated Modulation of Cell-Growth, Growth-Factor Binding, and Receptor Phosphorylation*. Journal of Biological Chemistry, 1984. **259**(11): p. 6818-6825.
151. Farooqui, T., et al., *GM1 inhibits early signaling events mediated by PDGF receptor in cultured human glioma cells*. Anticancer Research, 1999. **19**(6B): p. 5007-5013.
152. Mutoh, T., et al., *Ganglioside Gm1 Binds to the Trk Protein and Regulates Receptor Function*. Proceedings of the National Academy of Sciences of the United States of America, 1995. **92**(11): p. 5087-5091.
153. Kimura, M., et al., *Engagement of endogenous ganglioside GM1a induces tyrosine phosphorylation involved in neuron-like differentiation of PC12 cells*. Glycobiology, 2001. **11**(4): p. 335-343.
154. Saha, N., et al., *Ganglioside mediate the interaction between Nogo receptor 1 and LINGO-1*. Biochemical and Biophysical Research Communications, 2011. **413**(1): p. 92-97.
155. Chung, T.W., et al., *Ganglioside GM3 inhibits VEGF/VEGFR-2-mediated angiogenesis: Direct interaction of GM3 with VEGFR-2*. Glycobiology, 2009. **19**(3): p. 229-239.
156. Kim, S.J., et al., *Ganglioside GM3 participates in the TGF-beta 1-induced epithelial-mesenchymal transition of human lens epithelial cells*. Biochemical Journal, 2013. **449**: p. 241-251.
157. Kabayama, K., et al., *Dissociation of the insulin receptor and caveolin-1 complex by ganglioside GM3 in the state of insulin resistance*. Proceedings of the National Academy of Sciences of the United States of America, 2007. **104**(34): p. 13678-13683.
158. Tagami, S., et al., *Ganglioside GM3 participates in the pathological conditions of insulin resistance*. Journal of Biological Chemistry, 2002. **277**(5): p. 3085-3092.
159. Sekino-Suzuki, N., et al., *Involvement of gangliosides in the process of Cbp/PAG phosphorylation by Lyn in developing cerebellar growth cones*. Journal of Neurochemistry, 2013. **124**(4): p. 514-522.
160. Bremer, E.G., J. Schlessinger, and S. Hakomori, *Ganglioside-Mediated Modulation of Cell-Growth - Specific Effects of Gm3 on Tyrosine Phosphorylation of the Epidermal Growth-Factor Receptor*. Journal of Biological Chemistry, 1986. **261**(5): p. 2434-2440.
161. Hanai, N., et al., *Ganglioside-Mediated Modulation of Cell-Growth - Specific Effects of Gm3 and Lyso-Gm3 in Tyrosine Phosphorylation of the Epidermal Growth-Factor Receptor*. Journal of Biological Chemistry, 1988. **263**(22): p. 10915-10921.
162. Miura, Y., et al., *Reversion of the Jun-induced oncogenic phenotype by enhanced synthesis of sialosylsphingomyelinase (GM3 ganglioside)*. Proceedings of the National Academy of Sciences of the United States of America, 2004. **101**(46): p. 16204-16209.
163. Park, S.Y., et al., *Control of cell motility by interaction of gangliosides, tetraspanins, and epidermal growth factor receptor in A431 versus KB epidermoid tumor cells*. Carbohydrate Research, 2009. **344**(12): p. 1479-1486.
164. Toledo, M.S., et al., *Effect of ganglioside and tetraspanins in microdomains on interaction of integrins with fibroblast growth factor receptor. (vol 280,*

- pg 16227, 2005). *Journal of Biological Chemistry*, 2005. **280**(21): p. 20916-20916.
165. Nakayama, H., et al., *GSL-Enriched Membrane Microdomains in Innate Immune Responses*. *Archivum Immunologiae Et Therapiae Experimentalis*, 2013. **61**(3): p. 217-228.
 166. Wang, X.Q., P. Sun, and A.S. Paller, *Ganglioside induces caveolin-1 redistribution and interaction with the epidermal growth factor receptor*. *Journal of Biological Chemistry*, 2002. **277**(49): p. 47028-47034.
 167. Wang, X.Q., et al., *Suppression of epidermal growth factor receptor signaling by protein kinase C- α activation requires CD82, caveolin-1, and ganglioside*. *Cancer Research*, 2007. **67**(20): p. 9986-9995.
 168. Duan, J.F., et al., *Ganglioside GM2 modulates the erythrocyte Ca²⁺-ATPase through its binding to the calmodulin-binding domain and its 'receptor'*. *Archives of Biochemistry and Biophysics*, 2006. **454**(2): p. 155-159.
 169. Wang, J.F., et al., *Cross-Linking of GM1 Ganglioside by Galectin-1 Mediates Regulatory T Cell Activity Involving TRPC5 Channel Activation: Possible Role in Suppressing Experimental Autoimmune Encephalomyelitis*. *Journal of Immunology*, 2009. **182**(7): p. 4036-4045.
 170. Boscher, C., et al., *Galectin-3 Protein Regulates Mobility of N-cadherin and GM1 Ganglioside at Cell-Cell Junctions of Mammary Carcinoma Cells*. *Journal of Biological Chemistry*, 2012. **287**(39): p. 32940-32952.
 171. Handa, K. and S.I. Hakomori, *Carbohydrate to carbohydrate interaction in development process and cancer progression*. *Glycoconjugate Journal*, 2012. **29**(8-9): p. 627-637.
 172. Kojima, N. and S.I. Hakomori, *Molecular Mechanisms of Cell Motility .3. Cell-Adhesion, Spreading, and Motility of Gm3-Expressing Cells Based on Glycolipid-Glycolipid Interaction*. *Journal of Biological Chemistry*, 1991. **266**(26): p. 17552-17558.
 173. Santacroce, P.V. and A. Basu, *Probing specificity in carbohydrate-carbohydrate interactions with micelles and Langmuir monolayers*. *Angewandte Chemie-International Edition*, 2003. **42**(1): p. 95-98.
 174. Simons, K. and E. Ikonen, *Functional rafts in cell membranes*. *Nature*, 1997. **387**(6633): p. 569-572.
 175. van Meer, G., D.R. Voelker, and G.W. Feigenson, *Membrane lipids: where they are and how they behave*. *Nature Reviews Molecular Cell Biology*, 2008. **9**(2): p. 112-124.
 176. Todeschini, A.R. and S.I. Hakomori, *Functional role of glycosphingolipids and gangliosides in control of cell adhesion, motility, and growth, through glycosynaptic microdomains*. *Biochimica Et Biophysica Acta-General Subjects*, 2008. **1780**(3): p. 421-433.
 177. Kaiser, H.J., et al., *Order of lipid phases in model and plasma membranes*. *Proceedings of the National Academy of Sciences of the United States of America*, 2009. **106**(39): p. 16645-16650.
 178. Contreras, F.X., et al., *Molecular recognition of a single sphingolipid species by a protein's transmembrane domain*. *Nature*, 2012. **481**(7382): p. 525-529.
 179. Holthuis, J.C.M., et al., *The organizing potential of sphingolipids in intracellular membrane transport*. *Physiological Reviews*, 2001. **81**(4): p. 1689-1723.

180. D'angelo, G., et al., *Glycosphingolipids: synthesis and functions*. Febs Journal, 2013. **280**(24): p. 6338-6353.
181. Jacob, F., et al., *Serum antiglycan antibody detection of nonmucinous ovarian cancers by using a printed glycan array*. Int J Cancer, 2012. **130**(1): p. 138-46.
182. Jacob, F., et al., *The glycosphingolipid P(1) is an ovarian cancer-associated carbohydrate antigen involved in migration*. Br J Cancer, 2014. **111**(8): p. 1634-45.
183. Chen, F.Q., et al., *High-frequency genome editing using ssDNA oligonucleotides with zinc-finger nucleases*. Nature Methods, 2011. **8**(9): p. 753-U96.
184. Anugraham, M., et al., *A platform for the structural characterization of glycans enzymatically released from glycosphingolipids extracted from tissue and cells*. Rapid Commun Mass Spectrom, 2015. **29**(7): p. 545-61.
185. Boccuto, L., et al., *A mutation in a ganglioside biosynthetic enzyme, ST3GAL5, results in salt & pepper syndrome, a neurocutaneous disorder with altered glycolipid and glycoprotein glycosylation*. Hum Mol Genet, 2014. **23**(2): p. 418-33.
186. Suzuki, Y., et al., *Histone acetylation-mediated glycosyltransferase gene regulation in mouse brain during development*. J Neurochem, 2011. **116**(5): p. 874-80.
187. Gazieli-Sovran, A., et al., *miR-30b/30d regulation of GalNAc transferases enhances invasion and immunosuppression during metastasis*. Cancer Cell, 2011. **20**(1): p. 104-18.
188. Lauc, G., A. Vojta, and V. Zoldos, *Epigenetic regulation of glycosylation is the quantum mechanics of biology*. Biochimica Et Biophysica Acta-General Subjects, 2014. **1840**(1): p. 65-70.
189. Ropero, S., et al., *Epigenetic loss of the familial tumor-suppressor gene exostosin-1 (EXT1) disrupts heparan sulfate synthesis in cancer cells*. Human Molecular Genetics, 2004. **13**(22): p. 2753-2765.
190. Kohler, R.S., et al., *Epigenetic activation of MGAT3 and corresponding bisecting GlcNAc shortens the survival of cancer patients*. Oncotarget, 2016. **7**(32): p. 51674-51686.
191. Bull, C., M.H. den Brok, and G.J. Adema, *Sweet escape: sialic acids in tumor immune evasion*. Biochim Biophys Acta, 2014. **1846**(1): p. 238-46.
192. Bull, C., et al., *Sialic acids sweeten a tumor's life*. Cancer Res, 2014. **74**(12): p. 3199-204.
193. Dall'Olio, F., et al., *Sialosignaling: Sialyltransferases as engines of self-fueling loops in cancer progression*. Biochimica Et Biophysica Acta-General Subjects, 2014. **1840**(9): p. 2752-2764.
194. Lu, J., et al., *beta-Galactoside alpha2,6-sialyltransferase 1 promotes transforming growth factor-beta-mediated epithelial-mesenchymal transition*. J Biol Chem, 2014. **289**(50): p. 34627-41.
195. Pearce, O.M. and H. Laubli, *Sialic acids in cancer biology and immunity*. Glycobiology, 2016. **26**(2): p. 111-28.
196. Lemarier, N., et al., *The C-Ha-Ras Oncogene Induces Increased Expression of Beta-Galactoside Alpha-2,6-Sialyltransferase in Rat Fibroblast (Fr3t3) Cells*. Glycobiology, 1992. **2**(1): p. 49-56.

197. Seales, E.C., et al., *Ras oncogene directs expression of a differentially sialylated, functionally altered beta 1 integrin*. *Oncogene*, 2003. **22**(46): p. 7137-7145.
198. Seales, E.C., et al., *A protein kinase C/Ras/ERK signaling pathway activates myeloid fibronectin receptors by altering beta 1 integrin sialylation*. *Journal of Biological Chemistry*, 2005. **280**(45): p. 37610-37615.
199. Vierbuchen, M.J., et al., *Quantitative lectin-histochemical and immunohistochemical studies on the occurrence of alpha(2,3)- and alpha(2,6)-linked sialic acid residues in colorectal carcinomas. Relation to clinicopathologic features*. *Cancer*, 1995. **76**(5): p. 727-35.
200. Zhang, Z., et al., *Modification of glycosylation mediates the invasive properties of murine hepatocarcinoma cell lines to lymph nodes*. *PLoS One*, 2013. **8**(6): p. e65218.
201. Lin, S., et al., *Cell surface alpha 2,6 sialylation affects adhesion of breast carcinoma cells*. *Exp Cell Res*, 2002. **276**(1): p. 101-10.
202. Zhu, Y., et al., *Suppression of a sialyltransferase by antisense DNA reduces invasiveness of human colon cancer cells in vitro*. *Biochim Biophys Acta*, 2001. **1536**(2-3): p. 148-60.
203. Christie, D.R., et al., *ST6Gal-I expression in ovarian cancer cells promotes an invasive phenotype by altering integrin glycosylation and function*. *J Ovarian Res*, 2008. **1**(1): p. 3.
204. Schultz, M.J., et al., *ST6Gal-I sialyltransferase confers cisplatin resistance in ovarian tumor cells*. *Journal of Ovarian Research*, 2013. **6**.
205. Schultz, M.J., et al., *The Tumor-Associated Glycosyltransferase ST6Gal-I Regulates Stem Cell Transcription Factors and Confers a Cancer Stem Cell Phenotype*. *Cancer Research*, 2016. **76**(13): p. 3978-3988.
206. Swindall, A.F., et al., *ST6Gal-I Protein Expression Is Upregulated in Human Epithelial Tumors and Correlates with Stem Cell Markers in Normal Tissues and Colon Cancer Cell Lines*. *Cancer Research*, 2013. **73**(7): p. 2368-2378.
207. Bresalier, R.S., et al., *Cell surface sialoprotein alterations in metastatic murine colon cancer cell lines selected in an animal model for colon cancer metastasis*. *Cancer Res*, 1990. **50**(4): p. 1299-307.
208. Zhao, Y., et al., *Modification of sialylation mediates the invasive properties and chemosensitivity of human hepatocellular carcinoma*. *Mol Cell Proteomics*, 2014. **13**(2): p. 520-36.
209. Isaji, T., et al., *An oncogenic protein Golgi phosphoprotein 3 up-regulates cell migration via sialylation*. *J Biol Chem*, 2014. **289**(30): p. 20694-705.
210. Shaikh, F.M., et al., *Tumor cell migration and invasion are regulated by expression of variant integrin glycoforms*. *Exp Cell Res*, 2008. **314**(16): p. 2941-50.
211. Seales, E.C., et al., *Hypersialylation of beta1 integrins, observed in colon adenocarcinoma, may contribute to cancer progression by up-regulating cell motility*. *Cancer Res*, 2005. **65**(11): p. 4645-52.
212. Kim, C., F. Ye, and M.H. Ginsberg, *Regulation of Integrin Activation*. *Annual Review of Cell and Developmental Biology*, Vol 27, 2011. **27**: p. 321-345.
213. Schultz, M.J., A.F. Swindall, and S.L. Bellis, *Regulation of the metastatic cell phenotype by sialylated glycans*. *Cancer and Metastasis Reviews*, 2012. **31**(3-4): p. 501-518.

214. Pochec, E., et al., *Glycosylation profile of integrin alpha(3)beta(1) changes with melanoma progression*. *Biochimica Et Biophysica Acta-Molecular Cell Research*, 2003. **1643**(1-3): p. 113-123.
215. Pretzlaff, R.K., V.W. Xue, and M.E. Rowin, *Sialidase treatment exposes the beta1-integrin active ligand binding site on HL60 cells and increases binding to fibronectin*. *Cell Adhes Commun*, 2000. **7**(6): p. 491-500.
216. Seales, E.C., et al., *Ras oncogene directs expression of a differentially sialylated, functionally altered beta1 integrin*. *Oncogene*, 2003. **22**(46): p. 7137-45.
217. Semel, A.C., et al., *Hyposialylation of integrins stimulates the activity of myeloid fibronectin receptors*. *J Biol Chem*, 2002. **277**(36): p. 32830-6.
218. Seales, E.C., et al., *Hypersialylation of beta(1) integrins, observed in colon adenocarcinoma, may contribute to cancer progression by up-regulating cell motility*. *Cancer Research*, 2005. **65**(11): p. 4645-4652.
219. Amano, M., et al., *The ST6Gal I sialyltransferase selectively modifies N-glycans on CD45 to negatively regulate galectin-1-induced CD45 clustering, phosphatase modulation, and T cell death*. *Journal of Biological Chemistry*, 2003. **278**(9): p. 7469-7475.
220. Amano, M., et al., *Tumour suppressor p16INK4a-anoikis-favouring decrease in N/O-glycan/cell surface sialylation by down-regulation of enzymes in sialic acid biosynthesis in tandem in a pancreatic carcinoma model*. *Febs Journal*, 2012. **279**(21): p. 4062-4080.
221. Liu, Z.Y., et al., *ST6Gal-I Regulates Macrophage Apoptosis via alpha 2-6 Sialylation of the TNFR1 Death Receptor*. *Journal of Biological Chemistry*, 2011. **286**(45): p. 39654-39662.
222. Sanchez-Ruderisch, H., et al., *Galectin-1 sensitizes carcinoma cells to anoikis via the fibronectin receptor alpha(5)beta(1)-integrin*. *Cell Death and Differentiation*, 2011. **18**(5): p. 806-816.
223. Swindall, A.F. and S.L. Bellis, *Sialylation of the Fas Death Receptor by ST6Gal-I Provides Protection against Fas-mediated Apoptosis in Colon Carcinoma Cells*. *Journal of Biological Chemistry*, 2011. **286**(26): p. 22982-22990.
224. Sugrue, S.P. and E.D. Hay, *Response of basal epithelial cell surface and Cytoskeleton to solubilized extracellular matrix molecules*. *J Cell Biol*, 1981. **91**(1): p. 45-54.
225. Greenburg, G. and E.D. Hay, *Epithelia suspended in collagen gels can lose polarity and express characteristics of migrating mesenchymal cells*. *J Cell Biol*, 1982. **95**(1): p. 333-9.
226. Sugrue, S.P. and E.D. Hay, *The identification of extracellular matrix (ECM) binding sites on the basal surface of embryonic corneal epithelium and the effect of ECM binding on epithelial collagen production*. *J Cell Biol*, 1986. **102**(5): p. 1907-16.
227. Guan, F., K. Handa, and S.I. Hakomori, *Specific glycosphingolipids mediate epithelial-to-mesenchymal transition of human and mouse epithelial cell lines*. *Proc Natl Acad Sci U S A*, 2009. **106**(18): p. 7461-6.
228. Hay, E.D., *The mesenchymal cell, its role in the embryo, and the remarkable signaling mechanisms that create it*. *Dev Dyn*, 2005. **233**(3): p. 706-20.
229. Kalluri, R. and M. Zeisberg, *Fibroblasts in cancer*. *Nat Rev Cancer*, 2006. **6**(5): p. 392-401.

230. Lee, J.M., et al., *The epithelial-mesenchymal transition: new insights in signaling, development, and disease*. J Cell Biol, 2006. **172**(7): p. 973-81.
231. Li, L. and W.B. Neaves, *Normal stem cells and cancer stem cells: the niche matters*. Cancer Res, 2006. **66**(9): p. 4553-7.
232. Hugo, H., et al., *Epithelial--mesenchymal and mesenchymal--epithelial transitions in carcinoma progression*. J Cell Physiol, 2007. **213**(2): p. 374-83.
233. Turley, E.A., et al., *Mechanisms of disease: epithelial-mesenchymal transition--does cellular plasticity fuel neoplastic progression?* Nat Clin Pract Oncol, 2008. **5**(5): p. 280-90.
234. Polyak, K. and R.A. Weinberg, *Transitions between epithelial and mesenchymal states: acquisition of malignant and stem cell traits*. Nat Rev Cancer, 2009. **9**(4): p. 265-73.
235. Larue, L. and A. Bellacosa, *Epithelial-mesenchymal transition in development and cancer: role of phosphatidylinositol 3' kinase/AKT pathways*. Oncogene, 2005. **24**(50): p. 7443-54.
236. Haltiwanger, R.S. and J.B. Lowe, *Role of glycosylation in development*. Annu Rev Biochem, 2004. **73**: p. 491-537.
237. Hakomori, S., *Traveling for the glycosphingolipid path*. Glycoconj J, 2000. **17**(7-9): p. 627-47.
238. Miljan, E.A. and E.G. Bremer, *Regulation of growth factor receptors by gangliosides*. Sci STKE, 2002. **2002**(160): p. re15.
239. Rebbaa, A., P.M. Chou, and E.G. Bremer, *Modulation of Growth Factor response in brain tumors by complex carbohydrates*. Bull Cancer, 2004. **91**(4): p. E15-60.
240. Todeschini, A.R., et al., *Ganglioside GM2-tetraspanin CD82 complex inhibits met and its cross-talk with integrins, providing a basis for control of cell motility through glycosynapse*. J Biol Chem, 2007. **282**(11): p. 8123-33.
241. Stanley, P., *Regulation of Notch signaling by glycosylation*. Curr Opin Struct Biol, 2007. **17**(5): p. 530-5.
242. Bruckner, K., et al., *Glycosyltransferase activity of Fringe modulates Notch-Delta interactions*. Nature, 2000. **406**(6794): p. 411-5.
243. Batlle, E., et al., *The transcription factor Snail is a repressor of E-cadherin gene expression in epithelial tumour cells*. Nature Cell Biology, 2000. **2**(2): p. 84-89.
244. Hajra, K.M., D.Y.S. Chen, and E.R. Fearon, *The SLUG zinc-finger protein represses E-cadherin in breast cancer*. Cancer Research, 2002. **62**(6): p. 1613-1618.
245. Comijn, J., et al., *The two-handed E box binding zinc finger protein SIP1 downregulates E-cadherin and induces invasion*. Molecular Cell, 2001. **7**(6): p. 1267-1278.
246. Eger, A., et al., *DeltaEF1 is a transcriptional repressor of E-cadherin and regulates epithelial plasticity in breast cancer cells*. Oncogene, 2005. **24**(14): p. 2375-2385.
247. Perez-Moreno, M.A., et al., *A new role for E12/E47 in the repression of E-cadherin expression and epithelial-mesenchymal transitions*. Journal of Biological Chemistry, 2001. **276**(29): p. 27424-27431.
248. Yang, J., et al., *Twist, a master regulator of morphogenesis, plays an essential role in tumor metastasis*. Cell, 2004. **117**(7): p. 927-939.

249. Shapiro, I.M., et al., *An EMT-Driven Alternative Splicing Program Occurs in Human Breast Cancer and Modulates Cellular Phenotype*. Plos Genetics, 2011. **7**(8).
250. Xu, Y., et al., *Role of CK1 in GSK3 beta-mediated phosphorylation and degradation of Snail*. Oncogene, 2010. **29**(21): p. 3124-3133.
251. Wang, S.P., et al., *p53 controls cancer cell invasion by inducing the MDM2-mediated degradation of Slug*. Nature Cell Biology, 2009. **11**(6): p. 694-U22.
252. Hennessy, B.T., et al., *Characterization of a Naturally Occurring Breast Cancer Subset Enriched in Epithelial-to-Mesenchymal Transition and Stem Cell Characteristics*. Cancer Research, 2009. **69**(10): p. 4116-4124.
253. Wiklund, E.D., et al., *Coordinated epigenetic repression of the miR-200 family and miR-205 in invasive bladder cancer*. International Journal of Cancer, 2011. **128**(6): p. 1327-1334.
254. Corney, D.C., et al., *Frequent Downregulation of miR-34 Family in Human Ovarian Cancers*. Clinical Cancer Research, 2010. **16**(4): p. 1119-1128.
255. Gravgaard, K.H., et al., *The miRNA-200 family and miRNA-9 exhibit differential expression in primary versus corresponding metastatic tissue in breast cancer*. Breast Cancer Research, 2011. **13**.
256. Carvalho, J., et al., *Lack of microRNA-101 causes E-cadherin functional deregulation through EZH2 up-regulation in intestinal gastric cancer*. Journal of Pathology, 2012. **228**(1): p. 31-44.
257. Ono, M., et al., *GM3 ganglioside inhibits CD9-facilitated haptotactic cell motility: coexpression of GM3 and CD9 is essential in the downregulation of tumor cell motility and malignancy*. Biochemistry, 2001. **40**(21): p. 6414-21.
258. Mitsuzuka, K., et al., *A specific microdomain ("glycosynapse 3") controls phenotypic conversion and reversion of bladder cancer cells through GM3-mediated interaction of alpha3beta1 integrin with CD9*. J Biol Chem, 2005. **280**(42): p. 35545-53.
259. Toledo, M.S., et al., *Cell growth regulation through GM3-enriched microdomain (glycosynapse) in human lung embryonal fibroblast WI38 and its oncogenic transformant VA13*. J Biol Chem, 2004. **279**(33): p. 34655-64.
260. Guan, F., et al., *Functional role of gangliotetraosylceramide in epithelial-to-mesenchymal transition process induced by hypoxia and by TGF- β* . FASEB J, 2010. **24**(12): p. 4889-903.
261. Mathow, D., et al., *Zeb1 affects epithelial cell adhesion by diverting glycosphingolipid metabolism*. EMBO Rep, 2015. **16**(3): p. 321-31.
262. Freire-de-Lima, L., et al., *Involvement of O-glycosylation defining oncofetal fibronectin in epithelial-mesenchymal transition process*. Proc Natl Acad Sci U S A, 2011. **108**(43): p. 17690-5.
263. Sampaio, J.L., et al., *Membrane lipidome of an epithelial cell line*. Proc Natl Acad Sci U S A, 2011. **108**(5): p. 1903-7.
264. Liang, Y.J., et al., *Differential expression profiles of glycosphingolipids in human breast cancer stem cells vs. cancer non-stem cells*. Proceedings of the National Academy of Sciences of the United States of America, 2013. **110**(13): p. 4968-4973.
265. Thiery, J.P., et al., *Epithelial-mesenchymal transitions in development and disease*. Cell, 2009. **139**(5): p. 871-90.

266. Singh, S.K., et al., *Identification of a cancer stem cell in human brain tumors*. *Cancer Res*, 2003. **63**(18): p. 5821-8.
267. Bonnet, D. and J.E. Dick, *Human acute myeloid leukemia is organized as a hierarchy that originates from a primitive hematopoietic cell*. *Nature Medicine*, 1997. **3**(7): p. 730-737.
268. Igarashi, Y. and R. Kannagi, *Glycosphingolipids as mediators of phenotypic changes associated with development and cancer progression*. *Journal of Biochemistry*, 2010. **147**(1): p. 3-8.
269. Pattabiraman, D.R., et al., *Activation of PKA leads to mesenchymal-to-epithelial transition and loss of tumor-initiating ability*. *Science*, 2016. **351**(6277): p. 1042-+.

7. Abbreviations

GCS - Glucosylceramide synthase
EMT - Epithelial mesenchymal transition
MET – Mesenchymal epithelial transition
AGA - Anti glycan antibodies
GSLs - Glycosphingolipids
HGSC – High grade serous carcinoma
LGSC – Low-grade serous carcinoma
FIGO - International federation of gynecology and obstetrics
OSE - Ovarian surface epithelium
STIC - Serous tubal intraepithelial carcinomas
FTSEC - Fallopian tube secretory epithelial cells
ECM - Extra cellular matrix
GPI – Glycosylphosphatidylinositol
Asn – Asparagine
Ser - Serine
Thr - Threonine
O-GlcNAc - *O*-linked *N*-acetylglucosamine
O-Man - *O*-mannose
O-Fuc - *O*-fucose
O-Gal - *O*-galactose
GlcCer – Glucosylceramide
GalCer - Galactosylceramide
EGFR - Epidermal growth factor receptor
MMP9 - Matrix metalloproteinase-9
HGF - Hepatocyte growth factor
ER - endoplasmic reticulum
FACS - fluorescence-activated cell sorted
miR – microRNA
PKA - Protein kinase A

8. Appendix

8.1 Supplementary information for publication 4.1

4.1 The glycosphingolipid P₁ is an ovarian cancer-associated carbohydrate antigen involved in migration

F. Jacob, M. Anugraham, T. Pochechueva¹, B. W. C. Tse, S. Alam, R. Guertler, N. V. Bovin, A. Fedier, N. F. Hacker, M. E. Huflejt, N. Packer and V. A. Heinzelmann-Schwarz

British Journal of Cancer, 2014

SUPPLEMENTARY INFORMATION

Material and Methods

Cell cultures

Normal human ovarian surface epithelial cell line originated from the ovary (HOSE6-3) and ovarian cancer cell lines OVCAR3, SKOV3, A2780, IGROV1 were cultured in RPMI 1640 medium containing penicillin/streptomycin and 10% fetal calf serum (FCS). Ovarian cancer cells TOV112D and TOV21G (clear cell) were cultivated in DMEM containing 10% FCS and penicillin/streptomycin. Cell cultures were maintained at 37°C in 5% CO₂ and tested routinely for mycoplasma infection (VenorGeM® Mycoplasma Detection Kit (Biocene Pty Ltd, Rozelle, Australia) and (Uphoff & Drexler, 2005)).

Extraction of GSLs from cancer tissue samples

Fresh primary tumor samples from patients with serous ovarian cancer and endometrioid peritoneal cancer were washed twice with PBS. GSLs were extracted as previously described (Korekane *et al*, 2007). Briefly, tissues (~100mg) were homogenized in 5ml of chloroform:methanol (2:1) and stored for 2h at room temperature (RT), with intermittent sonication for 30sec every 30min. Prior to centrifugation at 1800xg for 15min, 2.5 ml of methanol was added to the homogenate. Supernatant was collected and residual tissue was homogenized again in 5ml of chloroform:methanol:water (1:2:0.8). The tissue homogenate was stored for 2h at RT and subjected to centrifugation at 1800xg for 15min. Supernatant was collected and combined with the previous supernatant and evaporated under vacuum. The dried residue containing the glycosphingolipid mixture was then re-dissolved in 100µl of chloroform:methanol (2:1).

Extraction of GSLs from IGROV1 cells

Ovarian cancer cell line IGROV1 was grown in large quantities (1×10^8), harvested and stored in -80°C until use. GSLs were extracted as previously described with some modifications (Durrant *et al*, 2006). Cells were harvested and washed thrice in 10ml of PBS and centrifuged at 1800xg for 15min. A volume of 5ml of chloroform: methanol (2:1) was added to the cell pellet and the tube was kept overnight in a 4°C incubator shaker prior to centrifugation at 1800xg for 15min. Supernatant was collected and pellet was re-extracted again as described above. The combined supernatants were subjected to centrifugation at 1800xg for 15min to remove residual protein pellet. The supernatant was evaporated to dryness under vacuum and the dried residue containing the glycosphingolipid mixtures was re-dissolved in 50 μl of chloroform: methanol (2:1).

PVDF blotting of extracted GSLs, enzymatic release of glycans and purification of glycan alditols

GSLs were blotted onto a polyvinylidene difluoride (PVDF) membrane, an adaptation from a previous method developed for the release of *N*- and *O*-glycans (Jensen *et al*, 2012). Re-dissolved glycosphingolipid mixtures (50 μl) were blotted (10 μl x 5 times) onto cut pre-activated PVDF spots which were placed in a chloroform-compatible 96-well microtitre plate. Neutral and acidic glycosphingolipid standards (10 μl) were blotted (2.5 μl x 4 times) on individual PVDF spots. The spots were air-dried at RT to ensure proper binding of GSLs to the membrane. Once the spots were dried, the glycosphingolipid mixture (acidic and neutral) was digested with 5mU of *Endoglycoceramidase* II (EGCase II, recombinant clone derived from *Rhodococcus sp.* and expressed in *Escherichia coli*, Sigma-Aldrich, St. Louis, USA) in 50 μl of 0.05M Sodium acetate buffer pH 5.0 for 16h at 37°C . The 96-well microtiter plate was sealed with parafilm to avoid sample evaporation. After incubation, approximately 50 μl was recovered from the individual PVDF spots and transferred to 1.5ml Eppendorf tubes. The sample wells were washed with 50 μl of water and combined with the enzyme mixture of

released glycans for each sample. The reaction was stopped by adding 1ml of chloroform:methanol:water (8:4:3) (Karlsson *et al*, 2010). The upper layer (methanol:water) containing the released oligosaccharides (~400µl) was dried and used for subsequent reduction and desalting steps.

Released glycans were reduced to alditols with 20µl of 200mM sodium borohydride in 50mM potassium hydroxide at 50°C for 2h. The reduction mixture was quenched using 3µl of 100% glacial acetic acid.

Glycan alditols were desalted using cation exchange columns that were prepared individually. Approximately 45µl of cation exchange resin beads (BioRad, Hercules, USA; AG50W-X8) were deposited onto reversed phase µ-C18 ZipTips (Perfect Pure, Millipore, Billerica, USA) that were placed in individual microfuge tubes. The tubes were then subjected to a brief spin and followed by a series of individual pre-washing steps with a) 50µl of 1M HCl, b) 50µl of methanol and c) 50µl of water. Each washing step was repeated three times, in which the columns were subjected to a brief spin after the addition of each solution. Approximately 20µl of glycan alditols were applied to the previously prepared cation exchange columns and they were eluted with water (50µl, twice) and dried. Residual borate was removed by drying the samples under vacuum after the addition of methanol (100µl, thrice). The purified glycan alditols were re-suspended in 15µl of water prior to mass spectrometry analysis.

Negative-mode LC-ESI-MS of released glycan alditols mixtures

Samples (4µl) were injected onto a Hypercarb porous graphitized carbon (PGC) capillary column (5 µm Hypercarb KAPPA, 180µm x 100mm, Thermo Hypersil, Runcorn, UK) using a Surveyor auto-sampler. The separation of glycans was carried out over a linear HPLC gradient of 0-45 % (v/v) acetonitrile/ 10mM ammonium bicarbonate for 35min followed by a 10min wash-step using 90 % (v/v) acetonitrile/ 10mM ammonium bicarbonate at a flow rate

of 3 μ l/ min. Glycans were analyzed by nanoLC-MS/MS using a LTQ linear ion-trap mass spectrometer (LC/MSD Trap XCT Plus Series 1100, Agilent Technologies, USA) which was connected to an ESI source (Agilent 6330, Agilent Technologies, USA). The MS spectra were obtained within the mass range of m/z 200 - m/z 1500. The temperature of the transfer capillary was maintained at 300°C and the capillary voltage was set at 3kV. Neutral and acidic glycans were detected in the negative ion reflector mode as $[M-H]^-$ ions and their signal intensities analyzed using Compass Data Analysis Version 1.1 software (Bruker Daltonics, Billerica, USA). The proposed oligosaccharide structures of experimental samples were verified through annotation using a fragmentation mass matching approach based on the MS/MS data and further validated based on the retention times of specific glycan masses of released glycans from glycosphingolipid standards.

Statistical analysis

All evaluations were performed using the R statistical programming language, version 2.15.1 (<http://www.r-project.org/>). Suspension array data are presented as logarithmized median fluorescence intensity (log(MFI)) which is defined as relative fluorescence unit (RFU). Two-group comparison was performed by Welch Two Sample t -test. Logistic regression was performed to predict low anti-P₁ trisaccharide antibody levels in the tumor group, with linear predictors being “cancer histotype”, “FIGO stage”, “grade”, “CA125”, “tumor origin”, “ABO blood group”, “past history of infections”, “BRCA1/2 status” and “smoking”. Cox regression was performed on relapse- and disease-free survival to investigate the prediction of anti-P₁ trisaccharide antibodies. Results are presented as differences of mean values with corresponding 95% confidence intervals (CI) and p -values. A p -value <0.05 was considered significant. Pearson’s correlation was applied to investigate the relationship between age and AGA levels.

In regards to printed glycan array experiments, the concordance correlation coefficient (CCC) was applied on total signal intensities as a median out of eight replicates (relative fluorescence unit, RFU) in order to calculate the correlation of AGA comparing ascites and blood plasma. The CCC was calculated on both printed glycan concentrations (10 and 50 μ M) for IgA+IgG+IgM together, as well as individually for IgA, IgG and IgM. The results were summarized in scatter plots.

In regards to xCELLigence experiment, to compare the effects of "P₁-high *versus* P₁-low" expressing IGROV1 cells with and without inhibitor araC, a linear mixed effects-model was applied across time points. Factors "high-low", "with/without inhibitor" and "time" were modified parameters. Measured cell indices were treated as a random effect. "P₁high-low" was nested in "Inhibitor", "Inhibitor" was nested in "time".

References

- Durrant LG, Harding SJ, Green NH, Buckberry LD, Parsons T (2006) A new anticancer glycolipid monoclonal antibody, SC104, which directly induces tumor cell apoptosis. *Cancer research* **66**(11): 5901-9
- Jensen PH, Karlsson NG, Kolarich D, Packer NH (2012) Structural analysis of N- and O-glycans released from glycoproteins. *Nature protocols* **7**(7): 1299-310
- Karlsson H, Halim A, Teneberg S (2010) Differentiation of glycosphingolipid-derived glycan structural isomers by liquid chromatography/mass spectrometry. *Glycobiology* **20**(9): 1103-16
- Korekane H, Tsuji S, Noura S, Ohue M, Sasaki Y, Imaoka S, Miyamoto Y (2007) Novel fucogangliosides found in human colon adenocarcinoma tissues by means of glycomic analysis. *Analytical biochemistry* **364**(1): 37-50
- Uphoff CC, Drexler HG (2005) Detection of mycoplasma contaminations. *Methods in molecular biology* **290**: 13-23

Table 1S Clinicopathological characteristics of ovarian cancer cohort (n=155)

Disease status		n	%	Total in %
Control group (81)	Healthy and benign	81	100	52.3
Tumors (74)	Borderline tumor	8	10.8	47.7
	Ovarian cancer	38	51.3	
	Peritoneal Cancer	19	25.7	
	Tubal Cancer	9	12.2	
FIGO Stage (74)	I	17	23.0	
	II	3	4.0	
	III	40	54.0	
	IV	9	12.2	
	unknown	5	6.8	
Grade (74)	Borderline	8	10.8	
	1	7	9.5	
	2	4	5.4	
	3	55	74.3	
Histotype (74)	Serous	53	71.6	
	Mucinous	10	13.6	
	Endometrioid	3	4.0	
	Mixed	3	4.0	
	Clear cell	2	2.7	
	Transitional cell	2	2.7	
	Undifferentiated	1	1.4	

Table 2S Summary of profiled printed glycans showed binding with ascites-derived anti-P₁ antibodies

Glycans are ranked from highest to lowest median RFU referring to AGA levels. The presence of particular disaccharide motifs is indicated by “X”. P₁ trisaccharide is highlighted in bold. Abbreviations: Lewis x (Le^x); Lewis y (Le^y); Lewis b (Le^b); H antigen (H); Tn antigen (TnSer); Lacto-N-fucopentaose I (LNFP-1).

	Median RFU	Spacered form of saccharide	Common name	Galβ1-4Glc(NAc)	Galα1-4Galβ
1.	19443	Galα1-4Galβ1-4Glcβ-sp3	P ^k , Gb3	X	X
2.	11807.5	GalNAcβ1-3Galα1-4Galβ1-4Glcβ-sp3	Gb4, P	X	X
3.	11209.5	Galα1-4Galβ1-4Glcβ-sp2	P ^k , Gb3	X	X
4.	8251	Galα1-3GlcNAcβ-sp3			
5.	7772	Fucα1-4(Fucα1-2Galβ1-3)GlcNAcβ1-3Galβ1-4Glcβ-sp4	Le ^b -Lac	X	
6.	7501	Fucα1-4(Fucα1-2Galβ1-3)GlcNAcβ-sp3	Le ^b		
7.	7218	Galβ1-4GlcNAcα1-6Galβ1-4GlcNAcβ-sp2		X	
8.	6224	Galα1-4Galβ1-4GlcNAcβ-sp2	P₁	X	X
9.	4380	Galα1-4(Galα1-3)Galβ1-4GlcNAcβ-sp3		X	X
10.	3855.5	Fucα1-2Galβ1-4(Fucα1-3)GlcNAcβ-sp3	Le ^y	X	
11.	3557	GalNAcβ-sp3	β-GalNAc		
12.	3492	Galα1-4(Fucα1-2)Galβ1-4GlcNAc		X	X
13.	3142.5	4-O-Su-Galβ1-4GlcNAcβ-sp3	4'-O-Su-LacNAc	X	
14.	2863.5	Manα1-6(Manα1-3)Manα1-6(Manα1-3)Manβ-sp4	Man5		
15.	1655	ManNAcβ-sp4	β-ManNAc		
16.	1647	Fucα1-2Galβ1-4(Fucα1-3)GlcNAcβ1-3Galβ1-4Glcβ-sp4	Le ^y -Lac	X	
17.	1471	GalNAcα-sp0	TnSer		
18.	1435	Galα1-4GlcNAcβ-sp3	α-LacNAc		

19.	1335.5	(Glc α 1-6) $_6\beta$ -sp4	maltohexaose	
20.	1302	Fuc α 1-2Gal β 1-3GlcNAc β 1-3Gal β 1-4GlcNAc β -sp2	H(type 1) penta	X
21.	1289	Gal β 1-3GlcNAc α 1-3Gal β 1-4GlcNAc β -sp3		X
22.	1250.5	Fuc α 1-2Gal β 1-4GlcNAc β -sp3	H (type 2)	X
23.	1132	Gal α 1-3Gal β 1-4GlcNAc β -sp3	α GalLe ^x	X
24.	1095.5	6-O-Su-GalNAc β 1-4GlcNAc β -sp3	6'-O-Su- LacdiNAc	
25.	1057.5	GlcNAc β 1-4Mur-L-Ala-D-i-Gln-Lys	GMDP-Lys	
26.	1020.5	Gal α 1-4GlcNAc β 1-3Gal β 1-4GlcNAc β -sp3		X
27.	985.5	Fuc α 1-2Gal β 1-3GlcNAc β 1-3Gal β 1-4Glc β -sp4	LNFP-I	X

Figure 1S Relationship of age and anti-P₁ antibody levels. Scatter plot showing anti-P₁ antibody levels (y-axis) and age (x-axis) in patient plasma for the control (grey) and tumor (black) group for IgM and IgG.

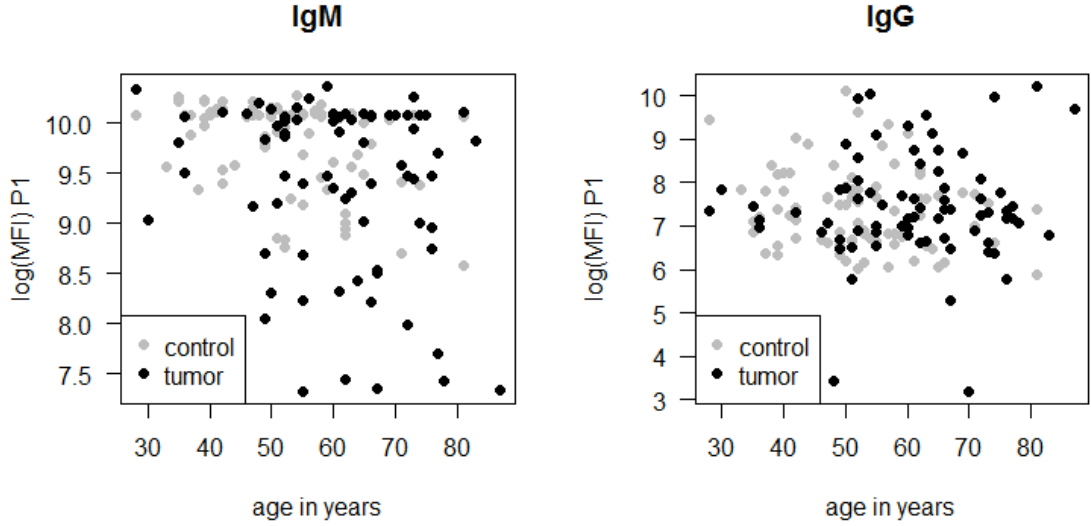


Figure 2S Identification of P₁ in ovarian cancer cell line (IGROV 1) using negative ion mode LC-ESI-MS/MS Base peak chromatogram is shown for glycans extracted from GSLs of ovarian cancer cell line, IGROV 1 **(A)**. Representative extracted ion chromatogram (EIC) of the P₁ pentasaccharide (Hex₄HexNAc₁) at m/z 870.3¹⁻ as indicated by the selected mass peak (red arrow) **(B)**. MS² spectrum of the m/z 870.3¹⁻ ion which corresponds to P₁ pentasaccharide (Gal α 1-4Gal β 1-4GlcNAc β 1-3Gal β 1-4Glc β 1)(C).

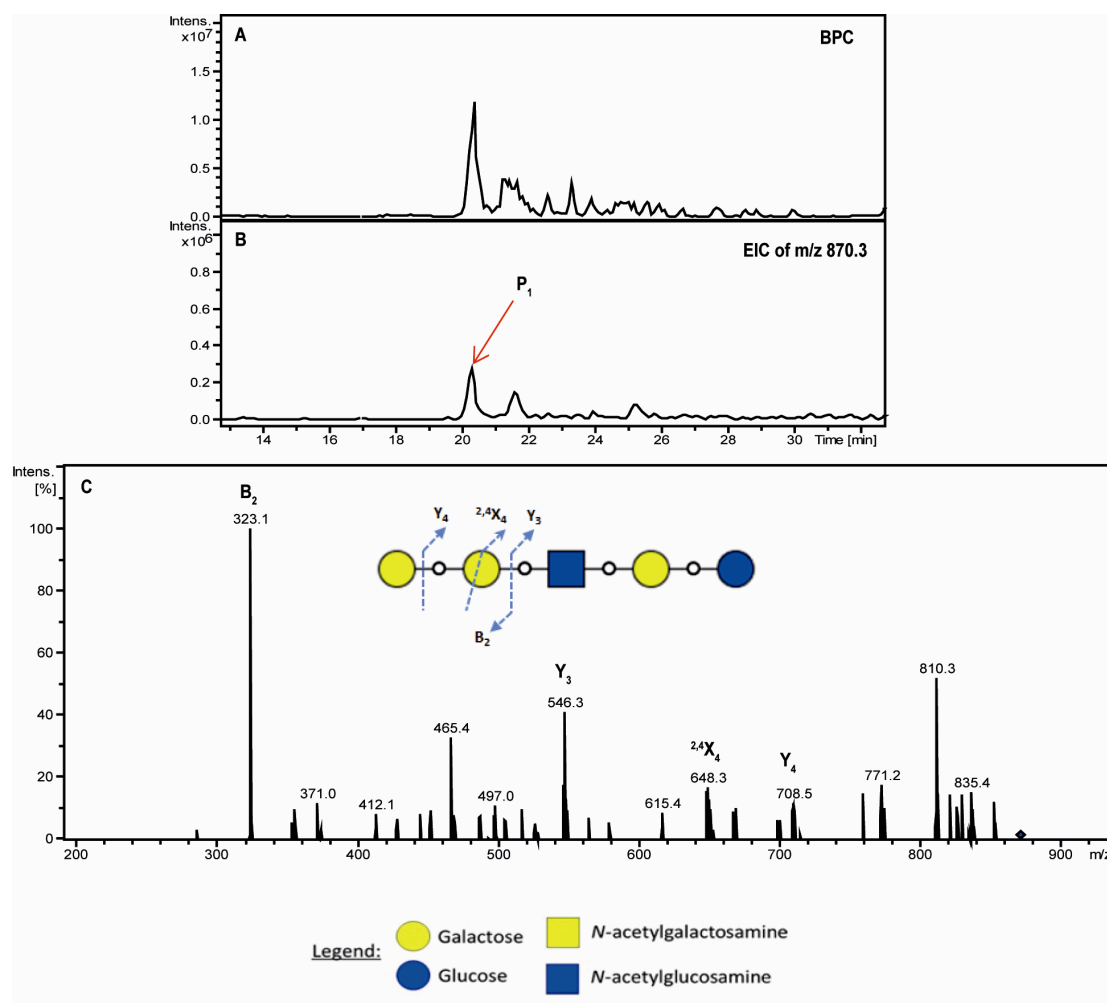


Figure 3S Representative fluorescence scan of randomly selected patient profiled for AGA in ascites (right panel) and blood plasma (left panel) on 50 μ M and 10 μ M prints

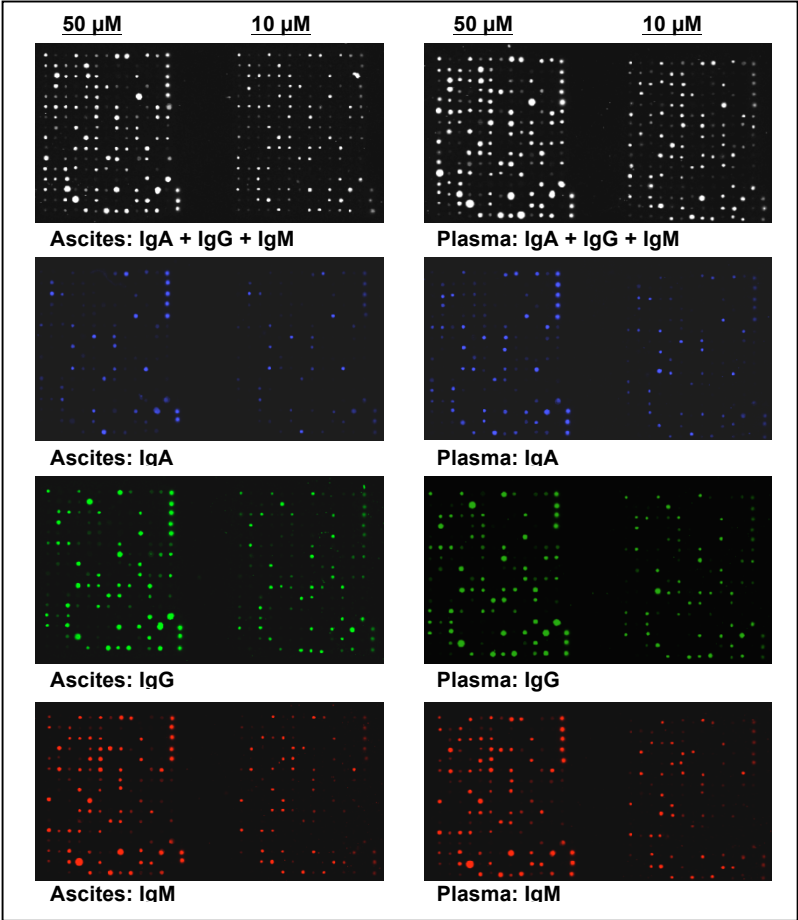
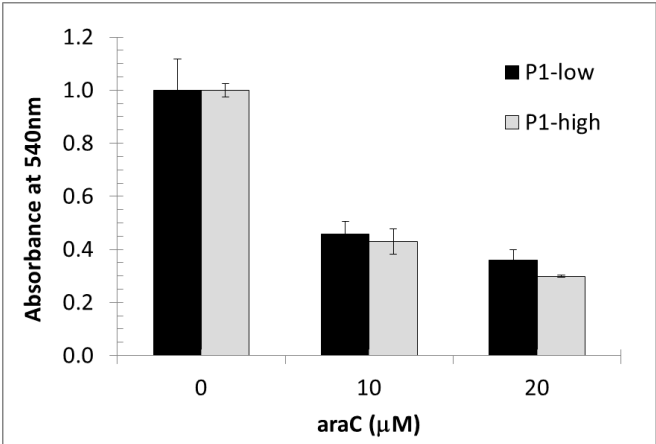


Figure 4S. Cell viability measured by MTT assay showed no statistical difference comparing P₁-low and -high expressing IGROV1 cells exposed to increasing concentrations of araC.



8.2 Supplementary information of Publication 4.4

4.4 Altered (neo-) lacto series glycolipid biosynthesis impairs α 2-6 sialylation on N-glycoproteins in ovarian cancer cells

Shahidul Alam*, Merrina Anugraham*, Yen-Lin Huang , Reto S. Kohler, Timm Hettich, Katharina Winkelbach, Yasmin Grether, Mónica Núñez López, Nailia Khasbiullina, Nicolai V. Bovin, Götz Schlotterbeck & Francis Jacob

Scientific Reports 2017

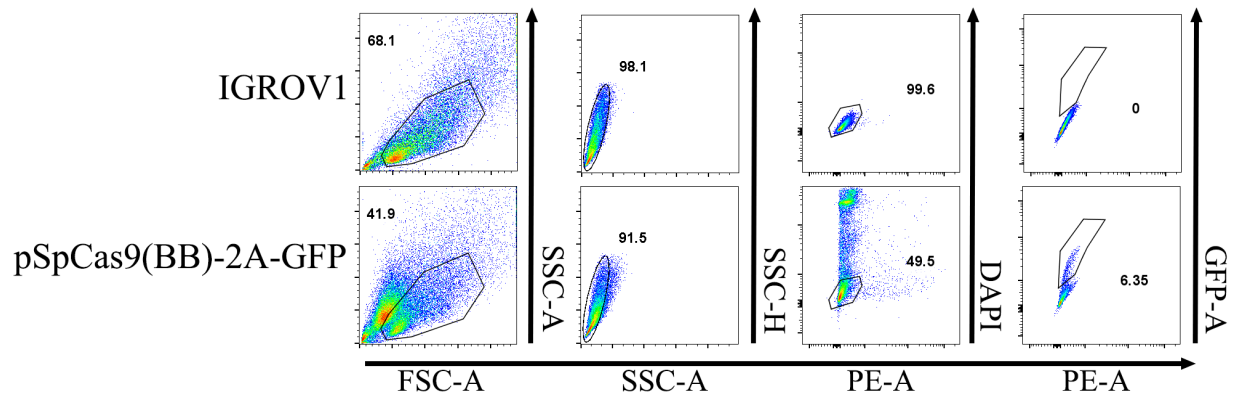
Altered (neo-) lacto series glycolipid biosynthesis impairs α 2-6 sialylation on *N*-glycoproteins in ovarian cancer cells

Shahidul Alam^{1,2+}, Merrina Anugraham¹⁺, Yen-Lin Huang¹, Reto S. Kohler¹, Timm Hettich³, Katharina Winkelbach¹, Yasmin Grether¹, Mónica Núñez López¹, Nailia Khasbiullina⁴, Nicolai V. Bovin⁴, Götz Schlotterbeck³, Francis Jacob^{1,2*}

Supplementary information

Supplemental Fig. S1

Single- cell selection after transient transfection of CRISPR- *Cas9* encoding plasmids. Representative gating of fluorescence activated single cell sorting into 96-well plates after transient delivery of pSpCas9(BB)-2A-GFP (PX458) encoding sgRNA.



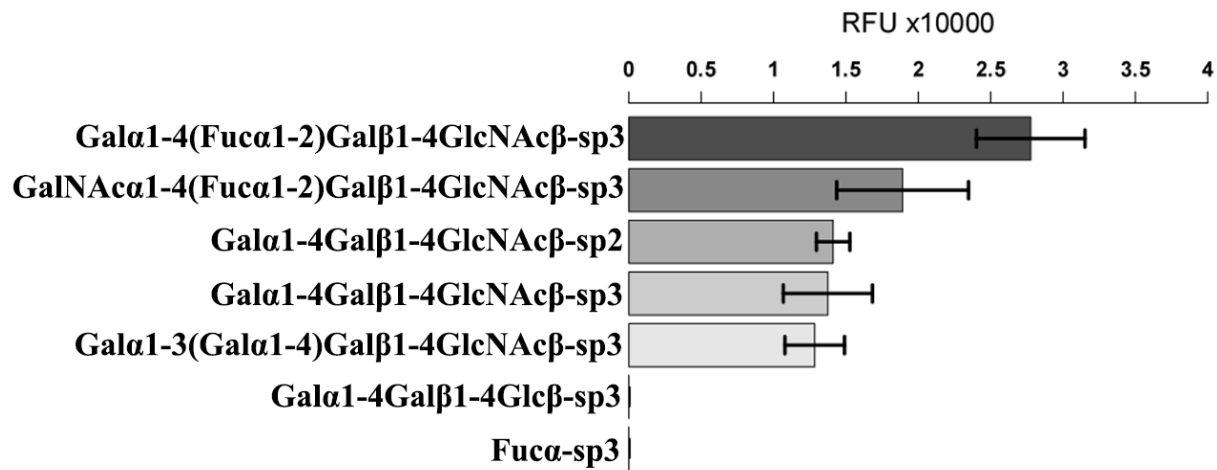
Supplemental Fig. S2

Determination and verification of potential off targets. *In silico* analysis revealed 50 and 17 potential off-targets for sgRNA_1 and sgRNA_2, respectively. The sgRNA_1 had only one predicted off-target in gene NM_001242377 chr5:+112339780 whereas sgRNA_2 was not predicted for an off-target site in a gene. Genomic sequences of predicted off-targets with highest score for each sgRNA were further amplified and sequenced, in which no mutations were observed. Off target DNA sequencing results for B3GNT5 wildtype (IGROV1) and knockout (clone KO_1 and KO_2) cells performed in triplicates. Genomic DNA sequence according to February 2009 human reference sequence (<http://genome.ucsc.edu/index.html>, GRCh37). Standard SP6 DNA Sequencing primer was used.

Off target	5'- ata cac aat tac agt ctt ttc aga aat tta gat -3'		GENOME
01_SP6_	5'- ata cac aat tac agt ctt ttc aga aat tta gat -3'	OK	clone KO_1
02_SP6_	5'- ata cac aat tac agt ctt ttc aga aat tta gat -3'	OK	clone KO_1
03_SP6_	5'- ata cac aat tac agt ctt ttc aga aat tta gat -3'	OK	clone KO_1
04_SP6_	5'- ata cac aat tac agt ctt ttc aga aat tta gat -3'	OK	clone KO_2
05_SP6_	5'- ata cac aat tac agt ctt ttc aga aat tta gat -3'	OK	clone KO_2
06_SP6_	5'- ata cac aat tac agt ctt ttc aga aat tta gat -3'	OK	clone KO_2
07_SP6_	5'- ata cac aat tac agt ctt ttc aga aat tta gat -3'	OK	IGROV1
08_SP6_	5'- ata cac aat tac agt ctt ttc aga aat tta gat -3'	OK	IGROV1
09_SP6_	5'- ata cac aat tac agt ctt ttc aga aat tta gat -3'	OK	IGROV1

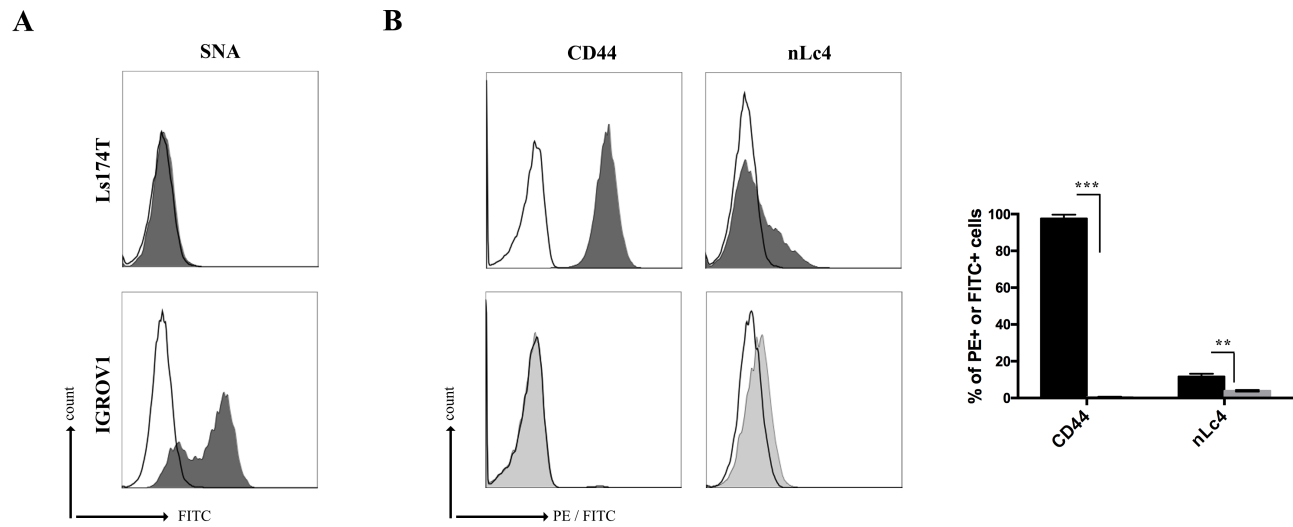
Supplemental Fig. S3

Determination of anti- P₁ IgM binding epitopes using printed glycan array. Barchart demonstrating the binding specificity for human anti-P₁ IgM P3NIL100 antibodies. We performed a broad screening of glycan binding specificity of the monoclonal antibody P3NIL100 across 381 glycans by utilizing glycan array technology. The results clearly demonstrated that antibody bound specifically to glycans with Gal α 1-4Gal β 1-4GlcNAc β as well as glycans terminating with Gal α 1-3(Gal α 1-4)Gal β 1-4 and GalNAc α 1-4Gal β 1-4, with some of these structures bearing α 1-2-linked fucose. As expected, there was no binding of the antibody to Gb3 glycan (Gal α 1-4Gal β 1-4Glc β -sp).



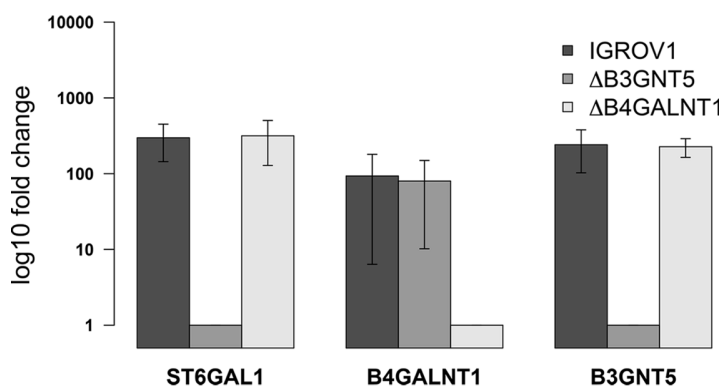
Supplemental Fig. S4

The epitope for anti- nLc4 IgM is present on glycoproteins in colon cancer cell line Ls174T. A) Histogram showing the absence of α 2-6 sialylation in Ls174T cells. **B)** Proteinase K treatment on Ls174T cells following staining for CD44 and nLc4. Representative histogram for unstained (white), Proteinase K - untreated (dark gray) and -treated cells (light gray). Data are represented as mean \pm s.d, *** $p < 0.001$, ** $p < 0.01$.



Supplemental Fig. S5

Quantitative gene expression of *ST6GAL1*, *B4GALNT1*, and *B3GNT5* in IGROV1, $\Delta B3GNT5$ -, and $\Delta B4GALNT1$ - cells. Bar chart represents three independent experiments. Data are represented as mean \pm s.d. RT-qPCR was performed in triplicates on three independent experiments.



Supplemental Table S1

Oligonucleotides used in the study.

single guided RNAs			Gene	Method
	oligonulceotide 5'-3'			
sgRNA 1	CAC CGA TAC ACG ATT ATA GCC GTT T	AAA CAA ACG GCT ATA ATC GTG TAT C	B3GNT5	Gene-editing
sgRNA 2	CAC CGA TCG ACG TTC CGG AAT TAG A	AAA CTC TAA TTC CGG AAC GTC GAT C	B3GNT5	Gene-editing
sgRNA 1	CAC CGT GGA TGC CGC GGT TTC GAC G	AAA CCG TCG AAA CCG CGG CAT CCA C	B4GALNT1	Gene-editing
sgRNA 2	CAA CGC CTT CAA ATA GTC CTC GGG A	AAA CTC CCG AGG ACT ATT TGA AGG C	B4GALNT1	Gene-editing
genotyping PCR primer			Gene	Method
	oligonulceotide 5'-3' (Forward)	oligonulceotide 5'-3' (Reverse)		
PCR_1	GTA TCT GCT TTC ATC CTG ACC AT	TGC CCA ACT GAA CTG CAT AAG	B3GNT5	Genotyping
PCR_2	GTA TCT GCT TTC ATC CTG ACC AT	TCG AGA CCA TAG AAC TTC GTG T	B3GNT5	Genotyping
PCR_3	GGC CTC GCT ACC AAT ACT T	TGC CCA ACT GAA CTG CAT AAG	B3GNT5	Genotyping
PCR_4	GAT GAG GAT AAA GCA GTG CAG AT	GCC TCA GCC CTG CTT CAA ATC	chr5:113003768+113004235	off target
PCR_1	AGA GCG TTA GAC AGG TCA GT	TGG AGG AAG GAG AGG ACA GA	B4GALNT1	Genotyping
PCR_2	CTG TGC GCT CTG GTC CTT	TGG AGG AAG GAG AGG ACA GA	B4GALNT1	Genotyping
PCR_3	CCA CTA CTT GCT CCT TGA TCC	TGG AGG AAG GAG AGG ACA GA	B4GALNT1	Genotyping
PCR_4	CCA CTA CTT GCT CCT TGA TCC	CTG TGC GCT CTG GTC CTT	B4GALNT1	Genotyping
PCR_5	GCA CAT ACT GAA GCG TTC ACA	ATC CCA GCT CCT CAG CTA CA	chr22:30296425-30296628	off target
PCR_6	TTG GCC AGA GGT TCA TGC TA	ACC GTC ACC CTA CTC AAG TG	chr12:52518025-52518321	off target

Supplemental Table S2

Details of target and reference genes, primers and amplicons investigated in this study by RT-qPCR. QPCR parameters are provided including efficiency (E in %; calculated based on the standard curve according to the equation $E=10^{(-1/\text{slope})}-1$) x 100 and expressed as percentage) and correlation coefficient (R^2).

Symbol	Gene name	Accession number	Chr. location	Forward Primer 5'-3'	Reverse Primer 5'-3'	Amplicon size in bp	E in %	R ²
<i>B3GNT5</i>	UDP-GlcNAc β -1,3-N-acetylglucosaminyl-transferase 5	NM_032047.4	3q28	GGCTTGAACCTTCGT GAGTTTCGC	TCGAGACCATAGAA CTTCGTGT	305	92.2	0.994
<i>ST6GALNAC1</i>	GalNAc α -2,6-Sialyltransferase I	NM_018414.3	17q25.1	CGAAATAGGAGGCC TTCAGACGAC	TTTCTGGAGCCACA GCGACTTG	76	74.1	0.999
<i>ST6GALNAC2</i>	GalNAc α -2,6-Sialyltransferase II	NM_006456.2	1q31.1	ATCGAATCTTGGGA CAGGAAAGGG	GATTGAACAGGCCA CGGAAGTG	92	83.9	0.899
<i>ST6GALNAC3</i>	GalNAc α -2,6-Sialyltransferase III	NM_001160011.1	1q31.1	AGCGCATGAGTTAC TGTGATGG	TGCATGGTCACTCT GTACTGTCC	69	103.9	0.999
<i>ST6GALNAC4</i>	GalNAc α -2,6-Sialyltransferase IV	NM_175039.3	9q34.11	ACCAGATCTCCAG GACGAGAC	TCTTCTCCCTGCAGT AGCTGTC	150	86.7	0.998
<i>ST6GALNAC5</i>	GalNAc α -2,6-Sialyltransferase V	NM_030965.1	1q31.1	TGACAATGGCACTG GAGCTCTG	GTGATTGGGATCCC TGCAGAAG	80	131.6	0.955
<i>ST6GALNAC6</i>	GalNAc α -2,6-Sialyltransferase VI	NM_013443.3	9q34.11	CATGCGGCAATTG ACGACCTC	CACGAATGAGACTT CTCCCTGTCC	66	106.1	0.999
<i>ST6GAL1</i>	β -galactosamide α -2,6-sialyltransferase 1	NM_173217.2	3q27-q28b	CCATCTCTGGGAT GCTTGGTATC	ACGTCAGTCTTGGC CTTGGATG	95	98.1	0.997
<i>ST6GAL2</i>	β -galactosamide α -2,6-sialyltransferase 2	NM_001142351.1	2q12.3	TTCTTGGGCGAGG AAATAGATTC	TCATAACCACGTGT AGGAGCAGAG	72	99.2	0.991
<i>B4GALNT1</i>	β -1,4-N-Acetyl-Galactosaminyl Transferase 1	NM_001276468	12q13.3	TGTGCGCTCTGGTCC TTCTG	TTGATCCTGACCGG GATGTGT	181	74.1	0.999
<i>HSPCB</i>	Heat shock protein 90kDa alpha (cytosolic)	NM_007355	6p12	TCTGGGTATCGGAA AGCAAGCC	GTGCACTTCCTCAG GCATCTTG	80	87.2	0.999
<i>YWHAZ</i>	Tyrosine 3-monooxygenase/tryptophan 5-monooxygenase activation protein	NM_003406	8q23.1	ACTTTTGGTACATTG TGGCTTCAA	CCGCCAGGACAAAC CAGTAT	94	94.1	0.999
<i>SDHA</i>	Succinate dehydrogenase complex, subunit A	NM_004168	5p15	TGGGAACAAGAGGG CATCTG	CCACCACTGCATCA AATTCATG	86	100.9	0.999

8.3 Supplementary information of Publication 4.5

4.5 Transition of mesenchymal and epithelial cancer cells depends on globosides

Francis Jacob*, Shahidul Alam*, Ching-Yeu Liang, Reto S. Kohler, Martina Konantz,
Arun V. Everest-Dass, Yen-Lin Huang, Andre Fedier, Andreas Schötzau, Monica
Nunez Lopez, Nicolle H. Packer, Claudia Lengerke, Viola Heinzelmann-Schwarz

Manuscript ready to submit

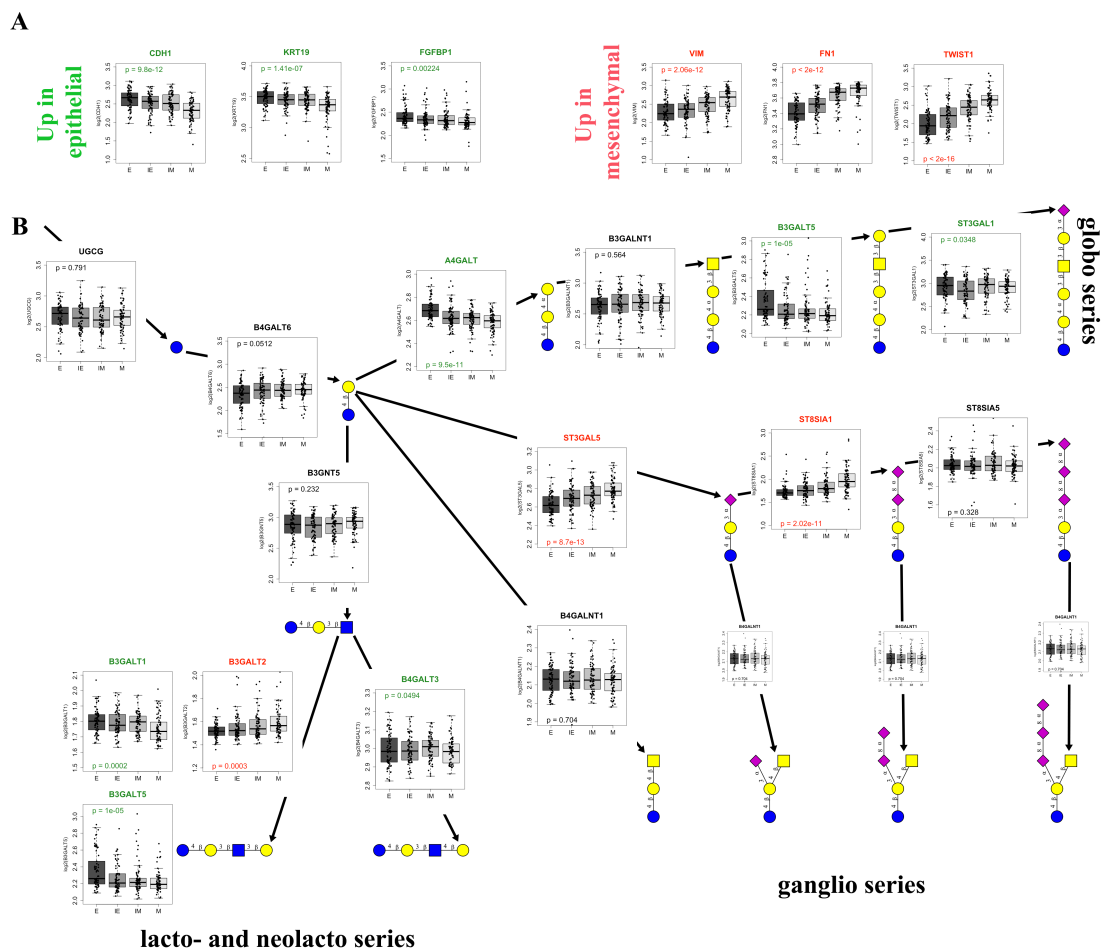
Transition of mesenchymal and epithelial cancer cells depends on globosides

Francis Jacob^{1*}, Shahidul Alam^{1,2*}, Ching-Yeu Liang¹, Reto S. Kohler², Martina Konantz³,
Arun V. Everest-Dass⁴, Yen-Lin Huang², Andre Fedier², Andreas Schötzau², Monica Nunez
Lopez², Nicolle H. Packer^{4,5}, Claudia Lengerke^{3,6}, Viola Heinzlmann-Schwarz^{2,7}

Supplementary information

Supplementary Figure S1

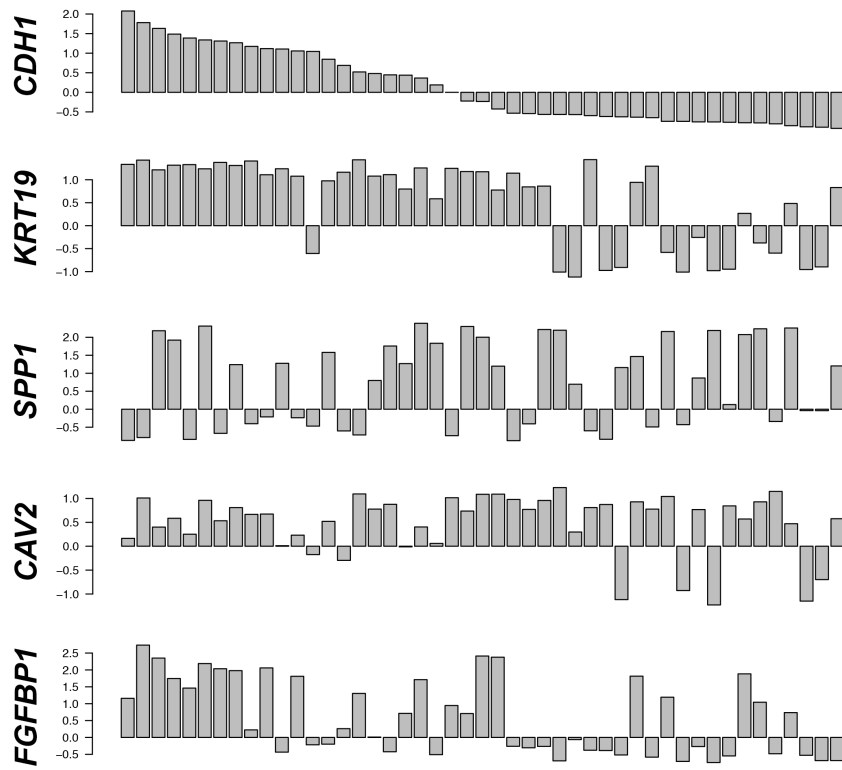
Globoside GSL synthesizing glycosyltransferases show elevated gene expression in epithelial tissue samples. Tohill transcriptomic data set was divided into four EMT states: epithelial (E), intermediated epithelial (IE), intermediate mesenchymal (IM), and mesenchymal based on previously developed EMT score (1). **A)** Upregulated EMT markers in epithelial (green) and mesenchymal (red) cells among four EMT states, respectively. **B)** KEGG annotated glycosyltransferases involved in glycosylceramide-related glycosphingolipids divided into three major series- globo, (neo-) lacto, and ganglio series glycosphingolipids. Boxplot showing expression of glycosyltransferase-encoding genes significantly up-regulated in epithelial (green), in mesenchymal (red), or without changes (black). Black solid arrows indicate elongation of glycan structures.



Supplementary Figure S2

EMT marker gene expression in 47 ovarian cancer cell lines. Normalized transcriptomic data were accessed *via* the <http://www.cbioportal.org>. The cell line CCLE Broad Cancer cell line encyclopedia (Novartis/ Broad, (2)) containing mRNA expression Z-scores (microarray) were sorted in descending order for *CDH1* expression in all available ovarian cancer cell lines (n=47) including IGROV1. Five corresponding epithelial markers (*KRT19*, *SPP1*, *CAV2*, and *FGFBP1*) and mesenchymal markers (*CDH2*, *VIM*, *FN1*, *TWIST1*, and *SERPINE1*) were plotted in bar charts accordingly. In addition, findings on EMT states in ovarian cancer cells published in Huang *et al.* 2013 (3) were highlighted for cell lines matching in both data sets (color code and legend below the figure).

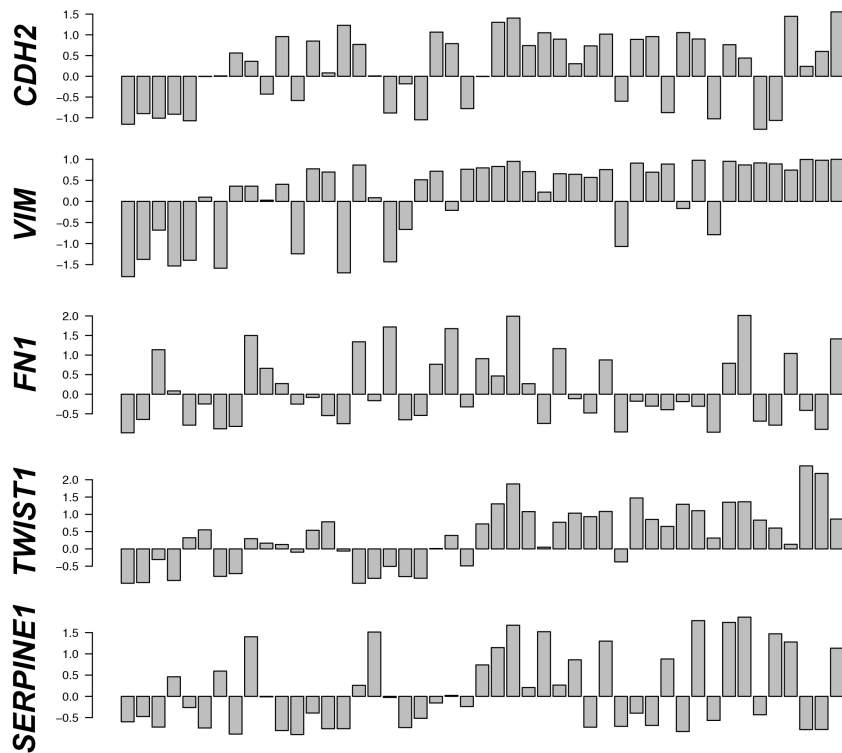
Genes Down-Regulated During EMT



Huang *et al.* 2013

- JHOIM2B
- MCAS
- RMGI
- FMUGS
- SNU119
- OVISE
- COV644
- OVKATE
- SNU840
- CAOV3
- CAOV4
- NIHOVCAR3
- OVSAHO
- CAW42
- CAW28
- EPD27
- OVCR44
- OVCR4
- JH90
- JH94
- OVMAH1
- KURANOCHI
- JH92
- IGROV1
- SKOV3
- COV594
- OV7
- COV318
- EPD21
- JHOC5
- FUDV1
- OC314
- OVCR8
- COV434
- COV982
- OC316
- OVTKO
- COLO704
- HEVA8
- OVK18
- ES2
- OV56
- OV21G
- TYKNU
- JHOM1
- TOV112D
- A2790
- X59M

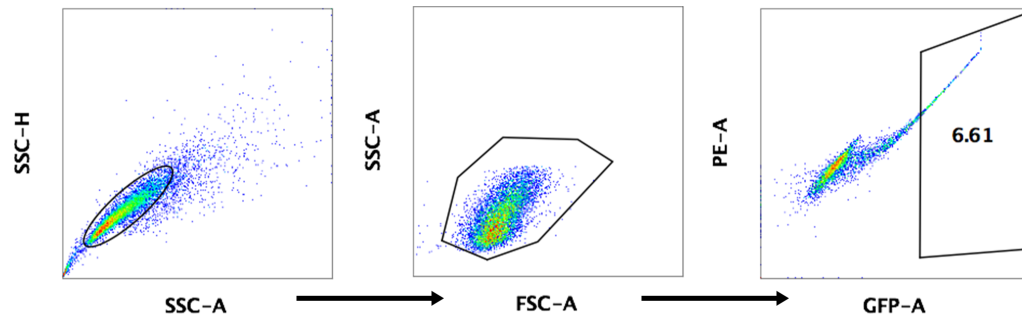
Genes Up-Regulated During EMT



Legend: ● epithelial ● intermediate-epithelial
 ● intermediate-mesenchymal ● mesenchymal

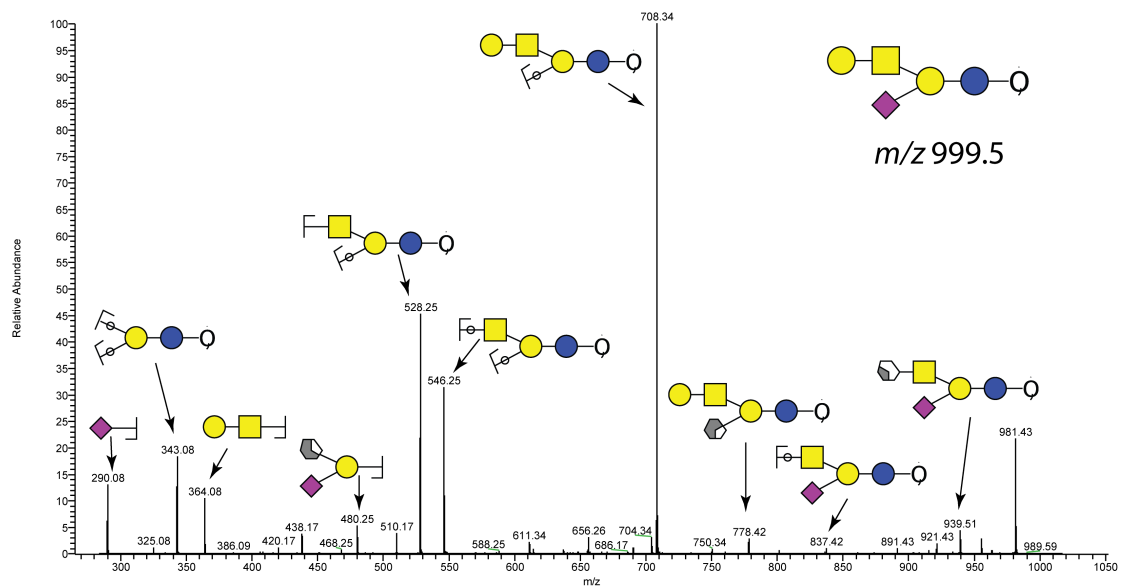
Supplementary Figure S3

Single cell sorting strategy after transient transfection of sgRNA CRISPR-Cas9 constructs. Cancer cell lines were transfected with equal amount of PX458 incorporating two different *A4GALT*-specific sgRNA in addition to *Cas9* and GFP. Single cell sorting was performed as exemplified for IGROV1 ovarian cancer cells.



Supplementary Figure S4

Quantification of glycans released from glycosphingolipids in wildtype and *AA4GALT* ovarian cancer cells using LC-ESI-MS/MS. Proposed GSL-glycan structures and their relative abundance as detected on the glycolipid membranes of ovarian epithelial cancer cells IGROV1 wild type and the knockout. GSL-glycan structures were enzymatically released from glycolipids and separated by PGC-LC-ESI MS/MS analysis. Structures were assigned based on MS/MS fragmentation (where possible) and biological GSL pathway constraints. Structures are depicted according to the CFG (Consortium of Functional Glycomics).



Supplementary Figure S5

Genetic depletion of *A4GALT* correlates with the absence of globosides in ovarian cancer cells representing the four different states of EMT.

A) PCR for initial verification of selected $\Delta A4GALT$ clones obtained from BG1 and SKOV3.

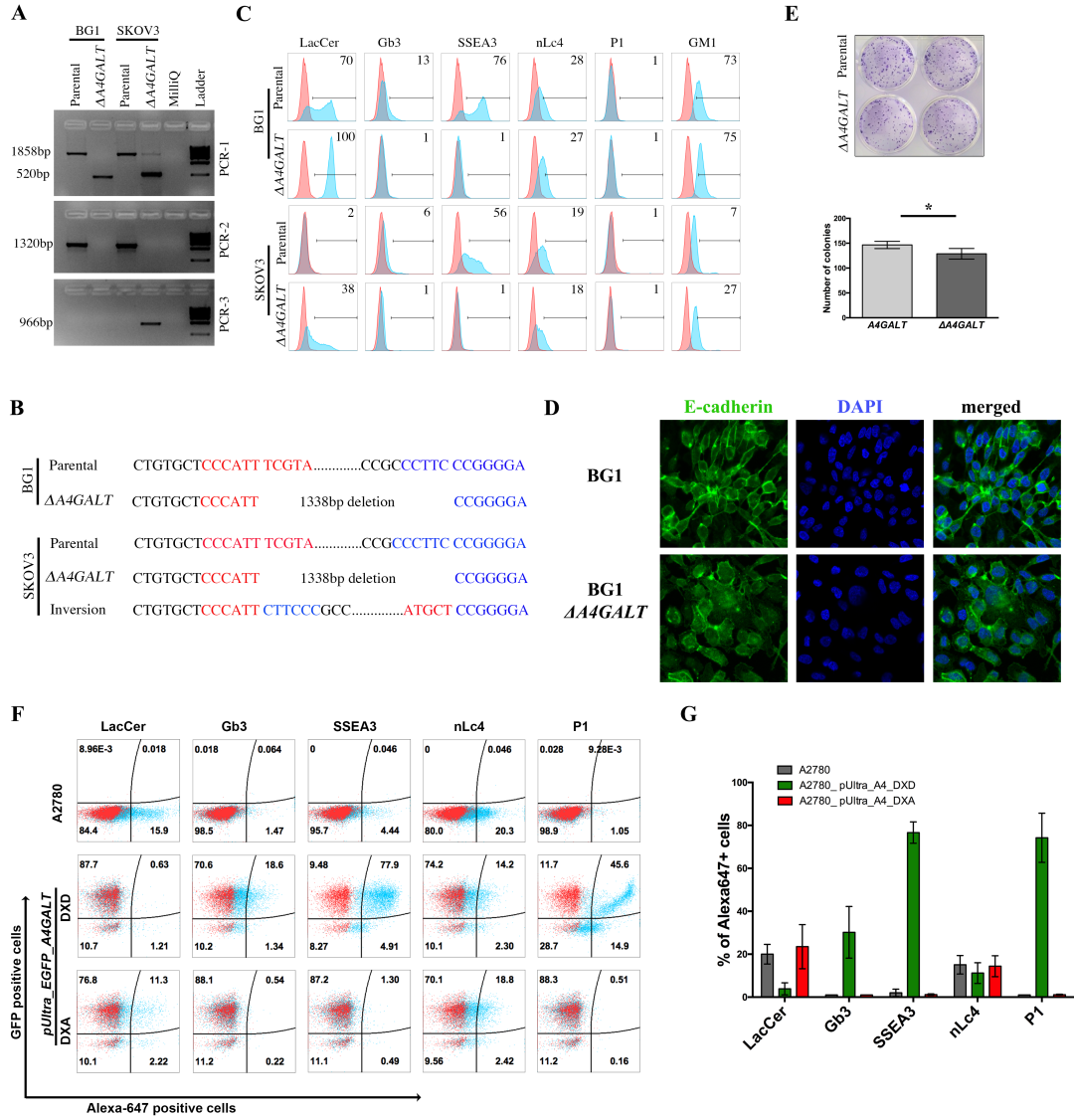
B) Sanger DNA sequencing results for selected clones at the *Cas9*-targeted region showing deletion and inversion in two additional genome edited cell lines. **C)** Corresponding flow

cytometry results shown as representative counter plots for validation of GSL expression in selected $\Delta A4GALT$. **D)** Anchorage-dependent growth investigated by colony formation assay

in SKOV3 and BG1 cells and their corresponding $\Delta A4GALT$ cell clones. **E)** Overexpression of A4GALT in A2780 cells negative for GSL expression. Counter plots display expression of










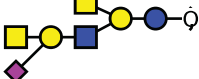

GSL expression in A2780 cells stably expressing A4GALT cloned into pUltra (co-expression with EGFP). **G)** Barchart summarizing three independent experiments for overexpression of

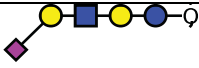
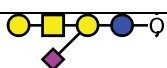
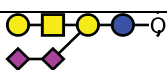
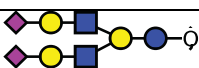
A4GALT in A28780 cells.



Supplementary Table S1

Quantification of glycans released from glycosphingolipids in wildtype and *AA4GALT* ovarian cancer cells using LC-ESI-MS/MS. Proposed GSL-glycan structures and their relative abundance as detected on the glycolipid membranes of ovarian epithelial cancer cells IGROV1 wild type and the knockout. GSL-glycan structures were enzymatically released from glycolipids and separated by PGC-LC-ESI MS/MS analysis. Structures were assigned based on MS/MS fragmentation (where possible) and biological GSL pathway constraints. Structures are depicted according to the CFG (Consortium of Functional Glycomics).

	[M-H] ⁻ ([M-2H] ²⁻)	Proposed structure	Wildtype Relative abundance % (SE)	<i>AA4GALT</i> Relative abundance % (SE)
1	505.3		3.8 (0.32)	
2a	708.3		3.3 (0.24)	2.6 (0.12)
2b	708.2		1.3 (0.08)	2.1 (0.03)
3	626.2	S {  }	6.9 (0.37)	0.8 (0.03)
4	837.4		0.3 (0.01)	0.4 (0.02)
5	911.4		2.6 (0.43)	0.4 (0.03)
6a	1202.5 (600.8)		2.2 (0.33)	1.7 (0.09)
6b	1202.5 (600.8)		4.6 (0.17)	2.4 (0.21)
7	634.2		13.9 (1.32)	17.0 (1.45)
8	1405.6 (702.3)		3.6 (0.43)	1.6 (0.23)
9a	999.5		1.6 (0.16)	0.1 (0.01)

9b	999.5		0.0	0.6 (0.03)
9c	999.5		13.4 (1.05)	29.4 (2.65)
10a	1290.6 (644.8)		40.4 (1.89)	38.5 (1.65)
11	1655.8 (827.4)		2.3 (0.24)	2.4 (0.17)

Supplementary Table S2

Cell lines used in this study. Table provides details of all cell lines including type of cells, name of the cell lines, culture media conditions, and supplements.

Cell types	Cell Lines	Culture media	Supplements
Normal	FT190	DMEM-Ham's F12 without HEPES Buffer, penicillin (100U/ml) and streptomycin (Sigma-Aldrich)	2% Ultroser™ (PALL, Life Science)
	FT133tag		
	FT237		
	FT240		
Ovarian Cancer	HOSE6.3	RPMI-1640 supplemented with 10% FBS, penicillin (100U/ml) and streptomycin (100µg/ml) (Sigma-Aldrich, Buchs, Switzerland)	1mM Sodium pyruvate (Sigma- Aldrich)
	HOSE17.1		
	IGROV1		
	A2780		
	SKOV3		
	OVCAR3		
	OVCAR4		
	OVCAR5		
	OVCAR8		
	BG1		
	OAW42		
	CAOV3		
	TOV21G		
	OVSAHO		
KURAMOCHI			
Tyk-Nu			
EFO27			
Breast Cancer	MCF7		
	T47D		
	MDA-MB-231		
Colon Cancer	HCT16		
	HCT116		
	HT29		
	LS174T		
Leukemia	THP-1		
	K562		
Cervical cancer	HeLa		
	ME-180		
Kidney	HEK293T		
Neuroblastoma	U521		

Supplementary Table S3

Table providing details of oligonucleotides used in this study. Name of oligonucleotides, DNA sequence, and method applying particular oligonucleotides are provided. RT-qPCR primer were established as recently described (4).

Oligonucleotide name	Sequences (5'–3')	Method
sgRNA1_Forward	Caccg TGG CTG CTC ACC TAC GAA ATG GG	CRISPR-Cas9
sgRNA1_Reverse	aaac ATT TCG TAG GTG AGC AGC CAC	CRISPR-Cas9
sgRNA2_Forward	caccgCAATCTTGCCCTCCCCGGGAA	CRISPR-Cas9
sgRNA2_Reverse	aaacTTCCCGGGGAGGCAAGATTGC	CRISPR-Cas9
Human U6_Forward	GAGGGCCTATTTCCCATGATTCC	Cloning
PCR_1,2_Forward	ACCAGGAAAGAGAGGTCTAATG	Genotyping A4GALT
PCR_1,3_Reverse	CTGTTGAGGAGCTGTGGGAG	Genotyping A4GALT
PCR_2,3_Reverse	CTCAACGGCGCGTTCCTGG	Genotyping A4GALT
T7_F	TAATACGACTCACTATAGGG	Cloning
Sequencing_A4_Forward	GGACCACTACAACGGCTGGAT	DNA Sequencing
Sequencing_A4_Reverse	ACGAAGTCCCGCATGCACA	DNA Sequencing
A4_qPCR_Forward	GTCTGCACCCTGTTCATCA	RT-qPCR
A4_qPCR_Reverse	AGAGCTGCCCTTTCTCCTTG	RT-qPCR
CDH1_Forward	GCCTCTGAAAAGAGAGTGAAG	RT-qPCR
CDH1_Reverse	TGGCAGTGTCTCTCCAAATCCG	RT-qPCR
Vimentin_Forward	TGCAGGAGGAGATGCTTCAGAG	RT-qPCR
Vimentin_Reverse	CAGAGACGCATTGTCAACATCCTG	RT-qPCR
HSPCB_Forward	TCTGGGTATCGGAAAGCAAGCC	RT-qPCR
HSPCB_Reverse	GTGCACCTCCTCAGGCATCTTG	RT-qPCR
YWHAZ_Forward	ACTTTTGGTACATTGTGGCTTCAA	RT-qPCR
YWHAZ_Reverse	CCGCCAGGACAAACCAGTAT	RT-qPCR
SDHA_Forward	TGGGAACAAGAGGGCATCTG	RT-qPCR
SDHA_Reverse	CCACCACTGCATCAAATTCATG	RT-qPCR
A4GALT_Exon3_NheI_F	CATGCTAGCGGATACCATGTCCAAGCC	Cloning
A4GALT_Exon3_XhoI_R1	CATCTCGAGTCACAAGTACATTTTCATGGC	Cloning
CMV_F	CAAATGGGCGGTAGGCGTG	Cloning
BGH_R	TAGAAGGCACAGTCGAGG	Cloning
A4GALT_DXA_forward	GTTCGGCGGCATCTAACTGGACACGGCATTTCATTG	Mutagenesis PCR
A4GALT_DXA_reverse	CCGCAGGTTCTTGAGAACAATGAAGTCCGTGCCAGGTAG	Mutagenesis PCR
InFusion_CDH1_F	CGCCTGGAGAATTGGATGGGCCCTTGGAGCCGC	Cloning
InFusion_CDH1_R	ATCCAGTCACTATGGCTAGTCGTCCTCGCCGCC	Cloning
InFusionIL2RCDH1_F	CGCCTGGAGAATTGGATGGATTACATACCTGCTGAT	Cloning
InFusionIL2RCDH1_R	ATCCAGTCACTATGGCTAGTGGTCTCGCCGCC	Cloning
CDH1_Bis_1F	ATTTTAGTAATTTTAGGTTAGAGGG	Bisulfite Sequencing
CDH1_Bis_1R	TCCAAAACCCATAACTAACC	Bisulfite Sequencing
CDH1_Bis_2F	AGTAATTTTAGGTTAGAGGGTT	Bisulfite Sequencing
CDH1_Bis_2R	CTAAAATCTAACTAACTTC	Bisulfite Sequencing

References

1. Tan TZ, *et al.* (2014) Epithelial-mesenchymal transition spectrum quantification and its efficacy in deciphering survival and drug responses of cancer patients. *EMBO Mol Med* 6(10):1279-1293.
2. Barretina J, *et al.* (2012) The Cancer Cell Line Encyclopedia enables predictive modelling of anticancer drug sensitivity. *Nature* 483(7391):603-607.
3. Huang RY, *et al.* (2013) An EMT spectrum defines an anoikis-resistant and spheroidogenic intermediate mesenchymal state that is sensitive to e-cadherin restoration by a src-kinase inhibitor, saracatinib (AZD0530). *Cell death & disease* 4:e915.
4. Jacob F, *et al.* (2013) Careful selection of reference genes is required for reliable performance of RT-qPCR in human normal and cancer cell lines. *PloS one* 8(3):e59180.

9. Acknowledgements

First of all I would like to thank my academic supervisor, Professor Viola Heinzlmann-Schwarz, for giving me the chance to do my PhD work in her lab and for her continuous support and guidance throughout the different projects I was working on. I would also like to thank my supervisor, Dr. Francis Jacob, for his tremendous support during the whole period of my PhD. The open door policy always made it easy to discuss with him anytime. I am very grateful for everything what they did for me!

Further, I am very thankful to my thesis committee members Professor Martin Spiess, and Professor Gerhard M. Christofori, who have also guided me throughout my PhD years. They have always been there to talk to, and have given great input for the projects.

I am also happy that I got the chance to work in such a great lab, which has become like a second family to me. We always had fun together, and you all made it a very enjoyable work environment. I miss the people who have already left, and I will miss everyone else, once I leave.

The 'good soul' of the lab is of course Monica Nunez Lopez. She keeps the whole lab running smoothly, and makes it a lot easier for us to do our work. In my case (as for many others), she has given so much support with experiments, discussions, and otherwise that she has helped me substantially with finishing my PhD. I would also like to think that she has become a friend over the past 5 years, with whom I have always enjoyed talking to. Many thanks also to Reto S. Kohler, Andre Fedier, Tatiana Pochechueva, Yen-Lin Huang, and Andreas Schötzau for being kind and patient when helping me with experiments and giving me scientific input when I had questions. Ana Bela, Ching-Yeu Liang, Natalie Rimmer, Terraneo Nastassja and Yasmin Grether, I want to thank you all for just being my friends, and being there for me. Coffee breaks, badminton games, lunches, discussions and so many other good times would not have been the same without all of you! I have also made other friendships and met so many great people at the DBM, but you guys are the most important.

I want to truly thank my parents Mohammed Musa and Shamsun Nahar Begum for letting me choose my own path, supporting my decisions, and for everything they have done for me. Last but definitely not least, I want to thank my family members

for their support throughout my PhD years and especially during the last few months of writing my thesis.

10. Curriculum vitae

MD. SHAHIDUL ALAM

Johanniter-Strasse 15
4056, Basel, Switzerland
+41 78 696 54 03
a.shahidul@unibas.ch
Skype ID: shahidgeb

Citizenship - Bangladeshi
Swiss Resident Permit B
Marital status – Single
Date of Birth – 18.11.1984



EDUCATION

- 02/2013 - to date PhD Student, Ovarian Cancer Research, Department of Biomedicine, University of Basel, Switzerland
- 01/2011 - 10/2012 M.Sc. in Biomedicine, Institute of Biology, University of Skövde, Sweden
- 04/2004 - 08/2010 B.Sc. (Hons), Genetic Engineering & Biotechnology, University of Chittagong, Bangladesh

RESEARCH EXPERIENCE

- 02/2013 - to date Graduate Research, Advisor Prof. Dr. Viola Heinzlmann, Supervisor Dr. Francis Jacob, Faculty representative Prof. Martin Spiess & Committee member Prof. Gerhard Christofori
- Dissecting the molecular functional of neutral glycosphingolipids in ovarian cancer by-
 - Establish CRISPR-Cas9 mediated genome editing
 - Developed assays for identification of glycosphingolipids on cancer cells derived from patient samples
 - Lenti- and retro-viral transduction to generate heritable and stable gene expression and valid rescue system
 - Utilize in-vitro assays to characterize clones and functional studies of glycosphingolipids
 - Establish and prepare glycan release for glycomics using LC-MS/MS
- 10/2012 - 01/2013 Research Trainee, Supervisor Dr. Francis Jacob, Glyco-oncology, Ovarian Cancer Research, DBM, University of Basel, Switzerland
- Identification of single nucleotide polymorphisms at the genomic locus of A4GALT, a glycosyltransferase synthesizing P blood group related antigens
- 01/2012 - 09/2012 M.Sc. Thesis, Supervisor Prof. Dr. Christian De Geyter, Gynecological Endocrinology, DBM, University of Basel, Switzerland
- Validations of the changes of gene expression induced by HRP in breast tissue of healthy postmenopausal women and identified by whole genome expression analysis

PUBLICATIONS

Peer-Reviewed

5. **Alam, S.**, Jacob, F., Liang, C.Y., Kohler, R.S., Konantz, M., Everest-Dass, A., Huang, Y.L., Fedier, A., Schötzau, A., Lopez, M.N., Packer, N.H., Lengerke, C., Schwarz, V.H.; Transition of mesenchymal and epithelial cancer cells depends on globosides. (Submitted to *Cell*)
4. **Alam, S.**, Anugraham, M., Huang, Y.L., Lopez, M.N., Kohler, R.S., Winkelbach, K., Greather, Y., Khasbiullina, N., Bovin, N.V., Hettich, T., Jacob, F.; (2017) Altered neo (-lacto) series glycolipid biosynthesis impairs α 2-6 sialylation on N-glycoproteins in ovarian cancer cells. *Scientific Reports*, DOI: 10.1038, **IF- 5.525**
3. **Alam, S.***, Pochechueva, T.*, Chinarev, A., Schötzau, A., Fedier, A., Bovin, N.V., Hacker, N.F., Jacob, F., Heinzelmann-Schwarz, V. (2017) Naturally occurring anti-glycan antibodies binding to Globo H-expressing cells identify ovarian cancer patients. *Journal of Ovarian Research*, 10 (1):8, **IF-2.502**, *Co-first author
2. **Alam, S.**, Fedier, A., Kohler, R.S., Jacob, F. (2015) Glucosylceramide synthase inhibitors differentially affect expression of glycosphingolipids. *Glycobiology*, 25(4): 351-356, **IF-3.528**
1. Jacob F., Anugraham M., Pochechueva, T., Tse, B.W.C., **Alam S.**, Guertler, R., Bovin, N.V., Fedier, A., Hacker, N.F., Huflejt, M.E., Packer, N., Heinzelmann-Schwarz, V. (2014) The glycosphingolipid P1 is an ovarian cancer mediated carbohydrates antigen involved in migration. *British Journal of Cancer*, 111: 1634- 1645, **IF-5.569**

Published Abstracts

4. Fedier, A., **Alam, S.**, Winkelbach, K., Kohler, R.S., Schwarz, V.H., Jacob, F. (2016) Neolacto glycosphingolipids promote Doxorubicin, Epirubicin, and organoarsenic PENAO sensitivity and hypoxia-induced HIF-1 α accumulation in ovarian cancer cells. *Geburtshilfe Frauenheilkd*, 76 - P070. **IF- 0.931**
3. **Alam, S.**, Fedier, A., Kohler, R. S., Lopez M. N., Heinzelmann-Schwarz, V.A., Jacob, F. (2015) Genetic disruption of A4GALT (α 1,4-galactosyltransferase) depletes globoside and P1 on IGROV1 ovarian cancer cells. *Glycoconjugate Journal*, 32(5): 173-342, **IF-1.828**
2. Jacob, F., Anugraham, M., Pochechueva, T., Tse, B.W.C., **Alam, S.**, Guertler, R., Bovin, N. V., Fedier, A., Hacker, N.F., Huflejt, M.E., Packer, N., Heinzelmann-Schwarz, V.A. (2015) Natural anti-glycan IgM recognize P1 glycosphingolipid expressed on ovarian cancer cells. *Clinical Cancer Research*, BIOL-1322, **IF-8.738**
1. Jacob, F., Anugraham, M., **Alam, S.**, Bovin, N., Packer, N., Hacker, N.,Heinzelmann-Schwarz, V.A. (2013) P1 glycosphingolipid is expressed on ovarian cancer cells recognized by naturally occurring anti-P1 antibodies. *Clinical Cancer Research*, OVCA13-B23, **IF-8.738**

CONFERENCE COMMUNICATIONS

Oral presentations

1. Glyco23, 23rd International Symposium on Glycoconjugates, Split, Croatia (2015)
2. DBM PhD Retreat, Schwarzsee, Friborg, Switzerland (2015)
3. DBM PhD Retreat, Hasliberg, Bern, Switzerland (2014)
4. Swiss Society for Gynecologists and Obstetricians (SGGG), Lugano, Switzerland (2013)

Poster presentations

1. Glycobiology Gordon Research Conference, Lucca, Italy (2015)
 2. Swiss Society for Gynecologists and Obstetricians (SGGG), Lugano, Switzerland (2015)
 3. Swiss Society for Gynecologists and Obstetricians (SGGG), Lugano, Switzerland (2014)
 4. DBM PhD Retreat, Hasliberg, Bern, Switzerland (2013)
-

MEMBERSHIPS

Executive Committee member of Basel-Bangladesh Association, Switzerland
Member of Young Biotechnologist Bangladesh
Member of Rotary Club of Chittagong, Bangladesh

OTHER INTREST

Travelling
Playing Football, Badminton, Cricket and Chess
Teaching Bengali to the non-residential Bangladeshi's in Basel, Switzerland
